NOTICE

AVIS

The quality of this microform is heavily dependent upon the quality of the original thesis submitted for microfilming. Every effort has been made to ensure the highest quality of reproduction possible.

La qualité de cette microforme dépend grandement de la qualité de la thèse soumise au microfilmage. Nous avons tout fait pour assurer une qualité supérieure de reproduction.

If pages are missing, contact the university which granted the degree.

S'il manque des pages, veuillez communiquer avec l'université qui a conféré le grade.

Some pages may have indistinct print especially if the original pages were typed with a poor typewriter ribbon or if the university sent us an inferior photocopy.

La qualité d'impression de certaines pages peut laisser à désirer, surtout si les pages originales ont été dactylographiées à l'aide d'un ruban usé ou si l'université nous a fait parvenir une photocopie de qualité inférieure.

Reproduction in full or in part of this microform is governed by the Canadian Copyright Act, R.S.C. 1970, c. C-30, and subsequent amendments.

La reproduction, même partielle, de cette microforme est soumise à la Loi canadienne sur le droit d'auteur, SRC 1970, c. C-30, et ses amendements subséquents.

Canada

UNIVERSITY OF ALBERTA

FINITE DIFFERENCE SIMULATION AND IMAGING OF SEISMIC WAVES
IN COMPLEX MEDIA

by   ©

NANXUN DAI

A THESIS

SUBMITTED TO THE FACULTY OF GRADUATE STUDIES AND RESEARCH

IN PARTIAL FULFILLMENT OF THE REQUIREMENTS FOR THE DEGREE

OF DOCTOR OF PHILOSOPHY

IN

GEOPHYSICS

DEPARTMENT OF PHYSICS

EDMONTON, ALBERTA

Spring 1993

The author has granted an irrevocable non-exclusive licence allowing the National Library of Canada to reproduce, loan, distribute or sell copies of his/her thesis by any means and in any form or format, making this thesis available to interested persons.

L'auteur a accordé une licence irrévocable et non exclusive permettant à la Bibliothèque nationale du Canada de reproduire, prêter, distribuer ou vendre des copies de sa thèse de quelque manière et sous quelque forme que ce soit pour mettre des exemplaires de cette thèse à la disposition des personnes intéressées.

The author retains ownership of the copyright in his/her thesis. Neither the thesis nor substantial extracts from it may be printed or otherwise reproduced without his/her permission.

L'auteur conserve la propriété du droit d'auteur qui protège sa thèse. Ni la thèse ni des extraits substantiels de celle-ci ne doivent être imprimés ou autrement reproduits sans son autorisation.

Canada

UNIVERSITY OF ALBERTA

RELEASE FORM

NAME OF AUTHOR   Nanxun Dai

TITLE OF THESIS   FINITE DIFFERENCE SIMULATION AND IMAGING OF SEISMIC WAVES IN COMPLEX MEDIA

DEGREE FOR WHICH THESIS WAS PRESENTED   Doctor of Philosophy

YEAR THIS DEGREE GRANTED   Spring 1993

(SIGNED) ....

PERMANENT ADDRESS:

405/55 Zhengnine Road

Shanghai China

DATED: January 8, 1993

PAGINATION ERROR.   ERREUR DE PAGINATION.

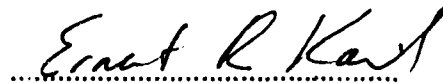TEXT COMPLETE.   LE TEXTE EST COMPLET.

UNIVERSITY OF ALBERTA
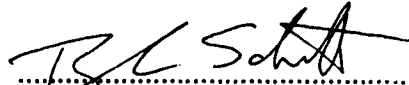
FACULTY OF GRADUATE STUDIES AND RESEARCH

The undersigned certify that they have read, and recommend to the Faculty of Graduate Studies and Research, for acceptance, a thesis entitled FINITE DIFFERENCE SIMULATION AND IMAGING OF SEISMIC WAVES IN COMPLEX MEDIA submitted by NANXUN DAI in partial fulfillment of the requirements for the degree of DOCTOR OF PHILOSOPHY in GEOPHYSICS.
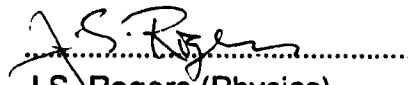
....
Supervisor
E.R. Kanasewich (Physics)

....
T.J.T. Spanos (Physics)
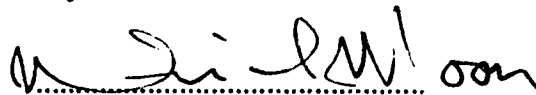
....
D.R. Schmitt (Physics)

....
J.S. Rogers (Physics)

....
R.J. Tait (Mathematics)

....
External Examiner, W.M. Moon
(Geological Sciences
University of Manitoba)

Date: January 4, 1993

Dedicated

To the fond memories of

my father, mother and mother-in-law.

ABSTRACT

Seismic wave propagation in two-dimensional non-homogeneous porous media is simulated with a finite difference method which solves the first order hyperbolic systems based on the theories developed by Biot, and de la Cruz and Spanos. Original solutions for a P-wave point or line source in a uniform porous medium are derived for the purposes of source implementation and algorithm testing. The existence of seismically observable differences due to the presence of pores has been examined through synthetic examples, which indicate that amplitude versus offset variations may be observed on receivers at increasing distance and could be diagnostic of the matrix and fluid parameters. These methods are applied in simulating seismic wave propagation over an expanded steam heated zone in Cold Lake Alberta area in enhanced oil recovery processing.

New approaches are developed to construct absorbing boundaries in wave modeling problems. A wave propagation modification technique and a one-way sponge filter technique are developed. Either of these approaches, when combined with the one-dimensional absorbing boundary conditions, absorbs not only the body waves but also surface waves effectively even in the poroelastic wave modeling where three types of waves may be present.

A velocity-pressure finite difference method is developed for modeling viscoacoustic wave propagation in heterogeneous media. A viscoacoustic medium is approximated by a generalized Maxwell body and a first order hyperbolic system is formulated to describe the wave motion. Viscoacoustic synthetic seismograms have been computed and compared with data from crosshole seismic experiments for monitoring steam injection projects in the Cold Lake area.

An original first order hyperbolic system is formulated for one-way waves in

heterogeneous media. This system is used in implementing absorbing boundaries and extrapolating wave field in the space-time domain. A back-propagation method is developed to implement seismic depth migration with a explicit finite difference scheme at a reduced computational cost. A number of examples illustrate the application of the one-way wave system in modelling, in absorbing reflections from the computational boundaries and in migrating pre-stack and post-stack synthetic seismic data.

ACKNOWLEDGEMENTS

TABLE OF CONTENTS

LIST OF TABLES

LIST OF FIGURES

.

CHAPTER 1

INTRODUCTION

Seismic waves, the mechanical vibrations propagating through the earth, have long been observed and studied for a variety of reasons. Natural earthquakes generate waves on the grandest scale providing data for studying the deeper parts of the earth. Artificially generated vibrations with relative smaller amount of energy and shorter wavelength are utilized in crustal investigation, mineral prospecting and intensively in exploration for oil and natural gas. In both exploration and earthquake seismology, the wave properties, such as the amplitude as a function of space and time, the propagation velocities, the vibratory frequency, the wave length, the attenuation, the dispersion and the polarization of particle motion are studied to deduce the information about the the internal structure and composition of the material of the earth.

Interpretation of seismic data invariably involves a conceptual "model" of the portion of the earth involved in seismic measurements. The model, either physical or mathematical, is a simplification of the real earth in which the only factors included are those expected to be most important in affecting the measurements (Sheriff and Geldart 1983).

Seismic modeling generally falls into two types, forward and inverse. In *forward modeling* one starts with an assumed earth model to generate the wave field by solving wave equations. Synthetic seismograms produced by forward modeling can aid in advancing our understanding of the kinematic and dynamic properties of seismic waves propagating through the earth as well as in the interpretation of wave patterns observed on

field seismograms. In order to gain an acceptable geological model, comparisons are often made between the synthetic and observed seismograms; errors are attributed to either inaccuracies in the model or other factors not accounted for. The model is then modified in an effort to account for the errors until adequate agreement has been reached. In contrast, in *inverse modeling* one attempts to construct a possible model from the observed seismic wave field. One of the most commonly used inverse modeling methods in seismic exploration is migration in which the recorded wave amplitudes are redistributed to their true spatial reflector positions to better assemble a two-dimensional or three dimensional *image* of the subsurface structure.

In this thesis new methods are described for simulating seismic wave responses in porous and viscoacoustic media, and for imaging complex subsurface constructions using seismic waves.

1.1 Seismic simulation

A basic problem of theoretical seismology is to determine the wave response of a given model to the excitation of an impulsive source by solving the wave equations under certain simplifications. When the geometric optic method of ray tracing is used only wave arrival times are determined. In a scalar approximation, the acoustic wave equation may be solved to evaluate the waveform but only compressional waves (P-waves) are considered. A more complete approach is to study the vector displacement field using the full elastic wave equation for modeling both P-waves and shear waves (S-waves). However, important wave properties such as attenuation and dispersion require a more sophisticated set of equations.

Exact analytical solutions do not exist even for the simplest acoustic wave equation for most subsurface geophysical configurations. Solutions for realistic models can be obtained

only through approximate approaches. In response to the growing desire for numerical seismic modeling a wide proliferation of methods of varying degrees of intricacy, accuracy and flexibility of implementation have been developed taking advantage of the prodigious advance in computational facilities.

Starting in the fifties, early synthetic seismograms were used to simulate the normal incidence reflections in a horizontally stratified model by simply applying wavelet convolution with a reflectivity sequence. Multi-dimensional waveform modeling became wide spread in the seventies. Many numerical methods stem from ray theory (Cerveny et al., 1977). Since the ray-theory based methods evaluate the wave energy from the contribution of individual rays, difficulties rise in specifying significant rays from the infinite possible ones. The ART (Asymptotic Ray Theory) method (Hron and Kanasewich, 1971) expands the solution of a wave equation into an infinite ray series but only the leading (zeroth) term is generally used to evaluate the amplitudes. A significant difference is shown when the first order term is further taken into account (Zheng 1989). The WKBJ seismogram technique (e.g. Chapman, 1978) provides an economical approach appliable to a smooth velocity section. The basic assumption inherent in WKBJ techniques is that the length scale defined by the material inhomogeneity should be much greater than the applied wavelength. Near grazing points and shadow zones, WKBJ results can be unreliable. In the reflectivity method (Fuchs and Muller, 1971) synthetic seismograms are generated by integrating numerically on the slowness vector which is appliable to vertical heterogeneous media. In the perturbation methods the seismic response is calculated by adding the effect of a model perturbation to a known solution of some simple (reference) model and an approximate (linear) scattering theory (e.g. the Born approximation) is used to estimate the effect of perturbation. The basic disadvantage of these methods lies in the limitation to the model of the media. On one hand, the reference model must be sufficiently simple for an exact solution to be known. On the other hand the perturbations defined as the difference

between the simple reference model and the true model, must be small everywhere in order that approximate scattering theory gives valid results.

A different group of approaches of seismic modeling may be classified as discrete-coordinate methods. This group includes the finite difference methods (Alterman and Loewenthal, 1970; Alford et al., 1974; Boore 1972; Keily et al. 1976), the finite element methods (Smith, 1975), and other methods which combine time-step advancing algorithms and integral transformations with respect to space variables such as the pseudo-spectral method (Gazdag, 1981; Kosloff and Baysal, 1982; Mikhailenko and Korneev 1984). These methods generally require large computer memory sizes and high performance speed. With the rapid advent of computer power they have received special attention, especially in exploration seismology, because they are the only methods capable of producing a complete synthetic seismogram for a realistic earth model.

Most previous seismic modeling methods treat the earth as a perfectly elastic single phase fluid or solid medium. The major features of seismic waves, such as the pattern of reflected and refracted body waves and the dispersion of surface waves which have been observed experimentally can be simulated on the basis of a purely elastic earth. However, there are differences between the observed and the synthetic seismograms. The principle difference is the energy loss in excess of that due to geometrical spreading and reflection at discontinuities. This extra loss, called intrinsic attenuation, reduces the penetrating depth of an observation but can supply information on the lithological properties.

Because of the increasing difficulty of exploring for natural resources and the growing realization that hydrocarbon reservoirs are more heterogeneous and complex than assumed in the past, it has become more important to better characterize the subsurface material lithologically and petrophysically by seismic methods. One of the efforts to meet this need is the search for suitable 'models of earth media'. The considerable literature in this area includes better models of wave propagation in viscoelastic and fluid filled porous media together with a proliferation of experimental work on this subject in the past few decades.

Biot developed a theory from the view point of continuum mechanics for wave motion in a porous elastic solid saturated with a viscous compressible fluid. The equations obtained by Biot were rederived by Johnson (1986) using a Lagrangian formulation. Katsube and Caroll (1987) extended Biot's theory by allowing a shear interaction between the viscous fluid and the solid at the microscopic level. Levy (1979), and Burridge and Keller (1981) derived coupled wave equations for time-harmonic motion in porous media through the use of the two-space method of homogenization that is used in statistical physics. Berryman and Thigpen (1985) and Berryman et al. (1988) derived wave equations for partially saturated porous media by using variational techniques. More recently de la Cruz and Spanos (1985, 1989, 1991a) constructed macroscopic wave equations for elastic porous media filled with viscous fluid by using volume averaging techniques in conjunction with physical arguments. Wave dispersion and dissipation in these models are mainly due to the viscous fluid motion relative to the solid matrix. The frequency dependence of the wave speed and attenuation are discussed by many authors (e.g. Biot 1956a, 1956b; Geertsma and Smit 1961; de la Cruz and Spanos 1985; Hickey 1990). These studies are simply based on the analysis of time harmonic plane waves in uniform porous space. However, because of the complexity, the well established wave equations for porous media have rarely been solved, either analytically or numerically, even for fairly simple models. The problem of calculating seismic wave fields in fluid saturated, heterogeneous media is the subject of the second chapter of this thesis (Dai et al 1992b; Dai et al 1992e).

Considerable progress has been also made in seismic wave attenuation for single phase material. In this context, seismic attenuation is taken to describe any irreversible energy losses, other than those due to spherical divergence, reflections, transmissions and mode conversions, which a seismic wave experiences as it propagates through a medium. This definition is a broader concept than is the mechanism of dissipation which describes energy

lost due to particular physical procedure such as friction between moving rock particles or fluid motion within rock pores. The most commonly used measures of attenuation is the dimensionless quality factor Q or its inverse Q^{-1} which is defined as $\frac{1}{Q} = -\frac{\Delta E}{2\pi E}$, where E is the peak strain energy stored in a volume of material and $-\Delta E$ is the energy lost in each cycle because of imperfections in the elasticity of the material (Aki and Richards 1980). Q can be measured directly   directly in laboratories or from observed seismic wave records.

The incorporation of absorption with arbitrary Q-laws for seismic simulation is not difficult in frequency-domain methods. However it has been almost impossible for the direct methods in the time domain to include attenuation because in the time domain the anelastic stress-strain relation has the form of a convolution integral which is intractable in numerical computation. To circumvent this problem Day and Minster (1984) transform the convolution integral operator into a convergent sequence of constant-coefficient differential operators of increased order based on the approach of Pade approximation. Emmerich and Korn (1987) utilized a generalized Maxwell body to approximate an arbitrary Q law yielding a second order differential equation system with extra intermediate variables for SH waves.

A first order hyperbolic system has been derived for anelastic acoustic wave motion by Dai et al.(1992d) based on the generalized Maxwell body approximation. The system is solved with a finite difference method for a realistic model of crosshole experiments which were carried out at Cold Lake, Alberta before and after a steam injection operation. Comparison is made between the synthetic seismograms and the observed ones.

1.2 Seismic Migration

On the conventional seismic time sections prior to migration the echo amplitudes are

displayed in a complex manner on graphs of receiver location versus travel time. In areas of steep dip, the reflection events appearing on the time sections are removed considerably from the true position of the reflector segment, thereby giving a distorted picture of the subsurface structure. Migration is a corrective data processing technique which attempts to assemble an image of the correctly positioned subsurface reflecting interface.

The interpretative value of migration techniques has been recognized since the beginning of seismic exploration. In the early years, migration was carried out manually with graphical methods, not directly to the seismic data itself but to the interpreted horizon sections or contour maps. In the sixties digital processing promoted the development of diffraction-stack method for migrating the common midpoint (CMP) stack seismic section. Based on Huygens' principle and the ray-theory concept, diffraction-stack migration considers a reflector as a sequence of diffracting points. Seismic amplitudes are summed along diffraction hyperbola on an unmigrated section to give the amplitude at the diffracting points on the migrated section. All modern seismic migration processes are based on wave theory. In these processes, the reflected field observed at the surface is used either as an initial conditions or a boundary conditions to reconstruct the subsurface wave field governed by the wave equation. An imaging principle is then applied to obtain the subsurface reflectivity map. Apart from a correct image, the wave-equation based migration processes also improve the lateral resolution by its property of focussing diffraction energy.

Migration can be performed in various combinations of time, space, frequency and wavenumber domain. (Berkhout 1982; Tsingas and Kanasewich, 1990). The numerical techniques employed in migration processes can generally be subdivided in three broad categories, namely, the finite difference approach (Claerbout 1970,1976), the summation approach (French, 1975; Schneider, 1978), and the transformation approach (Stolt, 1978; Gazdag, 1978).

Migration can be applied to either post-stack sections or prestack sections. Post-stack migration attempts to reposition reflected energy from its common midpoint position to its true subsurface location. Prestack migration works directly on the original data set such as a common shot gather. The fact that the common shot gather is acquired from a single physical experiment imposes fewer assumptions and restrictions on the subsequent data processing. Prestack migration avoids the CMP stacking artifacts and is therefore more consistent with the wave theory in principle. A single shot gather usually does not give a complete subsurface picture. Only the parts from which the reflection is seen by the receivers will show up in a single shot gather migration. A complete image with high signal noise ratio can be obtained by stacking a number of migrated shot gathers (Tsingas, 1990).

The conventional forms of wave-equation migration produces the migrated image in a distance-time reference frame and are referred to as *time migration*. Hubral (1977) showed ↑ a laterally inhomogeneous medium the diffraction pattern from subsurface scatterers can depart significantly from the normal hyperbolic shape; the Kirchhoff-summation method images seismic data at emergent "image ray" locations rather than at the desired positions vertically above the scatterers. The conventional finite difference method and frequency domain approach commit the same error and do not migrate seismic reflections to proper positions if there is a significant lateral variation in velocity (Larner et al., 1981). Larner et al (1981) proposed a partial solution to the later velocity variation problem by a two stage procedure consisting of a conventional migration followed by a depth conversion by an image-ray method based on the work of Hubral (1977). Judson et al. (1980) proposed a finite difference implementation to obtain a migrated depth section from a stacked time section. In their method the wave field extrapolation is processed in small increments of depth instead of time steps and a time shift term is applied to each trace to account for the transmission time changes resulting from the lateral velocity variation along the thin layer of depth increment. They noted that the additional operation within the migration algorithm can be difficult and expensive to implement. The same concept is

applied by Schultz and Sherwood (1980) to migrate the prestack seismic data. These methods give directly the image section on a distance-depth graph and are referred to as *depth migration*. Tsingas and Kanasewich (1990) performed depth-migration in the space-frequency domain in which a time-shifting or thin-lens term is involved where lateral variation of velocity is present.

Most extrapolation operators in wave theory based migrations are constructed from an one-way wave equation due to the fact that the signal recorded by the seismic surface survey come from the upward traveling wave field only. The one-way wave equations commonly obtained by seeking a polynomial or rational approximation to the dispersion relation of a square root form. Although successful in many situations, the method is limited by the assumptions made inherently in deriving the one-way wave equations. In particular it is assumed that spatial derivatives of the velocity can be ignored (Claerbout 1972, 1976; Stolt, 1978; Gazdag, 1978; and Van Wulfften Palthe, 1979). On the other hand, the existing one-way equations often fail in simulating the downgoing wave field at large propagating angles. In order to overcome these shortcomings, full wave equations were also employed for migration purpose (Kosloff and Baysal, 1983; Reshef and Kosloff, 1986). For strong lateral velocity variation and steep dips the two-way wave equation migration possesses certain advantages over the commonly used parabolic or paraxial wave equation but suffers from unwanted internal multiple reflections which are generated from strong velocity variations. This unwanted energy is especially troublesome if it is coherent and migrates to a time when the primaries are weak (Tsingas and Kanasewich, 1990).

Dai and Kanasewich (1992) and Dai et al. (1992a) developed a first order hyperbolic system for one-way waves in heterogeneous media. This system is accurate in simulating downgoing waves at propagating angles up to 80°. It is applied in performing two-dimensional post-stack and prestack depth migration through a back-propagating procedure

with a less expensive explicit finite difference scheme in the space-time domain with no unwanted internal reflections being present. The computational cost of this procedure can be the same as with forward modeling with the same finite difference scheme. Hence the extension of this method to three-dimensional one-pass migration can be economically feasible.

1.3 Finite difference methods

The finite difference method, since its introduction into computational seismology in the late sixties, has proved to be particularly versatile in extending the scope of solvable problems. The finite difference method is general, straightforward and flexible. It may be applied to an arbitrarily inhomogeneous medium and random source-receiver separation. As pointed out by Aki and Rechards (1980), the method is essentially similar to laboratory simulation using a scale model, but has greater advantage over the latter in accuracy of the result and in ease of implementation. The finite difference method offers a most direct solution to the problem expressed in terms of the basic equations, and the initial and boundary conditions. In the elastic case, the method automatically accounts not only for direct waves, primary and multiple reflection waves but also converted waves, head waves, diffraction waves and waves observed in ray-theoretical shadow zones.

Finite difference schemes can generally be placed in two broad categories: *explicit* and *implicit* (Kelly et al., 1976). In explicit schemes the response is evaluated exclusively at one space location at an advanced time directly from the response on the neighboring grid points already determined at previous times. In implicit schemes the response is evaluated simultaneously at all space locations at an advanced time from known values at previous times through a matrix inversion technique. The explicit operators are easier and more economical to implement but suffer from stability problems. For hyperbolic equations

explicit schemes are preferred because the stable conditions are not as severe as with parabolic equations.

Two distinct formulations are used in finite difference modeling (Kelly et al., 1976). The *homogeneous* approach solves the wave equations for every homogeneous layer separately. Boundary conditions must be explicitly imposed on the interfaces between different layers (Alterman and Karal, 1968; Alford et al., 1974). In contrast, the *heterogeneous* approach directly solves wave equations for the whole model. The wave equations in this case allow the physical properties to vary both laterally and vertically. In the heterogeneous approach, boundary conditions are satisfied implicitly and more complicated geometries can be accommodated with no extra effort.

The heterogeneous approach is based on wave equations which have continuously variable coefficients. When applying finite difference techniques to second order heterogeneous wave equations, additional approximations for the derivatives of the physical parameters are necessary (Kelly et al., 1976). First order hyperbolic systems which describe wave propagation in inhomogeneous media do not directly involve derivatives of physical parameters. When finite difference methods are applied to these first order systems, the error from numerical differentiation of the medium parameters are avoided. Finite difference methods were applied to first order hyperbolic systems by Virieux (1984,1986), Bayliss el al. (1986) and Vafidis et al. (1992) for modeling elastic SH and P-SV wave propagation in heterogeneous media.

Waves propagating on a discrete grid mesh become progressively dispersed with increasing travel time due to replacement of the differential equation by a difference equation. In any discretization, only the long waves are well approximated. Grid dispersion, depending highly on the number of grid points per wavelength, places restrictions on the applicability of the finite difference method in terms of the capability of the available computer making them more useful for finding the wave field in the vicinity of the seismic source or inhomogeneity. Higher-order accurate (in space) schemes have the

advantage of reducing the phase errors.

Numerical solutions from a finite difference method to a wave propagation problem are usually obtained over a finite region due to the limitation of the computer memory size. The techniques for construction of absorbing boundaries play an important role in reducing the artificial effects due to the existence of the computational boundaries. Widely used absorbing boundary conditions in seismic modeling are proposed by Clayton and Engquist (1977). They obtain the absorbing boundary conditions from the rational approximation of the one-way wave dispersion relation and their differential equation forms. The effectiveness of these absorbing boundaries are limited when waves are incident on the boundaries at large angles especially for elastic waves since shear waves are also involved in this case. To improve the absorbing effectiveness of these boundaries various techniques are introduced by Cerjan et al. (1985), Kosloff et al. (1986) and Sochacki et al. (1987) and Higdon (1987), to mention a few. These additional techniques improve the absorbing effectiveness but higher computational cost is required. Bayliss et al. (1986) in their forward modeling with first order hyperbolic systems employed absorbing boundaries based on one dimensional characteristic analysis (one dimensional absorbing boundaries). These absorbing boundaries are just as effective for waves impinging on the boundary perpendicularly and do not properly absorb surface waves. It is more challenging to construct absorbing boundaries for simulating waves in porous media where slow P waves may be present in additional to the regular P waves and S waves in solid elastic media.

New methods are proposed by Dai, Kanasewich and Vafidis (1992c) for assembling absorbing boundaries for modeling seismic waves in nonporous or porous media. The methods are based on the characteristic analysis of the first order hyperbolic system which describe the wave motion. The combinations of the one-dimensional absorbing boundary conditions and the wave propagation modification or sponge filter techniques not only effectively absorb all the types of body waves but also the surface waves.

1.4 Outline of the Thesis

The thesis consist of six chapters.

Chapter 1 contains an overview of the background and direction of this research work.

Chapter 2 describes the velocity-stress finite difference method for simulation of seismic waves in porous media. First, Biot's equations and de la Cruz-Spanos equations are reformulated into first order hyperbolic systems. Then the point and line source solutions of the system are derived for the purpose of numerical algorithm testing and the source implementation in the finite difference modeling procedures. Following a brief description of the finite difference scheme, a number of numerical example are given to illustrate the feasibility of the modeling methods.

In Chapter 3 the combined approaches of one dimensional absorbing boundary conditions with a wave propagation modification technique or alternately with a one-way sponge filter technique are developed to reduce artificial reflections from the margin of the computational region for numerical simulation of seismic wave in elastic and porous media with first order hyperbolic systems.

Chapter 4 describes a velocity-pressure finite difference method for simulation of seismic waves in viscoaoustic media in the space-time domain. A first order hyperbolic system is formulated by assembling a realistic quality factor law with generalized Maxwell bodies. This system is applied to model the seismic data observed from crosshole seismic experiments for monitoring steam injection projects in the Cold Lake area.

First order hyperbolic systems for one-way waves propagating in a heterogeneous medium are derived in Chapter 5. Based on these systems an elegant method for two-dimensional depth migration of seismic reflection data and a two-dimensional absorbing boundary technique are presented with a number of synthetic examples.

Chapter 6 is a brief overview summarizing the original contributions of the work presented in this thesis with some remarks on future directions.

CHAPTER 2

SIMULATION OF SEISMIC WAVES IN FLUID SATURATED POROUS MEDIA WITH BIOT EQUATIONS AND DE LA CRUZ-SPANOS EQUATIONS

2.1 INTRODUCTION

It has been long recognized that the data obtained from the observation of seismic waves which propagate through the earth carries information not only about the spatial allocation and geometrical configuration of interfaces between different rock types within the earth, but also about the physical properties of rocks, their mineralogical composition as well as their presentation state. Seismic methods, even though being very successful in locating structures and, in some cases, stratigraphic features favorable for oil and gas accumulation, have been used relatively little in directly locating the hydrocarbons themselves and in investigating the rock properties of direct interest to the hydrocarbon recovery such as porosity and permeability.

Since the resolution of seismic data has improved, detailed studies on the seismic response of hydrocarbon reservoirs are receiving more and more attention. In recent years, efforts have begun to be made in using seismic methods to evaluate and characterize hydrocarbon reservoirs and to monitor reservoir production and enhanced oil recovery (EOR) processes. In these developments the numerical modelling together with the basis theory of seismic waves plays an important role as they provide the basis for understanding

and interpreting the seismic characteristics.

The environment of hydrocarbon reservoirs is a composite multiphase media with gas or liquid occupying the voids between solid grains. Seismic modeling methods, however, have generally treated the medium as a single-phase elastic solid or more often as a layered fluid. In these modeling techniques no direct correlations are established between the seismic characteristics and the fundamental bulk characteristics of reservoirs in spite of the well known fact that seismic wave amplitude, velocity, attenuation and dispersion depend intrinsically on not only the solid mineralogy but also the porosity, the properties of pore fluids, confining pressure and other factors.

Biot's theory (1956a,b, 1962a,b) has long been regarded as the basis for solving wave propagation problems in porous media. The original equations (Biot 1956a) were set up for uniform porosity and isotropic composites. Later Biot (1962a) extended his theory to the non-uniform porosity case and further included anisotropic properties. Biot obtained his equations by deliberately ignoring the microscopic level and assuming that the concepts and principles of continuum mechanics can be applied to measurable macroscopic variables. Strictly speaking, it is only justified *a posteriori* by the agreement of the results that it provides with those obtained by other methods and experimental observations. In contrast, de la Cruz and Spanos (1985) equations, abbreviated as the C-S equation in what follows, for seismic wave propagation in fluid filled porous media were obtained by using the technique of volume averaging in passing from the well established physical laws at the microscopic level (in pore scale) to the macroscopic level. De la Cruz and Spanos (1989) later extended their theory to account for thermomechanical coupling. Recently de la Cruz et al. (1991a) examined the effects of inhomogeneity on the form of macroscopic equations and constructed equations of motion for heterogeneous porous media. The development of macroscopic equations through spatial averaging of the microscopic ones allows one to assign physical meaning to the theoretically assigned parameters. In this chapter both the

Biot equations and the C-S equations are studied in parallel for a comparison of their similarity and divergence.

Seismic wave propagation in generally inhomogeneous porous media can be simulated accurately with high order finite difference techniques. Finite difference numerical solutions to the acoustic and elastic wave equations have been presented by various authors (Alterman and Karal, 1968; Boore, 1972; Alford et al., 1974, Kelly et al., 1976; Vafidis et al., 1992). Recently proposed second order accurate finite difference solutions to the Biot's acoustic wave equations (Hassanzadeh, 1991) and to Biot's elastic wave equations (Zhu and McMechan, 1991) are based on the homogeneous approach. In this approach the homogeneous equations are numerically solved in each layer but boundary conditions should have been explicitly imposed on the interfaces (Kelly, et al. 1976). Hassanzadeh (1991) and Zhu and McMechan (1991) did not make any effort to compare their numerical solutions with analytic solutions.

In this development a finite difference solution for Biot's and C-S equations are proposed on the basis of the heterogeneous approach. One of the advantages of the heterogeneous approach is that boundary conditions are satisfied implicitly when the fluid phase is continuous. Therefore, complicated model geometries can be accommodated without imposing explicitly the boundary conditions on the interfaces.

In the velocity-stress finite difference method, Biot's and C-S equations are reformulated into first order systems whose vector of unknowns consists of the solid and fluid particle velocity components, the solid stress components and the fluid pressure. The first order systems are free of spatial derivatives of the physical parameters which are present in the second order Biot's and C-S wave equations for heterogeneous porous media. Consequently, the numerical approximation of the spatial derivatives of the physical parameters is not required in the velocity-stress finite difference method. Numerical approximation of these derivatives may sometimes result in large errors especially close to

interfaces where the physical parameters change quickly. This source of error is not present in our formulation of Biot's and C-S wave equations for heterogeneous media.

One of the key factors in finite difference simulations of wave propagation in porous media is source implementation. An original solution for the poroelastic wave equations is given in section 2.4 for an infinitely extended homogeneous porous medium with a pure dilatational point source or line source acting on both the solid and fluid parts.

In the following sections, we describe the velocity-stress finite difference method in solving Biot's and C-S equations. The finite difference scheme is based on dimensional splitting and consists of one-dimensional finite difference operators of MacCormack type which are fourth order accurate in space and of second order accuracy in time (Gottlieb and Turkel, 1976). The algorithm is fully vectorized by making use of the method of matrix multiplication by diagonals (Madsen et al., 1976; Vafidis et al., 1992). This finite difference method was successfully tested by comparing the numerical solutions with an exact known solution. Numerical examples are presented to illustrate the basic features of the wave field in porous media. The method is applied in simulating seismic wave propagation over an expanded steam heated zone during enhanced oil recovery (EOR) processing.

2.2 BIOT WAVE EQUATIONS FOR POROUS MEDIA

2.2.1 Macroscopic wave equations

Biot's linear theory for wave propagation in fluid saturated porous media is established under the following assumptions: 1) the fluid phase is continuous so that disconnected pores are supposed to belong to the solid matrix; 2) the porous medium is statistically isotropic, i.e. for all cross sections, the ratio of pore area to the solid occupied area is virtually constant; 3) the microscopic pore size is much smaller than the wavelength; 4) the deformations are small, which guarantees that the linearity of the mechanical processes; 5) the solid matrix is elastic hence all mechanisms of viscous origin related to the matrix is not under consideration. Also, it is assumed that the effect of the force of gravity and the temperature variations due to dissipation of energy can be neglected. According to Biot's theory, the equations of motion for a fluid-saturated, statistically isotropic, non-uniform porous medium are given by

$$\rho_{11} \frac{\partial^2 \mathbf{u}^s}{\partial t^2} + \rho_{12} \frac{\partial^2 \mathbf{u}^f}{\partial t^2} = \nabla \cdot \Sigma^s + b \frac{\partial}{\partial t} (\mathbf{u}^f - \mathbf{u}^s) ,$$

$$(2.2.1)$$

$$\rho_{12} \frac{\partial^2 \mathbf{u}^s}{\partial t^2} + \rho_{22} \frac{\partial^2 \mathbf{u}^f}{\partial t^2} = \nabla s - b \frac{\partial}{\partial t} (\mathbf{u}^f - \mathbf{u}^s) ,$$

Here, $\mathbf{u}^s$ and $\mathbf{u}^f$ are vectors of the macroscopic displacements of solid and fluid, respectively. The displacement vectors are defined as the average displacements over the volume of the particular phases in a representative element whose size is assumed to be

large compared to the pores. In terms of the average displacement vector $\mathbf{u}^f$ of the continuous fluid phase in the macroscopic element and the average displacement vector $\mathbf{u}^s$ of the solid particle, the elementary macroscopic flow rate dQ through an area dS with a normal $\mathbf{n}$ is given by (Biot 1956a)

$$dQ = \eta_o \left(\frac{\partial \mathbf{u}^f}{\partial t} - \frac{\partial \mathbf{u}^s}{\partial t} \right) \cdot \mathbf{n} \, dS \, . \tag{2.2.2}$$

where η_o denotes the porosity of the medium. The scalar s in equation (2.2.1) is related to the fluid pressure p and the porosity η_o according to

$$s = -\eta_o p . \tag{2.2.3}$$

Σ^s in equation (2.2.1) is a stress tensor

$$\Sigma^s = \begin{bmatrix} \sigma_{xx} & \sigma_{xy} & \sigma_{xz} \\ \sigma_{xy} & \sigma_{yy} & \sigma_{yz} \\ \sigma_{xz} & \sigma_{yz} & \sigma_{zz} \end{bmatrix} . \tag{2.2.4}$$

If we consider a unit cube of bulk material the components of Σ^s represent the force applied to the solid part of the faces, and s represents the force applied to the fluid part of these faces. The scalar s and the solid stress tensor Σ^s can be expressed in terms of the displacement vectors (see Appendix A):

$$s = Q \nabla \cdot \mathbf{u}^s + R \nabla \cdot \mathbf{u}^f + \frac{R}{\eta_o} \nabla \eta_o \cdot \left(\mathbf{u}^f - \mathbf{u}^s \right) , \tag{2.2.5}$$

$$\Sigma^s = (P - 2N) \nabla \cdot \mathbf{u}^s \mathbf{I} + N \left[\nabla \mathbf{u}^s + \left(\nabla \mathbf{u}^s \right)^T \right] + Q \nabla \cdot \mathbf{u}^f \mathbf{I} + \frac{Q}{\eta_o} \nabla \eta_o \cdot \left(\mathbf{u}^f - \mathbf{u}^s \right) \mathbf{I} , \tag{2.2.6}$$

where **I** is the second order identity tensor. The parameters P, Q, R and N are Biot's elastic constants and represent the mechanical properties of the fluid-saturated porous medium. The parameters ρ_{ij} in (2.2.1) represent the inertia of the two phases and are related to the mass densities of the solid and fluid, ρ_o^s and ρ_o^f,

$$\rho_{11} + \rho_{12} = (1 - \eta_o)\rho_o^s \equiv \rho_1 , \tag{2.2.7}$$

$$\rho_{12} + \rho_{22} = \eta_o \rho_o^f \equiv \rho_2. \tag{2.2.8}$$

The parameter b in (2.2.1) represents the resistive damping due to motion of the fluid relative to that of the solid and is expressed in terms of the porosity η_o, the fluid viscosity μ_f and the permeability K as:

$$b = \eta_o^2 \frac{\mu_f}{K} . \tag{2.2.9}$$

The relations between Biot's parameters and the basic physical parameters have been investigated by many authors (e.g. Biot and Willis, 1957; Stoll 1974; Feng and Johnson, 1983). These relations are given in Appendix A. Laboratory measurements of Biot's parameters for sandstones were reported by Yew and Jogi (1976, 1978) and Winkler (1985) among others.

2.2.2 First order hyperbolic system for 2-D P-SV waves

For a two-dimensional problem of wave propagation in porous media, it can be shown that SH waves decouple from P and SV waves. If we suppose all physical parameters and variables are independent of y, that is $\dfrac{\partial}{\partial y} \equiv 0$ in equations (2.2.1)—(2.2.6), then after taking the derivative of the macroscopic solid stress tensor Σ and scalar s with respect to time t and writing them in component form, the two dimensional P-SV wave equations can be formulated as:

$$\rho_{11}\frac{\partial v_x^s}{\partial t} + \rho_{12}\frac{\partial v_x^f}{\partial t} = \frac{\partial \sigma_{xx}}{\partial x} + \frac{\partial \sigma_{xz}}{\partial z} + b\left(v_x^f - v_x^s\right),$$
(2.2.10)

$$\rho_{11}\frac{\partial v_z^s}{\partial t} + \rho_{12}\frac{\partial v_z^f}{\partial t} = \frac{\partial \sigma_{xz}}{\partial x} + \frac{\partial \sigma_{zz}}{\partial z} + b\left(v_z^f - v_z^s\right),$$
(2.2.11)

$$\frac{\partial \sigma_{xx}}{\partial t} = P\frac{\partial v_x^s}{\partial x} + (P-2N)\frac{\partial v_z^s}{\partial z} + Q\left(\frac{\partial v_x^f}{\partial x} + \frac{\partial v_z^f}{\partial z}\right) + \frac{Q}{\eta_o}\left[\frac{\partial \eta_o}{\partial x}\left(v_x^f - v_x^s\right) + \frac{\partial \eta_o}{\partial z}\left(v_z^f - v_z^s\right)\right],$$
(2.2.12)

$$\frac{\partial \sigma_{zz}}{\partial t} = (P-2N)\frac{\partial v_x^s}{\partial x} + P\frac{\partial v_z^s}{\partial z} + Q\left(\frac{\partial v_x^f}{\partial x} + \frac{\partial v_z^f}{\partial z}\right) + \frac{Q}{\eta_o}\left[\frac{\partial \eta_o}{\partial x}\left(v_x^f - v_x^s\right) + \frac{\partial \eta_o}{\partial z}\left(v_z^f - v_z^s\right)\right],$$
(2.2.13)

$$\frac{\partial \sigma_{xz}}{\partial t} = N\left(\frac{\partial v_x^s}{\partial z} + \frac{\partial v_z^s}{\partial x}\right),$$
(2.2.14)

$$\rho_{12}\frac{\partial v_x^s}{\partial t} + \rho_{22}\frac{\partial v_x^f}{\partial t} = \frac{\partial s}{\partial x} - b\left(v_x^f - v_x^s\right),$$
(2.2.15)

$$\rho_{12}\frac{\partial v_z^s}{\partial t} + \rho_{22}\frac{\partial v_z^f}{\partial t} = \frac{\partial s}{\partial z} - b\left(v_z^f - v_z^s\right),$$
(2.2.16)

$$\frac{\partial s}{\partial t} = Q\left(\frac{\partial v_x^s}{\partial x} + \frac{\partial v_z^s}{\partial z}\right) + R\left(\frac{\partial v_x^f}{\partial x} + \frac{\partial v_z^f}{\partial z}\right) + \frac{R}{\eta_o}\left[\frac{\partial \eta_o}{\partial x}\left(v_x^f - v_x^s\right) + \frac{\partial \eta_o}{\partial z}\left(v_z^f - v_z^s\right)\right], \quad (2.2.17)$$

where $v_x^s = \frac{\partial u_x^s}{\partial t}$, $v_z^s = \frac{\partial u_z^s}{\partial t}$, $v_x^f = \frac{\partial u_x^f}{\partial t}$ and $v_z^f = \frac{\partial u_z^f}{\partial t}$ are the solid and fluid particle velocity

components. $v_y^s = \frac{\partial u_y^s}{\partial t}$, $v_y^f = \frac{\partial u_y^f}{\partial t}$, τ_{xy} and τ_{yz} do not appear in above equations because

they are related to SH wave motion and are independent of the rest of the unknowns.

The above equations can be written in matrix form as

$$E_0\frac{\partial u}{\partial t} = A_0\frac{\partial u}{\partial x} + B_0\frac{\partial u}{\partial z} + C_0 u , \qquad (2.2.18)$$

where

$$u = \begin{bmatrix} v_x^s \\ v_z^s \\ \sigma_{xx} \\ \sigma_{zz} \\ \sigma_{xz} \\ v_x^f \\ v_z^f \\ s \end{bmatrix}, \qquad (2.2.19)$$

$$E_0 = \begin{bmatrix} \rho_{11} & 0 & 0 & 0 & 0 & \rho_{12} & 0 & 0 \\ 0 & \rho_{11} & 0 & 0 & 0 & 0 & \rho_{12} & 0 \\ 0 & 0 & 1 & 0 & 0 & 0 & 0 & 0 \\ 0 & 0 & 0 & 1 & 0 & 0 & 0 & 0 \\ 0 & 0 & 0 & 0 & 1 & 0 & 0 & 0 \\ \rho_{12} & 0 & 0 & 0 & 0 & \rho_{22} & 0 & 0 \\ 0 & \rho_{12} & 0 & 0 & 0 & 0 & \rho_{22} & 0 \\ 0 & 0 & 0 & 0 & 0 & 0 & 0 & 1 \end{bmatrix}, \qquad (2.2.20)$$

$$\mathbf{A}_0 = \begin{bmatrix} 0 & 0 & 1 & 0 & 0 & 0 & 0 & 0 \\ 0 & 0 & 0 & 0 & 1 & 0 & 0 & 0 \\ P & 0 & 0 & 0 & 0 & Q & 0 & 0 \\ P-2N & 0 & 0 & 0 & 0 & Q & 0 & 0 \\ 0 & N & 0 & 0 & 0 & 0 & 0 & 0 \\ 0 & 0 & 0 & 0 & 0 & 0 & 0 & 1 \\ 0 & 0 & 0 & 0 & 0 & 0 & 0 & 0 \\ Q & 0 & 0 & 0 & 0 & R & 0 & 0 \end{bmatrix}, \quad (2.2.21)$$

$$\mathbf{B}_0 = \begin{bmatrix} 0 & 0 & 0 & 0 & 1 & 0 & 0 & 0 \\ 0 & 0 & 0 & 1 & 0 & 0 & 0 & 0 \\ 0 & P-2N & 0 & 0 & 0 & 0 & Q & 0 \\ 0 & P & 0 & 0 & 0 & 0 & Q & 0 \\ N & 0 & 0 & 0 & 0 & 0 & 0 & 0 \\ 0 & 0 & 0 & 0 & 0 & 0 & 0 & 0 \\ 0 & 0 & 0 & 0 & 0 & 0 & 0 & 1 \\ 0 & Q & 0 & 0 & 0 & 0 & R & 0 \end{bmatrix}, \quad (2.2.22)$$

$$\mathbf{C}_0 = \begin{bmatrix} -b & 0 & 0 & 0 & 0 & b & 0 & 0 \\ 0 & -b & 0 & 0 & 0 & 0 & b & 0 \\ -q_x & -q_z & 0 & 0 & 0 & q_x & q_z & 0 \\ -q_x & -q_z & 0 & 0 & 0 & q_x & q_z & 0 \\ 0 & 0 & 0 & 0 & 0 & 0 & 0 & 0 \\ b & 0 & 0 & 0 & 0 & -b & 0 & 0 \\ 0 & b & 0 & 0 & 0 & 0 & -b & 0 \\ -r_x & -r_z & 0 & 0 & 0 & r_x & r_z & 0 \end{bmatrix}, \quad (2.2.23)$$

and $q_x = \dfrac{Q}{\eta_o}\dfrac{\partial \eta_o}{\partial x}$, $q_x = \dfrac{Q}{\eta_o}\dfrac{\partial \eta_o}{\partial z}$,$r_x = \dfrac{R}{\eta_o}\dfrac{\partial \eta_o}{\partial x}$ and $r_x = \dfrac{R}{\eta_o}\dfrac{\partial \eta_o}{\partial z}$. Multiplying equation (2.2.18) by the inversion of $\mathbf{E}_0$,

$$\mathbf{E}_0^{-1} = \begin{bmatrix} R_{22} & 0 & 0 & 0 & 0 & -R_{12} & 0 & 0 \\ 0 & R_{22} & 0 & 0 & 0 & 0 & -R_{12} & 0 \\ 0 & 0 & 1 & 0 & 0 & 0 & 0 & 0 \\ 0 & 0 & 0 & 1 & 0 & 0 & 0 & 0 \\ 0 & 0 & 0 & 0 & 1 & 0 & 0 & 0 \\ -R_{12} & 0 & 0 & 0 & 0 & R_{11} & 0 & 0 \\ 0 & -R_{12} & 0 & 0 & 0 & 0 & R_{11} & 0 \\ 0 & 0 & 0 & 0 & 0 & 0 & 0 & 1 \end{bmatrix}, \quad (2.2.24)$$

where

$$R_{ij} = \frac{\rho_{ij}}{\rho_{11}\rho_{22} - \rho_{12}^2} \, , \qquad (2.2.25)$$

we obtain

$$\frac{\partial \mathbf{u}}{\partial t} = \mathbf{A}\frac{\partial \mathbf{u}}{\partial x} + \mathbf{B}\frac{\partial \mathbf{u}}{\partial z} + \mathbf{C}\mathbf{u} \, , \qquad (2.2.26)$$

where

$$\mathbf{A} = \begin{bmatrix} 0 & 0 & R_{22} & 0 & 0 & 0 & 0 & -R_{12} \\ 0 & 0 & 0 & 0 & R_{22} & 0 & 0 & 0 \\ P & 0 & 0 & 0 & 0 & Q & 0 & 0 \\ P-2N & 0 & 0 & 0 & 0 & Q & 0 & 0 \\ 0 & N & 0 & 0 & 0 & 0 & 0 & 0 \\ 0 & 0 & -R_{12} & 0 & 0 & 0 & 0 & R_{11} \\ 0 & 0 & 0 & 0 & -R_{12} & 0 & 0 & 0 \\ Q & 0 & 0 & 0 & 0 & R & 0 & 0 \end{bmatrix} \, , \quad (2.2.27)$$

$$\mathbf{B} = \begin{bmatrix} 0 & 0 & 0 & 0 & R_{22} & 0 & 0 & 0 \\ 0 & 0 & 0 & R_{22} & 0 & 0 & 0 & -R_{12} \\ 0 & P-2N & 0 & 0 & 0 & 0 & Q & 0 \\ 0 & P & 0 & 0 & 0 & 0 & Q & 0 \\ N & 0 & 0 & 0 & 0 & 0 & 0 & 0 \\ 0 & 0 & 0 & 0 & -R_{12} & 0 & 0 & 0 \\ 0 & 0 & 0 & -R_{12} & 0 & 0 & 0 & R_{11} \\ 0 & Q & 0 & 0 & 0 & 0 & R & 0 \end{bmatrix} \, , \quad (2.2.28)$$

$$C = \begin{bmatrix} -B_2 & 0 & 0 & 0 & 0 & B_2 & 0 & 0 \\ 0 & -B_2 & 0 & 0 & 0 & 0 & B_2 & 0 \\ -q_x & -q_z & 0 & 0 & 0 & q_x & q_z & 0 \\ -q_x & -q_z & 0 & 0 & 0 & q_x & q_z & 0 \\ 0 & 0 & 0 & 0 & 0 & 0 & 0 & 0 \\ B_1 & 0 & 0 & 0 & 0 & -B_1 & 0 & 0 \\ 0 & B_1 & 0 & 0 & 0 & 0 & -B_1 & 0 \\ -r_x & -r_z & 0 & 0 & 0 & r_x & r_z & 0 \end{bmatrix}, \qquad (2.2.29)$$

with

$$B_1 = b(R_{11} + R_{12}), \qquad (2.2.30)$$

$$B_2 = b(R_{12} + R_{22}). \qquad (2.2.31)$$

The system (2.2.26) predicts the existence of three types of body waves, one shear and two compressional ones with a faster and a slower velocity. The system is hyperbolic since both A and B have the same real eigenvalues ($-V_f$, $-V_r$, $-V_s$, 0, 0, V_s, V_r, V_f), where V_f, V_r, V_s are the propagating velocities of the fast P wave, S wave and slow P wave. This system is solved in the later sections.

2.3 DE LA CRUZ-SPANOS WAVE EQUATIONS FOR POROUS MEDIA

2.3.1 Macroscopic wave equations

In this section a partial differential equation system is developed for wave motion in fluid saturated heterogeneous porous media mainly following the procedures described by de la Cruz and Spanos (1985, 1989) and de la Cruz et al. (1991). A first order wave equation system is then formulated by neglecting the less important macroscopic viscous stress of fluid. This modified system is utilized for wave field simulation with the finite difference method in the following sections together with the system described in the previous section.

The volume averaging technique is simple and offers great clarity in explaining what kind of averaging occurs in the macroscopic quantities. The basic idea behind the approach is the following. First it is assumed that on the pore scale the continuum equations for an elastic solid and a viscous compressible fluid hold. These microscopic equations are then spatially averaged over a representative element, say a sphere, in the solid-fluid composite. The diameter of the elementary sphere should be both sufficiently small and sufficiently large, so that both the macroscopic and microscopic inhomogeneities do not affect the results of the averaging procedure. The solid movement and fluid movement are coupled through the microscop. Joundary conditions on the interfaces of the constituent phases of the materials.

In de la Cruz-Spanos theory, a porous medium is envisaged as an elastic matrix whose pores are filled with viscous compressible fluid. In the pore scale the motions of the solid and fluid materials in a fully saturated porous medium are supposed to obey the linear equations of motion for the particular single phases, that is,

$$\frac{\partial}{\partial t}\left(\rho^s\frac{\partial \mathbf{u}^s}{\partial t}\right) = \nabla \cdot \Sigma^s$$

(2.3.1)

and

$$\frac{\partial}{\partial t}\left(\rho^f \mathbf{v}^f\right) = -\nabla \cdot \left(p^f \mathbf{I} - \Sigma^f\right),$$

(2.3.2)

respectively, where $\mathbf{I}$ is the second order identity tensor, ρ^s, $\mathbf{u}^s$, denote the density and microscopic displacement of the solid material, while ρ^f, $\mathbf{v}^f$ and p^f denote the density, microscopic velocity of fluid particles and the pressure of the fluid, Σ^s and Σ^f are the stress tensor of the solid and fluid, respectively, given by

$$\Sigma^s = K_s\nabla \mathbf{u}^s \mathbf{I} + \mu_s\left[\nabla \mathbf{u}^s + \left(\nabla \mathbf{u}^s\right)^T - \frac{2}{3}\nabla \cdot \mathbf{u}^s \mathbf{I}\right]$$

(2.3.3)

and

$$\Sigma^f = \mu_f\left[\nabla \mathbf{v}^f + \left(\nabla \mathbf{v}^f\right)^T - \frac{2}{3}\nabla \cdot \mathbf{v}^f \mathbf{I}\right],$$

(2.3.4)

where K_s, μ_s, and μ_f are the bulk modulus, the shear modulus of the solid material and the viscosity of the fluid material, respectively. The theory developed by de la Cruz and Spanos is constructed by applying volume averaging theorems (Slattery 1969, Whitaker 1969) to equations (2.3.1) — (2.3.4) to provide the initial framework. Two microscopic boundary conditions at the interface of the solid and the fluid are used to introduce the interaction between the solid motion and the fluid motion. They are the no slip condition

$$\mathbf{v}^f = \partial_t \mathbf{u}^s$$

(2.3.5)

and the stress continuity condition

$$-p^f \mathbf{n} + \Sigma^f \cdot \mathbf{n} = \Sigma^s \cdot \mathbf{n} \ , \tag{2.3.6}$$

where $\mathbf{n}$ is the unit normal to the interface. In addition, order of magnitude considerations and plausible physical arguments are incorporated to formulate a set of macroscopic equations for seismic wave propagation in heterogeneous porous media, which can be written (See Appendix B) in tensor form as

$$D_{11}\frac{\partial^2 \mathbf{u}^s}{\partial t^2} + D_{12}\frac{\partial^2 \mathbf{u}^f}{\partial t^2} = \nabla \cdot \Sigma^s + b \left(\frac{\mathbf{v}^f}{\eta_o} - \frac{\mathbf{v}^s}{1 - \eta_o}\right) \ , \tag{2.3.7}$$

$$\Sigma^s = (A - 2\mu_s)\nabla \cdot \mathbf{u}^s \mathbf{I} + \mu_s \left(\nabla \mathbf{u}^s + (\nabla \mathbf{u}^s)^T\right) + B \ \nabla \cdot \mathbf{u}^f \mathbf{I}$$

$$+ N_f \left(\mathbf{u}^f \nabla \eta_o + \nabla \eta_o \mathbf{u}^f\right) + N_s \left(\mathbf{u}^s \nabla \eta_o + \nabla \eta_o \mathbf{u}^s\right)$$

$$+ H_A \mathbf{u}^s \cdot \nabla \eta_o \mathbf{I} - H_B \mathbf{u}^f \cdot \nabla \eta_o \mathbf{I} \tag{2.3.8}$$

$$D_{21}\frac{\partial^2 \mathbf{u}^s}{\partial t^2} + D_{22}\frac{\partial \mathbf{v}^f}{\partial t} = -\nabla p^f + \nabla \cdot \Sigma^f - b \left(\frac{\mathbf{v}^f}{\eta_o} - \frac{\mathbf{v}^s}{1 - \eta_o}\right) \ , \tag{2.3.9}$$

$$\Sigma^f = \mu_f \left(\nabla \mathbf{v}^f + (\nabla \mathbf{v}^f)^T - \frac{2}{3}\nabla \cdot \mathbf{v}^f \mathbf{I}\right) - \mu_f \frac{\delta}{\eta_o}\left(\mathbf{v}^f \nabla \eta_o + \nabla \eta_o \mathbf{v}^f\right)$$

$$-\mu_f \frac{1-\delta}{1-\eta_o}\left(\mathbf{v}^s \nabla \eta_o + \nabla \eta_o \mathbf{v}^s\right) + \frac{2}{3} \mu_f \left(\frac{\delta}{\eta_o}\mathbf{v}^s \nabla \eta_o + \frac{1-\delta}{1-\eta_o}\mathbf{v}^f \cdot \nabla \eta_o\right) \mathbf{I} \ , \tag{2.3.10}$$

$$\frac{\partial p^f}{\partial t} = - C \, \nabla \cdot v^s - E \, \nabla \cdot v^f + F_A \, \nabla \eta_o \cdot v^s - F_B \, \nabla \eta_o \cdot v^f - \frac{K_f}{\rho_o^f} \nabla \rho_o^f \cdot v^f , \qquad (2.3.11)$$

where u^f is macroscopic fluid displacement and $v^s = \frac{\partial u^s}{\partial t}$ is the macroscopic particle velocity of the solid material. It is important to note that two kinds of averages may show up in the averaging process (e.g. de Vries 1989). One is the average over the particular phase called "intrinsic volume average" and denoted by a bar over the variable, see equation (B.3); the other is the average over the representative element called "volume average" as such and denoted by the sign <>, see equation (B.4). The two kinds of average are related by a factor of the volume fraction of the pertaining phase (see equation (B.5)). In equations (2.3.7) - (2.3.11) the sign <> has been dropped for convenience, therefore all the variables Σ^s, Σ^f, p^f, u^s, u^f, v^s, and v^f from here on represent the their volume averages over a predefined volume of the representative element. The derivation of the macroscopic equations and the definitions of the coefficients are given in the Appendix B.

2.3.2 Neglect of macroscopic stress of fluid Σ^f

In order to examine the magnitude of Σ^f let us consider a uniform porous medium. For this case, the stress tensor in component form, from equation (2.3.10), is given by

$$\sigma_{ik}^f = \mu_f \left(\partial_k v_i^f + \partial_i v_k^f - \frac{2}{3} \delta_{ik} \partial_l v_l^f \right) . \qquad (2.3.12)$$

Inserting equation (2.3.12) into equation (2.3.9), and writing it in component form, we have

$$D_{21}\partial_i v_i^f - D_{22}\partial_i v_i^s = -\partial_i p_f + \partial_k \left[\mu_f \left(\partial_k v_i^f + \partial_i v_k^f - \frac{2}{3} \delta_{ik}\partial_l v_l^f \right) \right] - \frac{\mu_f \eta_o^2}{K} \left(\frac{v_i^f}{\eta_o} - \frac{v_i^s}{1-\eta_o} \right) .$$

$$(2.3.13)$$

Here we have used $b = \frac{\mu_f \eta_o^2}{K}$, as given in equation (B.23) in Appendix B, where K is the permeability. Let us compare the last two terms on the right hand side of equation (2.3.13). These terms represent the forces related to the viscosity of the fluid. For simplicity, we investigate the two-dimensional homogeneous case (i.e. $\frac{\partial}{\partial y} \equiv 0$). For $i = x$, the comparison of the last two terms in order of magnitude is expressed by

$$\mu_f \left(\frac{4}{3}\frac{\partial^2 v_x^f}{\partial x^2} + \frac{\partial^2 v_x^f}{\partial z^2} + \frac{1}{3}\frac{\partial^2 v_z^f}{\partial x \partial z} \right) \sim \frac{\mu_f \eta_o^2}{K} \left(\frac{v_x^f}{\eta_o} - \frac{v_x^s}{1-\eta_o} \right) .$$

$$(2.3.14)$$

If a plane harmonic wave is propagating in the z-direction, then v_x^f can be written as

$$v_x^f = A \sin(\omega t - kz + \varphi_o) .$$

$$(2.3.15)$$

If the solid and the fluid materials are moving differently and v_x^s has the same order of magnitude as v_x^f, then expression (2.3.14) can be written as

$$\mu_f k^2 A \sin(\omega t - kz + \varphi_o) \sim \frac{\mu_f \eta_o}{K} A \sin(\omega t - kz + \varphi_o') .$$

So, the magnitudes of the two terms is compared as

$$k^2 \sim \frac{\eta_o}{K}$$

$$(2.3.16)$$

If we suppose that the minimum velocity of seismic waves is 1,000 m/s and the maximum

frequency is 200 Hz, then the square of the wavenumber is

$$k^2 \leq \frac{4\pi^2(200)^2}{(1000)^2} \ m^{-2} \cong 1.58 \ m^{-2} \ . \tag{2.3.17}$$

For typical values of permeability $10^{-12} m^2$ and porosity $\eta_o = 10^{-1}$, their ratio is

$$\frac{\eta_o}{K} = 10^{11} m^{-2} \ . \tag{2.3.18}$$

We see that the magnitude of the left hand side of expression (2.3.14) is over 10 orders

smaller than the right hand side. Therefore, Σ^f is negligible in seismic wave propagation

problems. Similar considerations can be found in the literature (e.g. Biot, 1956a; Bourbie

et al., 1987). After dropping Σ^f we have a set of four macroscopic equations (2.3.7),

(2.3.8), (2.3.9) and (2.3.11), and equation (2.3.9) becomes

$$D_{21}\partial_t v^s + D_{22} \, \partial_t \, v^f = - \nabla p^f - b\left(\frac{v^f}{\eta_o} - \frac{v^s}{1 - \eta_o}\right) + \frac{p^f}{\eta_o}\nabla \eta_o \ . \tag{2.3.19}$$

2.3.3 First order hyperbolic system for 2-D P-SV waves

For a two dimensional wave propagation problem, it can be shown SH waves decouple

from P-SV waves. If we suppose all physical parameters and variables are constant in the

y-direction, that is $\frac{\partial}{\partial y} \equiv 0$ in equations (2.3.7), (2.3.8.)., (2.3.11) and (2.3.19), it is

readily shown that P-SV waves satisfy the following first order differential equations:

$$D_{11}\frac{\partial v_x^s}{\partial t} + D_{12}\frac{\partial v_x^f}{\partial t} = \frac{\partial \sigma_{xx}^s}{\partial x} + \frac{\partial \sigma_{xz}^s}{\partial z} + b\left(\frac{v_x^f}{\eta_o} - \frac{v_x^s}{1 - \eta_o}\right) ,$$

(2.3.20)

$$D_{11}\frac{\partial v_z^s}{\partial t} + D_{12}\frac{\partial v_z^f}{\partial t} = \frac{\partial \sigma_{xz}^s}{\partial x} + \frac{\partial \sigma_{zz}^s}{\partial z} + b\left(\frac{v_z^f}{\eta_o} - \frac{v_z^s}{1 - \eta_o}\right) ,$$

(2.3.21)

$$\frac{\partial \sigma_{xx}^s}{\partial t} = A\frac{\partial v_x^s}{\partial x} + (A - 2\mu_s)\frac{\partial v_z^s}{\partial z} + B\left(\frac{\partial v_x^f}{\partial x} + \frac{\partial v_z^f}{\partial z}\right)$$

$$+ (2N_s + H_A)\frac{\partial \eta_o}{\partial z} v_z^s + (2N_f + H_B)\frac{\partial \eta_o}{\partial x} v_x^f + H_A\frac{\partial \eta_o}{\partial x} v_x^s + H_B\frac{\partial \eta_o}{\partial x} v_x^f ,$$

(2.3.22)

$$\frac{\partial \sigma_{zz}^s}{\partial t} = (A - 2\mu_s)\frac{\partial v_x^s}{\partial x} + A\frac{\partial v_z^s}{\partial z} + B\left(\frac{\partial v_x^f}{\partial x} + \frac{\partial v_z^f}{\partial z}\right)$$

$$+ (2N_s + H_A)\frac{\partial \eta_o}{\partial z} v_z^s + (2N_f + H_B)\frac{\partial \eta_o}{\partial z} v_z^f + H_A\frac{\partial \eta_o}{\partial x} v_x^s + H_B\frac{\partial \eta_o}{\partial x} v_x^f ,$$

(2.3.23)

$$\frac{\partial \sigma_{xz}^s}{\partial t} = \mu_s\left(\frac{\partial v_z^s}{\partial x} + \frac{\partial v_x^s}{\partial z}\right) + N_f\left(\frac{\partial \eta_o}{\partial z} v_x^f + \frac{\partial \eta_o}{\partial x} v_z^f\right) + N_s\left(\frac{\partial \eta_o}{\partial z} v_x^s + \frac{\partial \eta_o}{\partial x} v_z^s\right) ,$$

(2.3.24)

$$D_{21}\frac{\partial v_x^s}{\partial t} + D_{22}\frac{\partial v_x^f}{\partial t} = -\frac{\partial p_f}{\partial x} - b\left(\frac{v_x^f}{\eta_o} - \frac{v_x^s}{1 - \eta_o}\right) ,$$

(2.3.25)

$$D_{21}\frac{\partial v_z^s}{\partial t} + D_{22}\frac{\partial v_z^f}{\partial t} = -\frac{\partial p_f}{\partial z} - b\left(\frac{v_z^f}{\eta_o} - \frac{v_z^s}{1 - \eta_o}\right) ,$$

(2.3.26)

$$\frac{\partial p_f}{\partial t} = -C\left(\frac{\partial v_x^s}{\partial x} + \frac{\partial v_z^s}{\partial z}\right) - E\left(\frac{\partial v_x^f}{\partial x} + \frac{\partial v_z^f}{\partial z}\right) + F_A\left(\frac{\partial \eta_o}{\partial x} v_x^s + \frac{\partial \eta_o}{\partial z} v_z^s\right)$$

$$- \left(F_B\frac{\partial \eta_o}{\partial x} + \frac{K_f}{\rho_f^o}\frac{\partial \rho_f^o}{\partial x}\right)v_x^f - \left(F_B\frac{\partial \eta_o}{\partial z} + \frac{K_f}{\rho_f^o}\frac{\partial \rho_f^o}{\partial z}\right)v_z^f .$$

(2.3.27)

Writing equations (2.3.20) - (2.3.21) in matrix form, we have

$$E_o\frac{\partial u}{\partial t} = A_o\frac{\partial u}{\partial x} + B_o\frac{\partial u}{\partial z} + C_o u ,$$

(2.3.28)

where

$$u = \begin{bmatrix} v_x^s \\ v_z^s \\ \sigma_{xx}^s \\ \sigma_{zz}^s \\ \sigma_{xz}^s \\ v_x^f \\ v_z^f \\ p_f \end{bmatrix},$$

(2.3.29)

$$E_o = \begin{bmatrix} D_{11} & 0 & 0 & 0 & 0 & D_{12} & 0 & 0 \\ 0 & D_{11} & 0 & 0 & 0 & 0 & D_{12} & 0 \\ 0 & 0 & 1 & 0 & 0 & 0 & 0 & 0 \\ 0 & 0 & 0 & 1 & 0 & 0 & 0 & 0 \\ 0 & 0 & 0 & 0 & 1 & 0 & 0 & 0 \\ D_{21} & 0 & 0 & 0 & 0 & D_{22} & 0 & 0 \\ 0 & D_{21} & 0 & 0 & 0 & 0 & D_{22} & 0 \\ 0 & 0 & 0 & 0 & 0 & 0 & 0 & 1 \end{bmatrix},$$

(2.3.30)

$$A_o = \begin{bmatrix} 0 & 0 & 1 & 0 & 0 & 0 & 0 & 0 \\ 0 & 0 & 0 & 0 & 1 & 0 & 0 & 0 \\ A & 0 & 0 & 0 & 0 & B & 0 & 0 \\ A-2\mu_s & 0 & 0 & 0 & 0 & B & 0 & 0 \\ 0 & \mu_s & 0 & 0 & 0 & 0 & 0 & 0 \\ 0 & 0 & 0 & 0 & 0 & 0 & 0 & -1 \\ 0 & 0 & 0 & 0 & 0 & 0 & 0 & 0 \\ -C & 0 & 0 & 0 & 0 & -E & 0 & 0 \end{bmatrix},$$

(2.3.31)

$$
\mathbf{B_o} = \begin{bmatrix}
0 & 0 & 0 & 0 & 1 & 0 & 0 & 0 \\
0 & 0 & 0 & 1 & 0 & 0 & 0 & 0 \\
0 & A-2\mu_s & 0 & 0 & 0 & 0 & B & 0 \\
0 & A & 0 & 0 & 0 & 0 & B & 0 \\
\mu_s & 0 & 0 & 0 & 0 & 0 & 0 & 0 \\
0 & 0 & 0 & 0 & 0 & 0 & 0 & 0 \\
0 & 0 & 0 & 0 & 0 & 0 & 0 & -1 \\
0 & -C & 0 & 0 & 0 & 0 & -E & 0
\end{bmatrix} ,
$$

$$(2.3.32)$$

$$
\mathbf{C_o} = \begin{bmatrix}
-\dfrac{b}{1-\eta_o} & 0 & 0 & 0 & 0 & \dfrac{b}{\eta_o} & 0 & 0 \\[2ex]
0 & -\dfrac{b}{1-\eta_o} & 0 & 0 & 0 & 0 & \dfrac{b}{\eta_o} & 0 \\[2ex]
N_A\dfrac{\partial \eta_o}{\partial x} & H_A\dfrac{\partial \eta_o}{\partial z} & 0 & 0 & 0 & N_B\dfrac{\partial \eta_o}{\partial x} & -H_B\dfrac{\partial \eta_o}{\partial z} & 0 \\[2ex]
H_A\dfrac{\partial \eta_o}{\partial x} & N_A\dfrac{\partial \eta_o}{\partial z} & 0 & 0 & 0 & -H_B\dfrac{\partial \eta_o}{\partial x} & N_B\dfrac{\partial \eta_o}{\partial z} & 0 \\[2ex]
N_s\dfrac{\partial \eta_o}{\partial z} & N_s\dfrac{\partial \eta_o}{\partial x} & 0 & 0 & 0 & N_f\dfrac{\partial \eta_o}{\partial z} & N_f\dfrac{\partial \eta_o}{\partial x} & 0 \\[2ex]
-\dfrac{b}{1-\eta_o} & 0 & 0 & 0 & 0 & -\dfrac{b}{\eta_o} & 0 & 0 \\[2ex]
0 & \dfrac{b}{1-\eta_o} & 0 & 0 & 0 & 0 & -\dfrac{b}{\eta_o} & 0 \\[2ex]
F_A\dfrac{\partial \eta_o}{\partial x} & F_A\dfrac{\partial \eta_o}{\partial z} & 0 & 0 & 0 & G_x & G_z & 0
\end{bmatrix} ,
$$

$$(2.3.33)$$

where

$$N_A = 2\,N_s + H_A ,$$

$$(2.3.34)$$

$$N_B = 2\,N_f - H_B ,$$

$$(2.3.35)$$

$$G_x = F_B \frac{\partial \eta_o}{\partial x} + \frac{K_f}{\rho_f^o} \frac{\partial \rho_f^o}{\partial x}$$

(2.3.36)

and

$$G_z = F_B \frac{\partial \eta_o}{\partial z} + \frac{K_f}{\rho_f^o} \frac{\partial \rho_f^o}{\partial z} .$$

(2.3.37)

Multiplying equation (2.3.28) by the inversion of $\mathbf{E_o}$,

$$\mathbf{E_o^{-1}} = \begin{bmatrix} R_{22} & 0 & 0 & 0 & 0 & -R_{12} & 0 & 0 \\ 0 & R_{22} & 0 & 0 & 0 & 0 & -R_{12} & 0 \\ 0 & 0 & 1 & 0 & 0 & 0 & 0 & 0 \\ 0 & 0 & 0 & 1 & 0 & 0 & 0 & 0 \\ 0 & 0 & 0 & 0 & 1 & 0 & 0 & 0 \\ -R_{21} & 0 & 0 & 0 & 0 & R_{11} & 0 & 0 \\ 0 & -R_{21} & 0 & 0 & 0 & 0 & R_{11} & 0 \\ 0 & 0 & 0 & 0 & 0 & 0 & 0 & 1 \end{bmatrix} ,$$

(2.3.38)

where

$$R_{ij} = \frac{D_{ij}}{D_{11}D_{22} - D_{12}D_{21}} ,$$

(2.3.39)

we obtain equation

$$\frac{\partial \mathbf{u}}{\partial t} = \mathbf{A} \frac{\partial \mathbf{u}}{\partial x} + \mathbf{B} \frac{\partial \mathbf{u}}{\partial z} + \mathbf{Cu} ,$$

(2.3.40)

where

$$\mathbf{A} = \begin{bmatrix} 0 & 0 & R_{22} & 0 & 0 & 0 & 0 & R_{12} \\ 0 & 0 & 0 & 0 & R_{22} & 0 & 0 & 0 \\ A & 0 & 0 & 0 & 0 & B & 0 & 0 \\ A-2\mu_s & 0 & 0 & 0 & 0 & B & 0 & 0 \\ 0 & \mu_s & 0 & 0 & 0 & 0 & 0 & 0 \\ 0 & 0 & -R_{21} & 0 & 0 & 0 & 0 & -R_{11} \\ 0 & 0 & 0 & 0 & -R_{21} & 0 & 0 & 0 \\ -C & 0 & 0 & 0 & 0 & -E & 0 & 0 \end{bmatrix} , \tag{2.3.41}$$

$$\mathbf{B} = \begin{bmatrix} 0 & 0 & 0 & 0 & R_{22} & 0 & 0 & 0 \\ 0 & 0 & 0 & R_{22} & 0 & 0 & 0 & R_{12} \\ 0 & A-2\mu_s & 0 & 0 & 0 & 0 & B & 0 \\ 0 & A & 0 & 0 & 0 & 0 & B & 0 \\ \mu_s & 0 & 0 & 0 & 0 & 0 & 0 & 0 \\ 0 & 0 & 0 & 0 & -R_{21} & 0 & 0 & 0 \\ 0 & 0 & 0 & -R_{21} & 0 & 0 & 0 & -R_{11} \\ 0 & -C & 0 & 0 & 0 & 0 & -E & 0 \end{bmatrix} , \tag{2.3.42}$$

$$\mathbf{C} = \begin{bmatrix} -\dfrac{B_2}{1-\eta_o} & 0 & 0 & 0 & 0 & \dfrac{B_2}{\eta_o} & 0 & 0 \\[2ex] 0 & -\dfrac{B_2}{1-\eta_o} & 0 & 0 & 0 & 0 & \dfrac{B_2}{\eta_o} & 0 \\[2ex] N_A\dfrac{\partial \eta_o}{\partial x} & H_A\dfrac{\partial \eta_o}{\partial z} & 0 & 0 & 0 & N_B\dfrac{\partial \eta_o}{\partial x} & -H_B\dfrac{\partial \eta_o}{\partial z} & 0 \\[2ex] H_A\dfrac{\partial \eta_o}{\partial x} & N_A\dfrac{\partial \eta_o}{\partial z} & 0 & 0 & 0 & -H_B\dfrac{\partial \eta_o}{\partial x} & N_B\dfrac{\partial \eta_o}{\partial z} & 0 \\[2ex] N_s\dfrac{\partial \eta_o}{\partial z} & N_s\dfrac{\partial \eta_o}{\partial x} & 0 & 0 & 0 & N_f\dfrac{\partial \eta_o}{\partial z} & N_f\dfrac{\partial \eta_o}{\partial x} & 0 \\[2ex] \dfrac{B_1}{1-\eta_o} & 0 & 0 & 0 & 0 & -\dfrac{B_1}{\eta_o} & 0 & 0 \\[2ex] 0 & \dfrac{B_1}{1-\eta_o} & 0 & 0 & 0 & 0 & -\dfrac{B_1}{\eta_o} & 0 \\[2ex] F_A\dfrac{\partial \eta_o}{\partial x} & F_A\dfrac{\partial \eta_o}{\partial z} & 0 & 0 & 0 & -G_x & -G_z & 0 \end{bmatrix} \tag{2.3.43}$$

$$B_1 = b(R_{11} + R_{21})$$
(2.3.44)

$$B_2 = b(R_{12} + R_{22})$$
(2.3.45)

The system (2.3.40) predicts the existence of three types of body waves, one shear and two compressional ones with a faster and a slower velocity. The system is hyperbolic since both A and B have the same real eigenvalues ($-V_f$, $-V_r$, $-V_s$, 0, 0, V_s, V_r, V_f), where V_f, V_r, V_s are the propagating velocities of the fast P wave, S wave and slow P wave for fluid viscosity $\mu_f = 0$, respectively (See Appendix D). System (2.3.40) has the same form as the Biot's wave system (2.2.26), but the C-S system has more independent parameters. In Biot equations the parameter corresponding to B and C in the C-S equations are restricted to be equal, a condition imposed by the assumption of the existence of a unique potential energy for a porous medium (Biot, 1956a). De la Cruz et al (1991a,b) released this restriction by envisaging a porous medium as two superimposed interacting continua, thus allowing two different energy potentials for the solid and fluid movement respectively. Other differences appear in parameters associated with densities, which arise because of the fact that Biot mixed the use of two different kinds of volume averages. From equation (2.2.2) it is clear that the "intrinsic volume average" is applied to the displacement vectors. On the other hand, from the definition of macroscopic solid stress (Biot, 1956a, 1962a) and equation (2.2.3), the solid stress in equation (2.2.1) and (2.2.6) and the scalar s in equation (2.2.1) denote the "volume average" of those variables. A comparison of the physical parameters in Biot's equation and the C-S equations are given in Appendix E.

2.4 POINT AND LINE SOURCE SOLUTIONS IN A UNIFORM POROUS MEDIUM

One of the key factors in finite difference simulations is source implementation. Analytic solutions of Biot's equations for waves generated by a unidirectional point force in a homogeneous porous medium were derived by applying Laplace transforms (Burridge and Vargas, 1979) and Fourier transforms (Norris, 1985, Bonnet, 1987). Burridge and Vargas (1979) obtained a far field solution by applying the "saddle-point" method. Boutin et al. (1987) obtained solutions not only for unidirectional point forces but also for a harmonic volume source which is related to fluid injection. In this development, the analytic solutions of Biot's equations and the C-S equations are presented for a P-wave point source and a P-wave line source with the source force acting on both solid and fluid materials, which is useful in the source implementation of finite difference simulations and in testing the accuracy of the finite difference algorithms. In this chapter the solutions are derived for the C-S equations. The corresponding solutions for Biot equations can be obtained by a comparison of the physical parameters in the C-S equation and the corresponding parameters in Biot's equations (Appendix E; Dai et al., 1992a).

2.4.1 Point source solutions

For a point source in a three dimensional uniform medium, after neglecting Σ^f and substituting (2.3.8) into (2.3.7), (2.3.11) into (2.3.9), we can write the macroscopic equations with a body force f as

$$D_{11}\partial_{tt}\mathbf{u}^s + D_{12}\partial_{tt}\mathbf{u}^f - b\left(\frac{\mathbf{v}^f}{\eta_o} - \frac{\mathbf{v}^s}{1-\eta_o}\right) + \nabla\left[(A - \mu_s)\nabla.\mathbf{u}^s + B\nabla.\mathbf{u}^f\right] + \mu_s\nabla^2\mathbf{u}^s = (1-q)\mathbf{f},$$

$$(2.4.1)$$

$$D_{21}\partial_{tt}\mathbf{u}^s + D_{22}\partial_{tt}\mathbf{u}^f + b\left(\frac{\mathbf{v}^f}{\eta_o} - \frac{\mathbf{v}^s}{1-\eta_o}\right) + \nabla\left[C\nabla.\mathbf{u}^s + R\nabla.\mathbf{u}^f\right] = q\,\mathbf{f},\qquad(2.4.2)$$

where q is an arbitrary quantity (≤ 1) which determine the force distribution in the two phases. It can be set equal to η_o, for instance. After Fourier transformation with respect to time t, (2.4.1) and (2.4.2) become

$$\omega^2\left(\tilde{D}_{11}\tilde{\mathbf{u}}^s + \tilde{D}_{12}\tilde{\mathbf{u}}^f\right) + \nabla\left[(A - \mu_s)\nabla.\tilde{\mathbf{u}}^s + B\nabla.\tilde{\mathbf{u}}^f\right] + \mu_s\nabla^2\tilde{\mathbf{u}}^s = (1-q)\tilde{\mathbf{f}},\qquad(2.4.3)$$

$$\omega^2\left(\tilde{D}_{21}\tilde{\mathbf{u}}^s + \tilde{D}_{22}\tilde{\mathbf{u}}^f\right) + \nabla\left[C\nabla.\tilde{\mathbf{u}}^s + R\nabla.\tilde{\mathbf{u}}^f\right] = q\,\tilde{\mathbf{f}},\qquad(2.4.4)$$

where $\tilde{\mathbf{u}}^s$, $\tilde{\mathbf{u}}^f$ and $\tilde{\mathbf{f}}$ are the Fourier transforms of the solid and fluid displacements and the body force, respectively, and

$$\tilde{D}_{m1} = D_{m1} - (-1)^m\frac{ib}{(1-\eta_o)\omega}\qquad(m = 1, 2),\qquad(2.4.5)$$

$$\tilde{D}_{m2} = D_{m1} + (-1)^m\frac{ib}{\eta_o\omega}\qquad(m = 1, 2).\qquad(2.4.6)$$

Introduce the potentials ϕ_1, ϕ_2, ψ_1, ψ_2, Φ and Ψ so that

$$\tilde{\mathbf{u}}^s = \nabla\phi_1 + \nabla\times\psi_1,\qquad(2.4.7)$$

$$\tilde{\mathbf{u}}^f = \nabla\phi_2 + \nabla\times\psi_2,\qquad(2.4.8)$$

$$\tilde{f} = \nabla\Phi + \nabla\times\Psi \, , \qquad\qquad (2.4.9)$$

with $\nabla\cdot\psi_1 = 0, \quad \nabla\cdot\psi_2 = 0, \quad \nabla\cdot\Psi = 0.$

If we suppose the source to be purely dilatational, then its rotational component $\Psi \equiv 0$ and so are ψ_1 and ψ_2. Substituting (2.4.7), (2.4.8) and (2.4.9) into equations (2.4.3) and (2.4.4) and letting $\Phi = \delta(r)S(\omega)$, we obtain an inhomogeneous system for the dilatational potentials ϕ_1 and ϕ_2

$$\omega^2[\tilde{D}_{11}\phi_1 + \tilde{D}_{12}\phi_2] + A\nabla^2\phi_1 + B\nabla^2\phi_2 = (1-q)\delta(r)S(\omega) \, , \qquad\qquad (2.4.10)$$

$$\omega^2[\tilde{D}_{21}\phi_1 + \tilde{D}_{22}\phi_2] + C\nabla^2\phi_1 + E\nabla^2\phi_2 = q\delta(r)S(\omega) \, . \qquad\qquad (2.4.11)$$

In this linear inhomogeneous differential equation system the right hand side terms are Dirac delta functions which are singular at the source location. This inhomogeneous system can be equivalently transformed into a problem described by the corresponding homogeneous system with certain regularity conditions at the source point.

In order to obtain the regularity conditions, we take volume integrals of equations (2.4.10) and (2.4.11) over a small spherical region with the center at the source and then let the radius σ of the sphere approach zero

$$\lim_{\sigma\to 0} \int_v \left\{ \omega^2[\tilde{D}_{11}\phi_1 + \tilde{D}_{12}\phi_2] + A\nabla^2\phi_1 + B\nabla^2\phi_2 \right\} dv = (1-q)S(\omega), \qquad\qquad (2.4.12)$$

$$\lim_{\sigma\to 0} \int_v \left\{ \omega^2[\tilde{D}_{21}\phi_1 + \tilde{D}_{22}\phi_2] + C\nabla^2\phi_1 + E\nabla^2\phi_2 \right\} dv = qS(\omega) \, . \qquad\qquad (2.4.13)$$

Since ϕ_1 and, ϕ_2 should be bounded at the origin from physical consideration, the volume integrals of ϕ_1 and, ϕ_2 approach zero as σ approaches to zero. After applying the Gaussian theorem to (2.4.12) and (2.4.13), the volume integrals are transformed into surface integrals

$$\lim_{\sigma \to 0} \int_{s_\sigma} \left(A\nabla\phi_1 + B\nabla\phi_2 \right) ds_\sigma = (1-q)S(\omega) , \qquad (2.4.14)$$

$$\lim_{\sigma \to 0} \int_{s_\sigma} \left(C\nabla\phi_1 + E\nabla\phi_2 \right) ds_\sigma = qS(\omega) , \qquad (2.4.15)$$

where s_σ is the surface of the sphere. Equation (2.4.14) and (2.4.15) are the regularity conditions which describe the flux of the potential gradients at the source region. Since ϕ_1 and, ϕ_2 are spherically symmetrical, one can write equation (2.4.14), (2.4.15) as

$$\lim_{\sigma \to 0} \int_{s_\sigma} \left(A\frac{\partial\phi_1}{\partial r} + B\frac{\partial\phi_2}{\partial r} \right) ds_\sigma = (1-q)S(\omega) , \qquad (2.4.16)$$

and

$$\lim_{\sigma \to 0} \int_{s_\sigma} \left(C\frac{\partial\phi_1}{\partial r} + E\frac{\partial\phi_2}{\partial r} \right) ds_\sigma = qS(\omega) . \qquad (2.4.17)$$

The problem expressed by the inhomogeneous equations (2.4.10) and (2.4.11) is now equivalent to the one that consists of the homogeneous equations

$$\omega^2\left[\tilde{D}_{11}\phi_1 + \tilde{D}_{12}\phi_2\right] + A\nabla^2\phi_1 + B\nabla^2\phi_2 = 0 ,$$

(2.4.18)

$$\omega^2\left[\tilde{D}_{21}\phi_1 + \tilde{D}_{22}\phi_2\right] + C\nabla^2\phi_1 + E\nabla^2\phi_2 = 0 ,$$

(2.4.19)

with the regularity conditions (2.4.16) and (2.4.17) at the source location. Since the solutions are spherically symmetrical we have

$$\nabla^2\phi_i = \frac{1}{r^2}\frac{d}{dr}\left(r^2\frac{d\phi_i}{dr}\right) = \frac{1}{r}\frac{d^2(r\,\phi_i)}{dr^2} ,$$

(2.4.20)

Substitution of (2.4.20) into equation (2.4.18) and (2.4.19) gives

$$\omega^2\left[\tilde{D}_{11}\Phi_1 + \tilde{D}_{12}\Phi_2\right] + A\frac{d^2\Phi_1}{dr^2} + B\frac{d^2\Phi_2''}{dr^2} = 0 ,$$

(2.4.21)

$$\omega^2\left[\tilde{D}_{21}\Phi_1 + \tilde{D}_{22}\Phi_2\right] + C\frac{d^2\Phi_1}{dr^2} + E\frac{d^2\Phi_2}{dr^2} = 0 ,$$

(2.4.22)

where $\Phi_i = r\phi_i$. Introducing the differential operator D defined by $D\Phi = \frac{d\Phi}{dr}$ and $D^2 = DD$, the general solution of the system can be found by using the differential operator method. Rewriting equation (2.4.21) and (2.4.22) with the differential operator D, we have

$$\left(\omega^2\tilde{D}_{11} + PD^2\right)\Phi_1 + \left(\omega^2\tilde{D}_{12} + BD^2\right)\Phi_2 = 0 ,$$

(2.4.23)

$$\left(\omega^2\tilde{D}_{21} + CD^2\right)\Phi_1 + \left(\omega^2\tilde{D}_{22} + ED^2\right)\Phi_2 = 0 .$$

(2.4.24)

To have nontrivial solutions for equation (2.4.23) and (2.4.24) requires

$$\det \begin{bmatrix} \omega^2 \tilde{D}_{11} + AD^2 & \omega^2 \tilde{D}_{12} + BD^2 \\ \omega^2 \tilde{D}_{21} + CD^2 & \omega^2 \tilde{D}_{22} + ED^2 \end{bmatrix} = 0 \ . \tag{2.4.25}$$

Equation (2.4.25) has the characteristic roots

$$D_1 = +ik_f, \qquad D_2 = -ik_f, \qquad D_3 = +ik_s, \qquad D_4 = -ik_s, \tag{2.4.26}$$

where

$$k_f = \frac{\omega}{V_f} \ , \tag{2.4.27}$$

$$k_s = \frac{\omega}{V_s} \ , \tag{2.4.28}$$

and

$$V_f^2 = \frac{s + \sqrt{s^2 - 4rt}}{2r} \ , \tag{2.4.29}$$

$$V_s^2 = \frac{s - \sqrt{s^2 - 4rt}}{2r} \ , \tag{2.4.30}$$

$$r = \tilde{D}_{11}\tilde{D}_{22} - \tilde{D}_{12}\tilde{D}_{21} \ , \tag{2.4.31}$$

$$s = \tilde{D}_{11}E + \tilde{D}_{22}A - \tilde{D}_{12}C - \tilde{D}_{21}B \ , \tag{2.4.32}$$

$$t = AE - BC \ . \tag{2.4.33}$$

Therefore the general solutions have the following forms

$$\Phi_1 = a\, e^{-ik_f r} + b\, e^{-ik_s r} + c\, e^{+ik_f r} + d\, e^{+ik_s r} \ ,$$

(2.4.34)

$$\Phi_2 = a^{'}\, e^{-ik_f r} + b^{'}\, e^{-ik_s r} + c^{'}\, e^{+ik_f r} + d^{'}\, e^{+ik_s r} \ ,$$

(2.4.35)

where a, b, c d a' b' c' and d' are underdetermined constants. Equation (2.4.34) and (2.4.35) indicate that there are two kinds of dilatational waves, characterized by different wave numbers k_f and k_s propagating in porous media. In our case the waves radiate from the source, hence c, d, c' and d' are equal to zero. Furthermore, from equation (2.4.23) or (2.4.24) we know that

$$\frac{\Phi_2}{\Phi_1} = A_f \qquad \text{for } D = \pm ik_f \ ,$$

(2.4.36)

$$\frac{\Phi_2}{\Phi_1} = A_s \qquad \text{for } D = \pm ik_s \ ,$$

(2.4.37)

where

$$A_f = - \frac{\tilde{D}_{11} V_f^2 - A}{\tilde{D}_{12} V_f^2 - B} = - \frac{\tilde{D}_{21} V_f^2 - C}{\tilde{D}_{22} V_f^2 - E} \ ,$$

(2.4.38)

$$A_s = - \frac{\tilde{D}_{11} V_s^2 - A}{\tilde{D}_{12} V_s^2 - B} = - \frac{\tilde{D}_{21} V_s^2 - C}{\tilde{D}_{22} V_s^2 - E} \ .$$

(2.4.39)

Therefore the general solutions become

$$\Phi_1 = a\, e^{-ik_f r} + b\, e^{-ik_s r} \ ,$$

(2.4.40)

$$\Phi_2 = aA_f e^{-ik_f\,r} + bA_s\,e^{-ik_s\,r}\ , \tag{2.4.41}$$

or

$$\phi_1 = \frac{a\,e^{-ik_f r} + b\,e^{-ik_s r}}{r}\ , \tag{2.4.42}$$

$$\phi_2 = \frac{aA_f e^{-ik_f r} + bA_s\,e^{-ik_s r}}{r}\ . \tag{2.4.43}$$

The arbitrary constants a and b can now be determined by making use of the regularity conditions. Substituting (2.4.42) and (2.4.43) into (2.4.16) and (2.4.17), we have

$$\lim_{\sigma\to 0}\left\{ \int_s \frac{-a(A+BA_f)\,exp(-ik_f\sigma)}{\sigma^2}\,\sigma^2 d\Omega\ + \int_s \frac{-b(A+BA_s)\,exp(-ik_s\sigma)}{\sigma^2}\,\sigma^2 d\Omega\ \right\} = (1-q)S(\omega) \ , \tag{2.4.44}$$

$$\lim_{\sigma\to 0}\left\{ \int_s \frac{-a(C+EA_f)\,exp(-ik_f\sigma)}{\sigma^2}\,\sigma^2 d\Omega\ + \int_s \frac{-b(C+EA_s)\,exp(-ik_s\sigma)}{\sigma^2}\,\sigma^2 d\Omega\ \right\} = qS(\omega), \tag{2.4.45}$$

where Ω is the solid angle. Or

$$(A + BA_f)a + (A + BA_s)b = -\frac{(1-q)S(\omega)}{4\pi}\ , \tag{2.4.46}$$

$$(C + EA_f)a + (C + EA_s)b = -\frac{qS(\omega)}{4\pi}\ . \tag{2.4.47}$$

Solving equations (2.4.46) and (2.4.47), we find the constants

$$a = \frac{\alpha}{4\pi}\,S(\omega)\ , \tag{2.4.48}$$

$$b = \frac{\beta}{4\pi} \, S(\omega) \, , \tag{2.4.49}$$

where

$$\alpha = \frac{(1 - q)(C + EA_s) - q(A + BA_s)}{(AE - BC)(A_f - A_s)} \, , \tag{2.4.50}$$

$$\beta = \frac{q(A + B\,A_f) - (1 - q)(C + EA_f)}{(AE - BC)(A_f - A_s)} \, . \tag{2.4.51}$$

Substitution of (2.4.48) and (2.4.49) into equation (50) and (51) gives dilatational potential solutions for a point source of pure P waves in the space-frequency domain

$$\phi_1(r,\omega) = \frac{S(\omega)\left(\alpha \, e^{-ik_f r} + \beta \, e^{-ik_s r}\right)}{4\pi r} \, , \tag{2.4.52}$$

$$\phi_2(r,\omega) = \frac{S(\omega)\left(\alpha \, A_f e^{-ik_f r} + \beta \, A_s \, e^{-ik_s r}\right)}{4\pi r} \, . \tag{2.4.53}$$

The corresponding solutions in the space and time domain are given by the inverse Fourier transformation of equations (2.4.52) and (2.4.53).

$$\phi_1(r, t) = \frac{1}{2\pi} \int \frac{S(\omega)\left(\alpha \, e^{-ik_f r} + \beta \, e^{-ik_s r}\right)}{4\pi r} e^{i \, \omega t} \, d\omega \, , \tag{2.4.54}$$

$$\phi_2(r, t) = \frac{1}{2\pi} \int \frac{S(\omega)\left(\alpha \, A_f e^{-ik_f r} + \beta \, A_s e^{-ik_s r}\right)}{4\pi r} e^{i \, \omega t} \, d\omega \, . \tag{2.4.55}$$

When the porous medium is saturated with an ideal fluid without viscosity, that is $b = 0$ in equations (2.4.1) and (2.4.2), all the coefficients in equations (2.4.52) and (2.4.53) are real. The solutions in the space-time domain are given by

$$\phi_1(r,t) = \frac{\alpha\, s\!\left(t - \frac{r}{V_f}\right) + \beta\, s\!\left(t - \frac{r}{V_s}\right)}{4\pi r} , \tag{2.4.56}$$

$$\phi_2(r,t) = \frac{\alpha\, A_f s\!\left(t - \frac{r}{V_f}\right) + \beta A_s\, s\!\left(t - \frac{r}{V_s}\right)}{4\pi r} , \tag{2.4.57}$$

where $s(t)$ is the time variation of the source function.

2.4.2 Line source solutions

In the finite difference simulation of two-dimensional P-SV waves it is necessary to implement a line source in the algorithm. For a P-wave line source along the y-axis, the source force f in the right hand side of (2.4.1) and (2.4.2) is given by

$$\mathbf{f} = \nabla \Phi = \nabla\!\left[\delta(x)\,\delta(z)\right] S(\omega) . \tag{2.4.58}$$

Equations (2.4.10) and (2.4.11) become

$$\omega^2\!\left[\tilde{D}_{11}\phi_1 + \tilde{D}_{12}\phi_2\right] + A\nabla^2\phi_1 + B\nabla^2\phi_2 = (1-q)\delta(x)\delta(z)S(\omega) , \tag{2.4.59}$$

$$\omega^2\!\left[\tilde{D}_{21}\phi_1 + \tilde{D}_{22}\phi_2\right] + C\nabla^2\phi_1 + E\nabla^2\phi_2 = q\delta(x)\delta(z)S(\omega) . \tag{2.4.60}$$

In order to find the solutions for ϕ_1 and ϕ_2, the simplest way is to integrate the point source solutions (2.4.56) and (2.4.57) along the whole y-axis

$$\phi_1(x, z, t) = \frac{1}{4\pi} \int_{-\infty}^{\infty} \frac{\alpha\, s\left(t - \frac{r}{V_f}\right) + \beta\, s\left(t - \frac{r}{V_s}\right)}{r}\, dy \ , \tag{2.4.61}$$

$$\phi_2(x, z, t) = \frac{1}{4\pi} \int_{-\infty}^{\infty} \frac{\alpha\, A_f s\left(t - \frac{r}{V_f}\right) + \beta A_s\, s\left(t - \frac{r}{V_s}\right)}{r}\, dy \ , \tag{2.4.62}$$

where $r = \sqrt{x^2 + y^2 + z^2}$. Since $dy/r = dr/y$ and r is even in y, we have

$$\phi_1(x, z, t) = \frac{1}{2\pi} \int_{r}^{\infty} \frac{\alpha\, s\left(t - \frac{r}{V_f}\right) + \beta\, s\left(t - \frac{r}{V_s}\right)}{y}\, dr$$

$$= \frac{\alpha H\,(t - d/V_f)}{2\pi} \int_{d/V_f}^{t} \frac{s(t - \tau)}{\sqrt{\tau^2 - d^2/V_f^2}}\, d\tau + \frac{\beta H\,(t - d/V_s)}{2\pi} \int_{d/V_s}^{t} \frac{s(t - \tau)}{\sqrt{\tau^2 - d^2/V_s^2}}\, d\tau \ , \tag{2.4.63}$$

where $H(\ )$ is a Heaviside step function and $d = \sqrt{x^2 + z^2}$. Similarly, we can get

$$\phi_2(x, z, t) = \frac{1}{2\pi} \int_{r}^{\infty} \frac{\alpha\, A_f s\left(t - \frac{r}{V_f}\right) + \beta\, A_s s\left(t - \frac{r}{V_s}\right)}{y}\, dr$$

$$= \frac{\alpha A_f H (t - d/V_f)}{2\pi} \int_{d/V_f}^{t} \frac{s(t - \tau)}{\sqrt{\tau^2 - d^2/V_f^2}} d\tau + \frac{\beta A_s H (t - d/V_s)}{2\pi} \int_{d/V_s}^{t} \frac{s(t - \tau)}{\sqrt{\tau^2 - d^2/V_s^2}} d\tau \ .$$

$$(2.4.64)$$

In the finite difference implementation we express the source in terms of the vector u which is evaluated from equations (2.3.8), (2.3.11) for the C-S equations and from equations (2.2.5) and (2.2.6) for Biot's equations after the potentials are determined from equations (2.4.63), (2.4.64), (2.4.7) and (2.4.8) for a line source . When equations (2.4.63) and (2.4.64) are used to calculate the potentials for Biot's equations, all of the physical parameters in the formulae for the parameters should be replaced according to Table E1 in Appendix E. A Gaussian function whose frequency response is practically band limited can be used to define the source excitation $s(t)$.

2.5 FINITE DIFFERENCE METHOD

A heterogeneous, explicit finite difference method is employed to solve the first order hyperbolic systems for wave propagation in porous media. In finite difference approximations there are three related problems of primary concern, namely, the accuracy, the stability and the numerical dispersion properties of the algorithm. Generally the numerical error depends on the grid spacing and the time step. The accuracy of a finite difference scheme is measured by its truncation error. The problem of stability consists of finding conditions under which the difference between the theoretical and numerical solutions of the difference equation remains bounded as time progresses (Mitchell and Griffiths, 1981). In common with most explicit finite difference approximations to partial differential equations, a condition relating the time and space intervals must be satisfied if the solution to the difference equations is to be stable. In wave propagation the stability condition of the finite difference schemes is not as restrictive as in the heat flow problems (Broore, 1972). The dispersion properties of difference approximations relate to the speed of propagation of the numerical solution (Turkel 1974). A measurement of dispersion is the phase error which occurs due to replacement of the differential equation by a difference equation. Phase errors produce a variation of phase velocity with frequency or wavenumber. Grid dispersion depends highly on the number of grid points per wavelength.

The first order systems, (2.2.26) and (2.3.40), are solved numerically for $t > 0$, subject to the initial conditions $u(x, z, t = 0)$. In order to set up the finite difference method, a grid mesh is superposed on a two-dimensional rectangular model The discrete points (x_j, z_m, t_n) are defined by $x_j = j \Delta x$ for each $j = 0, 1, \cdots J$; $z_m = m \Delta z$ for each $m = 0, 1, \cdots M$ and $t_n = n \Delta t$ for each $n = 0, 1, \cdots N$, while the numerical

approximation of the solution $u(x_j, z_m, t_n)$ is represented by u^n_{jm}.

The finite difference algorithm is based on the the concept of splitting in time (Strang, 1968). The numerical solution u is updated for one time step by first applying a one dimensional difference operator in the x direction and then in the z-direction. At successive time levels the difference directions are reversed. The advancing procedure from time level n to level $n+2$ can be expressed by

$$u^{n+2} = F^\dagger_z \, F^\dagger_x F_z \, F_x u^n \qquad (2.5.1)$$

where F_x and $F^\dagger_x$ are one-dimensional difference operators approximating the solution of the one- dimensional equation

$$\frac{\partial u}{\partial t} = A \frac{\partial u}{\partial x} + C^x u \qquad (2.5.2)$$

for constant z, while F_z and $F^\dagger_z$ are one-dimensional difference operators approximating the solution of the one- dimensional equation

$$\frac{\partial u}{\partial t} = B \frac{\partial u}{\partial z} + C^z u \qquad (2.5.3)$$

for constant x. In equation (2.5.2) and (2.5.3) the non-derivative term has been partitioned into two terms to maintain consistency in the one-dimensional case. The decomposition is arbitrary provided $C = C^x + C^z$. Each of the operators in (2.5.1) advances the time t by a half-step so that the final output of the combined four operators is for two time steps. One advantage of splitting methods is that stability properties are governed by the one-dimensional schemes. Furthermore, splitting methods have smaller phase error than a wide

class of unsplit schemes (Turkel, 1974).

A MacCormack-like scheme (Gottlieb and Turkel, 1976) applied to (2.5.2) consists of a predictor

$$\mathbf{u}_{j,m}^{(1)} = \mathbf{u}_{j,m}^n - \frac{\Delta t}{6\Delta x} \mathbf{A}_{j,m} (7\mathbf{u}_{j,m}^n - 8\mathbf{u}_{j+1,m}^n + \mathbf{u}_{j+2,m}^n) + \Delta t \, \mathbf{C}_{j,m}^x \mathbf{u}_{j,m}^n \qquad (2.5.4)$$

and a corrector

$$\mathbf{u}_{j,m}^{n+1/2} = \frac{1}{2} (\mathbf{u}_{j,m}^{(1)} + \mathbf{u}_{j,m}^n) + \frac{\Delta t}{12\Delta x} \mathbf{A}_{j,m} (7\mathbf{U}_{j,m}^{(1)} - 8\mathbf{u}_{j-1,m}^{(1)} + \mathbf{u}_{j-2,m}^{(1)}) + \frac{\Delta t}{2} \mathbf{C}_{j,m}^x \mathbf{u}_{j,m}^{(1)}$$

$$(2.5.5)$$

Equations (2.5.4) and (2.5.5) describe the operator F_x. $F_x^{\dagger}$ is described by equations similar to (2.5.4) and (2.5.5) where the direction of differencing is interchanged.

In order to define the operator F_z and $F_z^{\dagger}$, one replaces matrix $\mathbf{A}$ in operators F_x and $F_x^{\dagger}$ by matrix $\mathbf{B}$ and calculates the difference in the index m instead of j. The finite difference algorithm is second order accurate in time and fourth order accurate in space. A truncation error analysis of this scheme is given in Appendix C. Gottlieb and Turkel (1976) analysed its stability. They proved that the method is stable when

$$\frac{\Delta t}{\Delta x} v_{max} < \frac{2}{3}, \qquad (2.5.6)$$

where v_{max} is the maximum wave velocity. Due to the presence of the term $C^x u$ in equation (2.5.2) it is required that $\Delta t \le \rho(C^x)$, where $\rho(C^x)$ denotes the spectral radius of the matrix C^x.

One of the major advantage of this high order (in space) finite difference scheme is its smaller phase error compared to other (2,2) methods such as the popular Lax-Wendroff and leapfrog schemes (Gottlieb and Turkel, 1976). To avoid grid dispersion, the condition

$\Delta x < \lambda_{min}/6$ should be satisfied, where λ_{min} is the minimum wavelength present in the model. In the simulation of seismic waves in porous media the strict criterion imposed by the minimum slow P-wave velocity can be relaxed because the slow P-wave attenuates very fast in cases where the saturating fluid is viscous. In most case the minimum wave length of the S wave is taken into account.

The fourth order scheme requires values at two points in both x and z directions from the point for which new values are being computed. At points near the boundaries, there are not enough neighbors to implement the scheme, so values are defined at points outside the computational domain by a third order extrapolator (Turkel, 1980). A P-wave line source is employed for the generation of the synthetic seismograms. The method of Alterman and Karal (1968) was used for the source implementation. In the case where a free surface is modelled, the solid stress components and the fluid pressure must be zero at the surface while the velocity components are calculated by extrapolation of the characteristic variables of the hyperbolic systems (Bayliss et al., 1986).

A new absorbing boundary technique is used in this development. This absorbing boundary is implemented by adding a small transition zone adjacent to the artificial boundary. In the transition zone, the direction of propagation is adjusted gradually so that the wave reaches the boundary at normal angles. Then, the wave field is separated into outgoing and incoming waves and the characteristics of the incoming waves are allowed to vanish. Satisfactory absorbing effect is achieved when the width of zone is about one wavelength for the peak frequency of the source wavelet. The details on the absorbing boundary technique are described in Chapter 3.

The finite difference algorithm calculates the response over the whole mesh and is fully vectorized by applying the method of matrix multiplication by diagonals (Madsen et al., 1976; Vafidis et al., 1992). The computational time for 2400 iterations on the Convex 210 is 90 min for a mesh whose size is 300x300. Storage requirement for the velocity-stress

method is quite high due to the additional memory required for the extra unknowns (i.e. stress components) and for the intermediate variables present in the splitting schemes.

2.6 EXAMPLES OF NUMERICAL SOLUTIONS AND APPLICATIONS

Uniform model

The accuracy of the numerical solutions is examined by comparing them with the exact solutions given by (2.4.63) and (2.4.64). A homogeneous porous medium is considered whose parameters are those of layer 1 (Table 2.6.1 for Biot's equation and Table 2.6.2 for the C-S equation) with the damping coefficient b equal to zero. A P-wave line source located at $(x=0, z=0)$ employs a Gaussian time function whose peak frequency is at 30 Hz. The numerical solutions for two different grid spacings and the exact solution at $(x=100$ m, $z=100$ m) are displayed as functions of time (Figure 2.6.1 for Biot's equation and Figure 2.6.2 for the C-S equation). It is shown, in this case, that a fast P-wave and a slow P-wave are propagating in the porous medium. The oscillatory tails present in the numerical solutions with the grid spacing of 4 meters are due to numerical dispersion of slow P waves. When the grid spacing is equal to 2 meters, the numerical solutions fit the exact solutions very well.

Two layer model

Seismic responses are calculated for a simple two layer model using both the Biot and C-S equations in order to demonstrate the major features of seismic wave propagation in porous media. In both the Biot theory and the de la Cruz-Spanos theory the attenuation is related to the relative motion of the fluid to the solid through the damping coefficient b or the fluid viscosity μ^f. In these simulations, a small value of b or μ^f is assigned to Layer 1 and a larger value of b or μ^f to Layer 2 (See Table 2.6.1 and Table 2.6.2) in order to examine the affects of the damping coefficient b or the fluid viscosity μ^f to various wave types.

Figure 2.6.3 illustrates snapshots of the vertical components of the solid particle velocities (Figure 2.6.3a - 2.6.3c) and fluid particle velocities (Figure 2.6.3d — 2.6.3f)

Table 2.6.1 **Physical parameters of porous media for Biot's equation modeling**

	LAYER 1*	LAYER 2
ρ_{11} (kg/m^3)	2167	2430
ρ_{22} (kg/m^3)	191	255
ρ_{12} (kg/m^3)	-83	-100
b (N s m^4)	3000	700000
P (N / m^2)	2.0332E10	5.565E10
Q (N / m^2)	0.0953E10	0.07E10
R (N / m^2)	0.0331E10	0.079E10
μ_f (N s/ m^2)	0.684E10	1.2E1
q	0.1	0.1
Velocity of fast P-wave (m/s)**	3210	4860
Velocity of slow P-wave (m/s)**	1180	1740
Velocity of shear wave (m/s)**	1790	2240
α	-0.337E-10	-0.165E-10
β	0.719E-11	0.210E-11
A_f	1.1	0.585
A_s	-16.2	-48.2

*From Yew, C. H. and Jogi, P. N., 1978

** For $\mu_f = 0$

Table 2.6.2 Physical parameters of porous media
for the C-S equation modeling

	LAYER 1	LAYER 2
depth (m)	0 ~ 645	645 ~ 1000
ρ_o^s (kg/m^3)	2400	2500
ρ_o^f (kg/m^3)	1000	1000
ρ_{12} (kg/m^3)	-100	-100
η_o	0.3	0.3 ~ 0.25
K (m^2)	9.56E-13	9.56E-13 ~ 7.8E-13
K_s (Pa)	2.298E10	3.15E10
μ_s (Pa)	1.0E10	1.8E10
K_f (Pa)	2.17E9	2.17E9
μ_f (Pa s)	1.0E-7	1.0E-5
δ_s	0.28	0.27
δ_f	0.048	0.035
δ_l	0.8	0.8
δ	0.1	0.1
Velocity of fast P-wave (m/s)*	3348	4118 ~ 4165
Velocity of slow P-wave (m/s)*	1110	1164 ~ 1120
Velocity of shear wave (m/s)**	1997	2627 ~ 2633

* For $\mu_f = 0$
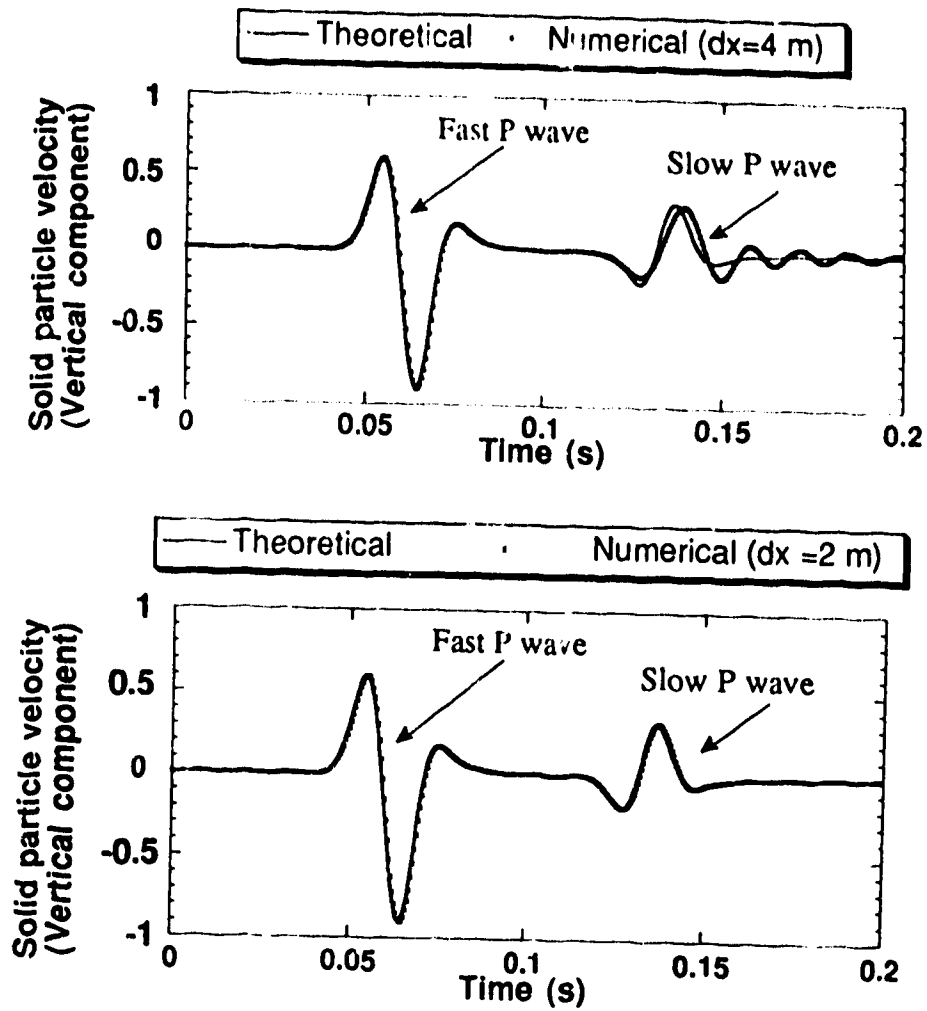
Figure 2.6.1 Comparison of analytical and numerical solutions of Biot equations for two different grid spacings Δx and the same time step Δt=0.0001 sec.. The vertical component of the solid part is shown as function of time. A P-wave line source generates waves propagating in a two-dimensional porous medium. Model parameters are those for layer 1 in Table 2.6.1. The oscillatory tails present at the large grid spacing are due to numerical dispersion.
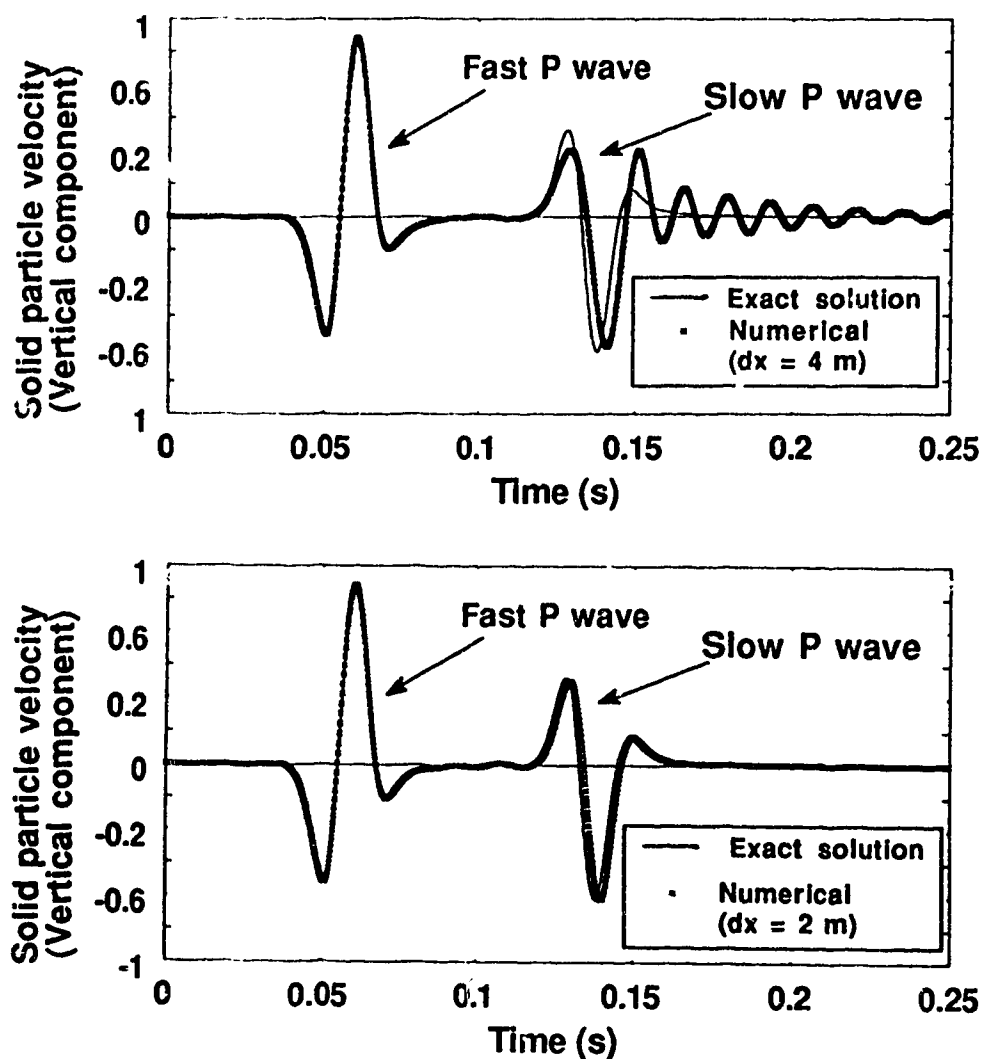
Figure 2.6.2 Comparison of analytical and numerical solutions of C-S equations for two different grid spacing Δx and time step Δt=0.0001 sec.. The vertical component of the solid part is shown as function of time. A P-wave line source generates waves propagating in a two-dimensional porous medium. Model parameters are shown in Table 2.6.2. The oscillatory tails present at the large grid spacing are due to numerical dispersion.
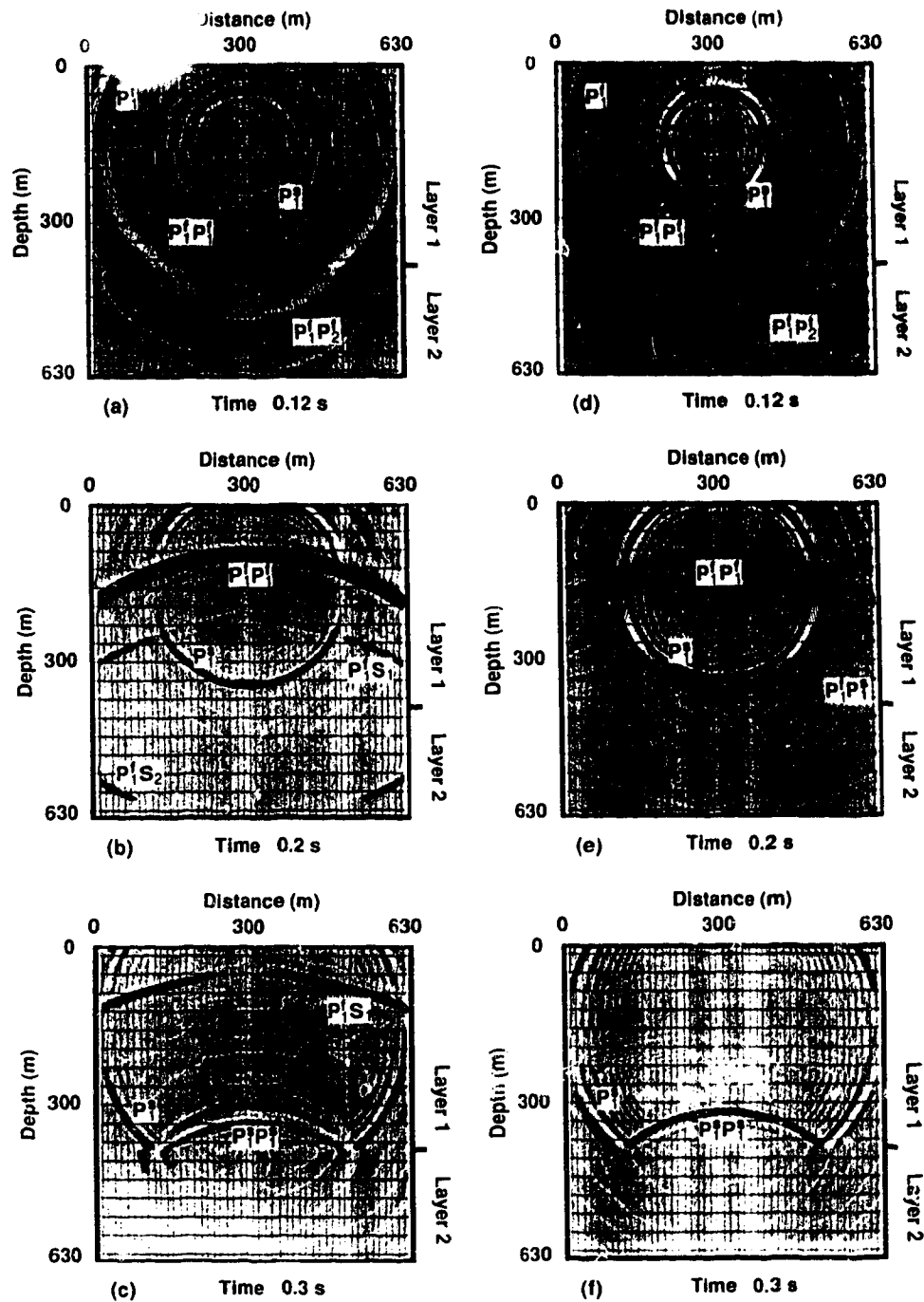
Figure 2.6.3 Snapshots of the vertical components of the solid (a)-(c) and fluid (d)-(f) particle velocities from the finite difference solution of Biot equations for a two-layer model. An infinitely extended model is simulated by applying absorbing boundary conditions on the computational boundaries. The model parameters are presented in Table 2.6.1. A P-wave line source, applied to both the solid and fluid parts, is located in the upper layer at a vertical distance of 244 m from the interface.

obtained by solving the Biot system. Infinitely extended models are simulated by applying the absorbing boundary techniques described in Chapter 3 on the computational boundaries. A P-wave line source is located in the upper layer at a distance of 244 m from the interface . In these diagrams various phases are indicated by arrows and nomenclature. The wave type W is indexed as P or S for a compressional or shear wave; a superscript is used for the phase velocity (f for fast and s for slow) and a subscript for the layer: i.e. $W_{layer}^{velocity}$. Multiple symbols are used to indicate reflected or transmitted phases.

The snapshots (Figure 2.6.3) at time $t = 0.12$ s show that the vertical components of the solid and fluid particle velocities are in phase for fast P-waves and out of phase for slow P-waves. At $t = 0.2$ s, we observe the reflections $P_1^f P_1^f$, $P_1^f S_1$ and $P_1^f P_1^s$, and a transmitted wave $P_1^f S_2$ of the fast P-wave as well as the slow P-wave which reaches the interface. Finally at $t=0.3$ s, the slow P-wave is reflected at the interface while the transmitted part is attenuated drastically since the fluid viscosity of the second layer is higher.

In Figure 2.6.4, we present the synthetic seismograms of the solid (Figure 2.6.4a) and fluid (Figure 2.6.4b) particle velocities (vertical components) from a solution of the Biot system with the model used in Figure 2.6.3. The receivers are located along the line running through the source and parallel to the interface. Among the various reflected phases indicated by arrows and the nomenclature, it is not surprising that the energy of the events associated with S waves is weaker in the fluid movement (Figure 2.6.4b) than that in the solid movement (Figure 2.6.4a), while the energy of the events associated with the slow P waves varies in the opposite way.

Figures 2.6.5 and 2.6.6 present the solution of the Biot system for the same two-layer model where the upper absorbing boundary is replaced by a free surface. In this case we use an explosive source whose stresses σ_{xx} and σ_{zz} are equal and proportional to a Gaussian time function. The source is located at a depth of 12 m from the free surface. The
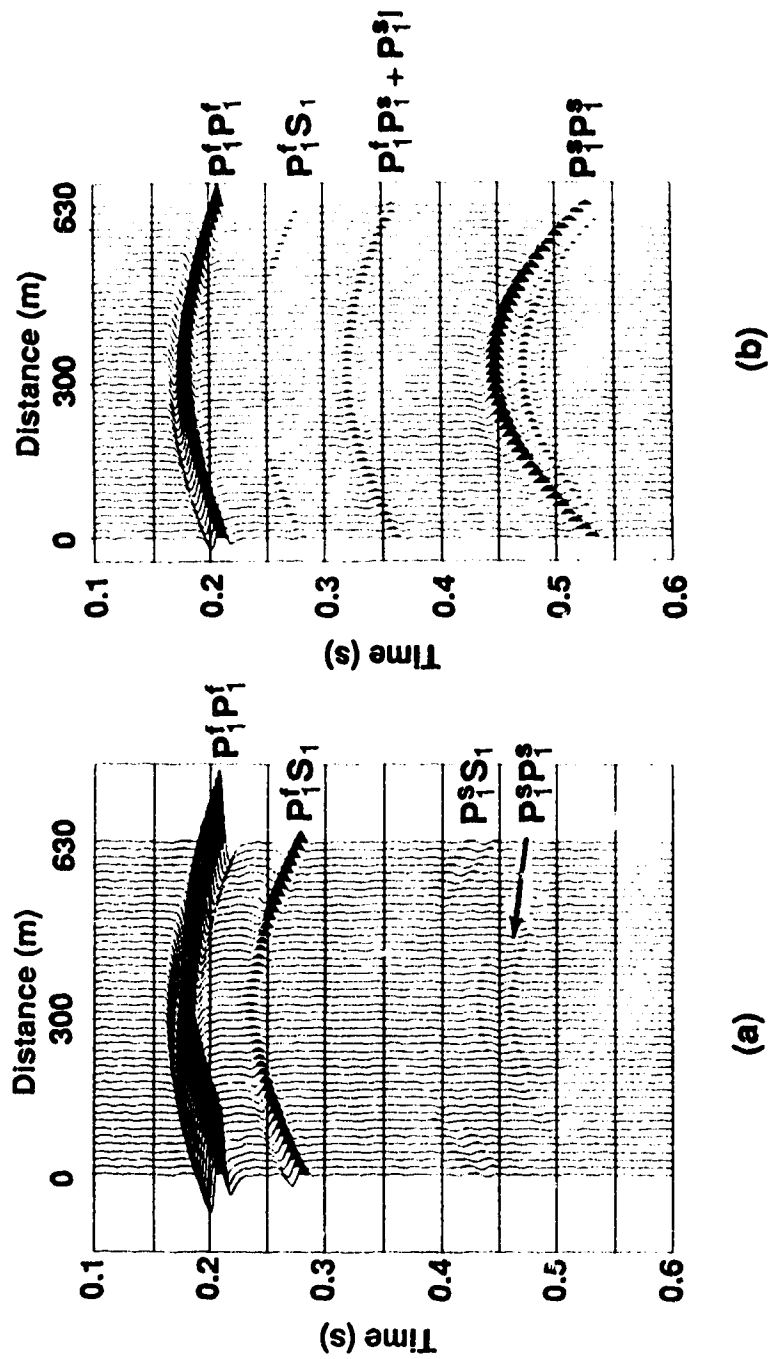
Figure 2.6.4 Synthetic seismograms of the solid (a) and fluid (b) particle velocities (vertical components) for the same model as in Figure 2.6.3. The receivers are located along the line through the source and parallel to the interface. The various phases are indicated by arrows and the nomenclature.

Figure 2.6.5. Snapshots of the vertical component of the solid particle velocity from the finite difference solution of Biot equations a two-layer model with the same physical parameters as for Figure 2.6.3. Here the upper boundary is a free surface. The source is located at a depth of 12 m and the interface is at 250 m.
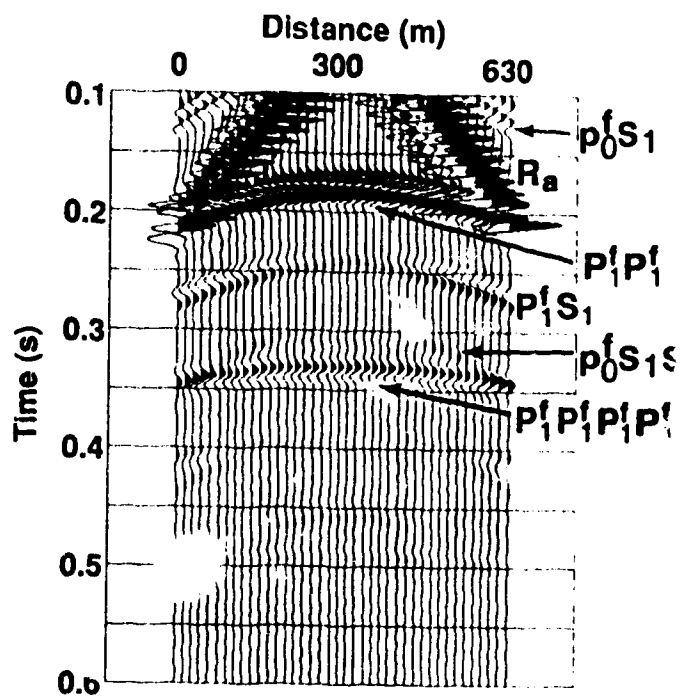
Figure 2.6.6 Synthetic seismograms of the solid particle velocities (vertical component) for the same model as for Figure 2.6.5. The various phases are indicated by arrows and the nomenclature.

interface is located at a depth of 250 m.

Figure 2.6.5 shows snapshots of the vertical component of the solid particle velocity. Any phase indicated with p_0^f is due to reflection of the original wave at the surface, i.e. a ghost. At $t=0.05$ s, it is seen that the wave-train of the direct fast P-wave is followed by the ghost reflection from the free surface. At $t=0.1$ s, we can see the converted reflections from the free surface ($p_0^f S_1$), the Raleigh waves (Ra) and the slow P-wave (P_1^s). At $t=0.15$ s, one part of the energy of the direct fast P-wave has been transmitted ($P_1^f P_2^f$ and another part has been reflected ($P_1^f P_1^f$). At $t=0.2$ s, we observe the reflected phase $p_0^f S_1 S_1$ and the transmitted phases $p_0^f S_1 S_2$ of $p_0^f S_1$ while $P_1^f P_1^f$ is reflected at the free surface ($P_1^f P_1^f P_1^f$). We also observe the converted phase of the direct fast P-wave from the interface ($P_1^f S_1$). At $t=0.25$ s, $P_1^f P_1^f P_1^f$ and slow P-wave reach the interface. At $t=0.3$ s, the surface reflected wave, $P_1^f P_1^f P_1^f P_2^f$, is propagating downward through the second layer and it catches up to $p_0^f S_1 S_2$. The slow P-wave is reflected ($P_1^s P_1^s$) and the transmitted part is drastically attenuated in the second layer.

Figure 2.6.6 shows the synthetic seismogram of the solid particle velocities (vertical component). The seismogram is dominated by the Raleigh wave. The late arriving phases are either reflections or multiples from the interface at a depth of 250 m.

The response of a two layer model is also calculated by solving the C-S system to demonstrate the major features of the wave field in porous media. The porosity is constant in the first layer and depth dependent in the second layer (Table 2.6.2). A P wave line source acting on both the fluid and the solid parts is located in the upper layer at a distance of 200 m from the interface. The time step is 0.2 ms and the grid spacing is 3.75 m in both the x and z directions. Figure 2.6.7 illustrates snapshots of the vertical components of the solid and fluid particle velocities. Similar phenomena are observed as in the results obtained by solving the Biot system.

The snapshots show that the solid (Figure 2.6.7a, b) and fluid (Figure 2.6.7c, d)
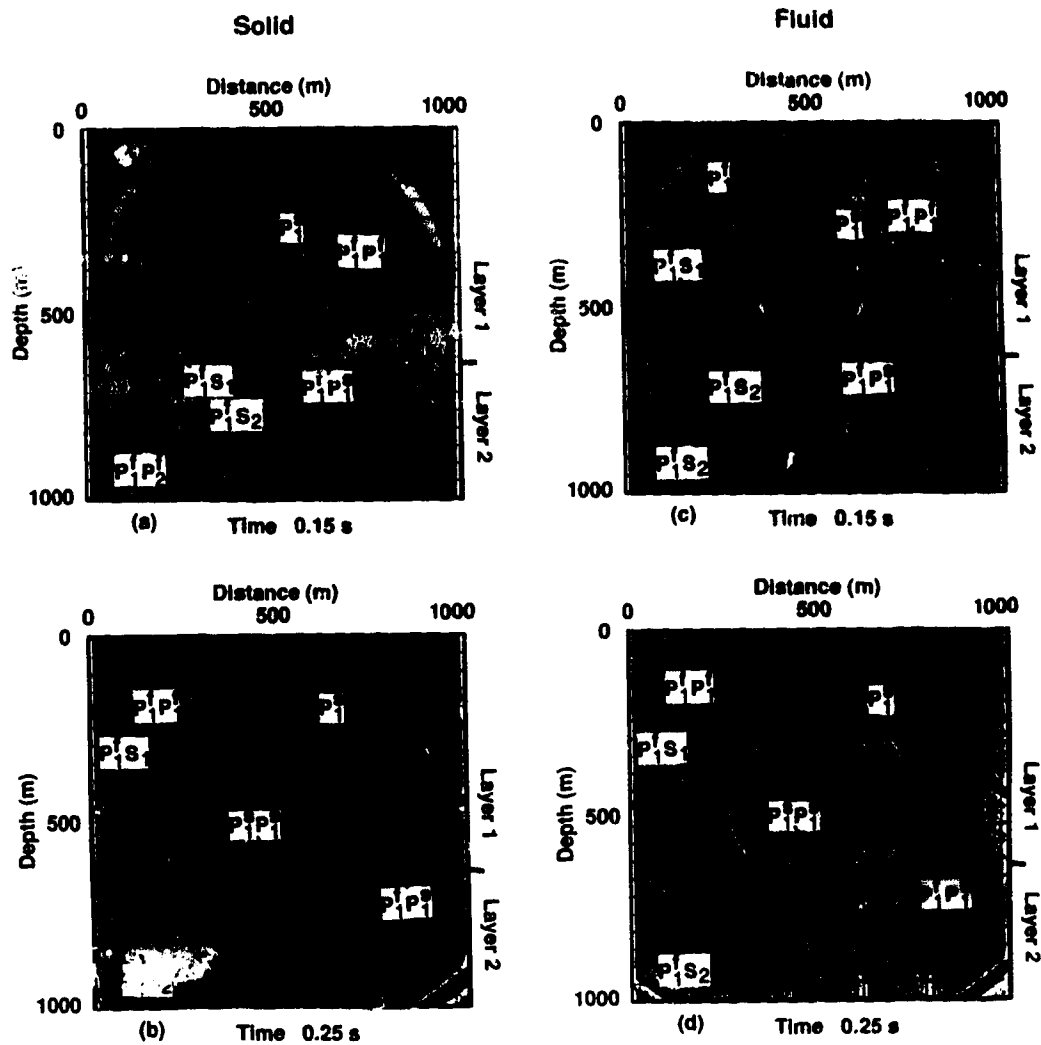
Figure 2.6.7. Snapshots at two different times of the vertical components of the solid (a, and fluid (c)-(d) particle velocities from the finite difference solution of C-S equations for a two-layer model. The model parameters are presented in Table 1. A P-wave line source, applied to both the solid and fluid parts, is located in the upper layer at a vertical distance of 200 m from the interface.

particle velocities are in phase for fast P-waves and out of phase for slow P-waves. At t = 0.15 s, we observe the reflections $P_1^f P_1^f$ and $P_1^f S_1$ of the fast P-wave as well as the slow P-wave which is approaching the interface. The fluid velocity snapshots also show clearly the converted slow P wave reflection $P_1^f P_1^s$ from the incident fast P wave. At t=0.25 s, the slow P wave is reflected ($P_1^s P_1^s$) at the interface while all the transmitted phases from the incident slow P wave are attenuated drastically since the fluid viscosity of the second layer is higher.

In figure 2.6.8, we present the synthetic seismograms of the fluid and solid particle velocity vertical components for the model used in Figure 2.6.7. The receivers are located along the line running through the source and parallel to the interface. It is observed again that the energy of the events associated with S waves is weaker in the fluid movement (Figure 2.6.8b) than that in the solid movement (Figure 2.6.8a), while the energy of the events associated with the slow P wave varies in the opposite way. This implies that the fast P waves and S waves are propagating through the solid framework and induce motion in the fluid in the pores via viscous coupling. In contrast, the slow P waves propagating through the connected fluid content also induce motion in the solid material.

If the saturated fluid is an ideal fluid with zero viscosity, there would be no energy dissipation in the wave motion. Figure 2.6.9 gives a synthetic example for this situation. The model is the same as for Figure 2.6.8 but here we let the fluid viscosity μ_f = 0. Compared to Figure 2.6.8 the energy of the the phases associated the slow P waves is much stronger in the seismogram for the vertical component of solid particle velocity (Figure 2.6.9a). In Figure 2.6.9b, which shows the seismogram for the vertical component of the fluid particle velocity, the slow P wave associated events have the same energy level as the others. This is because the attenuation of the slow P wave is very sensitive to the fluid viscosity. On the other hand, the fluid viscosity does not provide a dominant energy loss mechanism for the fast P waves and the S waves in porous media. The events
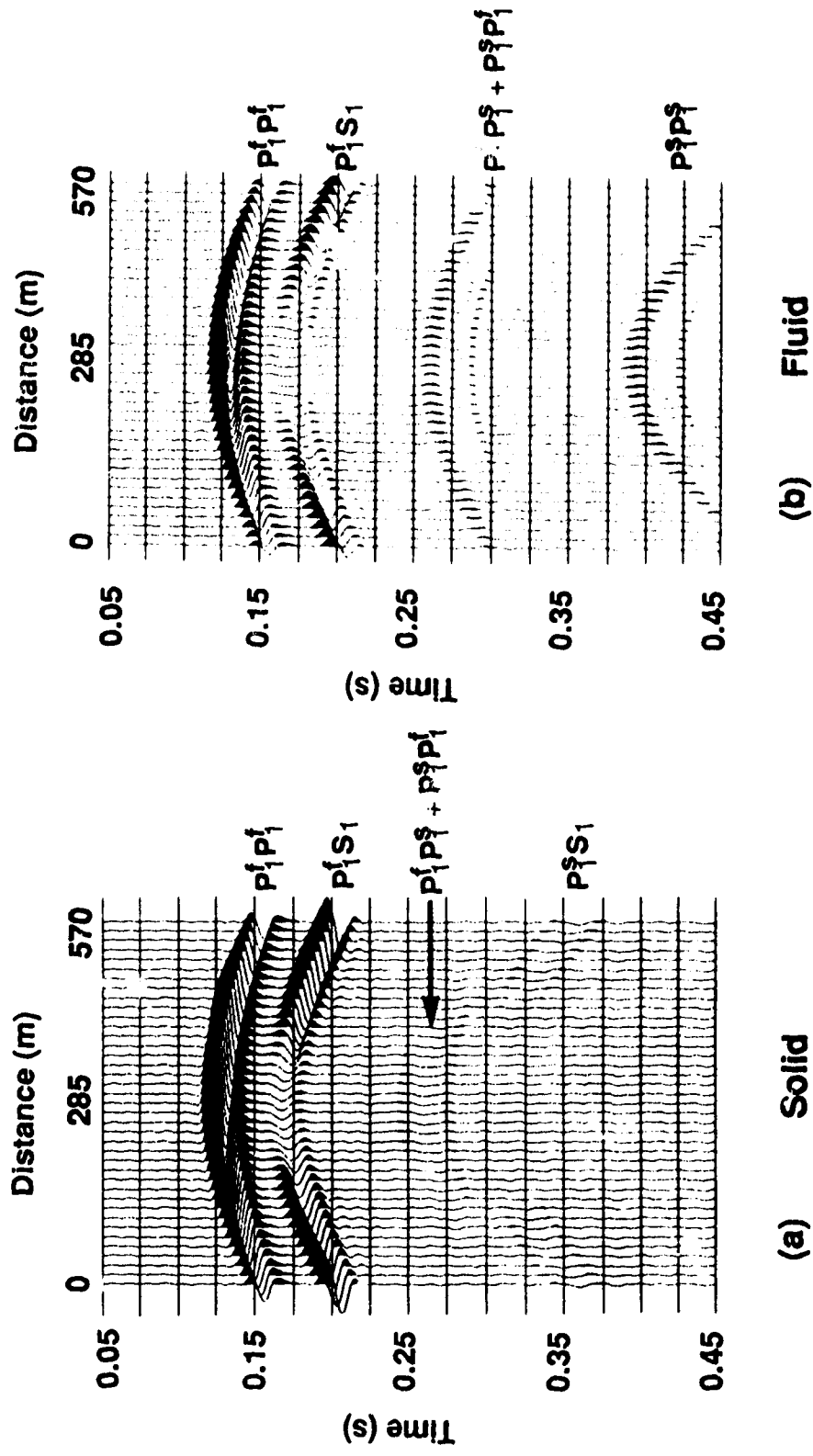
Figure 2.6.8. Synthetic seismograms of the vertical component of solid (a) and fluid (b) particle velocities. The model is the same one for Figure 2.6.7. The receivers are located along the line running through the source and parallel to the interface. The various phases are indicated by arrows and labels.
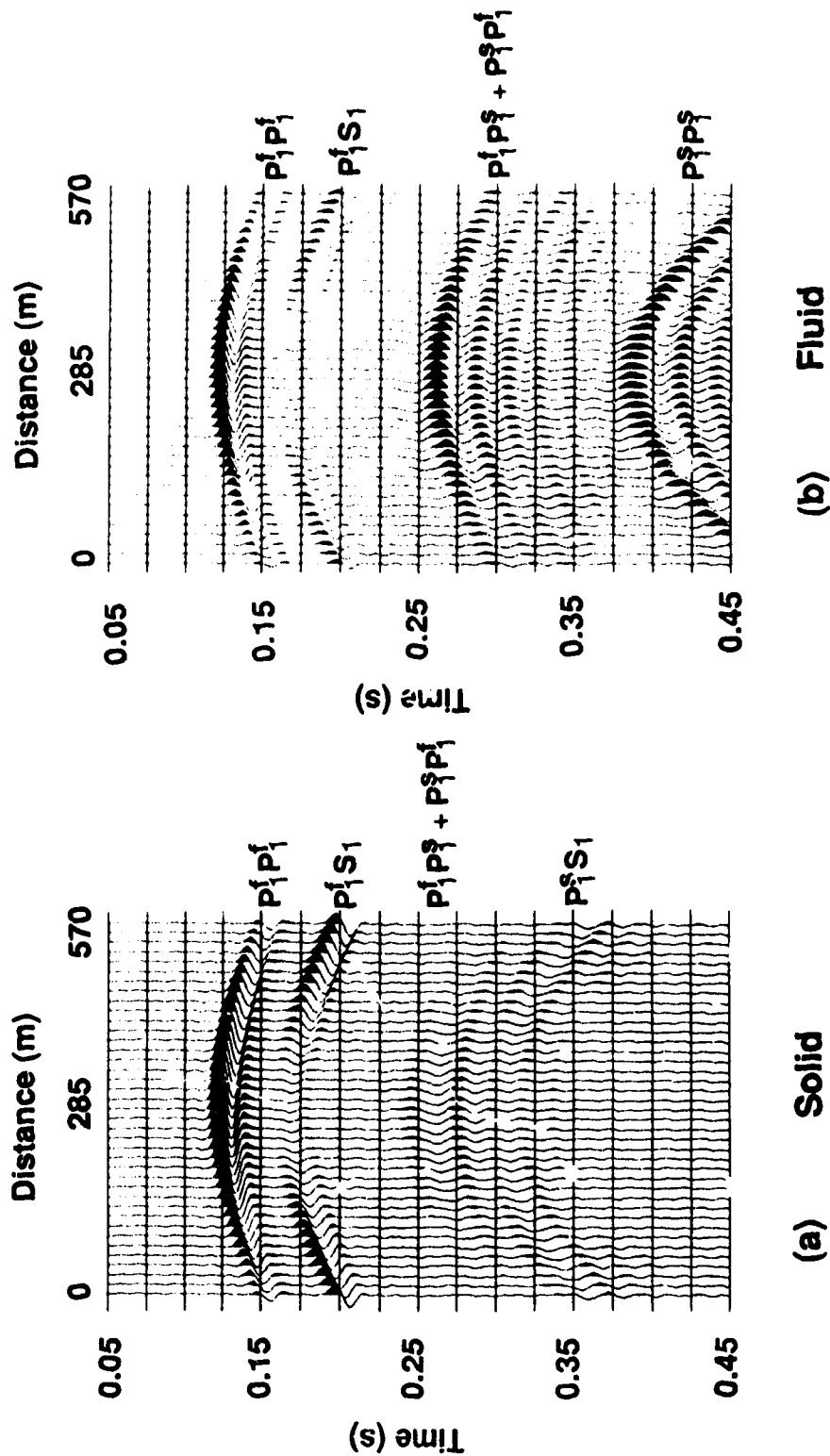
(a) Solid

(b) Fluid

Figure 2.6.9 Synthetic seismograms of the vertical components of solid (a) and fluid (b) particle velocities . The model is the same as for Figure 2.6.7 and Figure 2.6.8 but the fluid viscosity is zero here. The receivers are located along the line running through the source and parallel to the interface with a distance of 200 m. The various phases are indicated by arrows and labels.

Distance (m)
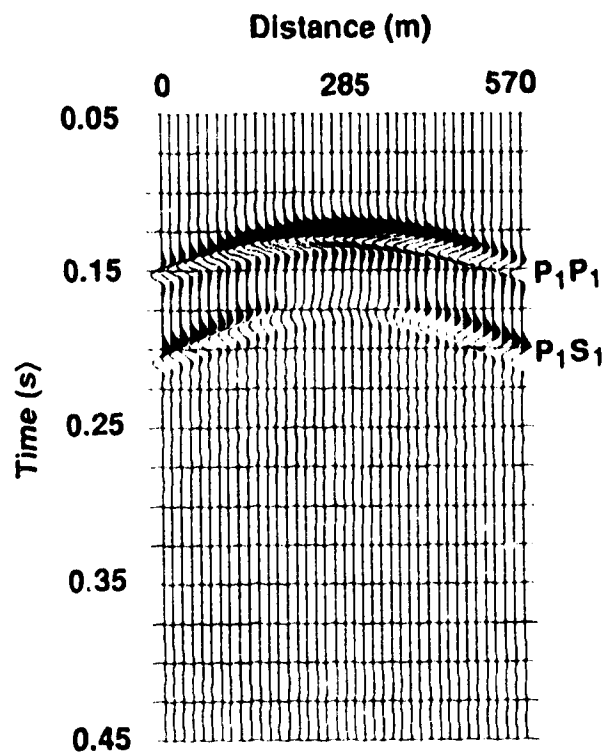
Figure 2.6.10. Synthetic seismogram of the particle velocity vertical component obtained from the numerical solutions of the C-S system. The model is the same as in Figure 2.6.9 but the porosity is set to be zero to simulate nonporous elastic solid media.

associated with the slow P wave in Figure 2.6.9 are shown with obvious numerical dispersion because of the low velocity of the slow P wave and the relatively large grid spacing (3.75 m) that we chose. The numerical dispersion, however, is less serious in the seismograms shown in Figure 2.6.8, since the slow waves are attenuated quickly in porous media saturated with viscous fluid. This suggests that the minimum slow P wave velocity criterion on numerical dispersion can be relaxed when realistic earth models are considered.

In the C-S system the porosity of the medium is included explicitly; the limiting cases of zero porosity should properly simulate the wave propagation in a single phase (solid) medium. Figure 2.6.10 is a synthetic seismogram showing the vertical component of the (solid) particle velocity which results when the porosity is zero in the model used in Figures 2.6.8 and 2.6.9. The result is exactly the same as would be obtained using an elastic wave equation.

The two layer examples verify the existence of a "slow" P-wave whose solid and fluid vertical components are out of phase. The "slow" P-wave is attenuated drastically at the lower layer where the fluid viscosity is higher. This is in accordance with theories given by Biot (1956) and de la Cruz-Spanos (1985) which predict increasing attenuation of "slow" P-wave as viscosity increases. Both the Biot theory and the da la Cruz-Spanos theory are limited in their ability to describe the attenuation of the "fast" P-wave and S-wave, because they have only one attenuation mechanism, related to the differential motion between solid and fluid, which is not the dominant one of "fast" P-wave and S-wave dissipation.

Reflectivity variation versus angle of incidence study

The variations of reflectivity versus angle of incidence in a shale-sandstone interface are studied for three different cases where the sandstone is fully saturated with gas, bitumen or water. The required parameters for the Biot system and the C-S system have been calculated from the properties of the rocks and fluids in the Cold Lake region (see Table F1

for shale and Table F2, F3, and F4 for sandstone saturated with gas, bitumk and water respectively in Appendix F). In calculating the P-P reflection coefficients, the maximum amplitudes of the reflected P-wave in a two layer model as they are recorded at a finite number of horizontal and vertical component receivers are added vectorially at each receiver location. The reflection coefficients are obtained by dividing the resulting value for each receiver by that of the direct wave in a uniform medium as recorded at the location symmetrical to the reflection wave receiver about the interface location in the two layer model. In this approach the effects of cylindrical spreading and attenuation are removed since the same effects are suffered by the reflection wave and the direct wave. The model geometry is given in Figure 2.6.11 where the depth from the receiver to the interface is 120 m which is large enough to ensure the separation of the P wave reflection from the converted S wave reflection.

Figure 2.6.12a shows the reflection coefficients extracted from the finite difference solutions of the Biot system. The P-P reflection coefficients from the shale-gas saturated sandstone interface are always greater than the P-P reflection coefficients from the other two interfaces. When the angle of incidence is equal to zero, the reflection coefficient of the interface between shale and gas saturated sandstone is 0.24, while the reflection coefficient of the interface between shale and bitumen saturated sandstone and the reflection coefficient of the interface between shale and water saturated sandstone are 0.1 and 0.08 respectively. The curves of the reflection coefficients versus the angle of incidence show a similar changing trend. They decrease slightly at first and then at about 50°, increase quickly. Figure 2.6.12b shows amplitude variation of the solid particle velocity versus angles of incidence. The vertical components show a general decreasing trend while the total amplitudes initially decrease and then increase at about 50°.

In figure 2.6.13 we present the results of amplitude variation versus angles of incidence as well as the reflection coefficients from gas-bitumen, gas-water and bitumen-water
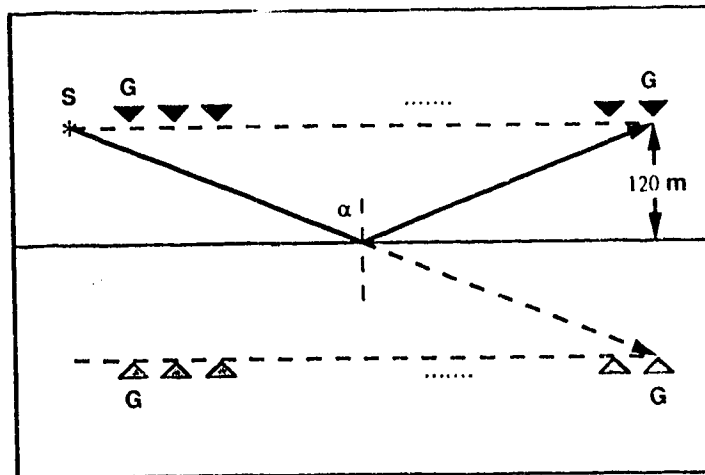
Figure 2.6.11 Model geometry used in th: finite difference study of reflectivity variation versus angle of incidence. "S" symbolizes a source and "G" symbolizes a receiver.
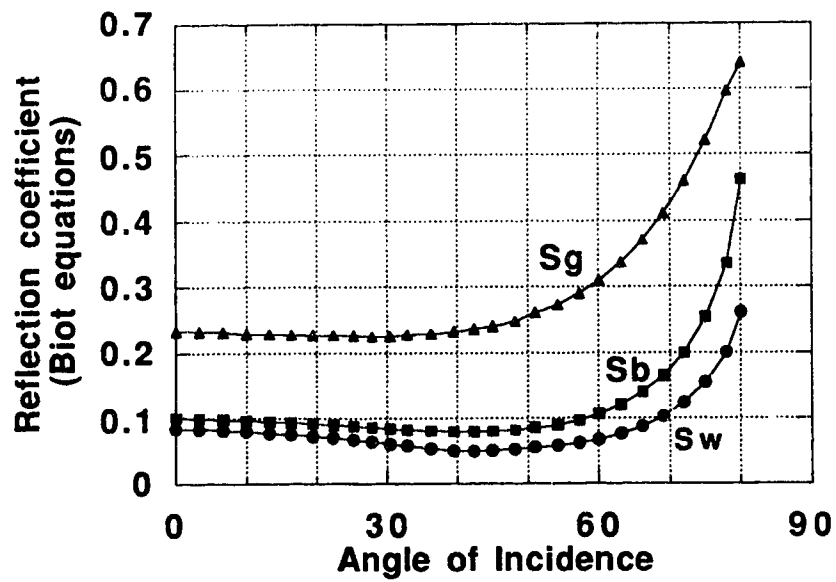
Figure 2.6.12a P-P reflection coefficients extracted from finite difference solutions of the

Biot system over interfaces of shale and gas saturated sandstone (Sg), shale and bitumen

saturated sandstone (Sb) and shale and water saturated sandstone (Sw).
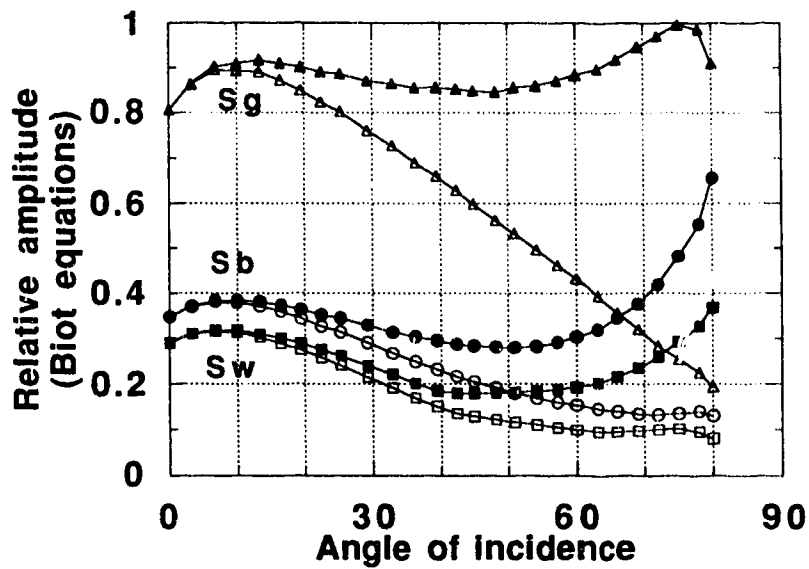
Figure 2.6.12b Relative P-P reflection amplitude extracted from finite difference solutions

of Biot system over interfaces of shale and gas saturated sandstone (Sg), shale and bitumen

saturated sandstone (Sb) and shale and water saturated sandstone (Sw). Solid symbols for

total amplitude of the particle velocity and open symbols for vertical components.
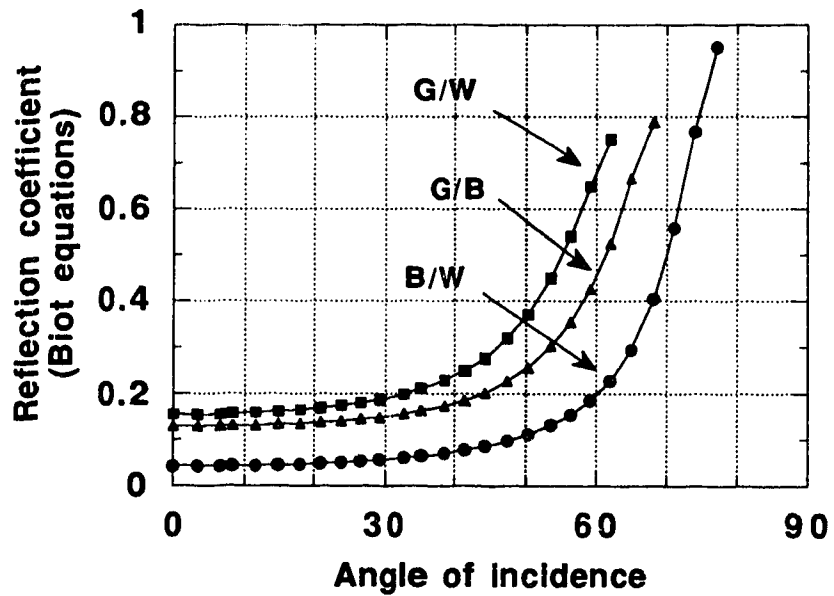
Figure 2.6.13a P-P reflection coefficients extracted from finite difference solutions of the Biot system over fluid contacts of gas and water in sandstone (G/W), gas and bitumen in sandstone (G/B) and bitumen and water in sandstone (B/W).
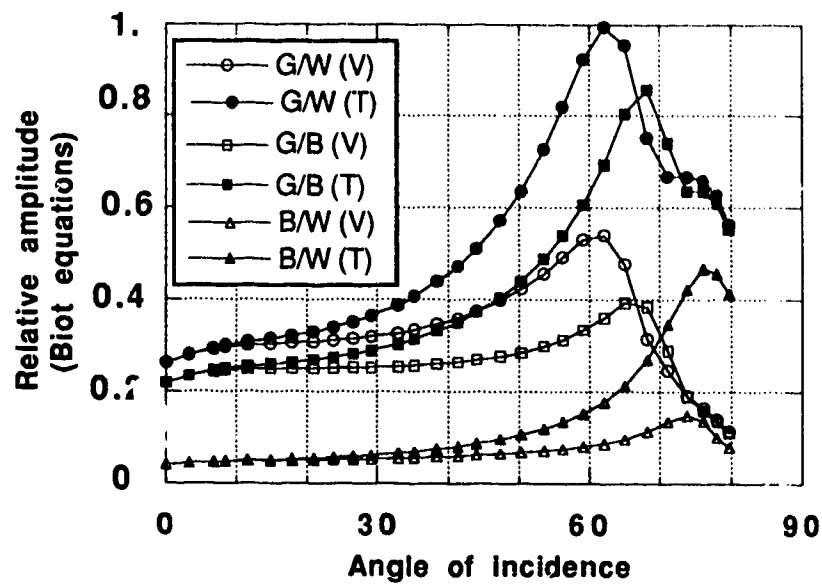
Figure 2.6.13b Relative P-P reflection amplitude extracted from finite difference solutions of the Biot system over fluid contacts of gas and water in sandstone (G/W), gas and bitumen in sandstone (G/B) and bitumen and water in sandstone (B/W). Solid symbols for total amplitude of the particle velocity and open symbols for vertical components. Beyond the critical angle the reflection interfered with headwaves.
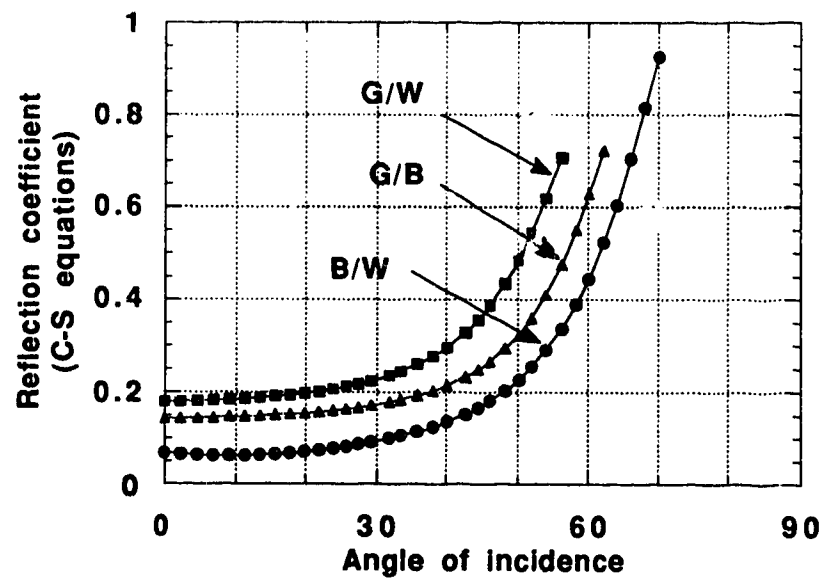
Figure 2.6.13c P-P reflection coefficients extracted from finite difference solutions of the

C-S system over fluid contacts of gas and water in sandstone (G/W), gas and bitumen in

sandstone (G/B) and bitumen and water in sandstone (B/W).
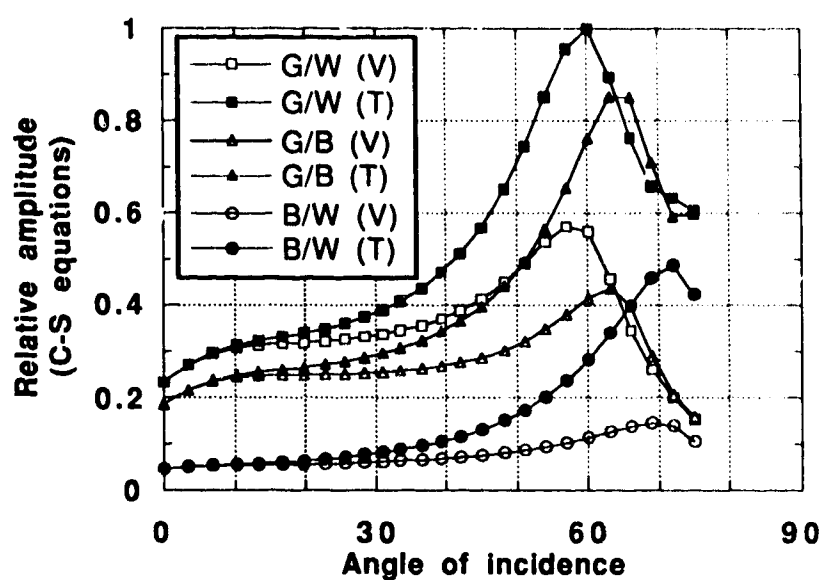
Figure 2.6.13d Relative P-P reflection amplitude extracted from finite difference solutions of the C-S system over fluid contacts of gas and water in sandstone (G/W), gas and bitumen in sandstone (G/B) and bitumen and water in sandstone (B/W). Solid symbols for total amplitude of the particle velocity and open symbols for vertical components. Beyond the critical angle the reflection interfered with headwaves.

contacts in a Cold Lake sandstone (Appendix F). Figure 2.6.13a and b are calculated with the Biot system while Figure 2.6.13c and d are the results of the C-S system. It can be seen that the gas-water contact has a slightly higher reflectivity than the gas-bitumen contact while the bitumen-water contact gives lov est reflectivity. All the curves of reflection coefficients monotonically increase with angle of incidence (Figure 2.6.13a and c). The solid particle amplitude curves also have a different pattern from those of the reflections from the shale-sandstone interface. All of the vertical and total amplitude curves for the solid particle velocity of the reflections from the gas-water, gas-bitumen and bitumen-water contacts generally increase with the angle of incidence (Figure 2.6.13b and d). The decrease in amplitude at large incident angle is related to the interference between reflection and head waves beyond the critical angles.

Field example

The methods of finite difference simulation of seismic waves in porous media described in this chapter are applied in modeling the seismic surface experiments over a thermally enhanced oil recovery (EOR) region. The largest, and potentially the most valuable, of Alberta's subsurface mineral deposits is the crude oil in buried oil sands deposits. Since only 7% of these deposits are accessible to surface mining, a large amount of research and many pilot plant studies are being carried out to examine the recovery of the oil through *in situ* methods. Most of these involve the application of heat to reduce the viscosity of bitumen so it may be pumped to the surface. In a steam injection project the steam is injected at pressures higher than the ambient formation pressure to increase the reservoir temperature in order to mobilize the heavy oil. It is always difficult to know the geometry of the heated zone. Drilling is very expensive and not always conclusive about the properties of the heated zone since the act of drilling disturbs the fluids and the strata. The measured effects of temperature and pressure on the elastic velocities strongly suggest that

it may be possible for a seismic survey to monitor thermal fronts in EOR projects Wang and Nur (1988) showed experimentally that by increasing the temperature from 20° to 120°C the compressional and the shear velocities decrease by 10%-60%. Crosshole seismic experiments have proven (Macrides, Kanasewich and Baratha 1988) to be useful tools in imaging steam-heated rocks since they can provide moderate resolution remote sensing of the anomalous zone. Hole to hole seismic measurements are expensive and a more cost effective procedure is to monitor with near surface sources and receivers. Before the field procedures are attempted it is useful to carry out computer simulation studies on various methods of carrying out the field procedures and also to develop methods for the interpretation of complex field data. The seismic modeling of a seismic surface survey over a EOR region based on finite difference soluti ns to the elastic wave equations was conducted by Dai et al. (1990). However, in the elastic simulations, no direct relationships were established between the seismic characteristics and the reservoir characteristics, such as the porosity and the bulk model of the fluid content in the pores etc..

Several seismic experiments have been conducted by ESSO Resources Canada for monitoring steam injection projects in the Cold Lake area. The computer simulations assist in the interpretation of the real data where the models are modified until a reasonable match is obtained between the field and the synthetic seismograms. In the following simulations synthetic seismograms are obtained by solving the Biot system using the finite difference method.

At Cold Lake the heavy oil or bitumen is contained in various sands of the lower Cretaceous Mannville group which averages 210 m in thickness. The Mannville group is subdivided into the McMurray, Clearwater, and Grand Rapids formations. The McMurray formation is up to 60 m thick and charaterized by a continuous basal sand section and an upper zone of thinner sands intersected with shales. The basal McMurray sands are mainly water bearing with upper thin sands containing minor amounts of bitumen when adequately

structured. The Clearwater formation, which consists mainly of highly saturated sands, is the target layer for most seismic surveys. It occurs at depths of 425-450 m having an approximate thickness of 50 m and an average porosity of 30% - 35%. The bitumen contained in the Clearwater formation accounts for approximately one-half of the total heavy oil reserves at the Cold lake area. The Grand Rapids is up to 100 m thick and primarily consists of thin sands imbedded with shales. Geological and geophysical descriptions of the Cold Lake region have been given by Harrison et al (1981) and Kanasewich (19ᵃᵃ).

In the present study, computer simulations of the Cold Lake models are carried out in order to examine the effects of the medium's porosity and the fluid contents on the wave amplitudes and velocites hence the arrival time of the seismic waves and to confirm the capability of surface seismic serveys in monitoring the EOR procedure. A simplified Cold Lake earth model with a steam heated zone is illustrated in Figure 2.6.14. The steam zone is considered along with a heated bitumen transition region. The P wave velocities and the porosities for each layer are indicated within the model. The maximum width of the steam zone is 150 m. The steam zone is truncated at the top by a shale layer whose porosity is 0.01 above the Clearwater sandstone with porosity of 0.33. The physical parameters of the model are given in Appendix G.

In the computer simulation with the finite difference method the time step is 0.25 ms, the grid spacing is 3.5 m and the dominant frequency of the Gaussian line source is 40 Hz. Figure 2.6.15 illustrates the seismic response during the process of steam injection. Figure 2. 6.15a shows the synthetic seismogram of a shot gather before the steam injection and Figure 2.6.15b shows the synthetic seismogram of a shot gather after the steam injection with the seismic source located above the center of the steam zone. The synthetic seismogram before injection (Figure 2.6.15a) shows regular P-P reflections as well as converted P-S reflection. As in real cases, no slow P wave phase is present because
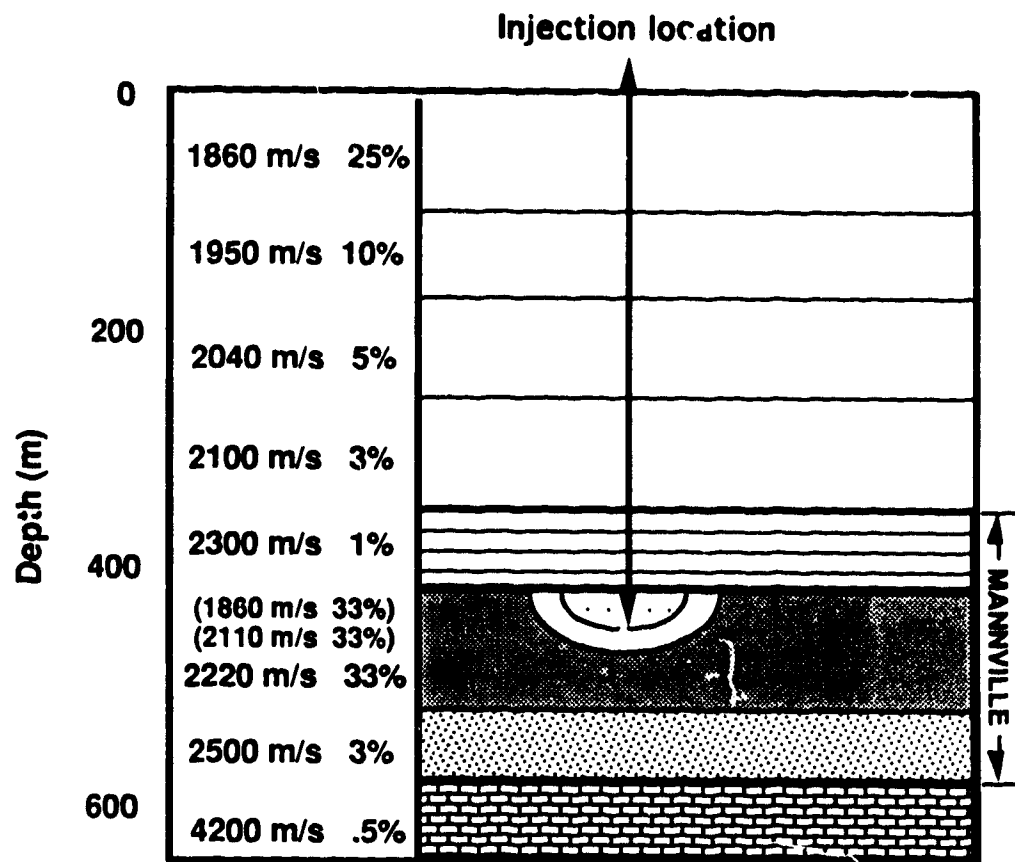
Figure 2.6.14. The Cold Lake depth model with a steam heated zone used for calculating synthetic seismograms. The fast P wave velocity and porosity of each layer are given in the left column; more physical parameters are given in Appendix G.
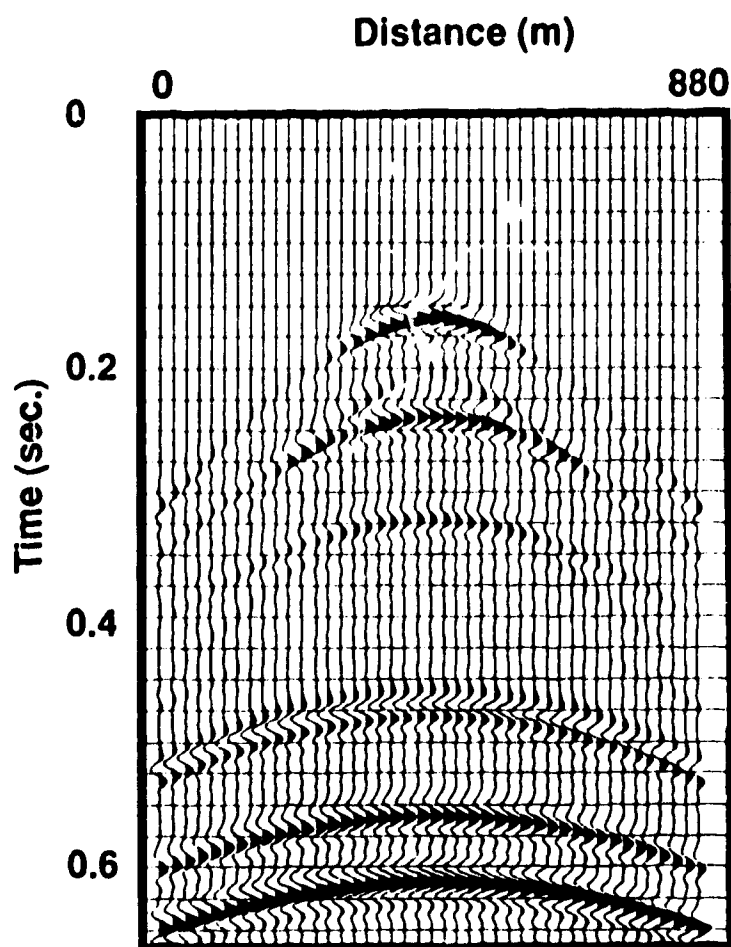
Figure 2.6.15a Synthetic seismic shot gather obtained from a finite difference solution

Biot equations for the model in Figure 2.6.14 before steam injection.
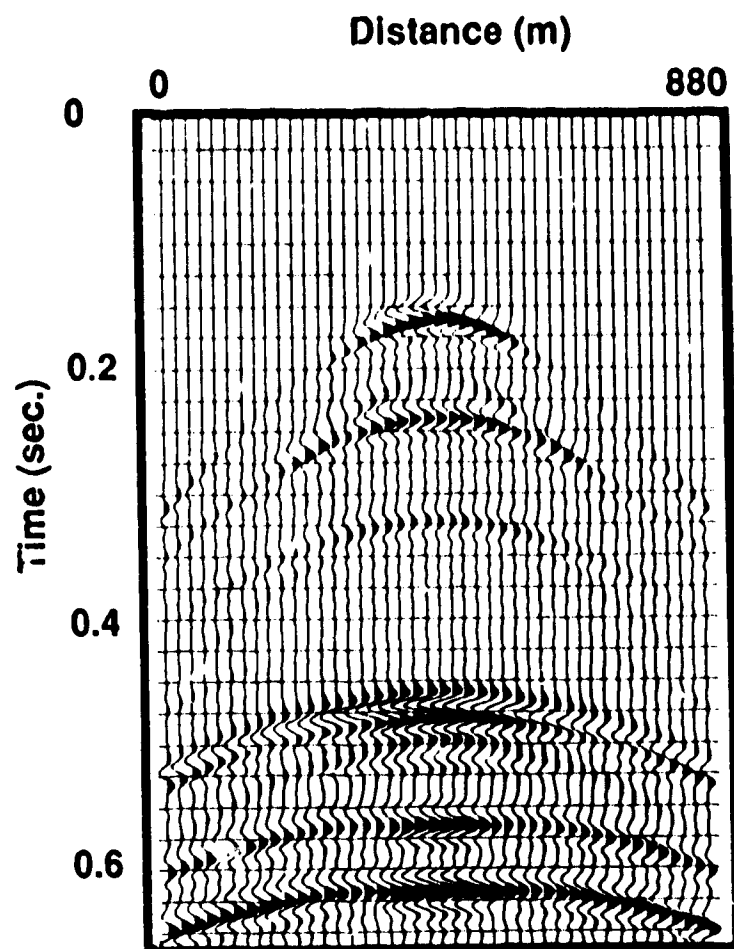
Figure 2.6.15b Synthetic seismic shot gather obtained from a finite difference solution o

Biot equations for the model in Figure 2.6.14 after steam injection.
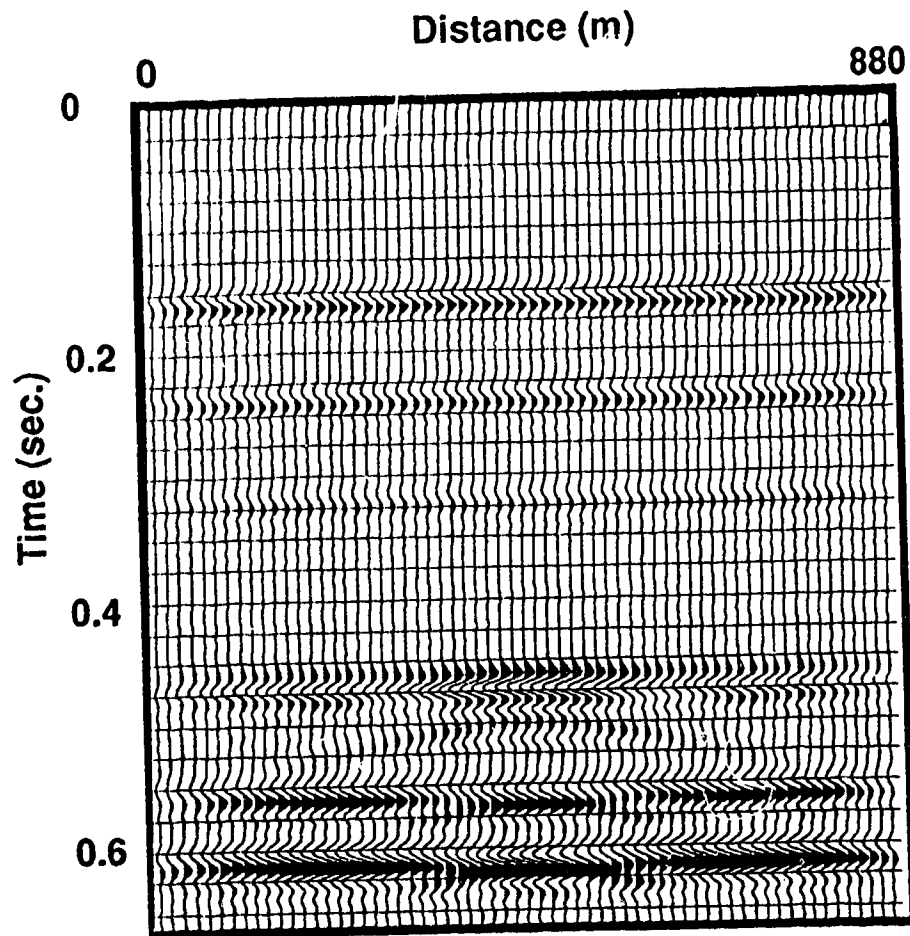
Figure 2.6.16 Synthetic zero-offset seismic section obtained from a finite difference solution of Biot equations for the model in Figure 2.6.14 after steam injection.

Distance **Steam injection location**

0 m (SE)   **982 m (NW)**

Injection level   Cold Lake Line 82
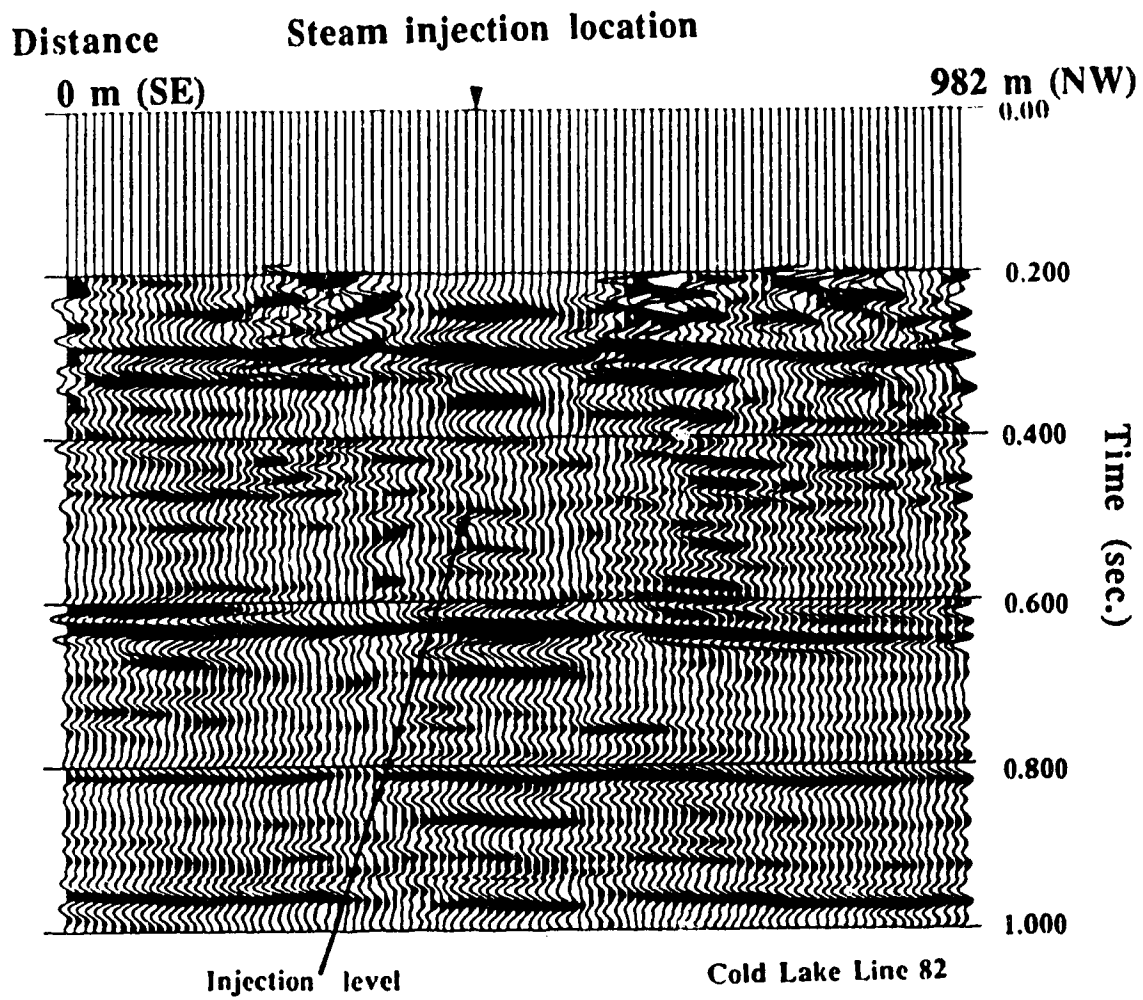
Figure 2.6.17 Common midpoint stack section obtained by Esso in a steam injection site near Cold Lake, Alberta, February 1984.

of its high attenuation property. The reflection at about 0.45 s. which comes from the interface between shale and bitumen saturated sandstone has a phase opposite to the others because the upper shale layer has higher velocity than the lower bitumen saturated sandstone layer. The synthetic seismogram after injection (Figure 2.6.15b) shows the reflection and diffraction waves from the steam zone in addition to the reflections present in Figure 2.6.15a. The reflection from the top of the steam zone shows stronger amplitude since the the fluid content (bitumen) in the Clearwater sandstone is replaced by steam and heated bitumen. It is also observed that the two reflections from the interfaces below the steam zone have been delayed which is attributed to the low velocity of the steam zone.

Forward modeling of zero offset seismic response is calculated by positioning a series of sources and receivers along the surface. The computed zero offset section (Figure 2.6.16) shows strong reflection from the top of the steam zone. The two lowest reflection events show a discontinuity due to the parts below the steam zone being delayed and the interference with the diffractions from the steam zone. The simulated section is compatible with the common-mid-point stack section of field data (Figure 2.6.17) which was obtained by Esso in a steam injection site near Cold Lake, Alberta, February 1984. Relative amplitude processing has been performed on the data. The section shown in Figure 2.6.16 is migrated with a new method described in Chapter 5. The migrated section properly images not only the steam zone but also the interfaces below the steam zone (see Figure 5.5.7) demonstrating the capability of the seismic reflection method in monitoring the thermally enhanced oil recovery (EOR) process.

2.7   CONCLUSION

An explicit, heterogeneous, high order finite difference method has been developed for the simulation of seismic waves propagating in inhomogeneous porous media. The simulation is based on the first order hyperbolic systems which are formulated from the Biot and de la Cruz-Spanos theories. This formulation enables one to obtain not only the particle velocity fields of the solid and fluid motion but also the solid stress and fluid pressure wave fields and to model the seismic response of a heterogeneous medium without introducing numerical approximations of the space derivatives of the physical parameters. Biot's equations and the C-S equations are analytically solved for point and line sources with the source force acting on both solid and fluid materials and generating a fast and a slow P-wave in a uniform porous medium.

Numerical solutions of Biot's equations and the C-S equations for simple earth model show similar features of the wave motion in porous media. Additional slow P-wave propagation can be observed in the synthetic seismograms when very low fluid viscosity is used, although the slow P-wave is not generally observable in the real world. Attenuation is more pronounced for the slow P-wave. This is in accordance with Biot's theory and the de la Cruz-Spanos theory where the attenuation is related to viscous dragging or to solid and fluid interactions. This attenuation mechanism, however, is of secondary importance for fast P-waves and for S-waves. In porous medium modeling, more rock properties of geophysical and petrophysical interests, such as porosity, fluid density, fluid bulk modulus and fluid viscosity, are taken into account in calculating the seismic response. The realistic examples and the studies of reflectivity variation versus angle of incidence over interfaces of different rock types and different fluid contents indicate the application potential of this method in seismic diagnosis of the rock type and fluid content.

CHAPTER 3

ABSORBING BOUNDARIES FOR THE NUMERICAL SIMULATION OF SEISMIC WAVES IN ELASTIC AND POROUS MEDIA

3.1 INTRODUCTION

First order hyperbolic systems of wave equations have been used to simulate seismic waves in elastic media (Virieux 1984, 1986; Bayliss et al. 1986; Vafidis et al. 1992) and porous media (Dai et al., 1992a, b) with a finite difference scheme in the time-space domain. Using the first order systems for forward modelling enables one to obtain not only the particle velocity but also the stress of the wave fields. In addition, a properly formulated first order system, in which each of the coefficient matrices relates to the mechanical properties of the medium in one spatial direction, makes it easy to deal with the complexity due to the anisotropy of the medium.

Numerical solutions to the problems involving wave propagation must be obtained over a finite region due to the limitation of computer memory size. The time evolution of the wave fields are governed not only by the state in the interior of the region but also by the waves entering the region through the boundaries. Therefore boundary conditions which describe the incoming waves should be specified to complete the description of these problems. In seismic modelling it is assumed that there is no energy coming from the area outside the region of computation. Then, the solution at the boundaries consists of

outgoing waves. It is desirable to impose non-reflecting or absorbing conditions which have the property of minimizing wave propagation from the boundaries.

A widely used absorbing condition in seismic wave modelling was proposed by Clayton and Enquist (1977). They used the one-way wave equations based on the paraxial approximations of the acoustic or elastic equations. Related material is given by Engquist and Majda (1977). Another popular algorithm of this type was proposed by Reynolds (1978). The effectiveness of these boundary conditions is limited for large angles of wave incidence to the artificial boundary. Instabilities associated with paraxial approximation methods for certain values of Poisson's Ratio were reported by Emerman and Stephen (1983), Mahrer (1986), and Stacey (1988). A more recent paraxial method for acoustic wave modeling has been developed by Keys (1985) and independently by Higdon (1986,1987) who used a product of one-way wave equations at the boundary. Higdon (1991) further extended his method for elastic waves. These methods all break down for surface waves and headwaves impinging on the model edges. Scandrett et al. (1986) used a first-order boundary condition to absorb Rayleigh waves near a free surface of an elastic medium. Cerjan et al. (1985) proposed a method by applying a simple spatial filter or sponge which is based on enlarging the computational domain and using a damping mechanism on the additional portion of the domain. Further discussion and extension are given by Kosloff and Kosloff (1986) and a similar approach was developed by Sochacki et al. (1987). In these methods the sponge effect must be applied smoothly over a transition zone of three to five wavelengths in thickness to avoid artificial scattering from the the sponge itself. Because of this extension of the computational domain, the sponge boundary conditions are more applicable with large memory supercomputers. The implementations of most of these methods are designed for second order wave equations. Hedstrom (1979) developed a non-reflecting boundary condition for one dimensional first order nonlinear hyperbolic systems and Thompson (1987) generalized it to multidimensional problems. A

thorough review of non-reflection boundary conditions is given by Kelly and Marfurt (1990).

A comprehensive description of the various damping mechanisms which allow the simulation of radiation problems in finite regions was given by Israeli and Orszag (1981). They also discussed the method of propagation modifications and they proposed a sponge filter for the approximation of one dimensional wave propagation problems.

In this development, we consider the imposition of absorbing boundary conditions for first order hyperbolic systems of which those describing seismic wave propagation in two dimensional elastic or porous media are special cases. We use the one dimensional absorbing boundary conditions which are based on the characteristic analysis of the hyperbolic systems and absorb the waves impinging on the boundaries perpendicularly. Two wave field modification approaches are employed in narrow transition zones near the boundaries. A wave propagation modification method is used to adjust the travelling directions of the waves so that they reach the boundaries at a right angle. A one-way sponge filter method gives a dissipation mechanism to the transition zone, which selectively damps the remaining incoming waves without affecting the outgoing waves. The combination of the one dimensional absorbing boundary conditions with either of these two approaches effectively absorbs not only the body waves but also the surface waves. These methods are efficient and robust. They are specially suited to problems involving multiple types of propagating waves. These methods are utilized in Chapter 2 for seismic wave simulation in porous media where "slow" P waves may be present in addition to the regular ("fast") P waves and S waves. Numerical examples are given in this chapter for P-SV wave propagation simulations in elastic media.

3.2   ONE DIMENSIONAL ABSORBING BOUNDARY CONDITIONS

The two dimensional seismic wave behavior in elastic and porous media can be described by a first order differential system

$$\frac{\partial u}{\partial t} = A\frac{\partial u}{\partial x} + B\frac{\partial u}{\partial z} + C\ u\ ,$$

(3.2.1)

where A, B and C are $n \times n$ coefficient matrices; u is a vector whose components consist of n dependent variables, such as the components of the particle velocity and the stress. Matrices A and B have n real eigenvalues with n independent eigenvectors. The elements of matrices A and B are given by the elastic properties of the medium in the x-direction and z-direction, respectively. The matrix C represents an inhomogeneous term (which often arises from wave-dissipation related properties). These matrices can be space coordinate dependent for heterogeneous media. To solve system (3.2.1) by a finite difference method in the space-time domain, special treatment at the computational boundaries is required to minimize the incoming waves from artificial boundary reflections. Difficulty arises in boundary condition specification since both incoming and outgoing waves are propagating at the boundaries.

It is easy, however, to isolate the wave characteristics propagating in the opposite directions for the one-dimensional problem, for instance in the z-direction:

$$\frac{\partial u}{\partial t} = B\frac{\partial u}{\partial z} + C\ u\ .$$

(3.2.2)

Let $u(z,t)$ be a solution of equation (3.2.2), and suppose that for $z \in (0, H)$, the

computational region, λ_i is an eigenvalue of **B** with the corresponding left eigenvectors $l_B^{(i)}$ (a row vector) and the right eigenvectors $r_B^{(i)}$ (a column vector). Then

$$l_B^{(i)}\mathbf{B} = \lambda_i l_B^{(i)} ,$$

(3.2.3)

$$\mathbf{B}r_B^{(i)} = \lambda_i r_B^{(i)} .$$

(3.2.4)

Because of the orthonormality of left and right eigenvectors we have

$$l_B^{(i)} r_B^{(j)} = \delta_{ij} .$$

(3.2.5)

It follows from equation (3.2.3) and (3.2.4) that

$$\mathbf{L}_B\mathbf{B}\mathbf{R}_B = \Lambda ,$$

(3.2.6)

where the rows of the matrix $\mathbf{L}_B$ are the normalized left eigenvectors $l_B^{(i)}$, the columns of the matrix $\mathbf{R}_B$ are the normalized right eigenvectors $r_B^{(i)}$, and the matrix Λ is diagonal, with $\Lambda_{ii} = \lambda_i$, ordered so that $\lambda_1 \leq \lambda_2 ... \leq \lambda_n$.

It follows from the linear transformation $\mathbf{w} = \mathbf{L}_B \mathbf{u}$ that equation (3.2.2) becomes

$$\frac{\partial \mathbf{w}}{\partial t} = \Lambda \frac{\partial \mathbf{w}}{\partial z} + \mathbf{C}^*\mathbf{w},$$

(3.2.7a)

where $\mathbf{C}^* = \mathbf{L}_B\mathbf{C}\mathbf{R}_B$, or in component form

$$\frac{\partial w_i}{\partial t} = \lambda_i \frac{\partial w_i}{\partial z} + \sum_{j=1}^{n} C_{ij}^* w_j \qquad (i=1,....n),$$

(3.2.7b)

provided that **B** is spatially independent. Equation (3.2.7) is the standard form of the first order hyperbolic system with an inhomogeneous term. If $C = 0$, equation (3.2.7b) becomes

$$\frac{\partial w_i}{\partial t} = \lambda_i \frac{\partial w_i}{\partial z} , \tag{3.2.8}$$

which is a set of elastic wave equations for waves traveling at the characteristic velocity $-\lambda_i$. Three different situation are possible. For $\lambda_i < 0$, the wave given by w_i travels in the positive z-direction (down in geophysical convention), which is the incoming wave at $z = 0$, the top boundary and is the outgoing wave at $z = H$, the bottom boundary. For $\lambda_i > 0$, w_i travels in the negative z-direction (or up), the outgoing wave at the top boundary and is the incoming wave at the bottom boundary.

At the boundaries the outgoing waves depend on the information at and within the boundaries. Therefore they can be found from a properly designed numerical approximation of the solution of equation (3.2.2), such as a one-sided finite difference method involving only interior and boundary points. To let the incoming waves at the boundaries vanish, for general cases, we can specify the absorbing boundary conditions as

$$w_i = 1_B^{(i)} \mathbf{u} = 0 , \tag{3.2.9}$$

if λ_i corresponds to an incoming wave. Equation (3.2.9) is the equivalent form of the absorbing condition given by Hedstrom (1979) (also see Tompson, 1987)

$$\left. \left(\frac{\partial w_i}{\partial t} \right) \right|_{z = 0, H} = 0 , \tag{3.2.10}$$

which implies that the amplitude of the incoming wave w_i is constant in time at the boundaries. Since we assume an initial state of equilibrium at the boundaries, condition (3.2.9) ensures that there are no waves coming from the boundaries.

If we denote u_I as the values of u at the boundary calculated by a certain numerical scheme using interior points, then the above discussion leads to the implementation of the absorbing boundary condition (3.2.9) by letting

$$l_B^{(i)} u(t) = 0 , \qquad \text{(for the incoming waves)}$$

$$\text{(3.2.11)}$$

$$l_B^{(i)} u(t) = l_B^{(i)} u_I(t), \qquad \text{(for the others)}$$

at the boundaries. At the bottom boundary $(z = H)$, for instance, if $\lambda_i > 0$, for $i = r+1, ..., n$, then we can write

$$L_B u(t) = g_I \qquad \text{(3.2.12)}$$

where

$$g_I = \begin{bmatrix} l_B^{(1)} u_I(t) \\ \vdots \\ l_B^{(r)} u_I(t) \\ 0 \\ \vdots \\ 0 \end{bmatrix}. \qquad \text{(3.2.13)}$$

We can therefore determine the values of the variables at the boundary by solving equation

(3.2.12). It follows that

$$u(t) = R_B g_i \qquad (3.2.14)$$

at the bottom boundary.

A straightforward extension of the problem from one dimension to two dimensions for the commonly used rectangular models can be made by simply applying system (3.2.14) to the boundary of $z = H$, and applying its analogous forms to the other boundaries.

This idea was first applied by Bayliss et al. (1986) to the two dimensional P-SV elastic wave modelling. It is theoretically obvious that this method can only absorb the reflections of waves which impinge at the artificial boundaries perpendicularly. When a free surface boundary condition is applied to the top boundary, Bayliss et al. (1986) claimed that this simple extension does not absorb the Raleigh waves.

3.3 WAVE FIELD MODIFICATION APPROACHES

In order to improve the absorption of the outgoing waves Israeli and Orszag (1981) suggested modifying the propagation characteristics of the waves near the boundaries. They examined the one dimensional scalar wave equation and found that the artificial reflection can be effectively decreased by smoothly modifying the wave speed as the space coordinates approach the boundaries to match the approximate absorbing boundary conditions applied.

This concept of wave propagation modification can be effectually generalized to multi dimensional problems. In this development we adjust the wave propagation directivity and the non-derivative term in a transition strip adjacent to a boundary so that the outgoing

waves at the boundary are described by the wave equation with a zero inhomogeneous term and impinge the boundaries perpendicularly. Then the one dimensional absorbing boundary conditions can be effectively applied to the corresponding boundaries. Our numerical experiments show that this method absorbs successfully not only the body waves but also the surface waves.

Taking the bottom boundary for an example, we introduce a transition zone of thickness L on the top of the boundary. In the transition zone the wave equation (3.2.1) is modified to

$$\frac{\partial u}{\partial t} = m(z) \, A \frac{\partial u}{\partial x} + B \frac{\partial u}{\partial z} + m(z) \, C \, u \, ,$$ (3.3.1)

where $m(z)$ is a smooth monotonic function introduced to impose the propagation modification. When $m(z) = 1$, equation (3.3.1) is exactly equation (3.2.1) while $m(z) = 0$, equation (3.3.1) is modified into the one dimension form (3.2.2) with the inhomogeneous term equal to zero. We choose

$$m(z) = \frac{1}{2} + \frac{1}{2} \cos\left(\frac{z - H + L}{L} \pi\right) \qquad z \in (H - L, H)$$ (3.3.2)

for a given L, so $m(H-L) = 1$ and $m(H) = 0$.

The eigenvalues of the coefficient matrix $m(z)$ A, which are the characteristic velocities in the x components are now given by $m(z)$ λ_i. Thus the transition zone is an anisotropic layer in which the characteristic velocities in the x-direction change smoothly to zero while z approaches H. Therefore the outgoing waves are vertically incident on the bottom boundary and the imposition of the absorbing boundary condition according to equation (3.2.14) will effectively reduce the artificial reflections from the boundary. The only energy returning to the modelling region comes from the reflections due to the horizontal

velocity change in the transition zone. These reflections are controlled by the smoothness of the function $m(z)$. When equation (3.3.2) is used, we find that l equal to one wavelength for the peak frequency gives very satisfactory results.

Another way to minimize the incoming reflections is to introduce a damping term in the transition zones. Having isolated the incoming and outgoing waves we can determine the proper forms of the damping terms that selectively affect the incoming waves while letting the outgoing waves leave the domain without effect. This method can be called one-way sponge filtering in order to distinguish it from the sponge method introduced by Cerjan et al (1985). Taking the bottom boundary as an example, we rewrite equation (3.2.7a) into

$$\frac{\partial w}{\partial t} = \Lambda \frac{\partial w}{\partial z} + L_B C R_B w - Dw$$

(3.3.3)

in the transition zone. Here D is a matrix of damping coefficients. To attenuate the remaining incoming waves from the bottom boundary, we choose

$$D = v(z) \begin{bmatrix} 0 & & & & & \\ & \ddots & & & & \\ & & 0 & & & \\ & & & \lambda_{r+1} & & \\ & & & & \ddots & \\ & & & & & \lambda_n \end{bmatrix},$$

(3.3.4)

where $v(z) > 0$, if $\lambda_i > 0$ for $i = r+1,...n$. An extra dissipative factor $e^{-v(z)|\Delta z|}$ is imposed on the incoming waves of each type by the additional damping term in a depth step $|\Delta z|$. Reflections are caused by the introduction of the damping coefficient $v(z)$ which changes the mechanical properties of the medium in the transition zone. However, if we let $v(z)$ vary smoothly with z, only small reflections result. One choice of $v(z)$ is given by

$$v(z) = \frac{v}{2}\left[1 - \cos\left(\frac{z - H + L}{L} 2\pi\right)\right] \qquad z \in (H - L, H) , \qquad (3.3.5)$$

which vanishes at the edges of the transition zone.

Multiplying equation (3.3.3) by $\mathbf{R}_B$ gives

$$\frac{\partial \mathbf{u}}{\partial t} = \mathbf{B}\frac{\partial \mathbf{u}}{\partial z} + \mathbf{C}_D\mathbf{u} , \qquad (3.3.6)$$

where $\mathbf{C}_D = \mathbf{C} - \mathbf{R}_B\mathbf{DL}_B$. Therefore it is easy to combine the selective damping term into the existing codes. Analogous selective damping terms can be obtained for the other boundaries.

3.4 EXAMPLES FOR TWO-DIMENSIONAL P-SV ELASTIC WAVES

The absorbing boundaries described in the previous section can be directly implemented in all time advance schemes for wave field modelling with first order hyperbolic systems. Here we present the numerical examples for the two dimensional isotropic elastic P-SV system. The applications in the seismic wave simulation in porous media are given by Dai et al. (1992a) for Biot's equations and Dai et al (1992 b) for the de la Cruz-Spanos equations.

In two dimensional isotropic elastic media the P-SV waves are described by the first order hyperbolic system.

$$\frac{\partial \mathbf{u}}{\partial t} = \mathbf{A}\frac{\partial \mathbf{u}}{\partial x} + \mathbf{B}\frac{\partial \mathbf{u}}{\partial z} , \qquad (3.4.1)$$

where

$$\mathbf{u} = \begin{bmatrix} u \\ w \\ \sigma_{xx} \\ \sigma_{zz} \\ \sigma_{xz} \end{bmatrix} \, , \tag{3.4.2}$$

$$\mathbf{A} = \begin{bmatrix} 0 & 0 & \rho^{-1} & 0 & 0 \\ 0 & 0 & 0 & 0 & \rho^{-1} \\ \lambda+2\mu & 0 & 0 & 0 & 0 \\ \lambda & 0 & 0 & 0 & 0 \\ 0 & \mu & 0 & 0 & 0 \end{bmatrix} \, , \tag{3.4.3}$$

and

$$\mathbf{B} = \begin{bmatrix} 0 & 0 & 0 & 0 & \rho^{-1} \\ 0 & 0 & 0 & \rho^{-1} & 0 \\ 0 & \lambda & 0 & 0 & 0 \\ 0 & \lambda+2\mu & 0 & 0 & 0 \\ \mu & 0 & 0 & 0 & 0 \end{bmatrix} \, . \tag{3.4.4}$$

Here, u, and w are the horizontal and vertical components of the particle velocity respectively while σ_{xx}, σ_{zz} and σ_{xz} denote the components of the stress. ρ, λ and μ are the density, the Lame constant and the shear modulus of the medium. Equation (3.4.1) is numerically solved by applying the dimensional splitting method with an one dimensional MacCormack type finite difference scheme which is an explicit scheme of fourth order accuracy in space and second order accuracy in time (Vafidis et al., 1992).

It is easy to show that the matrices $\mathbf{A}$ and $\mathbf{B}$ have the same eigenvalues

$$(\lambda_1, \lambda_2, \lambda_3, \lambda_4, \lambda_5) = (-V_p, -V_s, 0, V_s, V_p), \tag{3.4.5}$$

where

$$V_p = \sqrt{\frac{\lambda + 2\mu}{\rho}} \ , \qquad (3.4.6)$$

and

$$V_s = \sqrt{\frac{\mu}{\rho}} \ , \qquad (3.4.7)$$

are the P-wave and S-wave velocities respectively. The left eigenvector matrix L_B and the right eigenvector matrix R_B of the matrix B are given, respectively, by

$$L_B = \frac{1}{\sqrt{2}} \begin{bmatrix} 0 & 1 & 0 & \frac{-1}{V_p\rho} & 0 \\ 1 & 0 & 0 & 0 & \frac{-1}{V_s\rho} \\ 0 & 0 & \sqrt{2} & \frac{-\sqrt{2}\lambda}{\lambda + 2\mu} & 0 \\ 1 & 0 & 0 & 0 & \frac{1}{V_s\rho} \\ 0 & 1 & 0 & \frac{1}{V_p\rho} & 0 \end{bmatrix} , \qquad (3.4.8)$$

and

$$
\mathbf{R}_B = \frac{1}{\sqrt{2}}
\begin{bmatrix}
0 & 1 & 0 & 1 & 0 \\
1 & 0 & 0 & 0 & 1 \\
\frac{-\lambda}{V_p} & 0 & \sqrt{2} & 0 & \frac{\lambda}{V_p} \\
-V_p\rho & 0 & ' & 0 & V_p\rho \\
0 & -V_s\rho & 0 & V_s\rho & 0
\end{bmatrix} .
\tag{3.4.9}
$$

Substituting the left eigenvectors given in equation (3.4.8) into equation (3.2.13) we obtain the vector g_I which is given by

$$
g_I =
\begin{bmatrix}
\frac{1}{\sqrt{2}}\left(w^{(l)} - \frac{\sigma_{zz}^{(l)}}{V_p\rho}\right) \\
\frac{1}{\sqrt{2}}\left(u^{(l)} - \frac{\sigma_{xz}^{(l)}}{V_s\rho}\right) \\
0 \\
0 \\
0
\end{bmatrix} ,
\tag{3.4.10}
$$

where $u^{(l)}$, $w^{(l)}$, $\sigma_{zz}^{(l)}$ and $\sigma_{xz}^{(l)}$ are the values of u, w, σ_{zz} and σ_{xz} at the bottom boundary calculated by the finite difference scheme with the inner points. To impose the one dimensional absorbing boundary condition to the bottom boundary we use equation (3.2.14) and obtain

$$
\begin{bmatrix} u \\ w \\ \sigma_{xx} \\ \sigma_{zz} \\ \sigma_{xz} \end{bmatrix} = \frac{1}{2}
\begin{bmatrix}
0 & 1 & 0 & 1 & 0 \\
1 & 0 & 0 & 0 & 1 \\
\frac{-\lambda}{V_p} & 0 & 1 & 0 & \frac{\lambda}{V_p} \\
-V_p\rho & 0 & 0 & 0 & V_p\rho \\
0 & -V_s\rho & 0 & V_s\rho & 0
\end{bmatrix}
\begin{bmatrix}
w^{(l)} - \frac{\sigma_{zz}^{(l)}}{V_p\rho} \\
u^{(l)} - \frac{\sigma_{xz}^{(l)}}{V_s\rho} \\
0 \\
0 \\
0
\end{bmatrix} . \qquad (3.4.11)
$$

For a one-way sponge filter an additional term $\mathbf{C}_D\mathbf{u}$ is to added to the right hand side of equation (3.4.1) in a transition zone on the top of the bottom boundary, where

$$
\mathbf{C}_D = \mathbf{R}_B\mathbf{D}\mathbf{L}_B . \qquad (3.4.12)
$$

From equations (3.3.4), (3.4.2), (3.4.5) and (3.4.12) we have

$$
\mathbf{C}_D\mathbf{u} = \frac{1}{2} v(z)
\begin{bmatrix}
V_s u + \frac{\sigma_{xz}}{\rho} \\
V_p w + \frac{\sigma_{zz}}{\rho} \\
\lambda u_z + \frac{\lambda\sigma_{zz}}{V_p\rho} \\
V_p^2\rho u_z + V_p\sigma_{zz} \\
V_s^2\rho u_x + V_s\sigma_{xz}
\end{bmatrix} \qquad (3.4.13)
$$

with $v(z)$ given in equation (3.3.5).

The performance of the absorbing boundaries is illustrated by a two dimensional two layer model of which the physical parameters are given in Table 3.4.1. The modelling region is a 900 m square with a uniform grid spacing of 3 m.

For the first case, absorbing boundary conditions are imposed on all the margins of the computational domain to simulate an infinitely extended model. The interface is positioned 550 m below the top margin. A line source of pure P waves is located in the upper layer 250 m above the interface. The time function of the source is of Gaussian form with a peak frequency of 30 Hz. The receivers are placed along the line running through the source and parallel to the interface.

Figure 3.4.1a displays the resulting seismograms for the vertical component of particle velocity when only the one dimensional absorbing boundary is implemented with equation (3.4   )r the bottom boundary and its analogous forms for the others. Prominent artificial reflections are observed since only the perpendicularly impinging waves are absorbed at the boundaries. Figure 3.4.1b is an enlarged trace from Figure 3.4.1a, which shows how the quality of the synthetic record has deteriorated.

Figure 3.4.2a shows the improvement of the seismogram by applying the one-way sponge filters in combination with the one dimensional absorbing boundary conditions. The width of the transition zone L is equal to 120 m which is less than the peak wavelength of 133 m and the damping coefficient v in equation (3.3.4) is chosen to be 0.025/m. The seismogram shows weak artifacts on the reflections recorded in the transition zone in the use of the one-way sponge filters (the first and last 8 traces). Figure 3.4.2b can be compared to Figure 3.4.1b showing that the artificial reflections have been reduced.

The effectiveness of wave propagation modification is illustrated in Figure 3.4.3 which exhibits the receiver output between 105 m and 795 m from the left boundary. The traces

are of high quality and the artificial reflections are very weak as seen on the enlarged trace in Figure 3.4.3b which is recorded at the same location as those in Figure 3.4.1b and 3.4.2b.

Table 3.4.1 Physical parameters of a two layer elastic model

	Layer 1		Layer 2	
depth (m)	250.			
r (kg/m^3)	2300.0		2500.0	
λ (Pa)	0.69E10		1.33E10	
μ (Pa)	0.69E10		1.33E10	
V_p (m/s)	3000.0		4000.0	
V_s (m/s)	1732.1		2309.4	
	case 1	case 2	case 1	case 2
depth (m)	0	0	550	250
source depth (m)	250	15		

The second case, as shown in Table 3.4.1, is for a two layer model in a half space with a free surface at the top margin of the computational domain. The interface is now at a depth of 250 m. The source is located 15 m below the surface.

When only the one dimensional absorbing boundary conditions are employed on the other boundaries, strong artificial reflections of the Raleigh wave are observed among the others as shown in Figure 3.4.4. In contrast, the combination of the wave propagation modification technique and the one dimensional absorbing conditions absorbs both surface
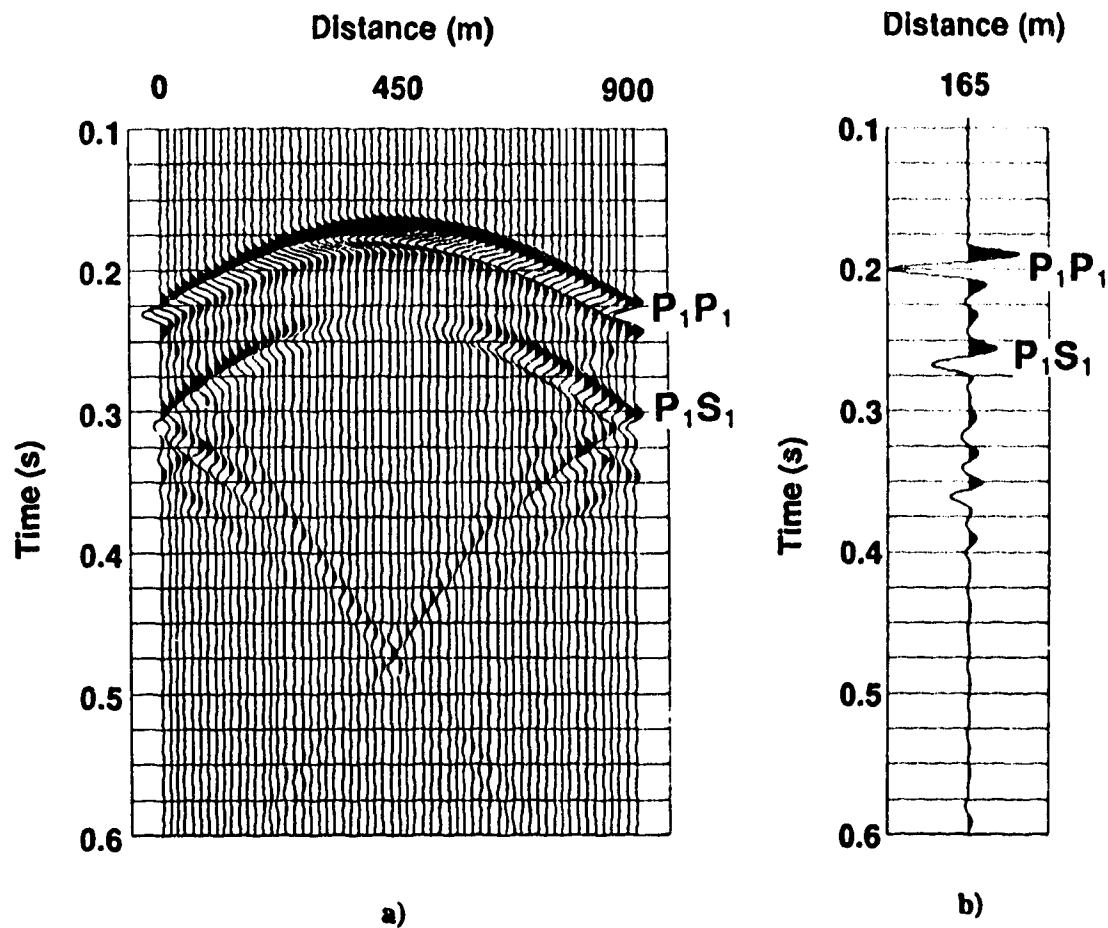
Figure 3.4.1 (a) Seismogram for a two layer elastic model with the one dimensional absorbing boundary conditions imposed on all the computational margins. (b) An enlarged trace from (a).
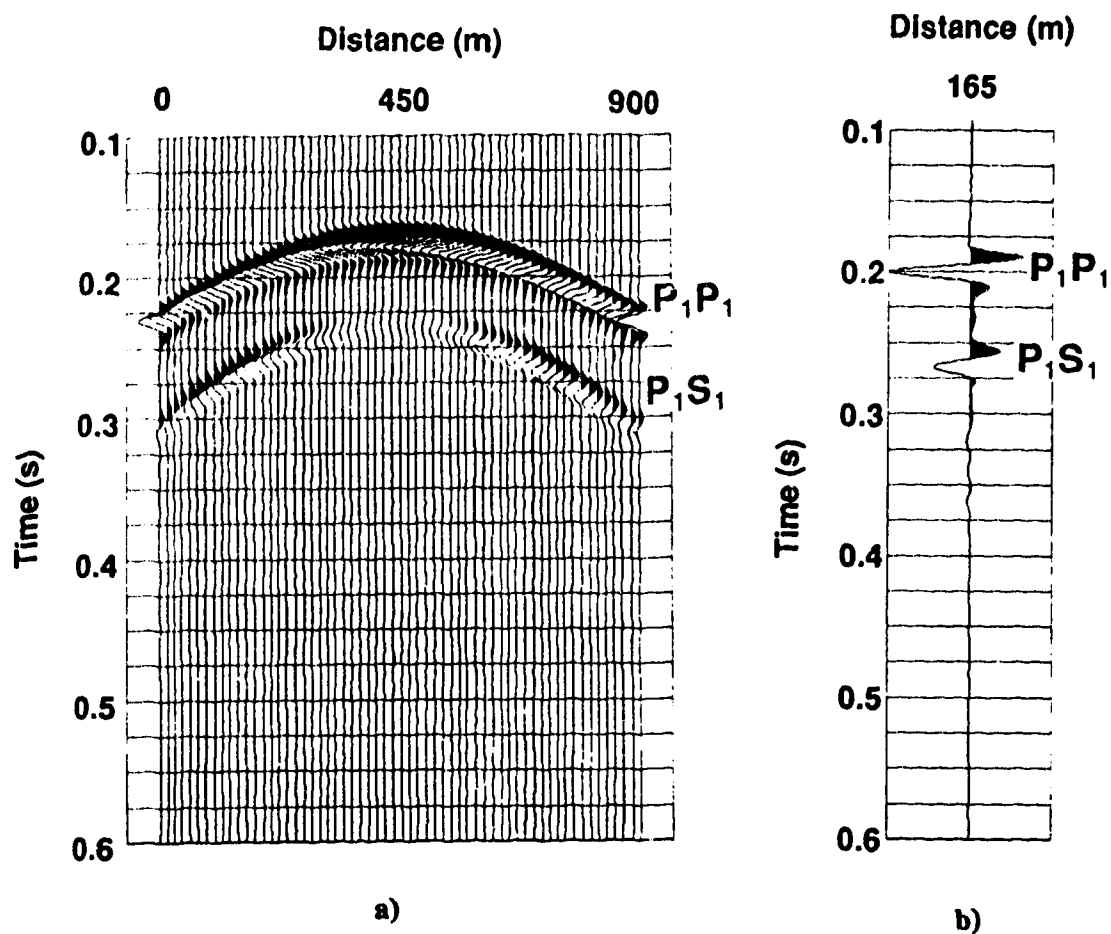
Figure 3.4.2 (a) Seismogram for the same two layer elastic model. The one-way sponge filter approach is applied to all computational margins in combination with the one-dimensional absorbing boundary conditions. (b) An enlarged trace from (a).

Distance (m)

105   450   795

0.1

0.2 P_1P_1

P_1S_1

0.3

Time (s)

0.4

0.5

0.6

a)

Distance (m)

165

0.1

0.2 P_1P_1

P_1S_1

0.3

Time (s)

0.4

0.5

0.6

b)
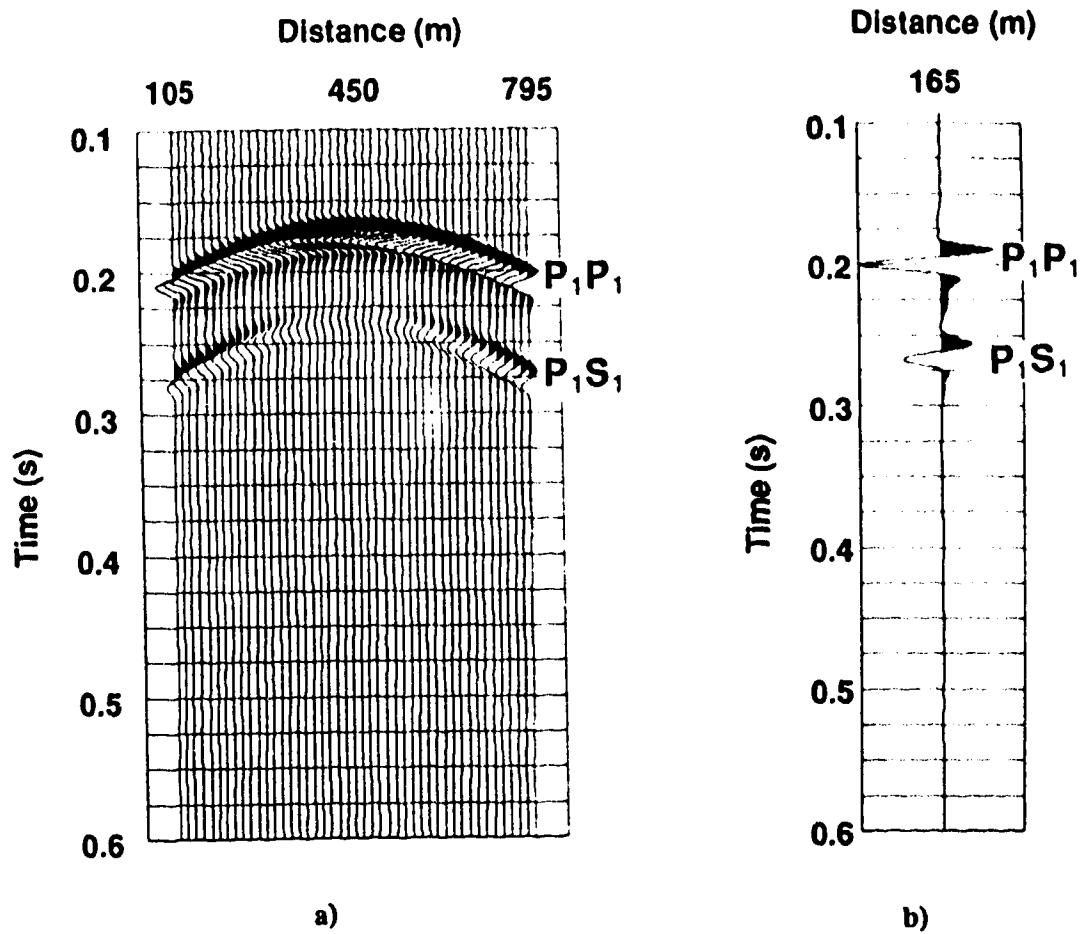
Figure 3.4.3 (a) Seismogram for the same two layer elastic model. The wave propagation modification approach is applied for all computational margins in combination with the one-dimensional absorbing boundary conditions. (b) An enlarged trace from (a).

and body waves effectively as shown in figure 3.4.5. This yields high quality synthetic seismograms with surface waves and multiple reflections in addition to primary reflected events.

The one-way sponge filter has also been tested on the surface waves. It gives satisfactory results too. It is yet possible to combine the wave propagation modification and the one-way sponge filter approaches in the same transition zone. Very little more is gained with this method and it does not appear to be cost effective.

For the one-way sponge filter the selection of an optimum damping coefficient v is important in order to obtain effective dissipation of the incoming waves and to avoid the extra reflections from the transition zone. The one-way sponge filter d es not introduce significant distortion in the outgoing waves. In contrast, the wave propagation modification approach is more efficient since it requires almost no extra computational time although the information is degraded in a transition zone whose width is less than a wave length.

3. 5   CONCLUSION

In this chapter, sevaral approaches are proposed for the construction of absorbing boundaries for numerical simulation of seismic waves in nonporous or porous media with first order hyperbolic systems. When the one dimensional absorbing boundary conditions are combined with a one-way sponge filter or wave propagation modification approach, it absorbs effectively all incident waves without imposing local conditions. The one-way sponge filter does not introduce significant distortion of the outgoing waves while the wave propagation modification approach is more robust. A combination of these two modifying approaches is possible but it seems not necessary. Comparisons of the new absorbing
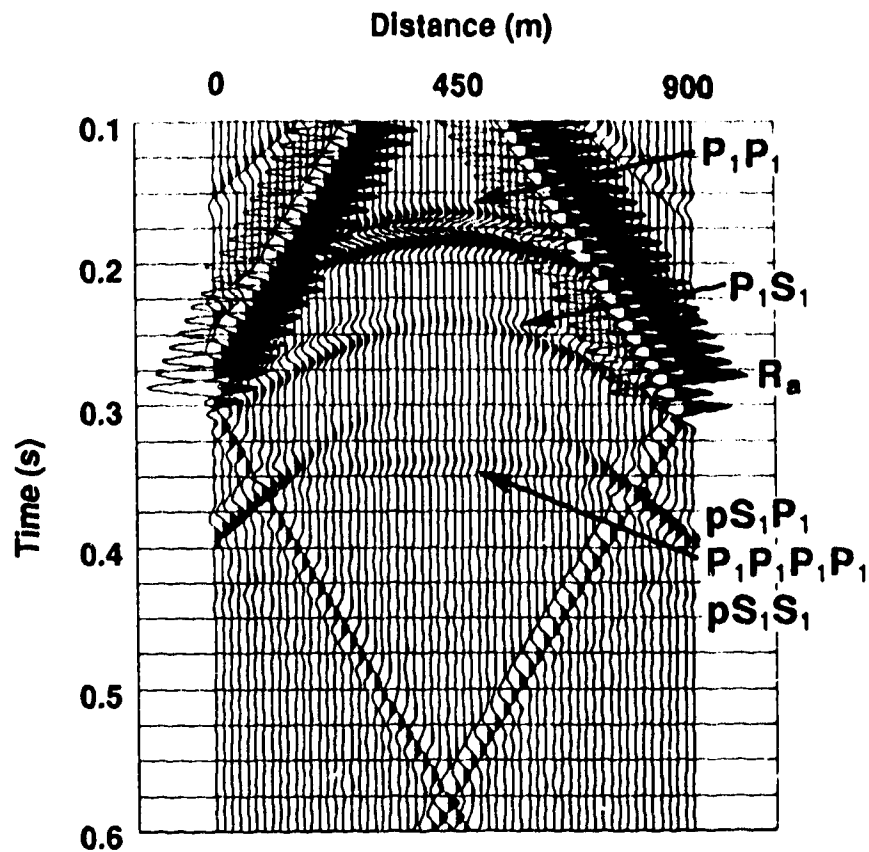
Figure 3.4.4 (a) Seismogram for the same two layer elastic model but the top margin of the computational domain being a free surface. The one dimensional absorbing boundary conditions are imposed on all other computational margins.
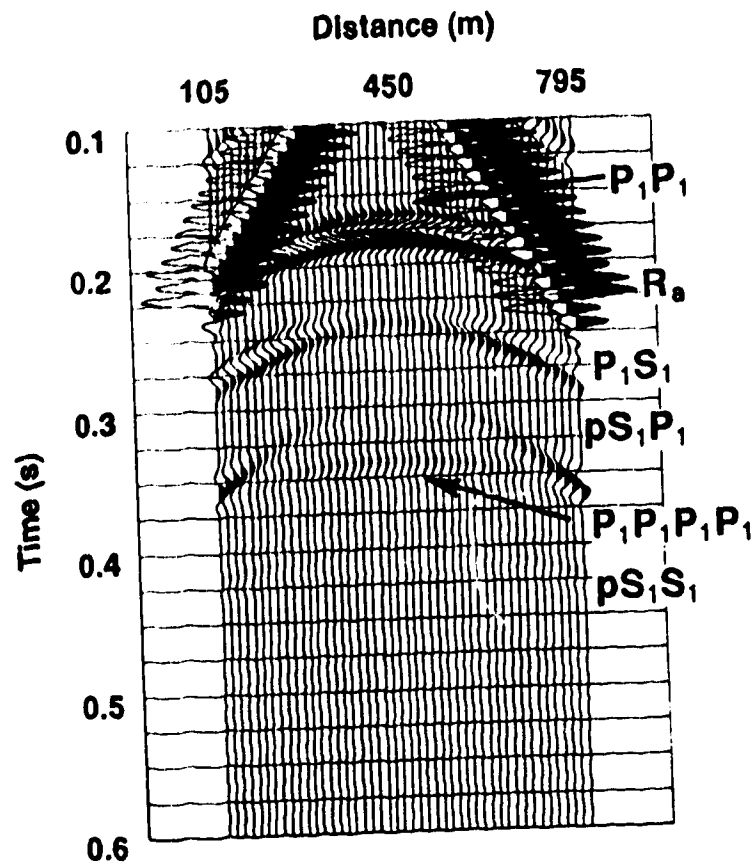
Figure 3.4.5 (a) Seismogram for the same two layer elastic model as for Figure 3.4.4. The wave propagation modification approach is applied for all other computational margins in combination with the one-dimensional absorbing boundary conditions.

boundary approaches with the existing ones indicate its superiority. The extension of these methods to three dimensions is straightforward.

CHAPTER 4

WAVE PROPAGATION IN VISCOACOUSTIC HETEROGENEOUS MEDIA

4.1 INTRODUCTION

Considerable progress has been made during the past two decades on aspects of seismic attenuation. By seismic wave attenuation one means any irreversible energy losses other than spherical divergence, transmission losses and mode conversions which a seismic wave experiences as it propagates through a medium. Evidence from different experiments supports the fact that several physical mechanisms must contribute to seismic attenuation in rocks. The dramatic increase in attenuation due to the addition of trace amounts of water to a dry porous rock has focused attention on details of flow within fine cracks (Nur et al., 1980). Coulomb friction between grains yields attenuation which depends upon the amplitude of vibration. The motion of lattice dislocations within the solid gives the right dependence on frequency and the correct magnitude of attenuation in granite and makes this an attractive choice for the energy loss mechanism (Mason, 1969).

For seismic waves in the shallow crust, the attenuation is usually proportional to frequency. In principle, velocity must depend upon frequency in an attenuating medium. Several attempts have been made to find modifications of Hooke's law that would account for the effects of inelasticity. The attempts to account for the observed variation of quality factor$Q$ with frequency can be divided into two groups: those invoking linear models and

those invoking non linear models (Knopoff, 1964). Non linearity seems to have been largely ignored, because of the mathematical difficulties associated with non linear systems.

In perfect elasticity, strain is linearly proportional to stress and independent of the duration of the stress. When the stress is removed the original form is recovered at once. In viscoelasticity, the strain under constant stress increases at a decreasing rate. When the stress is removed there is an immediate recovery by the amount of the initial strain and the strain decreases further, ultimately tending to zero (Jeffreys, 1976). In Boltzmann's early theory (1876) to explain the nature of acoustic loss, the strain due to an applied stress is delayed by some sort of 'memory' behavior in the material. For a stress excitation, which is a complicated function of time this can be expressed as a convolution with an elementary creep function which expresses the delay.

It is difficult to incorporate attenuation in time-domain methods because of the presence of a convolution integral which describes Boltzmann's superposition principle. Day and Minster (1984) proposed a method based on Pade approximations where the viscoelastic modulus is expressed by a series of rational functions. Then, the convolution integral which describes the stress-strain relation is transformed into a differential form. Carcione et al. (1988a, b) and Tal-Ezer et al.(1990) apply a similar approximation and solve numerically the wave propagation problem using the pseudospectral method. In practice, the technique based on Pade approximations gives valid results only for relatively short paths. Emmerich and Korn (1987) proposed a method for incorporating attenuation in the time domain based on the rheological model of the generalized Maxwell body. The advantage of this technique is that the results are satisfactory for longer propagation paths and/or strong attenuation.

In this chapter, the viscoacoustic modulus which describes an arbitrary Q law is approximated by the modulus of a generalized Maxwell body which is expressed in a rational function in frequency domain. A first order hyperbolic system is formulated in the

time domain and the velocity-pressure finite difference method is presented as it is applied to the viscoacoustic wave system. Finally the results from the application of the method in a crosshole experiment are presented and compared to the real data.

4.2 PROBLEM FORMULATION

4.2.1 Generalized Maxwell body approximation

In a two dimensional viscoacoustic heterogeneous medium, the equations of motion can be expressed in terms of the particle displacement components u_x, u_z and the pressure p as

$$\rho \frac{\partial^2 u_x}{\partial t^2} = \frac{\partial p}{\partial x} ,$$

(4.2.1)

$$\rho \frac{\partial^2 u_z}{\partial t^2} = \frac{\partial p}{\partial z} ,$$

(4.2.2)

where ρ is the density. The viscoacoustic constitutive relation is expressed by

$$p(t) = \int_{-\infty}^{t} K(t-\tau)\, \varepsilon(\tau)\, d\tau ,$$

(4.2.3)

where K is the viscoacoustic modulus and ε is the strain defined by the dilatation

$$\varepsilon = \frac{\partial u_x}{\partial x} + \frac{\partial u_z}{\partial z} .$$

(4.2.4)

The relationship between stress and strain given in (4.2.3) was first introduced by Boltzmann (1876) with a different notation. Equation (4.2.3) is not useful in forward modeling with finite difference methods because the numerical integration of the strain history at each point of the medium and each time step would require an immense amount of computer time and memory.

In the frequency domain, equation (4.2.3) is formulated as

$$p(\omega) = K(\omega) \, \varepsilon(\omega),$$
(4.2.5)

where $K(\omega)$ is the complex viscoacoustic modulus.

If we apply a strain of unit step $H(t)$, equation (4.2.3) gives the relaxation function

$$R(t) = \int_{-\infty}^{t} K(t - \tau) \, H(\tau) \, d\tau$$
(4.2.6)

which implies that $K(t)$ is the first time derivative of the relaxation function,

$$K(t) = \frac{dR(t)}{dt} \, ,$$
(4.2.7)

that is, $R(t)$ can be expressed as (see Figure 4.2.1)

$$R(t) = \left[K_R + K_\delta \int_0^\infty r(\omega) e^{-\omega t} d\omega \right] H(t) \, ,$$
(4.2.8)

where K_R denotes the relaxed modulus defined by

$$K_R = \lim_{t \to \infty} R(t) \, ; \tag{4.2.9}$$

K_δ represents the difference of the relaxed modulus K_R from the unrelaxed modulus K_u which is defined by

$$K_u = K_R + K_\delta = \lim_{t \to 0} R(t) \, ; \tag{4.2.10}$$

$r(\omega)$ is the normalized relaxation spectrum with

$$\int_0^\infty r(\omega) \, d\omega = 1. \tag{4.2.11}$$

If the relaxation spectrum consists of n single peaks of strength a_j at discrete relaxation frequencies ω_j, that is

$$r(\omega) = \sum_{j=1}^n a_j \delta(\omega - \omega_j) \, ; \qquad \sum_{j=1}^n a_j = 1, \tag{4.2.12}$$

then from equation (4.2.8)

$$R(t) = \left[K_R + K_\delta \sum_{j=1}^n a_j e^{-\omega_j t} \right] H(t) \tag{4.2.13}$$

and the corresponding modulus in frequency domain $K_n(\omega)$ is

$$K_n(\omega) = K_U - K_\delta \sum_{j=1}^n \frac{a_j \omega_j}{i\omega + \omega_j} \tag{4.2.14}$$
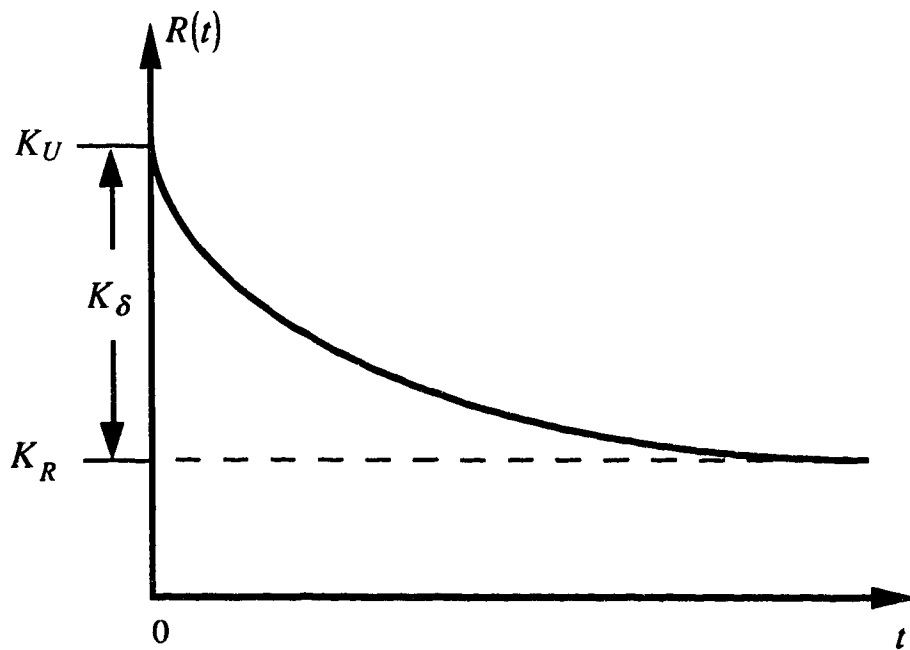
Figure 4.2.1 A typical relaxation function $R(t)$. K_U is the unrelaxed modulus;

$K_R = K_U - K_\delta$ is the relaxed modulus.

Equation (4.2.14) expresses the frequency modulus in a rational form which allows the viscoacoustic constitutive relation in the time domain to be expressed in differential form through some intermediate variables (Emmerich and Korn, 1987).

An equivalent expression of equation (4.2.14) is the complex modulus of the rheological model of the generalized Maxwell body

$$K_n(\omega) = K_R + K_\delta \sum_{j=1}^{n} \alpha_j \frac{i\omega}{i\omega + \omega_j} \,. \tag{4.2.15}$$

Each term of the sum in equation (4.2.15) can be interpreted as a classical Maxwell body with viscosity $\alpha_j K_\delta/\omega_j$ and elastic modulus $\alpha_j K_\delta$ (e.g. Christensen, 1982), and the term K_R represents an additional elastic element (Emmerich and Korn, 1987; see Figure 4.2.2). The quality factor Q for the generalized Maxwell body is described by

$$Q^{-1}(\omega) = \frac{Im\,K_n(\omega)}{Re\,K_n(\omega)} = \frac{K_\delta}{K_R} \frac{\displaystyle\sum_{j=1}^{n} \alpha_j \frac{\omega/\omega_j}{1+(\omega/\omega_j)^2}}{1 + \dfrac{K_\delta}{K_R} \displaystyle\sum_{j=1}^{n} \alpha_j \frac{(\omega/\omega_j)^2}{1+(\omega/\omega_j)^2}} \,. \tag{4.2.16}$$

For a given function $Q(\omega)$, a generalized Maxwell body model can be found as an approximation by determining the unknown weighting factors α_j through a fitting procedure. Following Emmerich and Korn (1987), we utilize the values of $\tilde{Q}^{-1}(\omega)$ at certain discrete frequencies $\tilde{\omega}_k$ with $k = 1, ..., K$ which are uniformly distributed on a logarithmic scale. Then, from equation (4.2.16), we obtain an over-determined linear system
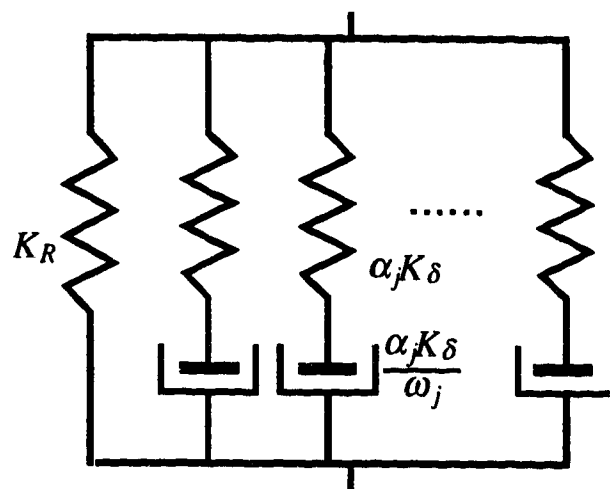
Figure 4.2.2 Generalized Maxwell body with viscosities $\dfrac{\alpha_j K_\delta}{\omega_j}$, elastic moduli $\alpha_j K_\delta$ and an additional elastic element K_R.

$$\sum_{j=1}^{n} \frac{\tilde{\omega}_k \left[\omega_j - \tilde{\omega}_k \tilde{Q}^{-1}(\tilde{\omega}_k) \right]}{\omega_j^2 + \tilde{\omega}_k^2} \, y_j = \tilde{Q}^{-1}(\tilde{\omega}_k) , \qquad k = 1,\ldots,K , \tag{4.2.17}$$

which is solved for $y_j = \alpha_j \dfrac{\delta\lambda}{\lambda_R}$ by applying a least-squares method. The normalization condition (4.2.12) can be expressed in terms of y_j as

$$\sum_{j=1}^{n} y_j = \sum_{j=1}^{n} \alpha_j \frac{K_\delta}{K_R} = \frac{K_\delta}{K_R} . \tag{4.2.18}$$

.

The obtained generalized Maxwell body approximation for a arbitrary Q law can then be expressed in terms of the solutions of the linear equation (4.2.17) as

$$K_n(\omega) = K_R \left(1 + \sum_{j=1}^{n} y_j \, \frac{i\omega}{i\omega + \omega_j} \right) . \tag{4.2.19}$$

4.2.2 A first order hyperbolic system for viscoelastic waves

If we replace $K(\omega)$ in equation (4.2.5) with $K_n(\omega)$ in equation (4.2.19), then the constitutive relation becoming

$$p(\omega) = K_R \left(1 + \sum_{j=1}^{n} y_j \, \frac{i\omega}{i\omega + \omega_j} \right) \varepsilon(\omega) \tag{4.2.20}$$

or

$$p(\omega) = K_R \varepsilon(\omega) + \sum_{j=1}^{n} \eta_j(\omega) \ ,$$
(4.2.21)

where

$$\eta_j(\omega) = y_j \ \frac{i\omega}{i\omega + \omega_j} \ \varepsilon(\omega) \ .$$
(4.2.22)

After inverse Fourier transforming, equation (4.2.21) and (4.2.22) become

$$p(t) = K_R \left(\frac{\partial u_x}{\partial x} + \frac{\partial u_z}{\partial z} \right) + \sum_{j=1}^{n} \eta_j(t)$$
(4.2.23)

and

$$\frac{\partial \eta_j}{\partial t} + \omega_j \eta_j = K_R y_j \left(\frac{\partial^2 u_x}{\partial x \partial t} + \frac{\partial^2 u_z}{\partial z \partial t} \right) \ , \quad j = 1\ 2, \ldots n \ .$$
(4.2.24)

After taking the time derivative on equation (4.2.23) and denoting the first order time derivative of the two displacement components with v_x and v_z, the particle velocity components, equations (4.2.1), (4.2.2), (4.2.23) and (4.2.24) form a system which, in matrix form, can be written as

$$E_0 \frac{\partial u}{\partial t} = A_0 \frac{\partial u}{\partial x} + B_0 \frac{\partial u}{\partial z} + C_0 u \ .$$
(4.2.25)

Therefore, the convolution integral present in the constitutive relation (equation 4.2.3) has been replaced by a set of first order differential equations with a number of intermediate

variables. By keeping the number of terms in (4.2.23) or in (4.2.17) small, this method of incorporating attenuation into the time-domain computations of the seismic wavefield is quite tractable.

If we chose $n = 5$, then the vector of unknowns of system (4.2.25) is

$$\mathbf{u} = \begin{bmatrix} v_x \\ v_z \\ p \\ \eta_1 \\ \eta_2 \\ \eta_3 \\ \eta_4 \\ \eta_5 \end{bmatrix} \qquad (4.2.26)$$

and the matrices become

$$\mathbf{E}_0 = \begin{bmatrix} \rho & 0 & 0 & 0 & 0 & 0 & 0 & 0 \\ 0 & \rho & 0 & 0 & 0 & 0 & 0 & 0 \\ 0 & 0 & 1 & -1 & -1 & -1 & -1 & -1 \\ 0 & 0 & 0 & 1 & 0 & 0 & 0 & 0 \\ 0 & 0 & 0 & 0 & 1 & 0 & 0 & 0 \\ 0 & 0 & 0 & 0 & 0 & 1 & 0 & 0 \\ 0 & 0 & 0 & 0 & 0 & 0 & 1 & 0 \\ 0 & 0 & 0 & 0 & 0 & 0 & 0 & 1 \end{bmatrix}, \qquad (4.2.27)$$

$$\mathbf{A}_0 = \begin{bmatrix} 0 & 0 & 1 & 0 & 0 & 0 & 0 & 0 \\ 0 & 0 & 0 & 0 & 0 & 0 & 0 & 0 \\ K_R & 0 & 0 & 0 & 0 & 0 & 0 & 0 \\ y_1 K_R & 0 & 0 & 0 & 0 & 0 & 0 & 0 \\ y_2 K_R & 0 & 0 & 0 & 0 & 0 & 0 & 0 \\ y_3 K_R & 0 & 0 & 0 & 0 & 0 & 0 & 0 \\ y_4 K_R & 0 & 0 & 0 & 0 & 0 & 0 & 0 \\ y_5 K_R & 0 & 0 & 0 & 0 & 0 & 0 & 0 \end{bmatrix}, \qquad (4.2.28)$$

$$\mathbf{B_o} = \begin{bmatrix} 0 & 0 & 0 & 0 & 0 & 0 & 0 & 0 \\ 0 & 0 & 1 & 0 & 0 & 0 & 0 & 0 \\ 0 & K_R & 0 & 0 & 0 & 0 & 0 & 0 \\ 0 & y_1 K_R & 0 & 0 & 0 & 0 & 0 & 0 \\ 0 & y_2 K_R & 0 & 0 & 0 & 0 & 0 & 0 \\ 0 & y_3 K_R & 0 & 0 & 0 & 0 & 0 & 0 \\ 0 & y_4 K_R & 0 & 0 & 0 & 0 & 0 & 0 \\ 0 & y_5 K_R & 0 & 0 & 0 & 0 & 0 & 0 \end{bmatrix} \qquad (4.2.29)$$

and

$$\mathbf{C_o} = \begin{bmatrix} 0 & 0 & 0 & 0 & 0 & 0 & 0 & 0 \\ 0 & 0 & 0 & 0 & 0 & 0 & 0 & 0 \\ 0 & 0 & 0 & 0 & 0 & 0 & 0 & 0 \\ 0 & 0 & 0 & -\omega_1 & 0 & 0 & 0 & 0 \\ 0 & 0 & 0 & 0 & -\omega_2 & 0 & 0 & 0 \\ 0 & 0 & 0 & 0 & 0 & -\omega_3 & 0 & 0 \\ 0 & 0 & 0 & 0 & 0 & 0 & -\omega_4 & 0 \\ 0 & 0 & 0 & 0 & 0 & 0 & 0 & -\omega_5 \end{bmatrix} . \qquad (4.2.30)$$

Multiplying equation (4.2.25) by $\mathbf{E_0^{-1}}$,

$$\mathbf{E_o^{-1}} = \begin{bmatrix} \rho^{-1} & 0 & 0 & 0 & 0 & 0 & 0 & 0 \\ 0 & \rho^{-1} & 0 & 0 & 0 & 0 & 0 & 0 \\ 0 & 0 & 1 & 1 & 1 & 1 & 1 & 1 \\ 0 & 0 & 0 & 1 & 0 & 0 & 0 & 0 \\ 0 & 0 & 0 & 0 & 1 & 0 & 0 & 0 \\ 0 & 0 & 0 & 0 & 0 & 1 & 0 & 0 \\ 0 & 0 & 0 & 0 & 0 & 0 & 1 & 0 \\ 0 & 0 & 0 & 0 & 0 & 0 & 0 & 1 \end{bmatrix} , \qquad (4.2.31)$$

we obtain

$$\frac{\partial u}{\partial t} = A\frac{\partial u}{\partial x} + B\frac{\partial u}{\partial z} + Cu ,$$ (4.2.32)

where

$$A = \begin{bmatrix} 0 & 0 & \rho^{-1} & 0 & 0 & 0 & 0 & 0 \\ 0 & 0 & 0 & 0 & 0 & 0 & 0 & 0 \\ A_{31} & 0 & 0 & 0 & 0 & 0 & 0 & 0 \\ y_1 K_R & 0 & 0 & 0 & 0 & 0 & 0 & 0 \\ y_2 K_R & 0 & 0 & 0 & 0 & 0 & 0 & 0 \\ y_3 K_R & 0 & 0 & 0 & 0 & 0 & 0 & 0 \\ y_4 K_R & 0 & 0 & 0 & 0 & 0 & 0 & 0 \\ y_5 K_R & 0 & 0 & 0 & 0 & 0 & 0 & 0 \end{bmatrix} ,$$ (4.2.33)

$$B = \begin{bmatrix} 0 & 0 & 0 & 0 & 0 & 0 & 0 & 0 \\ 0 & 0 & \rho^{-1} & 0 & 0 & 0 & 0 & 0 \\ 0 & B_{32} & 0 & 0 & 0 & 0 & 0 & 0 \\ 0 & y_1 K_R & 0 & 0 & 0 & 0 & 0 & 0 \\ 0 & y_2 K_R & 0 & 0 & 0 & 0 & 0 & 0 \\ 0 & y_3 K_R & 0 & 0 & 0 & 0 & 0 & 0 \\ 0 & y_4 K_R & 0 & 0 & 0 & 0 & 0 & 0 \\ 0 & y_5 K_R & 0 & 0 & 0 & 0 & 0 & 0 \end{bmatrix} ,$$ (4.2.34)

$$C = \begin{bmatrix} 0 & 0 & 0 & 0 & 0 & 0 & 0 & 0 \\ 0 & 0 & 0 & 0 & 0 & 0 & 0 & 0 \\ 0 & 0 & 0 & -\omega_1 & -\omega_2 & -\omega_3 & -\omega_4 & -\omega_5 \\ 0 & 0 & 0 & -\omega_1 & 0 & 0 & 0 & 0 \\ 0 & 0 & 0 & 0 & -\omega_2 & 0 & 0 & 0 \\ 0 & 0 & 0 & 0 & 0 & -\omega_3 & 0 & 0 \\ 0 & 0 & 0 & 0 & 0 & 0 & -\omega_4 & 0 \\ 0 & 0 & 0 & 0 & 0 & 0 & 0 & -\omega_5 \end{bmatrix} ,$$ (4.2.35)

and

$$A_{31} = B_{32} = K_R + K_R \sum_{j=1}^{5} y_j = K_R + K_\delta = K_U \ . \tag{4.2.36}$$

The characteristic equations of matrices A and B are

$$\lambda^6 \left(\lambda^2 - \frac{A_{31}}{\rho} \right) = 0 \tag{4.2.37}$$

and

$$\lambda^6 \left(\lambda^2 - \frac{B_{32}}{\rho} \right) = 0 \tag{4.2.38}$$

respectively. Therefore, the matrices A and B have the same eigenvalues

$$\left(\lambda_1, \lambda_2, \lambda_3, \lambda_4, \lambda_5, \lambda_6, \lambda_7, \lambda_8 \right) = (-v, 0, 0, 0, 0, 0, 0, v) \ , \tag{4.2.39}$$

where $v = \sqrt{\frac{A_{31}}{\rho}}$, is the high frequency limit velocity of wave propagation.

Since the eigenvalues of A and B are real and their eigenvectors are independent, system (4.2.25) is hyperbolic. The first order system is free of spatial derivatives of the physical parameters which are present in the second order wave equations for heterogeneous media. Consequently, the numerical approximation of the spatial derivatives of the physical parameters is not required in the velocity-pressure finite difference method. Numerical approximation of these derivatives may sometimes result in large errors especially at the location close to interfaces where the physical parameters change quickly. This source of error is not present in the above formulation of viscoacoustic wave

equations for heterogeneous media.

4.3 NUMERICAL SOLUTION

The generalized Maxwell body approximation method can be applied to an arbitrary Q law of frequency dependence. In a seismic application, the quality factor Q is normally assumed to be frequency-independent or nearly frequency-independent. To test the quality of the Maxwell body approximation we have computed $Q_n(\omega)$ numerically according to the approach described in the previous section for $n = 5$ and $n = 9$ over a range of frequency up to 250 Hz. The results are compared with the assumed exact value of a constant Q model with $Q = 30$ in Figure 4.3.1.

In the viscoacoustic case, when a pressure-dilatation relation is combined with the equilibrium equation, the resulting one-dimensional wave equation has a solution which can be written in a form analogous to the classical case:

$$u_x(x,t) = e^{i[\omega t - k(\omega)x]} \tag{4.3.1}$$

or

$$u_x(x,t) = e^{-\alpha(\omega)x} e^{i[\omega t - x/V(\omega)]} ; \tag{4.3.2}$$

where

$$k(\omega) = \left(\frac{K(\omega)}{\omega^2 \rho}\right)^{-\frac{1}{2}}. \tag{4.3.3}$$

Figure 4.3.1a The inverse Q versus frequency for a constant Q model with Q=30 (solid line) and its generalized maxwell body approximation for n = 5 and a frequency range of 0 to 250 Hz.

Figure 4.3.1b The inverse Q versus frequency for a constant Q model with Q=30 (solid

line) and its generalized Maxwell body approximation for n = 9 and a frequency range of 0

to 250Hz.

the attenuation coefficient $\alpha(\omega)$, in unite of inverse length, is

$$\alpha(\omega) = -\text{Im } k(\omega) \qquad (4.3.4)$$

and the phase velocity,$V(\omega)$, is given by

$$V(\omega) = \frac{\omega}{\text{Re } k(\omega)} , \qquad (4.3.5)$$

respectively.

For a constant Q , the modulus $K(\omega)$ is given by (Kjartansson, 1979)

$$K(\omega) = |K(\omega_o)| \left(\frac{i\omega}{\omega_o}\right)^{\frac{2}{\pi}\tan^{-1}\left(\frac{1}{Q}\right)} ; \qquad (4.3.5)$$

the phase $v \cdots \cdots V(\omega)$ and the attenuation coefficient $\alpha(\omega)$ are given by

$$V(\omega) = \left(\frac{K(\omega_o)}{\rho}\right)^{1/2} \frac{1}{\cos\left[\frac{1}{2}\tan^{-1}\left(\frac{1}{Q}\right)\right]} \left|\frac{\omega}{\omega_o}\right|^{\frac{1}{\pi}\tan^{-1}\left(\frac{1}{Q}\right)} \qquad (4.3.6)$$

and

$$\alpha(\omega) = \frac{\omega}{V(\omega)} \tan\left[\frac{1}{2}\tan^{-1}\left(\frac{1}{Q}\right)\right] . \qquad (4.3.7)$$

Numerical computations of $K_n(\omega)$ and velocity $V_n(\omega)$ with the generalized Maxwell body approach are shown in Figures 4.3.2 and 4.3.3 for $n = 5$ and $n = 9$ together with the exact values calculated with equations (4.3.5) and (4.3.6).
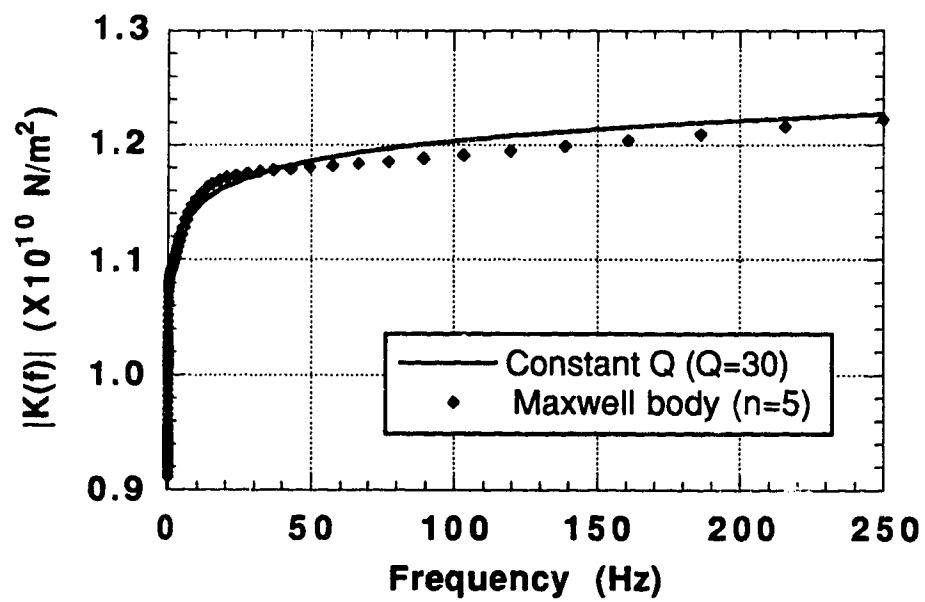
Figure 4.3.2a The absolute value of the complex modulus versus frequency for a constant Q model with $Q=30$ and its generalized Maxwell body approximation for $n = 5$ and a frequency range of 0 to 250 Hz.
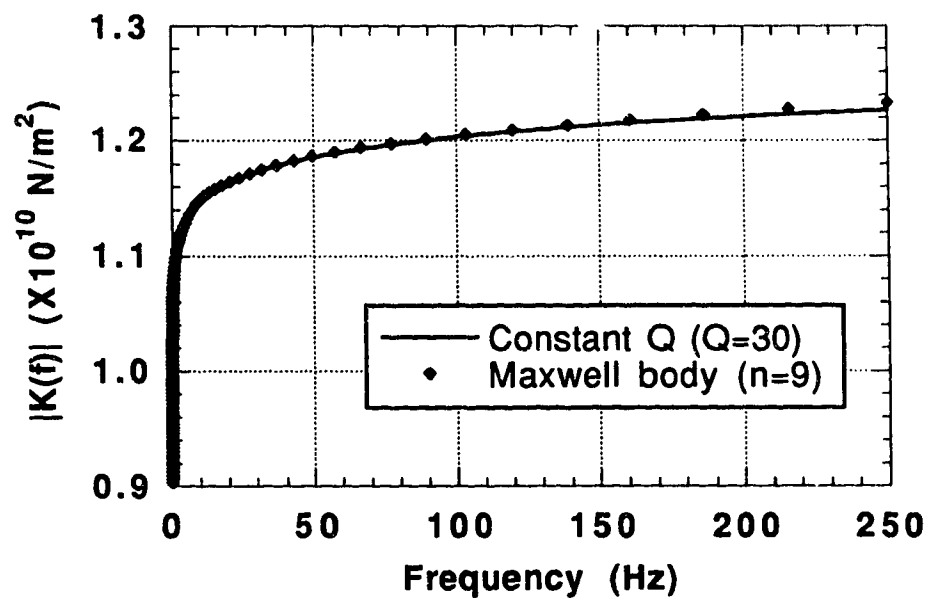
Figure 4.3.2b The absolute value of the complex modulus versus frequency for a constant

Q model with Q=30 (solid line) and its generalized Maxwell body approximation for n =

9 and a frequency range of 0 to 250 Hz.
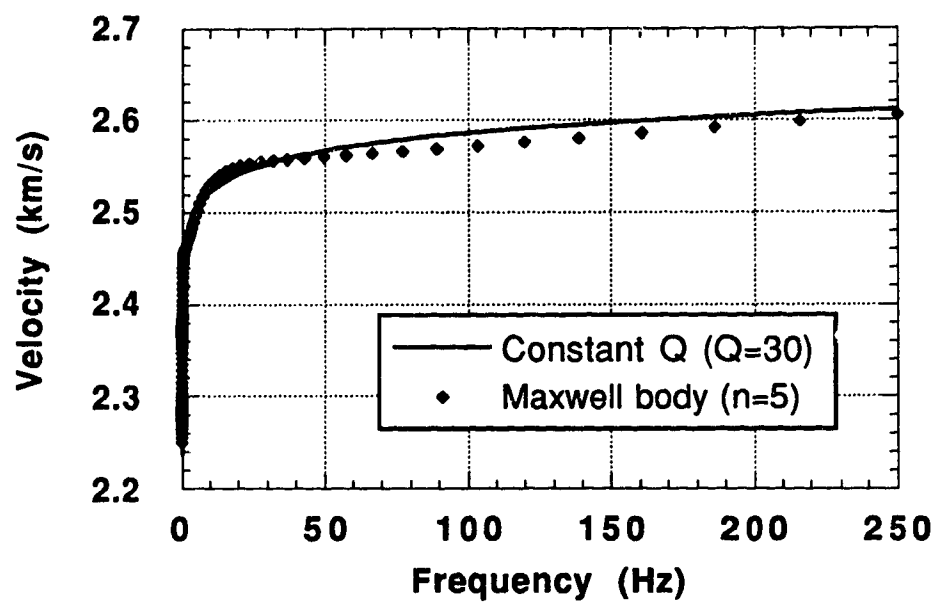
Figure 4.3.3a The velocity versus frequency for a constant Q model with $Q=30$ (solid line) and its generalized maxwell body approximation for $n = 5$ and a frequency range of 0 to 250 Hz.
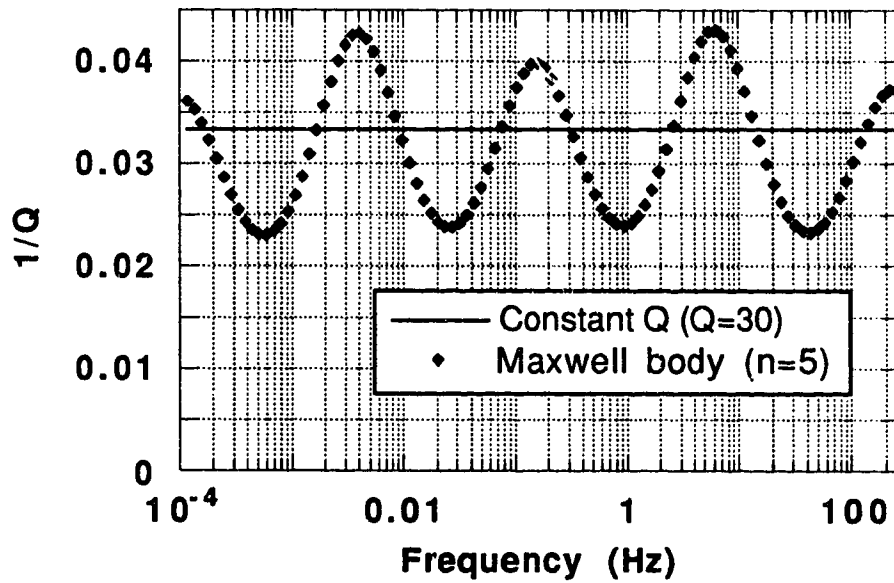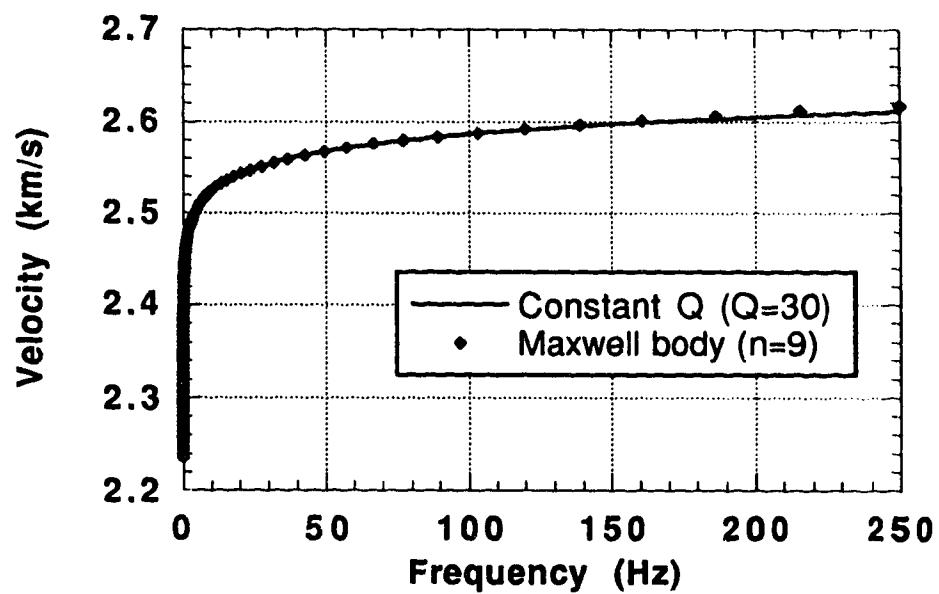
Figure 4.3.3b The velocity versus frequency for a constant Q model with $Q=30$ (solid

line) and its generalized Maxwell body approximation for $n = 9$ and a frequency range of 0
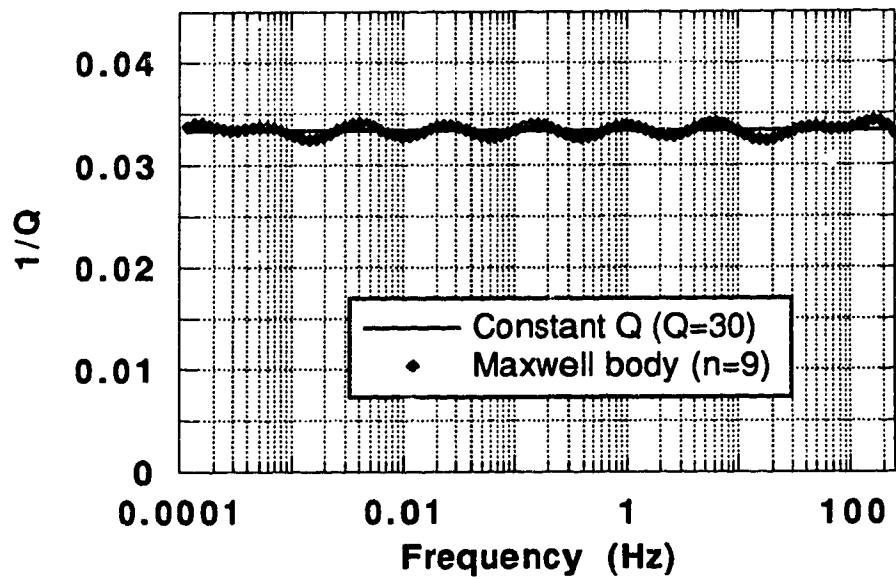
to 250Hz.

The impulse response, which is the waveform resulting from a delta function source at a given distance, is of particular interest since the waveform that results from an arbitrary source is obtained by simply convolving the source with the impulse response. The spectrum of the impulse response is obtained by omitting the $i\omega t$ term in equation (4.3.1) or (4.3.2). Figure (4.3.4) shows the spectrum amplitude of the impulse response at a distance of 500 m for a constant Q model ($Q = 30$) and its generalized Maxwell body approximation for $n = 5$ (Figure 4.3.4a) and $n = 9$ (Figure 4.3.4b). Figure (4.3.5) shows the response for a source whose time variation is the second derivative of the Gaussian function with a dominant frequency of 30 Hz (Figure 4.3.5a) at distance of 500 m for a constant Q model ($Q = 30$) and its generalized Maxwell body approximation for $n = 5$ (Figure 4.3.5a) and $n = 9$ (Figure 4.3.5b).

The first order system (4.2.32) is solved numerically for $t > 0$, subject to the initial condition, $u(x, z, t = 0)$. The concept of dimensional splitting (Strang, 1968) is applied to the system (4.2.32). A two step MacCormack-type finite difference operator is then employed to solve the differential system alternately in the x and z directions. The fully vectorized finite difference algorithm, which is second order accurate in time and fourth order in space, is described in section 2.5. The fact that all the non-zero elements in matrices A and B in system (4.2.32) are in the first three columns allows the difference operations in space to be implemented only to the first three components in the variable vector (4.2.25) as is the case for an acoustic wave system. Therefore an increase of the number n of the terms in equation (4.2.15) will require more computer memory but will not result in a significant increase of the computational time. On a Convex 210, the calculation of 1500 time steps for a model with a 500x480 mesh costs about 90 minutes of CPU time for $n = 9$. The absorbing boundary techniques described in Chapter 3 are also utilized in this development in order to reduce the artificial reflections from the margins of the computational region.
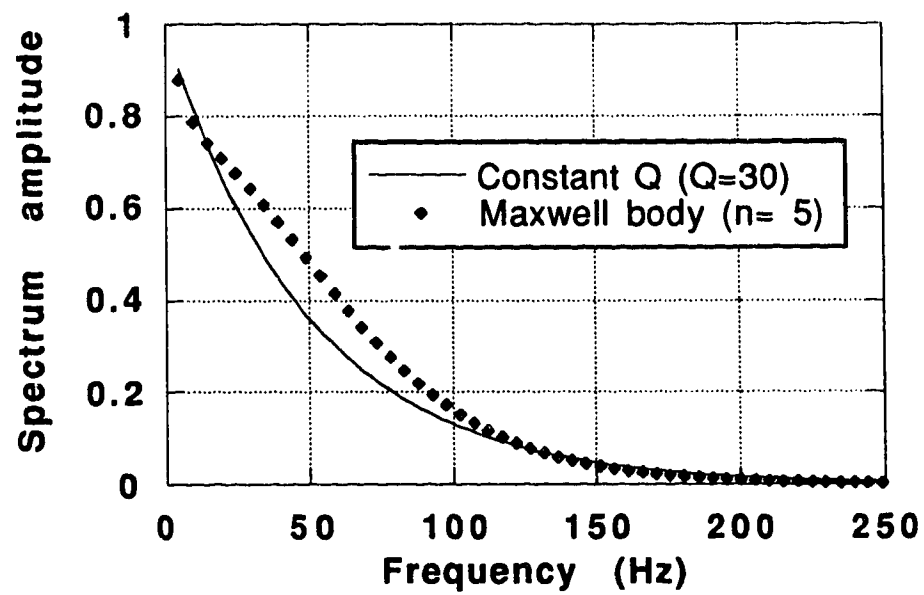
Figure 4.3.4a The amplitude of impulse response spectrum of a constant Q model with Q=30 (solid line) and its generalized Maxwell body approximation for $n = 5$, resulting from a unit impulse plane wave source at distance $x = 500$ m.
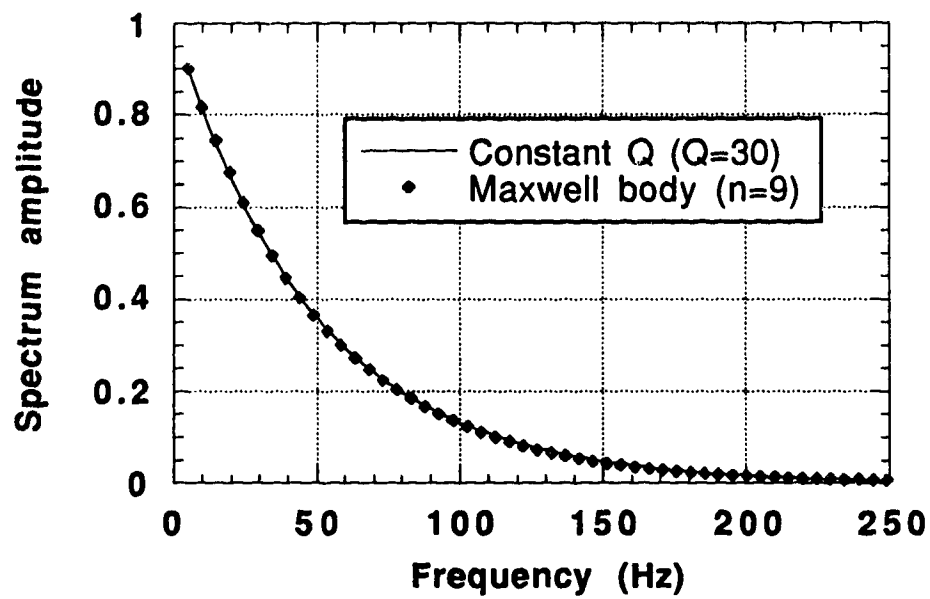
Figure 4.3.4b The amplitude of impulse response spectrum of a constant Q model with $Q=30$ (solid line) and its generalized Maxwell body approximation for $n = 9$, resulting from a unit impulse plane wave source at distance $x = 500$ m.
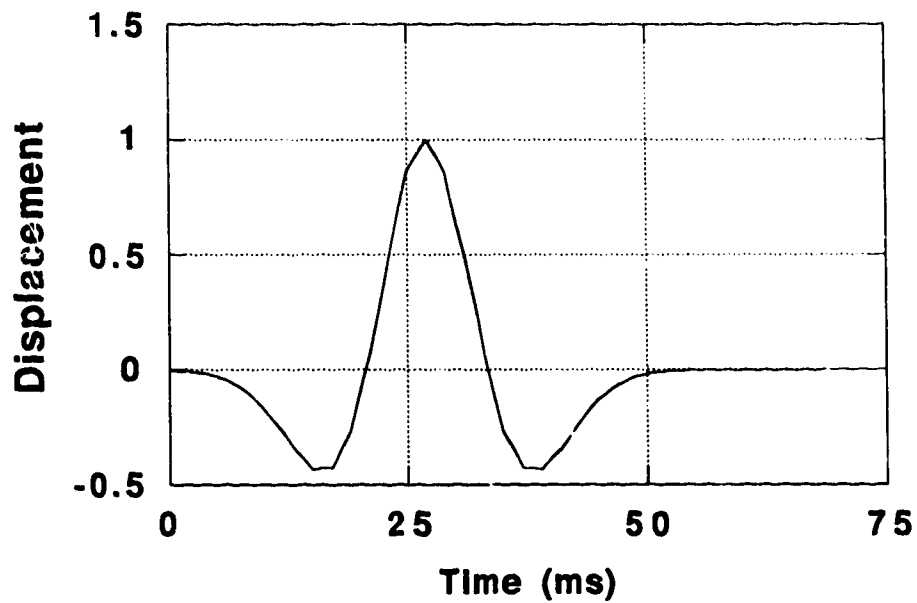
Figure 4.3.5a Time variation of a seismic pulse source which is the second derivative of
Gaussian function with a dominant frequency of 35 Hz. The source is used in calculating
the results shown in Fig 4.3.5b and c.
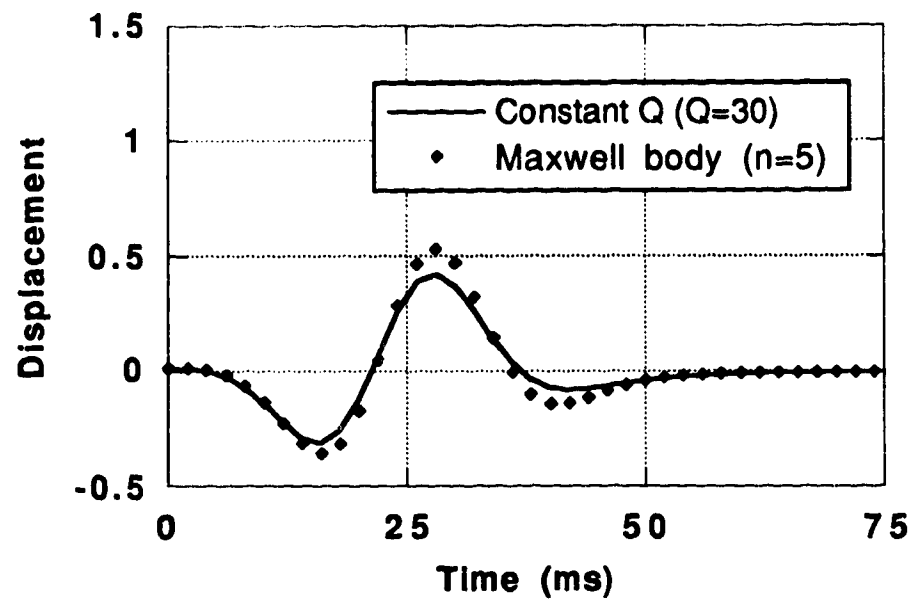
Figure 4.3.5b The waveform at distance x = 500 m resulting from a plane wave source with the shape shown in Fig 4.3.5a for a constant Q model with Q=30 (solid line) and its generalized Maxwell body approximation for n = 5 and frequency range of 0 to 250 Hz.
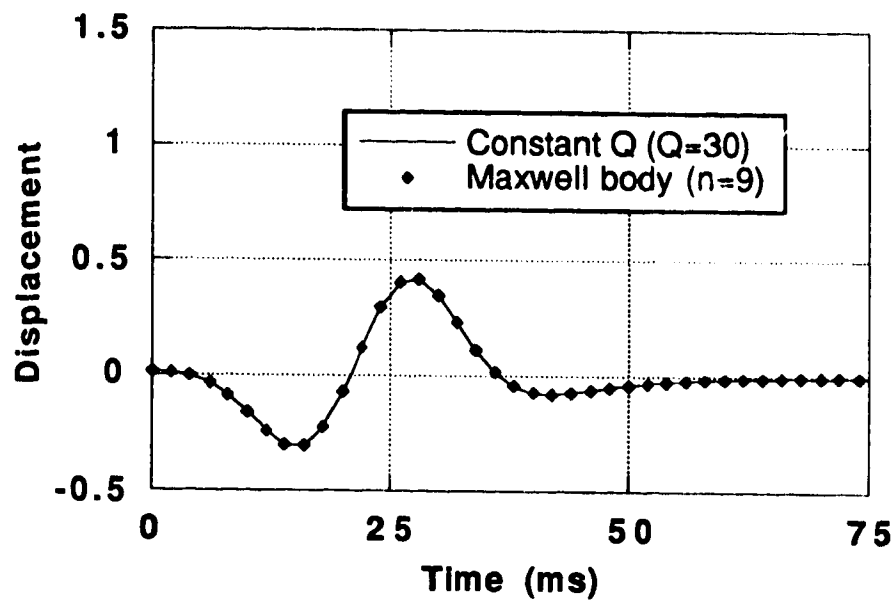
Figure 4.3.5c The waveform at distance x = 500 m resulting from a plane wave source with the shape shown in Fig 4.3.5a for a constant Q model with Q=30 (solid line) and its generalized Maxwell body approximation for n = 9 and frequency range of 0 to 250 Hz.

4. 4   FIELD EXAMPLE

The bitumen from the oil sands of Alberta is normally recovered by an enhanced oil recovery (EOR) operation. Many of these involve steam injection to make the oil mobile. From the reservoir engineer point of view it is important to monitor the growth of the steam fronts and to assess the changes occurring in the reservoir as a result of the steam stimulation. In particular, a knowledge of the size, position and physical state of the heated zone around the injection well is desired in the development of efficient heavy oil extraction techniques. Invasive techniques, such as drilling observation wells, are expensive and limited in spatial resolution. Non-invasive or remote sensing geophysical techniques, especially seismic method has proven to be a successful tool in delineating information about the heated zone.

ESSO Resource Canada Limited carried out crosshole seismic experiments in the Cold Lake, Alberta area to monitor a steam injection process. A velocity-depth model with a steam heated zone and the geometry of an initial crosshole experiment are illustrated in Figure 4.4.1. The source well and the receiver well are separated by 200 m. An explosive source (100 grams of Primacord charge) was shot repeatedly at a depth of 440 m within the source well for various positions of a receiver, generating high frequency waves up to 500 Hz. A well-locking vertical component seismometer was used for recording and was positioned at depths between 372 m and 462 m within the receiver well. The data was recorded at a sample rate of 1/ms.

Steam was injected from a well located half way between the receiver and source wells into the Clearwater (CLGW) formation in order to mobilize the heavy oil. The velocity model is derived from well log data (Kanasewich, 1983; Figure 4.4.1b). The top and bottom boundaries of the Clearwater are at depths of 415 m and 465 m respectively. The
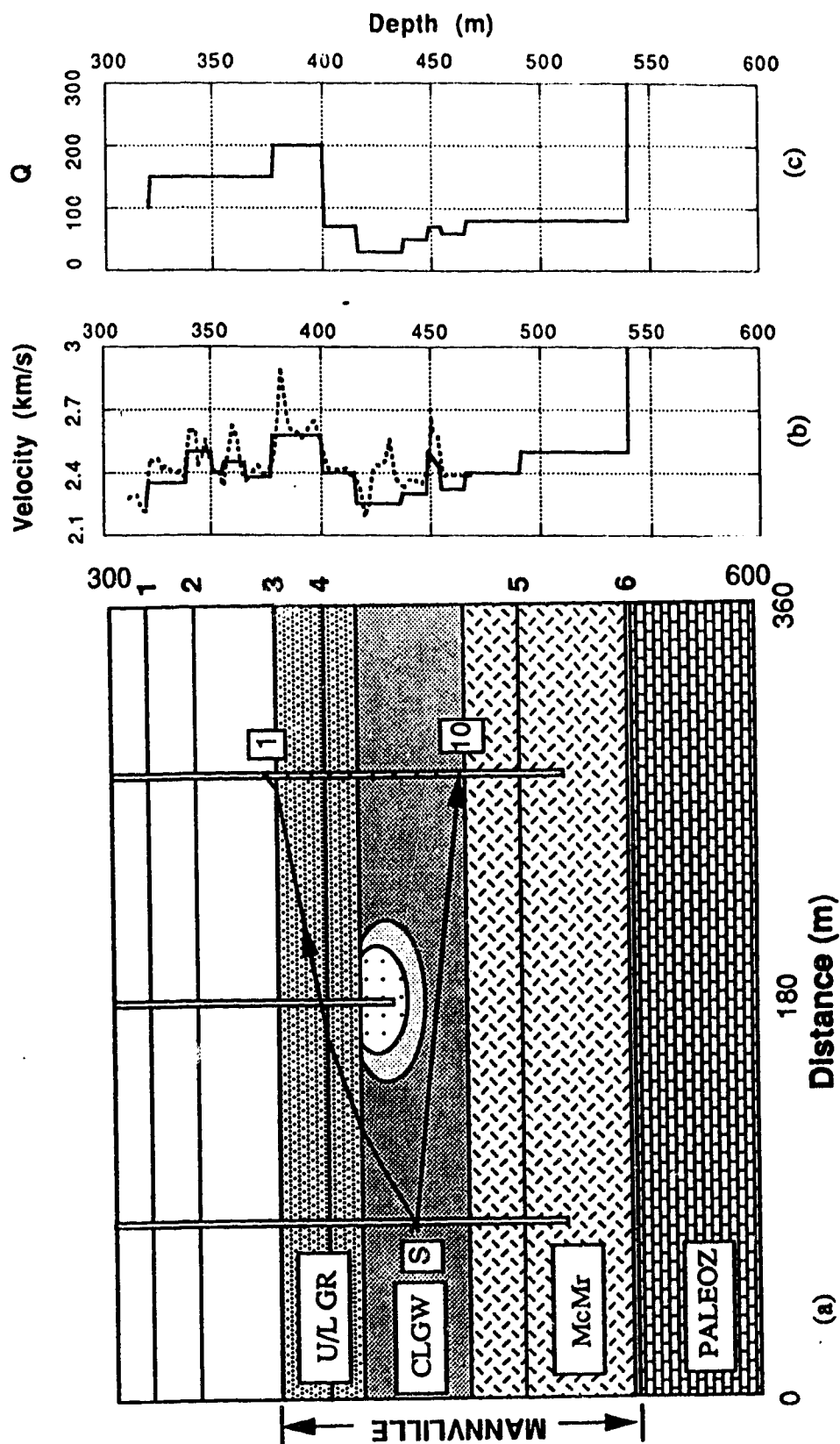
Figure 4.4.1. (a) Earth model for seismic crosshole experiment modeling. (b) Velocity ⸱⸱n curves, dash line from a well log data. (c) Quality factor Q-depth curve used in viscoacoustic ⸱. g. The quality factor Q in the inner and outer zones of steam heated region is 10 and 20, respectively.

top boundary is marked by the impermeable Grand Rapids (GP) shale formation which prevents the steam from escaping upwards. Two concentric ellipses are used to model the heated zone which are truncated at the top by a plane interface. In the inner zone the velocity is reduced 25% and the outer zone is the transition zone where the velocity increases linearly from the velocity of the inner zone to the normal value for the Clearwater layer.

The field experiment was conducted twice: the first time was before steam injection and the second was after injecting steam at a pressure of 10 Mpa for 48 days. The first 147 ms of the before and after steam injection experiments are shown in Figure 4.4.2. Delays of up to 2 ms are measured after steam injection in the first arrivals at receivers 6 to 10. The amplitudes of the arrivals from the two experiments show significant changes on traces 6 to 9, and are lower in the after injection traces. Reflections from layers below and above the Clearwater are difficult to identify in the records. Macrides et al. (1987) studied this data set and, based on evidence from theoretical and experimental studies (Tosaya et al., 1984; Nur et al., 1980), modeled it with ray tracing with a P-velocity drop of 20% within the steam zone. P-SV simulations with a finite difference method carried out by Vafidis and Kanasewich (1991) provided insight into the later arrivals which correspond to converted phases. Macrides et al. (1987) also studied the amplitudes and the power spectra of the real data and they reported that in the steam zone the quality factor Q is equal to 10 while in the Clearwater formation the quality factor Q is equal to 30. The decrease of Q as the temperature increases was explained by the increased saturation of heated bitumen and steam condensate within the zone affected by the steam injection and the increase of mobilization of the fluid contents. In addition, the increased microcrack porosity created in the heated zone by the injection of highly pressurized steam is expected to further contribute to an increase of attenuation in the anomalous zone (Macrides and Kanasewich, 1987).
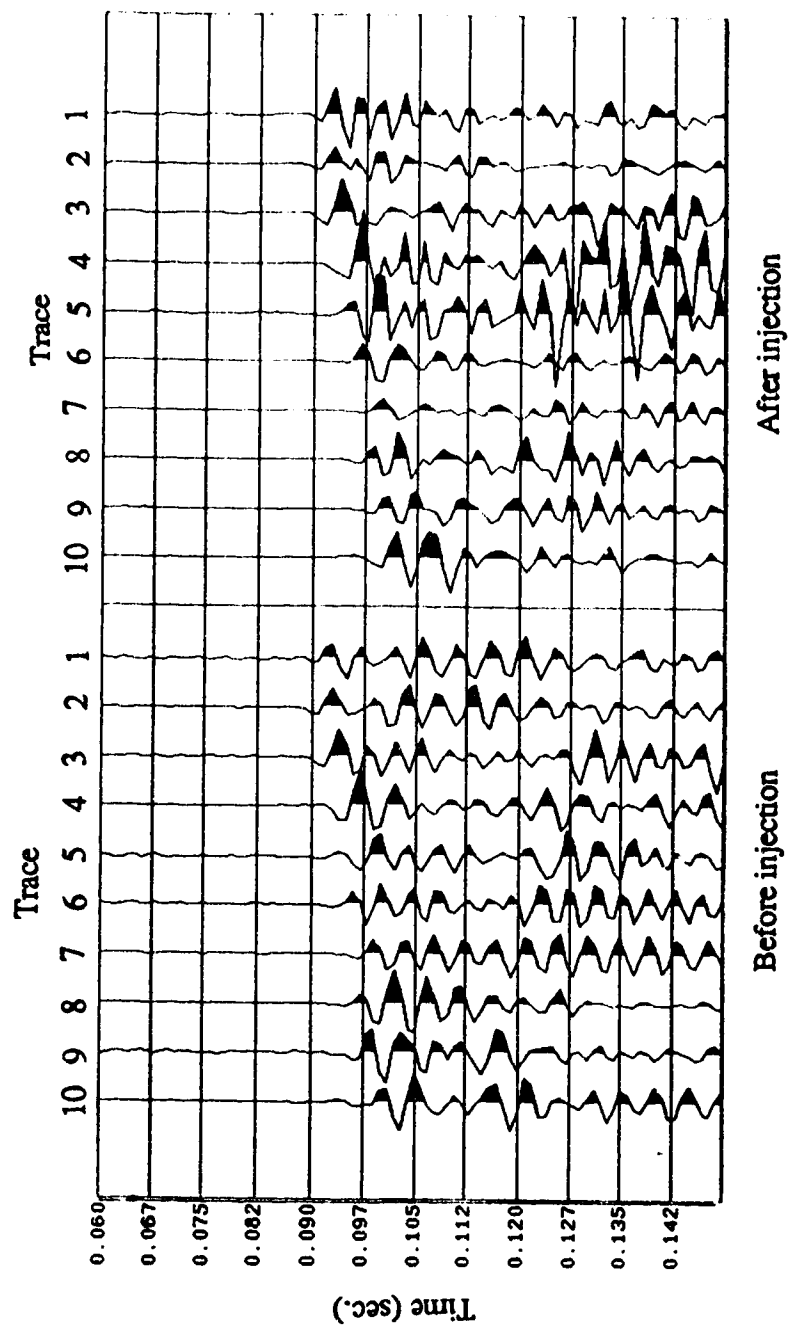
Figure 4.4.2 Observed data of the crosshole seismic experiment before and after steam injection.

In order to verify the validity of these interpretation points, we carried out realistic simulations of the acoustic wave propagation in attenuating media. The time step, in the finite difference method, is 0.05 ms and the grid spacing is 0.5 m. The excitation of the P-wave line source is a Gaussian function with a dominant frequency of 400 Hz.

The modeling is started by using the acoustic wave equation without considering the attenuation. Figure 4.4.3 illustrates the resulting seismogram for the vertical component of particle velocity. The reflection events are labeled by the number of the interface (see also Figure 4.4.1) from which the reflection occurred. The frequency content of the synthetic data is much higher than that of the observed data. The first arrival time delays on traces 6 to 10 can be observed. The dominant amplitude is related to the reflections from interfaces 6 and 4, which is too high compared to the real data. In the synthetic after injection seismogram the amplitude of the reflections from interface 4 and 5 reduces due to effect of the low velocity in the steam heated zone. However, it is still too high, especially in traces 6 and 7, as compared to the seismic section in Figure 4.4.2. Those reflections from the interfaces 1, 2 and 6 do not show significant decay across the synthetic seismograms except that due to geometrical spreading, since they are not affected by the steam zone.

In order to take into account the attenuation of the different layers, especially the quality factor change which occurred due to steam injection, viscoacoustic modeling is carried out for the same model by using the method described in the previous two sections and the same source function as the one used in acoustic modeling. The quality factor Q is assigned 30, 10, and 20 for the Clearwater layer, the inner steam zone, and the transition zone, respectively, according to Macrides et al. (1987). The quality factor Q versus depth curve is given in Figure 4.4.1c. A constant Q model is approximated by a generalized Maxwell body of 9 basic elements ($n = 9$). The elastic moduli and the viscosities of the elements are determined by a least-squares fitting procedure for a frequency range up to
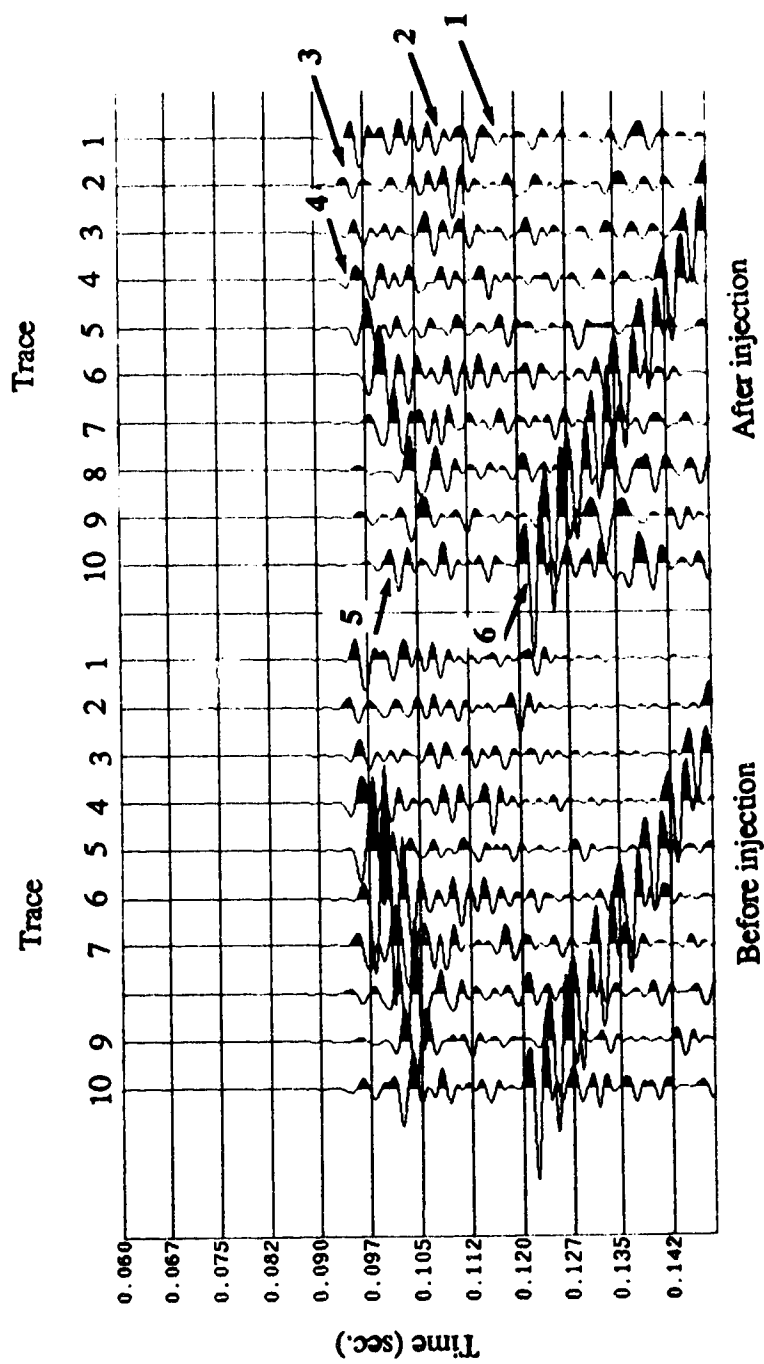
Figure 4.4.3 Synthetic sections from acoustic modeling of the crosshole seismic experiment before and after steam injection.
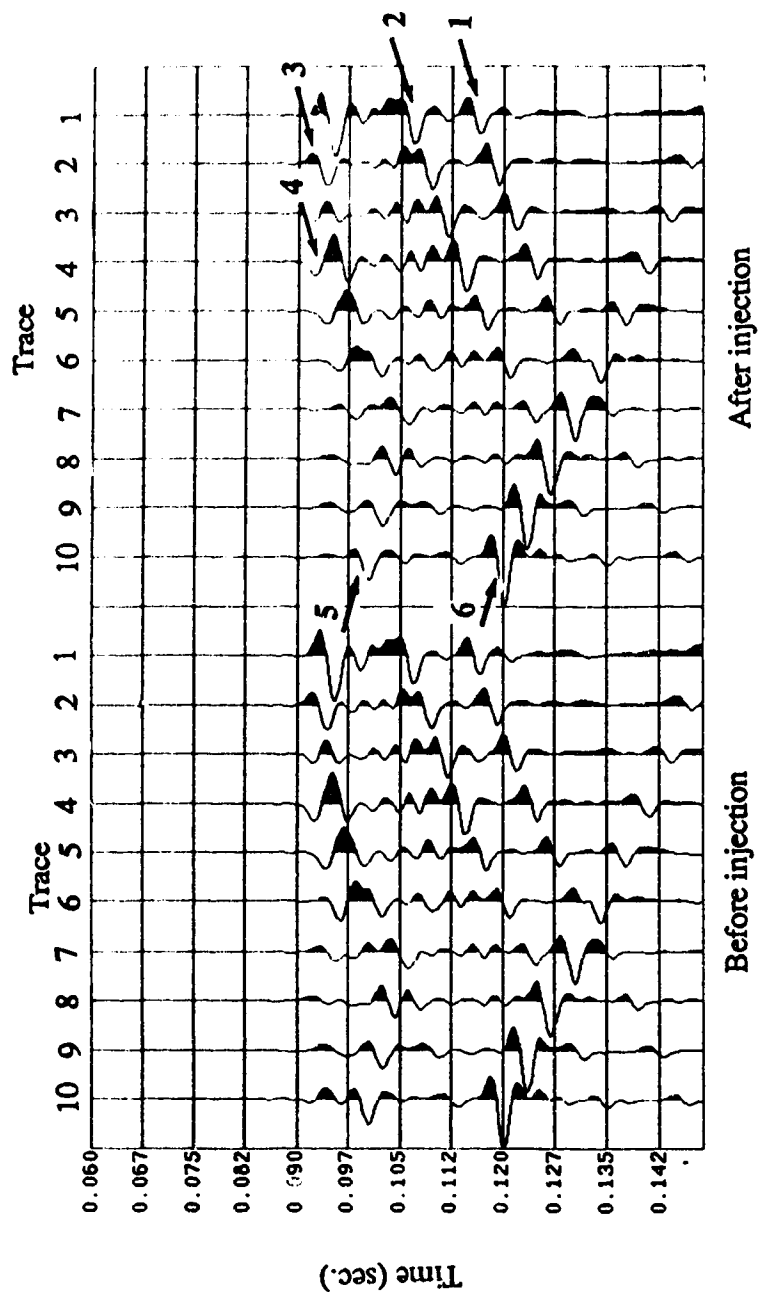
Figure 4.4.4 Synthetic sections from viscoacoustic modeling of the crosshole seismic experiment before and after steam injection.

800 Hz.

Figure 4.4.3 gives the synthetic seismograms from the viscoacoustic modeling before steam injection and after steam injection. The frequency content of the data is lower and more comparable with the real measurements than the results from acoustic modeling since the higher frequency content suffers more severe attenuation in viscoacoustic wave propagation. Apart from the first arrival time delays at receivers 7 to 10 of the after injection traces, the synthetic seismograms from the viscoacoustic modeling give a compatible energy distribution on the sections with that of the field data. At receivers 6 to 9 the amplitude of the after injection traces are lower than the amplitude of the before injection traces which is in agreement with the explanation given by Macrides et al. (1987). Significant decays of the downgoing and upcoming reflections from the lower and upper interfaces can be observed when the reflections travel into and through the Clearwater layer, which is one of the factors making the reflection events difficult to be identified in the real seismic observation when the data is contaminated by noise.

This model by no means explains the complexity of the real data but realistic finite difference simulations with attenuation helped in the verification of the interpretation made previously. These complications will not be covered here so that the focus is kept on the main features of the example and the difference between the acoustic modeling and the viscoacoustic modeling. Some minor amplitude difference arise because a two dimensional model and a line source are used to model the three-dimensional case with a point source in the field example and from the fact that converted phases are not included in the acoustic wave simulations.

4.5 CONCLUSION

In the velocity-pressure finite-difference method, attenuation is incorporated by expressing the convolution integral, which is present in the viscoacoustic constitutive relation, in a differential form. The equations of motion, the viscoacoustic constitutive relation, and the additional differential equations form a first order hyperbolic system which describes the wave motion in a heterogeneous medium. This system is solved by applying a dimensional splitting approach and the MacCormack-type two step finite difference operators which is second order accurate in time and fourth order accurate in space.

Viscoacoustic synthetic seismograms have been compared with field data from crosshole seismic experiments for monitoring steam injection projects in the Cold Lake area and with the synthetic data from acoustic modeling. The viscoacoustic modeling produces synthetic seismograms which are more compatible with the field measurements in terms of the frequency content and energy distribution. The simulations assist in interpreting the field data by establishing the relationship between the features of the seismic sections, such as the wave events, arrival time and amplitude changes, and the velocity and quality factor models and their changes after steam injection.

CHAPTER 5

SEISMIC MIGRATION AND ABSORBING BOUNDARIES WITH A ONE-WAY WAVE SYSTEM IN HETEROGENEOUS MEDIA

5.1 INTRODUCTION

Wave equation migration is an imaging technique performed in either the space-time domain (Claerbout, 1971; Sun and McMechan, 1986), in the space-frequency domain (Tsingas and Kanasewich, 1990), in the wavenumber-frequency domain (Stolt, 1978) or in the wavenumber-time domain (Baysal et al., 1983). In the space-time (x-t) domain, the wave equation migration method, known as time migration, is based on the paraxial approximation and gives accurate results only if there are no lateral velocity variations. Reverse time migration (Sun and McMechan, 1986) incorporates lateral velocity variations into the space-time operations by solving the two-way wave equation but suffers from unwanted internal multiple reflections which are generated from strong velocity variations. This unwanted energy is especially troublesome if it is coherent and migrates to a time when the primaries are weak (Tsingas and Kanasewich, 1990).

The most commonly used wave equation migration method is performed in the space-frequency (x-ω) domain where the paraxial approximation is expressed by parabolic partial differential equations. Although successful in many situations, the method is limited by the assumptions made in deriving the one-way wave equations. In particular it is assumed that spatial derivatives of the velocity can be ignored (Claerbout and Doherty,

1972, Claerbout 1976; Stolt 1978; Gazdag 1980; Berkhout and Van Wulfften Palthe, 1979). In x-ω or x-t migration techniques based on the paraxial approximation, implicit finite difference schemes are applied to avoid instabilities but Claerbout (1985) finds that "in space dimensions higher than one the implicit method becomes prohibitively costly".

The one-way wave equations are commonly obtained by seeking a polynomial or rational approximation to the dispersion relation of a square root form. They are not only used as seismic migration extrapolators but also as absorbing boundary conditions. The absorbing boundaries which are obtained from low order approximations fail to absorb waves impinging at large incident angles. Similarly in seismic migration, wave extrapolators based on low order approximations do not properly image subsurface structures especially in a geological region with complex structure. Higher order approximations improve the imaging at an expense of computational effort.

In this chapter, a hyperbolic system is derived which describes downgoing acoustic waves propagating in heterogeneous media. It is demonstrated that the corresponding dispersion relation is in accordance with the exact dispersion relation tor propagation angles up to $80°$. This first order hyperbolic system is equivalent to a third order partial differential equation, which, for homogeneous media, is reduced into the same form as the $45°$ paraxial wave equation. The one-way wave first order hyperbolic system is solved by applying a (2, 4) explicit finite difference scheme. The resulting snapshots illustrate the behavior of this system.

When the first order system is applied to the x-t migration problem, it offers a number of improvements over conventional depth migration techniques. In particular, posing the migration problem as an extrapolation in time instead of depth avoids problems associated with evanescent energy (Kosloff and Baysal, 1982). Also, unwanted energy related to internal reflections is not present because only downgoing propagating waves are present. Since the instability of explicit schemes is less severe for hyperbolic one-way equations or

systems (x-t domain) than for parabolic ones (ω-x), explicit rather than implicit schemes are applied in order to reduce the computational cost of the one-way wave equation migration in the space-time domain.

A new set of absorbing boundary conditions are constructed based on the one-way wave system. It is shown that these two-dimensional absorbing boundaries improve the absorbing effectiveness. In the last section, examples are presented of the application of the one-way wave system in modelling, in absorbing artificial reflections from the model boundaries, and in migrating prestack synthetic seismic data with large propagation angles.

5.2 ONE-WAY WAVE SYSTEM

The basic equations of motion for two-dimensional acoustic wave propagation in a heterogeneous medium, in the absence of body forces, are:

$$\rho \frac{\partial^2 u_x}{\partial t^2} = \frac{\partial p}{\partial x} \tag{5.2.1}$$

$$\rho \frac{\partial^2 u_z}{\partial t^2} = \frac{\partial p}{\partial z} \tag{5.2.2}$$

with p, u_x, and u_z denoting the negative pressure, the x and z components of the particle displacement respectively, and ρ denoting the density. The pressure can be expressed in terms of the particle displacement components as

$$p = K \left(\frac{\partial u_x}{\partial x} + \frac{\partial u_z}{\partial z} \right), \tag{5.2.3}$$

where K is the bulk modulus. By taking the time derivative of (5.2.3) and replacing particle displacements with particle velocities in (5.2.1), (5.2.2) and (5.2.3), we obtain a first order hyperbolic system

$$\frac{\partial u}{\partial t} = A \frac{\partial u}{\partial x} + B \frac{\partial u}{\partial z} \, , \qquad (5.4.4)$$

where u is given by

$$u = \begin{bmatrix} p \\ v_x \\ v_z \end{bmatrix} \, , \qquad (5.4.5)$$

with v_x, and v_z denoting the x and z components of the particle velocity; A and B are coefficient matrices given by

$$A = \begin{bmatrix} 0 & K & 0 \\ \frac{1}{\rho} & 0 & 0 \\ 0 & 0 & 0 \end{bmatrix} , \qquad (5.4.6)$$

$$B = \begin{bmatrix} 0 & 0 & K \\ 0 & 0 & 0 \\ \frac{1}{\rho} & 0 & 0 \end{bmatrix} . \qquad (5.4.7)$$

Through a characteristic analysis of the one dimensional wave equation in the z direction

$$\frac{\partial \mathbf{u}}{\partial t} = \mathbf{B}\frac{\partial \mathbf{u}}{\partial z} \quad , \tag{5.2.8}$$

it is possible to isolate the upcoming and the downgoing waves. Suppose λ_i be an eigenvalue of $\mathbf{B}$ with corresponding left eigenvectors $\mathbf{l}_B^{(i)}$ (a row vector) and right eigenvectors $\mathbf{r}_B^{(i)}$ (a column vector). Then

$$\mathbf{l}_B^{(i)}\mathbf{B} - \lambda_i\mathbf{l}_B^{(i)} \quad , \tag{5.2.9}$$

$$\mathbf{B}\mathbf{r}_B^{(i)} = \lambda_i\mathbf{r}_B^{(i)} \tag{5.2.10}$$

The orthonormality of the left and right eigenvectors is described by

$$\mathbf{l}_B^{(i)}\mathbf{r}_B^{(j)} = \delta_{ij} \quad . \tag{5.2.11}$$

From (5.2.9) and (5.2.10) it follows that

$$\mathbf{L}_B\mathbf{B}\mathbf{R}_B = \Lambda \tag{5.2.12}$$

where the rows of the matrix $\mathbf{L}_B$ are the normalized left eigenvectors $\mathbf{l}_B^{(i)}$; the columns of the matrix $\mathbf{R}_B$ are the normalized right eigenvectors $\mathbf{r}_B^{(i)}$; and the matrix Λ is diagonal, with $\Lambda_{ii} = \lambda_i$, ordered so that $\lambda_1 \leq \lambda_2 ... \leq \lambda_n$.

Through the linear transformation $\mathbf{w} = \mathbf{L}_B\mathbf{u}$, equation (5.2.8) can be written

$$\frac{\partial \mathbf{w}}{\partial t} = \Lambda\frac{\partial \mathbf{w}}{\partial z} \quad . \tag{5.2.13}$$

provided **B** independent of z. In component form equation (5.2.13) is

$$\frac{\partial w_i}{\partial t} = \lambda_i \frac{\partial w_i}{\partial z} ,$$

(5.2.14)

which describes a wave traveling with a characteristic velocity $-\lambda_i$. For $\lambda_i < 0$, the wave w_i travels in the positive z-direction (down in a geophysical convention). For $\lambda_i > 0$, w_i travels in the negative z-direction (or up). In heterogeneous media (i.e. **B** depends on both x and z) equation (5.2.8) can be expressed as

$$\frac{\partial \mathbf{u}}{\partial t} = \mathbf{R}_B \Lambda \mathbf{L}_B \frac{\partial \mathbf{u}}{\partial z} .$$

(5.2.15)

It can be easily shown that the eigenvalues of matrix **B** are

$$(\lambda_1, \lambda_2, \lambda_3) = (-V, 0, V) ,$$

(5.2.16)

where

$$V = \sqrt{\frac{K}{\rho}}$$

(5.2.17)

is the velocity of the acoustic waves, while

$$\mathbf{L}_B = \frac{1}{\sqrt{2}} \begin{bmatrix} 1 & 0 & -\sqrt{K\rho} \\ 0 & \sqrt{2} & 0 \\ 1 & 0 & \sqrt{K\rho} \end{bmatrix}$$

(5.2.18)

and

$$
\mathbf{R}_B = \frac{1}{\sqrt{2}} \begin{bmatrix} 1 & 0 & 1 \\ 0 & \sqrt{2} & 0 \\ \frac{-1}{\sqrt{K\rho}} & 0 & \frac{1}{\sqrt{K\rho}} \end{bmatrix} . \tag{5.2.19}
$$

By letting $\lambda_3 = 0$ in (5.2.15), we obtain the wave system which describes only downgoing waves

$$
\frac{\partial}{\partial t} \begin{bmatrix} p \\ v_x \\ v_z \end{bmatrix} = \frac{1}{2} \begin{bmatrix} 1 & 0 & 1 \\ 0 & \sqrt{2} & 0 \\ \frac{-1}{\sqrt{K\rho}} & 0 & \frac{1}{\sqrt{K\rho}} \end{bmatrix} \begin{bmatrix} -\sqrt{\frac{K}{\rho}} & 0 & 0 \\ 0 & 0 & 0 \\ 0 & 0 & 0 \end{bmatrix} \begin{bmatrix} 1 & 0 & -\sqrt{K\rho} \\ 0 & \sqrt{2} & 0 \\ 1 & 0 & \sqrt{K\rho} \end{bmatrix} \frac{\partial}{\partial z} \begin{bmatrix} p \\ v_x \\ v_z \end{bmatrix} \tag{5.2.20}
$$

or

$$
\frac{\partial}{\partial t} \begin{bmatrix} p \\ v_x \\ v_z \end{bmatrix} = \frac{1}{2} \begin{bmatrix} -\sqrt{\frac{K}{\rho}} & 0 & K \\ 0 & 0 & 0 \\ \frac{1}{\rho} & 0 & -\sqrt{\frac{K}{\rho}} \end{bmatrix} \frac{\partial}{\partial z} \begin{bmatrix} p \\ v_x \\ v_z \end{bmatrix} . \tag{5.2.21}
$$

By replacing the negative signs in (5.2.21) with positive ones this wave system describes upcoming waves.

In two dimensions, since we have no restriction for waves propagating in the positive or negative x-directions, a good approximation for a downgoing wave equation can be obtained by replacing the second term on the right hand side of (5.2.1) with the right side term of (5.2.21), that is

$$\frac{\partial}{\partial t}\begin{bmatrix} p \\ v_x \\ v_z \end{bmatrix} = \begin{bmatrix} 0 & K & 0 \\ \frac{1}{\rho} & 0 & 0 \\ 0 & 0 & 0 \end{bmatrix} \frac{\partial}{\partial x}\begin{bmatrix} p \\ v_x \\ v_z \end{bmatrix} + \frac{1}{2}\begin{bmatrix} -\sqrt{\frac{K}{\rho}} & 0 & K \\ 0 & 0 & 0 \\ \frac{1}{\rho} & 0 & -\sqrt{\frac{K}{\rho}} \end{bmatrix} \frac{\partial}{\partial z}\begin{bmatrix} p \\ v_x \\ v_z \end{bmatrix}$$

or

$$\frac{\partial \mathbf{u}}{\partial t} = \mathbf{A}\frac{\partial \mathbf{u}}{\partial x} + \mathbf{D}\frac{\partial \mathbf{u}}{\partial z} \ . \tag{5.2.22}$$

This system has the general solution of the form

$$\begin{bmatrix} p \\ v_x \\ v_z \end{bmatrix} = \begin{bmatrix} \hat{p} \\ \hat{v}_x \\ \hat{v}_z \end{bmatrix} e^{i(\omega t - k_x x - k_z^* z)} \ . \tag{5.2.23}$$

The necessary condition for (5.2.23) to be a non-trivial solution of the system (5.2.22) gives the dispersion relation, which is refer to as D1, for downgoing waves,

$$D1{:}k_z^* = \frac{k^2 - k_x^2}{k^2 - \frac{1}{2}k_x^2}\,k \ , \tag{5.2.24}$$

where

$$k = \frac{\omega}{V} \tag{5.2.25}$$

and

$$k_x = \frac{\omega}{V} \sin \theta ,$$ (5.2.26)

with θ denoting the wave propagation angle measured from the z-axis to the x-axis. This dispersion relation may be compared to the exact downgoing wave dispersion

$$k_z = \sqrt{k^2 - k_x^2}$$ (5.2.27)

in Figure 5.2.1. Slightly lower values of k_z^* appear at incident angles above 45°. This can be improved by multiplying matrix A in (5.2.22) with $\sqrt{\alpha}$ ($0 < \alpha < 1$) to slightly reduce the characteristic velocity in the x-direction. i.e.

$$\frac{\partial u}{\partial t} = \sqrt{\alpha}\, A\, \frac{\partial u}{\partial x} + D\, \frac{\partial u}{\partial z} .$$ (5.2.28)

The corresponding dispersion relation, which is refered to as D2, then becomes,

$$D2: \quad k_z^* = \frac{k^2 - \alpha k_x^2}{k^2 - \frac{1}{2}\alpha k_x^2}\, k .$$ (5.2.29)

By minimizing the root mean square error of k^*_z relative to k_z for angles up to 80° it is found that $\alpha = 0.905$. The dispersion relation D2 is shown in Figure 5.2.1. The system (5.2.28) is hyperbolic because both coefficient matrices A and D have real eigenvalues and independent eigenvectors. Eliminating v_x and v_z from system (5.2.28) an equivalent third order partial differential equation can be obtained as

$$\frac{1}{2}\frac{\partial^3 p}{\partial t^2 \partial z} + \frac{V\rho}{2}\frac{\partial}{\partial z}\left(\frac{1}{V\rho}\frac{\partial^2 p}{\partial t^2}\right) - \frac{\alpha}{2} V\rho\frac{\partial}{\partial z}\left[V\frac{\partial}{\partial x}\left(\frac{1}{\rho}\frac{\partial p}{\partial x}\right)\right] + \frac{1}{V}\frac{\partial^3 p}{\partial t^3} - \alpha V\rho\frac{\partial}{\partial x}\left(\frac{1}{\rho}\frac{\partial^2 p}{\partial t\partial x}\right) = 0$$

$$(5.2.30)$$

which describes the pressure wave in a heterogeneous media. If we assume a homogeneous medium, equation (5.2.30) can be reduced into

$$\frac{\partial^3 p}{\partial t^2 \partial z} - \frac{\alpha}{2} V^2\frac{\partial^3 p}{\partial x^2 \partial z} + \frac{1}{V}\frac{\partial^3 p}{\partial t^3} - \alpha V\frac{\partial^3 p}{\partial t\partial x^2} = 0 \ ,$$

$$(5.2.31)$$

where for $\alpha = 1$ or 0.905, one obtains the differential equation corresponding to the dispersion relations D1 or D2, respectively.

Originally, one-way wave equations have been obtained by seeking a polynomial or rational approximation to the dispersion relation (5.2.27). The continued fraction method (Hildebrand, 1956) is commonly applied to (5.2.27) to obtain a rational approximation. Clayton and Engquist (1977) proposed the dispersion relation A3

A3:

$$\frac{k_z^*}{k} = \frac{1 - \frac{3}{4}(k_x/k)^2}{1 - \frac{1}{4}(k_x/k)^2}$$

$$(5.2.32)$$

Equation (5.2.32) after inverse Fourier transforming becomes

$$\frac{\partial^3 p}{\partial t^2 \partial z} - \frac{V^2}{4}\frac{\partial^3 p}{\partial x^2 \partial z} + \frac{1}{V}\frac{\partial^3 p}{\partial t^3} - \frac{3V}{4}\frac{\partial^3 p}{\partial t\partial x^2} = 0$$

$$(5.2.33)$$

This equation is known as the 45° paraxial approximation of the acoustic wave equation and describes downgoing acoustic waves. In deriving equation (5.2.33) a homogeneous

vel⋅ ⋅ty model is assumed (Claerbout 1972, 1976; Stolt 1978; Gazdag 1980; Berkhout and Van Wulfften Palthe, 1979).

The dispersion relation A3 and its error relative to the exact dispersion relation are shown in Figure 1. A3 is called the 45° approximation since the error becomes large beyond this angle. Similarly, higher order approximations can be obtained. However, higher order differentials involved in the corresponding differential equations increase the computational cost.

The dispersion relation D1 (see Figure 5.2.1) coincides with the exact relation at both 0° and 90°. The error at angles above 45°, however, is higher than that for A3. By sacrificing the accuracy at 90° which is not important in practice, D2 gives high accuracy ⋅ propagation angles ranging up to 80°.

The dispersion relations D1 and D2 correspond to the sat   ⋅   ⋅ the first order differential system as the full wave equation system (5.2.1   ⋅   ⋅t order system (5.2.28) describing wave motion in heterogeneous media has the ⋅⋅   ⋅tage in applications over the scalar equatior ⋅ 2.30) not only because of the lower order differential operators involved but also because of the absence of derivatives of elastic parameters. It avoids the errors due to numerical differentiation of the physical parameters which are required in finite difference approximations of higher order differential equations for wave   ⋅⋅⋅ion in heterogeneous media. Hyperbolic systems and equations can be solved numerically at a reduced cost by applying explicit rather than implicit finite difference s ⋅emes. Instabilities of explicit schemes are not so severe for hyperbolic equations as they are for parabolic equations (Vafidis, 1983).

In order to demonstrate the effectiveness of the one-way wave system we consider a simple two layer model. The wave propagation problem is solved twice, the first time using the full wave system (5.2.4) and the second time using the one-way wave system (5.2.28). The snapshots of the pressure field fr⋅ n the two methods are shown in figure
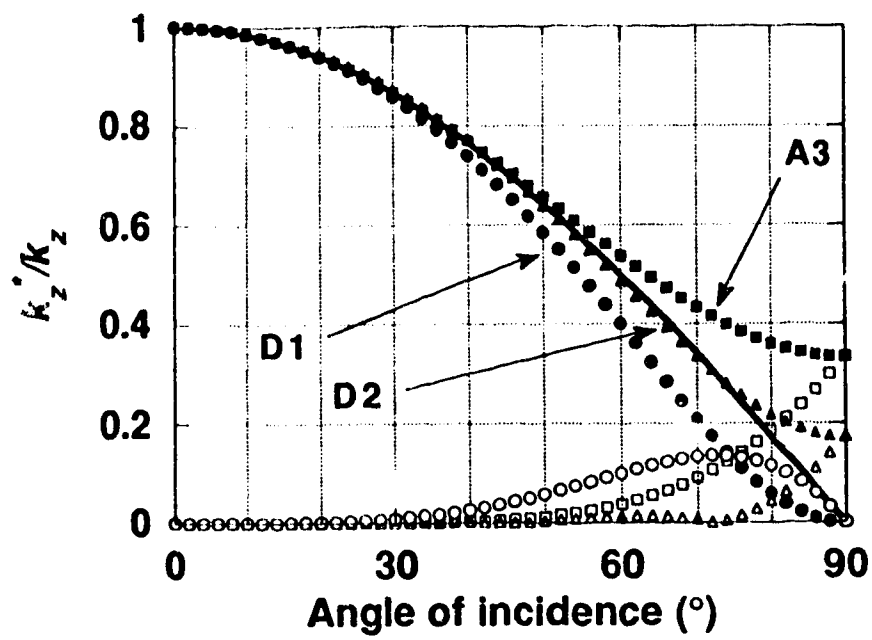
Figure 5.2.1 A comparison of the exact dispersion relation (continuous line) for the acoustic wave equation with the dispersion relations A3 (squares), D1 (circles), D2 (triangles) and their errors (open symbols).

5.2.2. It is obvious that the upcoming wave shown in the full wave equation snapshot is not present in the one-way wave equation snapshot. The downgoing wave is of the same quality in both snapshots. With this property, the one-way wave equation can be applied in seismic migration and in construction of absorbing boundaries for numerically solving the problem involving wave propagation.

5.3 SEISMIC MIGRATION WITH THE ONE-WAY WAVE SYSTEM

Seismic migration consists of two steps: (1) propagating the reflected waves back along their upcoming path and (2) imaging the waves at the reflecting interfaces. With the seismic section considered as the surface record of an upcoming wave field, the major concern in seismic migration is the formulation of equations which properly describe downgoing waves in order to accomplish extrapolation of the reflected wave field. Most of the wave equation migration techniques are based on dispersion relations of different accuracy in terms of describing waves propagating at large angles. Full wave equations were also used to implement wave field extrapolation.

Here, we use the downgoing wave system (5.2.28) as the wave field extrapolator. A M Co finite difference scheme of fourth order accuracy in space and second order accuracy in time and a dimensional splitting technique is applied to system (5.2.28). Two of the main advantages of the splitting methods are that stability properties are governed by one dimensional schemes and that splitting schemes have smaller phase errors than a wide s of unsplit schemes (Turkel, 1974). The stability condition of the MacCormack explicit finite difference scheme is $p\,V_{max} < 2/3$, where V_{max} is the maximum P-wave velocity in m/s, $p = \Delta t/\Delta x$, Δt is the time step in seconds and Δx is the grid size in meters. To avoid grid dispersion, $\Delta x < \lambda_{min}/6$ where λ_{min} is the minimum wavelength present in the
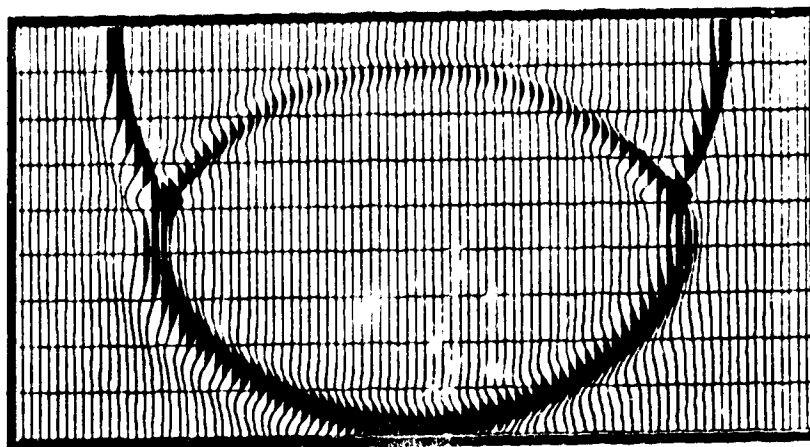
(a)
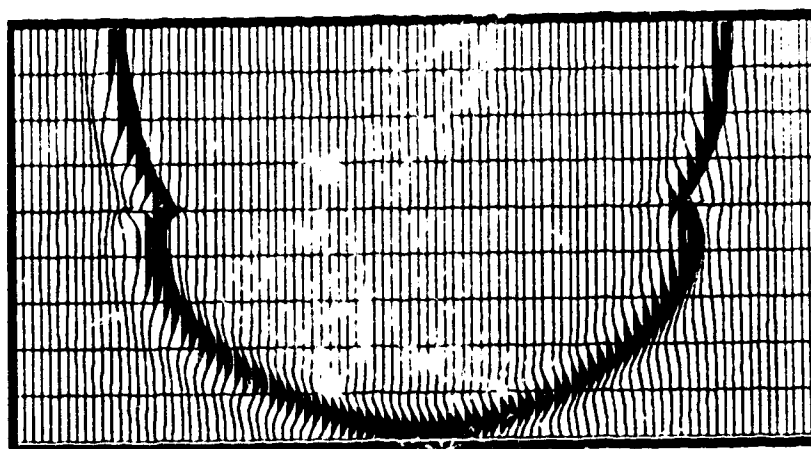
(b)

Figure 5.2.2   Snapshots for waves described by the full wave equation (a) and for waves described by the one-way wave equation (5.2.28) which corresponds to the dispersion relation D2 (b).

seismograms. The detailed description of the finite difference scheme is given in section 5 of chapter 2.

The procedure for migrating seismic data with the one-way wave system (5.2.28) is similar to reverse time migration (McMechan 1983, Baysal et al. 1983). Here, we consider the time reversed seismogram of a common shot gather or a CDP stacked section as the time variation of wave sources along the receiver line. In other words, our method solves an initial value problem rather than a boundary value problem which is encountered in reverse time migration. The wave field is downward propagated by solving numerically the acoustic one-way wave system. One of the advantages of migrating with the one-way wave system is that during the extrapolation procedure, practically no reflections exist at the discontinuities of the velocity model. Also, during the extrapolation procedure, the geometric spreading of the reflected wave energy is compensated. So, the total energy of each reflection event is carried back to the reflector. Hence, a reflectivity proportional image of the subsurface can be obtained by this migration technique for long enough receiver lines when geometric compensation of the incident waves is performed.

In post-stack migration, the velocity model is halved and the image step is taken for all space points at time zero. For pre-stack data, the extrapolated wave field is imaged at the first arrival time of each space point. Absorbing boundaries are constructed to prevent the artificial reflections from the borders of the computational domain.

5.4 ABSORBING BOUNDARIES

An important application of one-way wave equations is to construct absorbing boundaries. The literature on this subject was reviewed in Chapter 3. The effectiveness of the various absorbing boundaries can be predicted by finding out the reflectivity at the boundary. If we use a full acoustic wave equation in the interior of the model and an appropriate one-way equation at the boundary, it can be shown that the effective reflectivity at the boundary is given by

$$ r = \frac{k_z - k_z^*}{k_z + k_z^*} \tag{5.4.1} $$

or

$$ r = \frac{\sqrt{1 - \left(\frac{V}{\omega}k_x\right)^2} - \left[1 - \phi\left(\frac{V}{\omega}k_x\right)^2\right]\left[1 - \varphi\left(\frac{V}{\omega}k_x\right)^2\right]^{-1}}{\sqrt{1 - \left(\frac{V}{\omega}k_x\right)^2} + \left[1 - \phi\left(\frac{V}{\omega}k_x\right)^2\right]\left[1 - \varphi\left(\frac{V}{\omega}k_x\right)^2\right]^{-1}}, \tag{5.4.2} $$

where $\phi = 1$, $\varphi = 1/2$ for dispersion relation D1, $\phi = \alpha$, $\phi = \alpha/2$ for dispersion relation D2 and $\phi = 3/4$, $\varphi = 1/4$ for dispersion relation A3. By using equation (5.2.26) the reflectivity can be written as

$$ r(\theta) = \frac{\cos\theta - \left(1 - \phi\sin^2\theta\right)\left(1 - \varphi\sin^2\theta\right)^{-1}}{\cos\theta + \left(1 - \phi\sin^2\theta\right)\left(1 - \varphi\sin^2\theta\right)^{-1}}, \tag{5.4.3} $$

where θ denotes the incident angle of the impinging wave. Figure 5.4.1 shows the absolute values of the reflection coefficients for the dispersion relations D1, D2 and A3. It is seen that for D2 the reflection coefficient is smaller than those for A3 and D1 and a significant increase of the reflection coefficient of D2 appears at the incident angle about 80°. Therefore, using D2 or its corresponding differential equation as an absorbing boundary condition, no additional techniques are required for compressing artificial reflections in most practical problems unless waves propagating at angles larger than 80° are present. Switching the boundary condition from A3 to D2 requires little change in the existing codes.
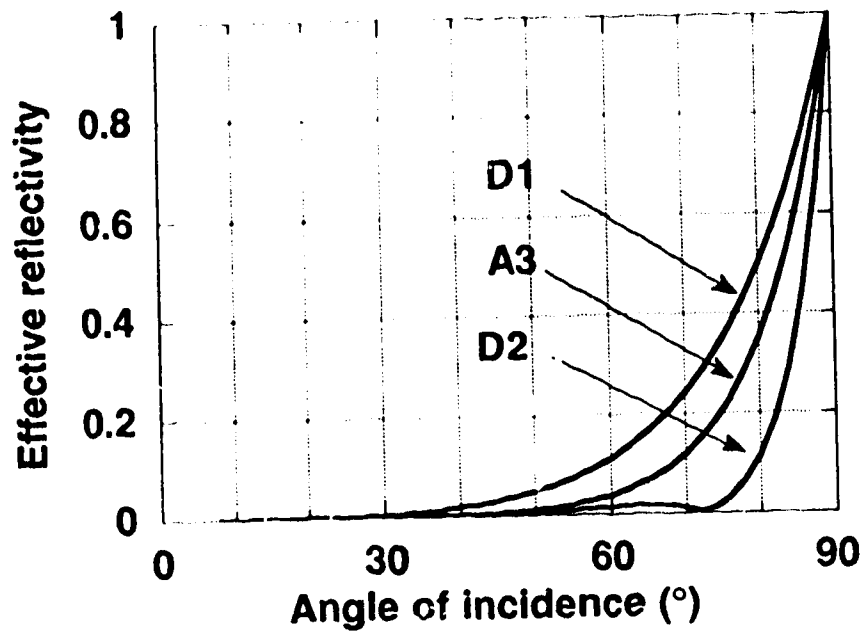
Figure 5.4.1   Reflection coefficients for absorbing boundaries with equations corresponding to dispersion relations A3, D1 and D2.

5.5 NUMERICAL EXAMPLES

The migration technique proposed in this paper is tested for a synthetic model (Figure 5.5.1) which consists of a dipping layer, a graben like structure and a horizontal layer. The physical parameters for the layers are given in Table 5.5.1. Synthetic shot gathers with split spread configuration have been generated using a finite difference technique for acoustic or P-SV wave propagation (Vafidis et al., 1992). Figure 5.5.2 shows a common shot synthetic seismogram from acoustic wave simulation at shot 5 (See Figure 5.5.1). This shot gather is used as the input in the migration procedures using the one-way wave systems (5.2.22) and (5.2.28) which are corresponding to the dispersion relations D1 and D2 respectively. Figure 5.5.3 shows the migrated sections. Pre-stack migration with the one-way wave system (5.2.28) (corresponding to D2) (Figure 5.5.3b) gives a better image for the portions of the reflectors where the reflected waves propagate at high angles relative to the z-axis than that with system corresponding to D1(Figure 5.5.3a).

Table 5.5.1 **Physical parameters for model in Figure 5.5.1**

	V_p (m/s)	V_s (m/s)	ρ (kg/m^3)
Layer 1	3500	2020	2300
Layer 2	4000	2310	2350
Layer 3	4500	2600	2400
Layer 4	4800	2780	2450
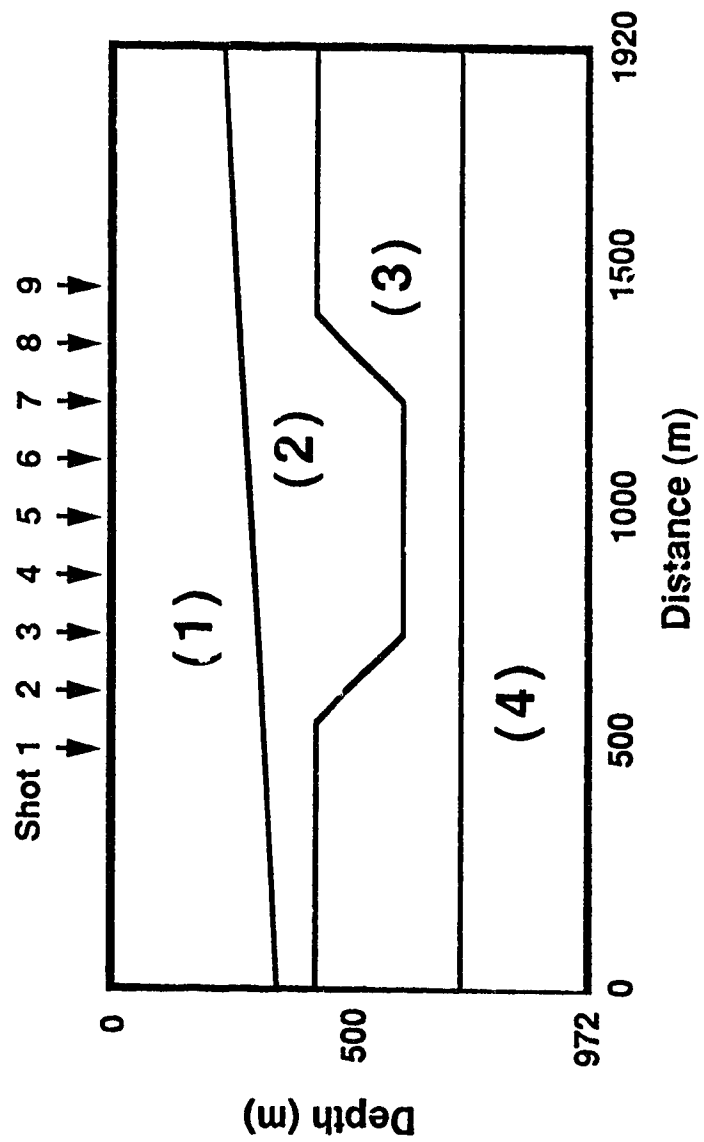
Figure 5.5.1   Model geometry for the migration example. The physical parameters is given

in Table 5.5.1.
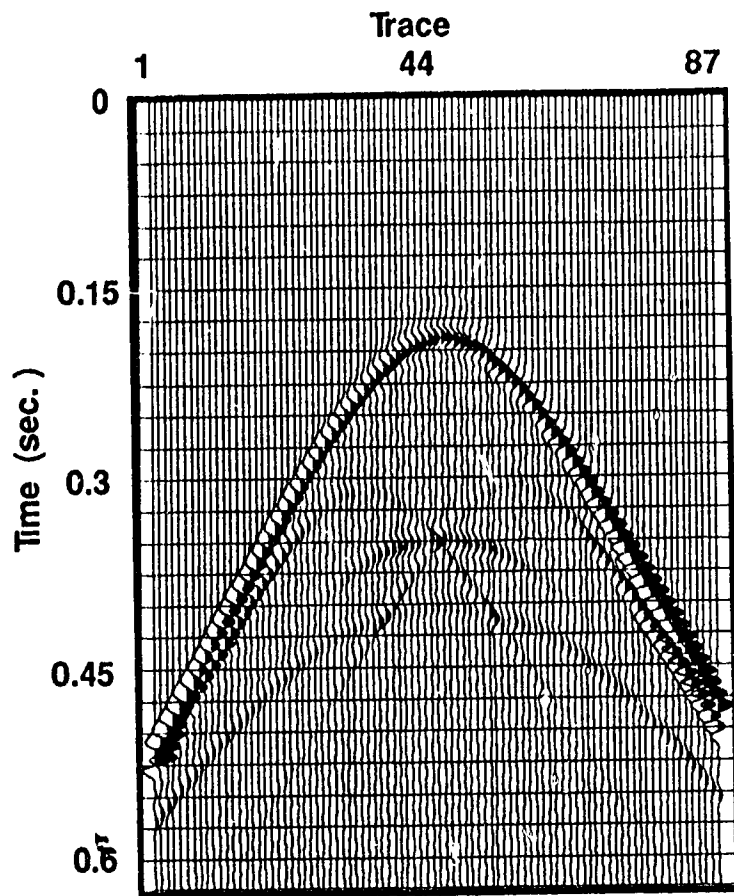
Figure 5.5.2   Shot gather from acoustic wave simulation at Shot #5.

172
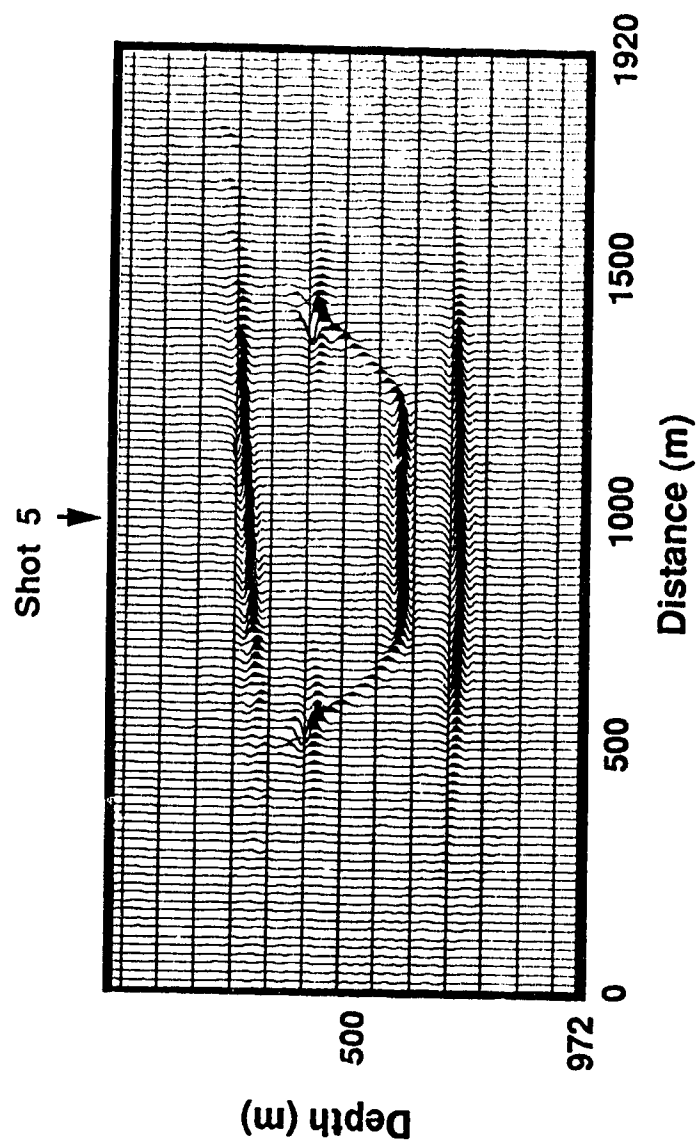
Figure 5.5.3a Migrated sections of the shot gather displayed in figure 5.5.2 with one-way wave equation(5.2.22) which corresponds to the dispersion relation D1.
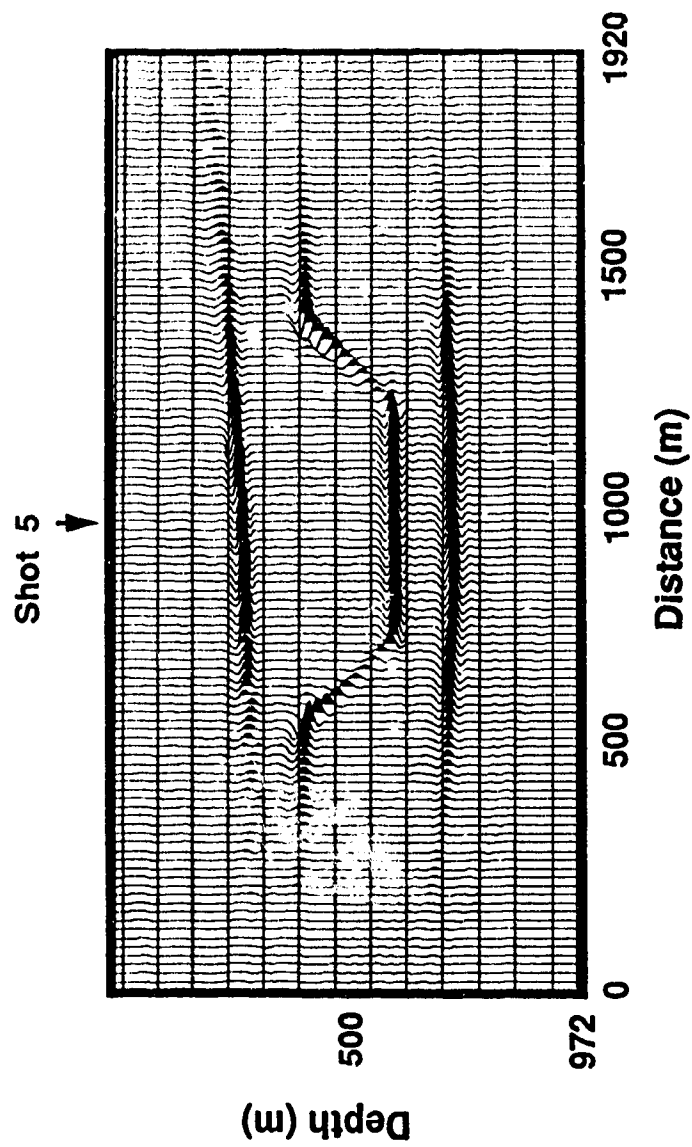
Figure5.5.3b Migrated sections of the shot gather displayed in figure 5.5.2 with one-way
wave equation (5.2.28) which corresponds to the dispersion relation D2.

Figure 5.5.4 shows three shot gathers for shots #3, #4, and #5 from a P-SV wave simulation where, apart from the P-P reflections, additional converted phases are observed. Figure 5.5.5 shows the migrated sections for the shot gathers displayed in Figure 5.5.4. The migration properly images those portions of the reflectors from which reflections are recorded by the receivers. The spots at depth around 450 m in the section of Figure 5.5.5 are observed at locations with different x-coordinates for different shot gathers. These spots are related to converted phases and they are not present in the migrated sections (see F·gure 5.5.3) for acoustic shot gathers. By stacking nine shot migrated sections for shots #$_1$ to #9, a very high quality image (Figure 5.5.6) is obtained. Stacking after migration removes effects which are related to converted phases and other inherent noise. Figure 5.5.7 gives an example of post-stack migration section. The original zero-offset section, given in Figure 2.6.16, is obtained from porous medium seismic modeling with Biot's equation. The earth model is given in Figure 2.6.14.

The superiority of the absorbing boundaries proposed in this chapter is also illustrated by comparing them with the one dimensional absorbing boundaries (Bayliss et al., 1986) available for solving first order hyperbolic systems. The synthetic seismograms displayed in figure 5.5.8 have been calculated from acoustic wave simulations with one dimensional (a) and two dimensional (b) absorbing boundaries. The two dimensional absorbing boundaries based on the one-way wave system (5.2.25) effectively absorb the artificial reflections from the model boundaries. In the synthetic traces from the one dimensional absorbing boundaries, we still observe energy related to the artificial reflections, because only the waves impinging the boundary at normal incidence are properly absorbed.
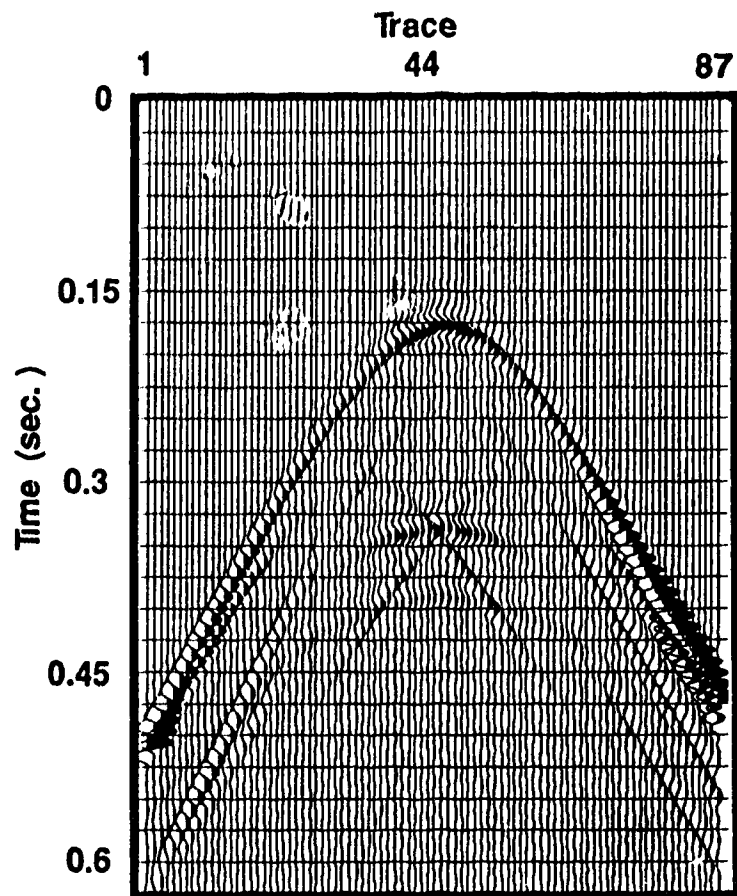
Figure 5.5.4 a Shot gather from elastic wave simulation at Shot #5.
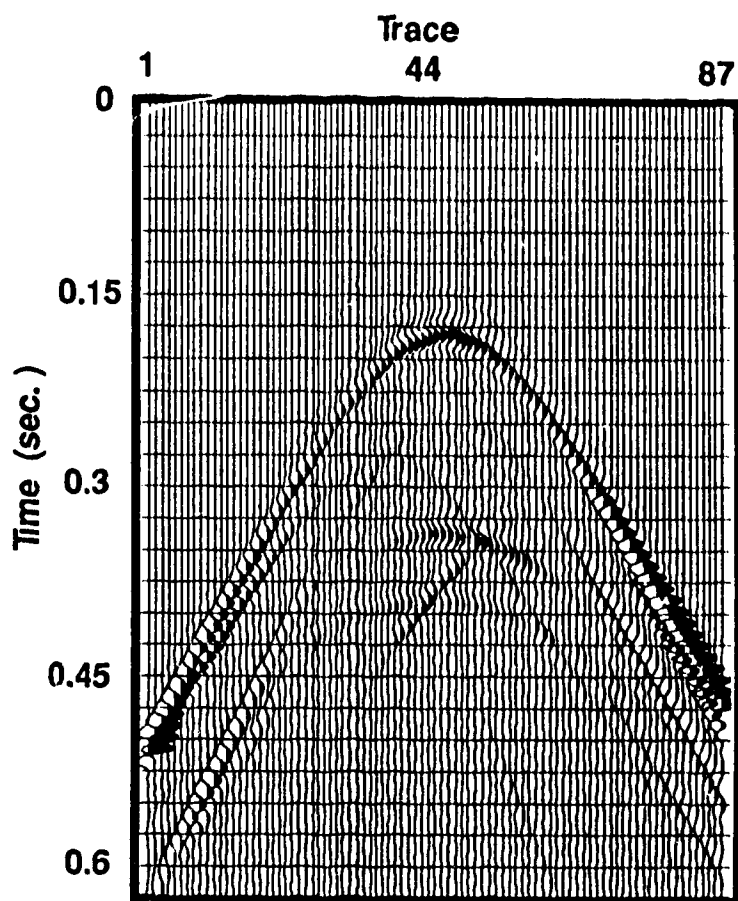
Figure 5 5.4b Shot gather from elastic wave simulation at Shot #4.
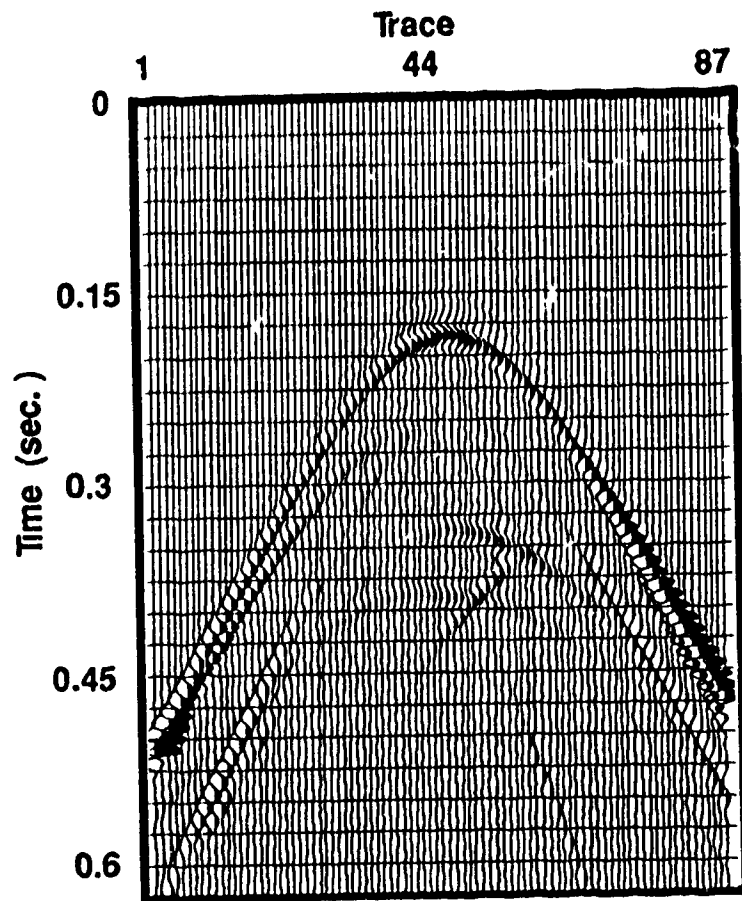
Figure 5.5 4c Shot gather from elastic wave simulation at Shot #3.
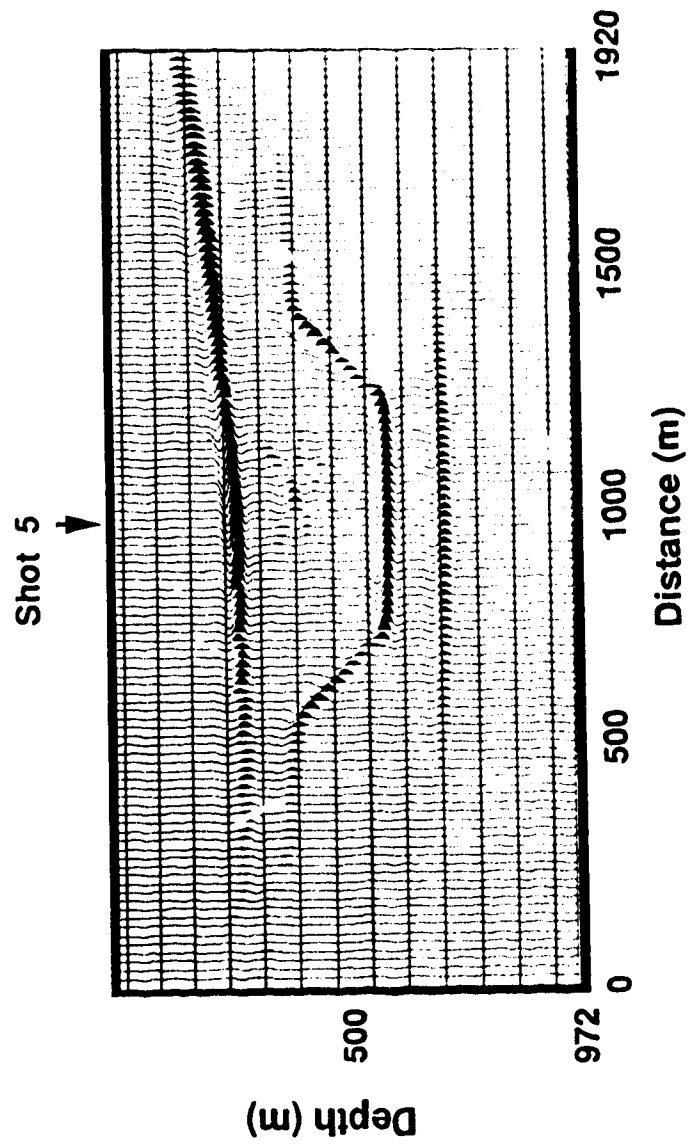
Figure 5.5.5a, Migrated sections of the shot gather displayed in Figure 5.5.4a with one-way wave equation D2.
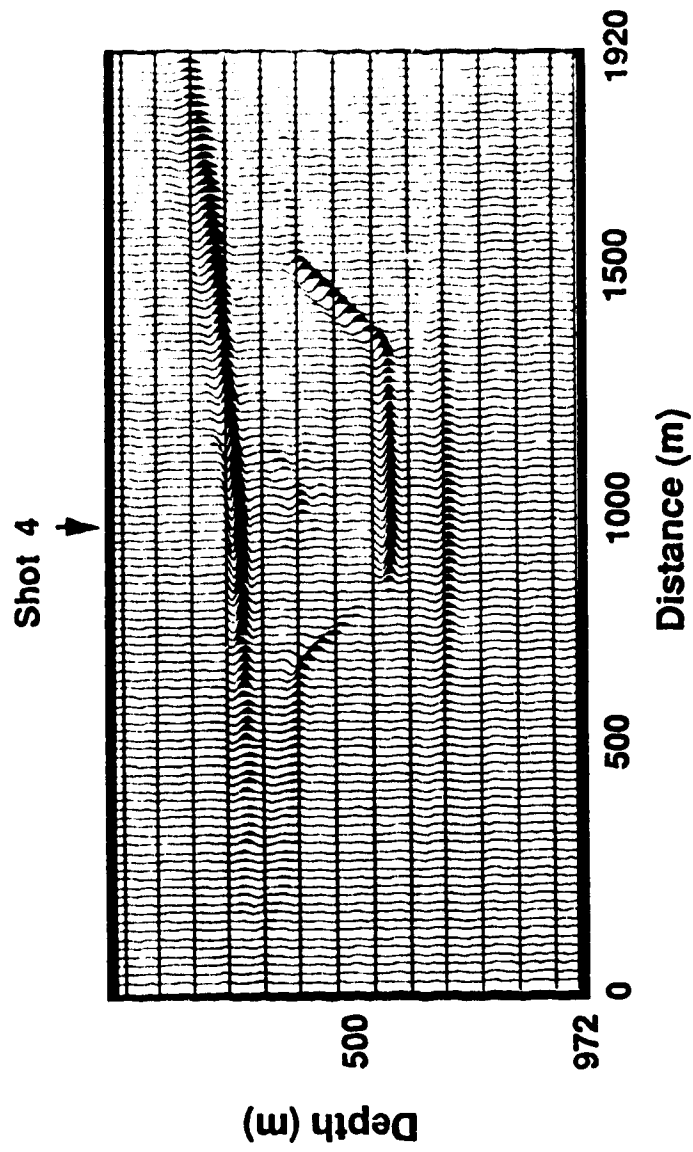
Figure 5.5.5b Migrated sections of the shot gather displayed in figure 5.5.4b with one-way wave equation D2.
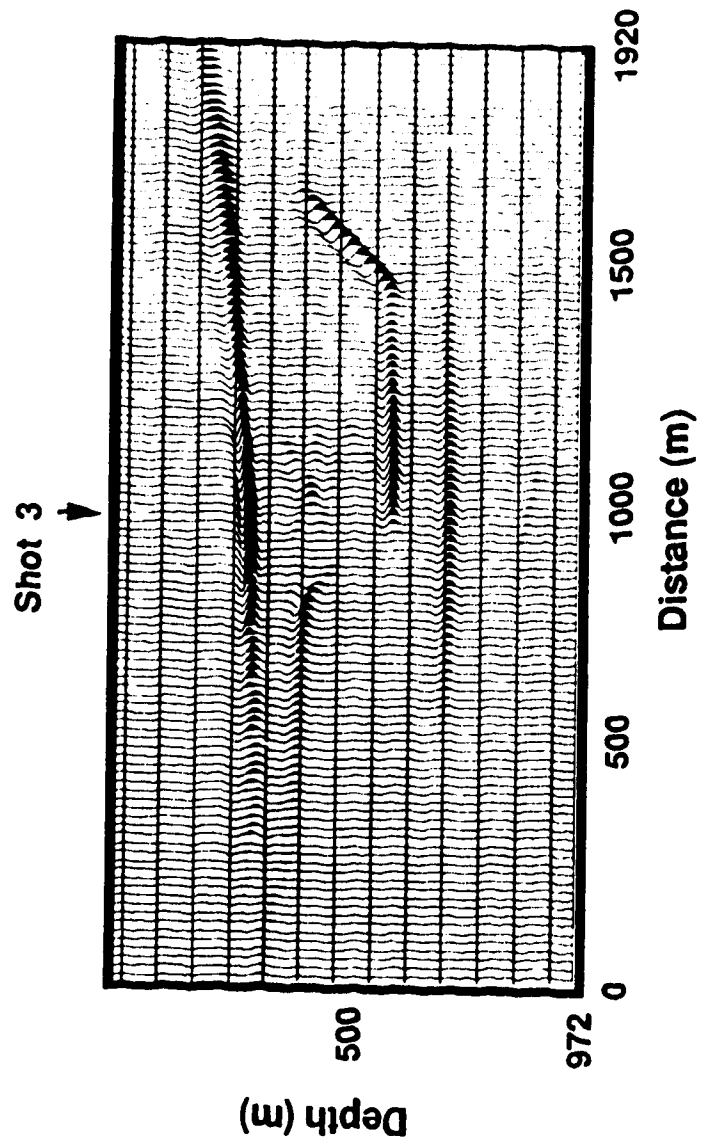
Figure 5.5.5c Migrated sections of the shot gather displayed in figure 5.5.4c with one-way wave equation D2.
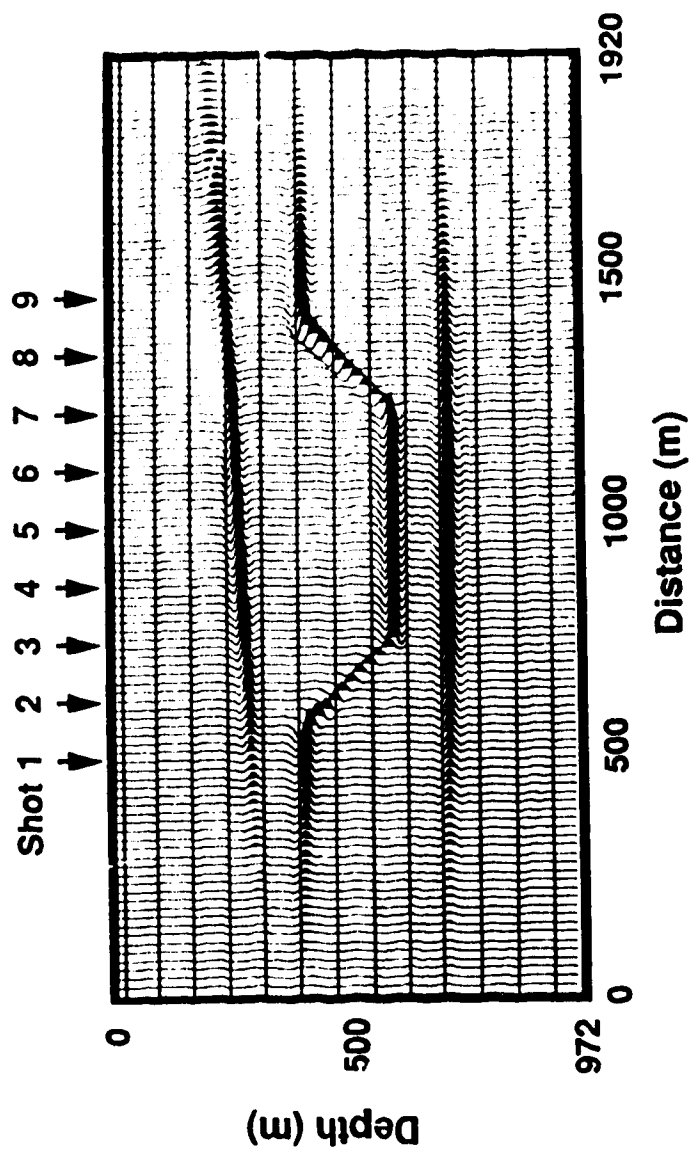
Figure 5.5.6 Stacked section of migrated P-SV data from shot #1 to Shot #9.
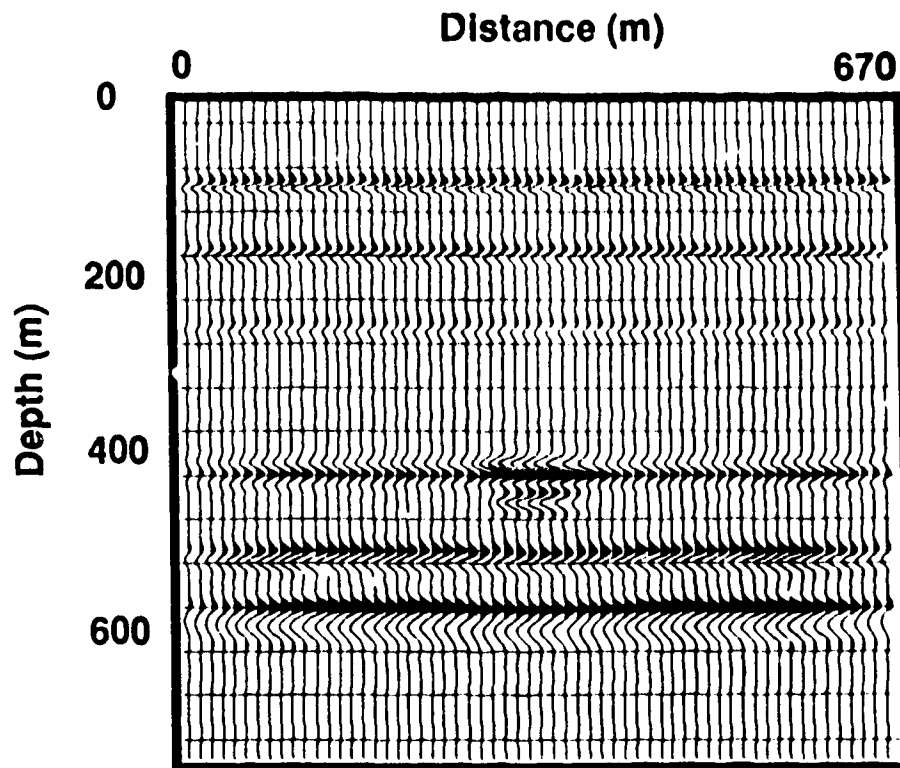
Figure 5.5.7 Post-stack migration section. The input zero-offset section, given in Figure 2.6.16, is from porous medium seismic modeling with Biot equation. The earth model is given in Figure 2.6.14.
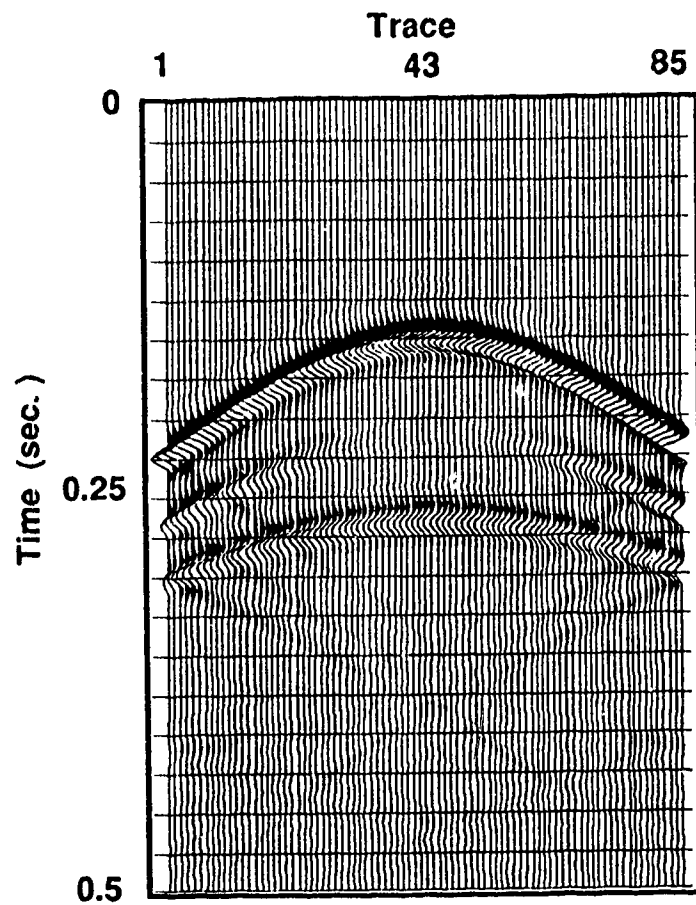
Figure 5.5.8a   Common shot synthetic seismogram with one-dimensional absorbing boundaries.
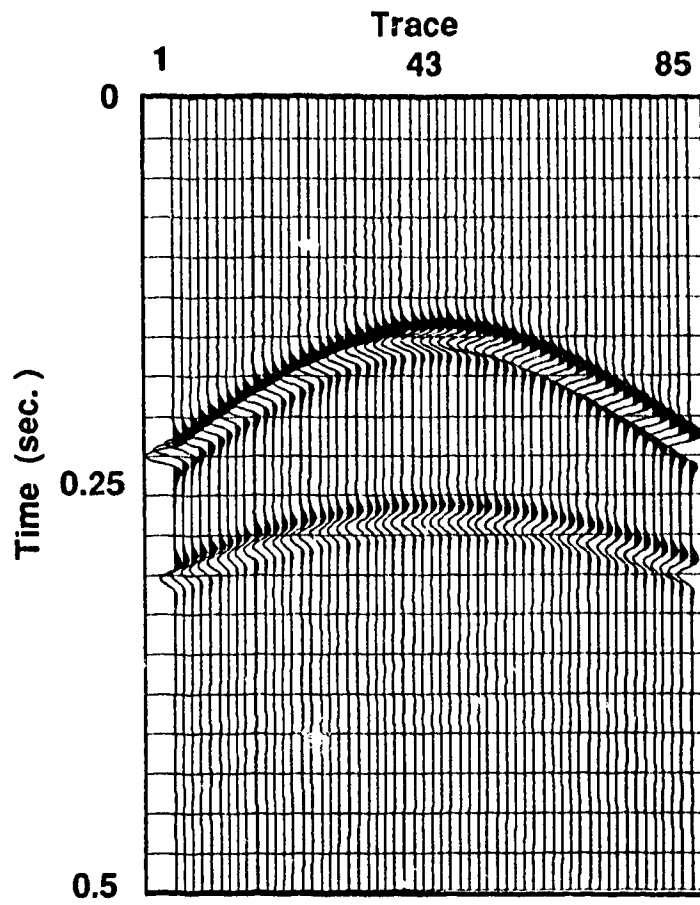
Figure 5.5.8b Common shot synthetic seismogram with the two-dimensional absorbing boundaries constructed from the one-way wave equation D2.

5.6   CONCLUSIONS

A first order hyperbolic system, describing one-way wave propagation in heterogeneous media, is formulated. Its dispersion relation is a close approximation for waves propagating with angles of incidence up to 80°. This system provides the basis for constructing absorbing boundaries and wave field extrapolation operators. Its equivalent scalar differential equation is in third order. For homogeneous media the scalar equation has the same form as the existing 45° paraxial wave equation.

A migration method is developed inherently for heterogeneous media based on the one-way wave system. By comparing dispersion relations, it has been shown that this space-time migration technique is more accurate than existing wave equation methods based on the 45° paraxial approximation. A (2,4) explicit finite difference scheme is employed in the downward wave extrapolation procedure. The application of this new method in synthetic acoustic or P-SV shot gathers results in high quality migrated sections.

The new absorbing boundaries have smaller effective reflectivity at large incident angles than those of the absorbing boundaries proposed by Clayton and Engquist (1977). Synthetic seismograms illustrate that the two-dimensional absorbing boundaries have better absorbing performance than existing one-dimensional absorbing boundaries for the first order hyperbolic system of acoustic waves.

CHAPTER 6

CONCLUSION AND DIRECTION

Seismic wave propagation in an inhomogeneous fluid saturated poroelastic medium has been accurately simulated by using the velocity stress finite-difference method. The development of the first order hyperbolic systems for wave motion in non-homogeneous porous media from Biot's theory and the de la Cruz-Spanos theory allows one to model the fluid and solid particle velocities, the solid stress components, and the fluid pressure simultaneously. Since the first order systems are free of spatial derivatives of the physical parameters, except the porosity, errors due to the numerical approximation of the spatial derivatives of those physical parameters are avoided. The application of the dimensional splitting method and the high order MacCormack finite difference scheme is effective in reduceing the phase error (numerical dispersion) in the numerical solutions. General analytic solutions have been derived for waves generated by a P-wave point or line source whose body forces act on both the solid and fluid part of a poroelastic medium. These solutions are useful not only in demonstrating the wave properties but also in source implementation of finite difference modeling and in algorithm testing.

Biot's theory was developed based on the *a priori* assumption that the concepts and principles of continuum mechanics can be applied to the measurable macroscopic variables whereas the de la Cruz-Spanos theory was developed through the technique of volume averaging in passing from the well established physical laws at the microscopic level to the macroscopic level. Although each thoery's start point and development are different, both

theories give similar results in the numerical simulations presented in this thesis.

In simulations with two layer models of porous media, "slow" compressional incident, transmitted and reflected phases are present in addition to the regular ("fast") P waves and S waves in solid elastic media when we deliberately set the fluid viscosity of the porous media unusually small. Forward modeling with wave equations for porous media establishes the relationships between the measurable wave characteristics, such as the wave propagation velocities, the amplitude, the waveform etc, and the physical properties of the solid framework and the fluid contents of the rocks, such as their elastic moduli, densities, the porosity of the rock, etc. The different patterns of the reflection amplitude and reflectivity variations versus angle of incidence extracted from the finite difference modeling over the interfaces of shale to sandstone saturated with different fluid contents and the contact interfaces of different types of fluids within sandstone indicate that these methods are applicable in diagnosing the rock properties of direct interest to hydrocarbon exploration and recovery.

In these simulations, it is observed that attenuation is more pronounced for the "slow" compressional waves especially at high fluid viscosities. This is in accordance with Biot's theory and the de la Cruz-Spanos theory where the attenuation is related to viscous dragging or to solid and fluid interactions. It is also observed that this attenuation mechanism is of secondary importance for "fast" compressional waves and for rotational waves. So, in porous media the other main attenuation mechanism should be related to the inelasticity of the solid matrix and finite difference modeling should be extended to porous viscoelastic media.

In order to incorporate the quality factor Q into seismic wave simulation in the time domain a first order hyperbolic system has been established for wave motion in inhomogeneous viscoacoustic media by transforming the convolution integral which is present in the constitutive relation into several differential equations through the

introduction of intermediate variables. In this development a general anelastic medium is approximated by a generalized Maxwell body. The residual error decreases as the number of the basic elements of the generalized Maxwell body increases for a given frequency range. In the finite difference modeling with the first order system, although the increase of the element number requires more computer memory, it does not result in significant increase of computational time. This method may be extended to the viscoelastic problem and, furthermore, may be combined with the Biot or C-S wave equations for porous media in order to cooperate the attenuation due to the inelasticity of the solid matrix into the finite difference modeling of seismic waves in porous media.

The formulation of absorbing boundary conditions have been difficult for elastic wave modeling due to the presence of S waves. It is even more challenging to construct absorbing boundaries in wave simulation in porous media since additional "slow" P waves may be present. In this thesis several approaches are proposed for constructing absorbing boundaries which are applicable to wave propagation problems in elastic and porous media. The one dimensional absorbing boundary conditions are formulated to separate outgoing waves from incoming waves for all wave types based on the characteristic analysis of the wave equations, and to absorb the waves impinging upon the artificial boundaries perpendicularly. The wave propagation modification approach is used to adjust gradually the wave propagation direction in a transition zone so that the waves hit the artificial boundaries at a right angle. The one-way sponge filters are designed for damping the remaining incoming waves in the transition zone without affecting the outgoing waves. The combination of the one-dimensional absorbing boundary conditions with either the wave propagation modification approach or the one-way sponge filter approach effectively absorbs all incident waves at the artificial boundaries. The one-way sponge filter approach is distinguished from the existing sponge method (i.e. Cerjan et al., 1985) not only because it is used in combination with the one-dimensional absorbing boundary conditions but also

in its one-way damping property. In the application of these techniques the thickness of the transition zone is reduced to about one wave-length for the wave of dominate frequency and highest velocity. The extension of these methods to three-dimensional problems is straightforward.

The first order hyperbolic system formulated in Chapter 5 for describing one-way waves in heterogeneous media provides the basis for a new method of performing pre-stack and post-stack seismic depth migration. It has been shown that the corresponding dispersion relation is in accordance with the exact dispersion relation for propagation angles up to $80°$. When this first order system is applied to the migration problem in the space and time domain, it offers a number of improvements over the conventional depth migration techniques. In particular, posing the depth migration as a back-propagation procedure in time instead of an extrapolation in depth avoids problems associated with evanescent energy. Since the depth migration method here was developed inherently for heterogeneous media based on the one-way wave system, no effort is needed for additional operations for the time-shift or thin-lens term to account for the lateral variation of velocity as is required in conventional depth migration. Also the unwanted image noise and energy loss related to internal reflections in migration with the full wave equation are not present because only downgoing propagating waves are involved in the present method. Since we work with a first order system which is free of the space derivative of the physical parameters, the error from the numerical approximation of the space derivative of the physical parameters is avoided even though we are dealing with heterogeneous media. Because the instability problem of explicit schemes is less severe for the hyperbolic one-way wave system (in the x-t domain) than for parabolic ones (in the ω-x domain), the less expensive explicit finite difference scheme rather than the implicit scheme can be applied in order to reduce the computational cost in finite difference depth migration in the space-time domain. This is important because it makes the extension of this method to three-dimensional depth migration economically feasible. In fact, the computational cost of this migration method is

exactly the same as that of acoustic forward modeling when the same finite difference scheme is used.

The present one-way wave system is also successfully applied in constructing absorbing boundaries in acoustic wave forward modeling problems and migration problems. It is possible to extend this method to elastic wave propagation problems.

BIBLIOGRAPHY

Alford, R.M., Kelly, K.R., and Boore, D.M., 1974, Accuracy of finite-difference modeling of the acoustic wave equation, *Geophysics*, **39**, 834-842.

Alterman, Z. S., and Karal, F.C., 1968, Propagation of elastic waves in layered media by finite-difference methods, *Bull. Seis. Soc. Am.*, **58**, 367-398.

Alterman, Z. S., and Loewenthal, D., 1970, Seismic waves in a quarter and three-quarter plane, *Geophys. J. Roy. Astr. Soc.*, **20**, 101-126.

Aki, K., and Richards, P.G., 1980, *Quantitative Seismology: Theory and Methods*, Freeman, San Francisco.

Bayliss, A., Jordan, K.E., LeMesurier, B.J. and Turkel, E., 1986, A fourth order accurate finite-difference scheme for the computation of elastic waves, *Bull. Seis. Soc. Am.*, **76**, 1115-1132.

Baysal, E., Kosloff,D.D., and Sherwood, J.W.C., 1983, Reverse time migration, *Geophysics*, **48**, 1514-1524.

Berkhout, A. J., 1982, *Seismic migration: Imaging of acoustic energy by wave field extrapolation. A. Theoretical aspects*, Elsevier Science Publishers, N. Y..

Berkhout, A. J., and Van Wulfften Palthe, D. W., 1979, Migration in terms of spatial deconvolution, *Geophy. Prosp.*, **27**, 261-291.

Berryman, J.G., and Thigpen, L., 1985, Linear dynamic poroelasticity with microstructure for partially saturated porous solids, *J. Appl. Mech.*, **52**, 345-350.

Berryman, J.G., Thigpen, L., and Chin, R.C.Y., 1988, Bulk elastic wave propagation in partially saturated porous solids, *J. Acoust. Soc. Am.*, **84**, 360-373.

Biot, M. A., 1956a, Theory of propagation of elastic waves in a saturated porous solid, I, Low-frequency range, *J. Acoust. Soc Am.*, **28**, 168.

Biot, M. A., 1956b, Theory of propagation of elastic waves in a saturated porous solid, II, High-frequency range, *J. Acoust. Soc Am.*, **28**, 179.

Biot, M. A., 1962a, Mechanics of deformation and acoustic propagation porous media, *J. Appl. Phy.*, **33**, 1482-1498.

Biot, M. A., 1962b, Generalization theory of acoustic propagation in porous media, *J. Acoust. Soc Am.*, **34**, 1254.

Biot, M. A., and Willis, D. G., 1957, The elastic coefficients of the theory of consolidation, *J. Appl. Mech.* **24**, 594-601.

Bultmann, L., 1876, Zur Theorie der elastiche Nachwirkung, *Ann. Phys. Chem. Erqanzung*, **7**, 24-654.

Bonnet, G., 1987, Basic singular solutions for a poroelastic medium in the dynamic range, *J. Acoust. Soc. Am.*, **82**, 1758-1762.

Boore, D.M., 1972, Finite-difference methods for seismic wave propagation in heterogeneous materials, *in* Bolt B.A., Ed., *Methods in Computational Physics*, **11**, Academic Press Inc., 1-37.

Bourbie, T., Coussy, O., and Zinszner, B., 1987, *acoustics of porous media*, Institute francais du petrole publications, Gulf Publishing Company.

Boutin, C., Bonnet, G., and Bard, P.Y., 1987, Green functions and associated sources in infinite and stratified poroelastic media, *Geophys. J. R. astr. Soc.*, **90**, 521-550.

Burridge, R., and Vargas, C.A., 1979, The fundamental solution in dynamic poroelasticity, *Geophys. J. R. Astr Soc.*, **58**, 61-90.

Burridge, R., and Keller, J.B., 1981, Poroelasticity equations derived from microstructure, *J. Acoust. Soc. Am.*, **70**, 1140-1146.

Carcione, J. M., Kosloff, D., and Kosloff, R., 1988a, Wave propagation simulation in a linear viscoelastic medium, *Geoph. J. R. Astr. Soc.*, **95**, 393-407.

Carcione, J. M., Kosloff, D., and Kosloff, R., 1988b, Wave propagation simulation in a linear viscoacoustic medium, *Geophysics*, **53**, 769-777.

Cerjan, C., Kosloff, D., Kosloff, R., and Reshef, M., 1985, A nonreflecting boundary condition for discrete acoustic and elastic wave equations, *Geophysics*, **50**, 705-708.

Cerveny, V., Molotkov, I. A., and Psencik, I., 1977, *Ray Method in Seismology*, University of karlova, Praha.

Chapman, C. H., 1978, A new method for computing synthetic seismograms, *Geophys. J. R. Astr. Soc.*, **54**, 481-518.

Christensen, R. M., 1982, *Theory of viscoelasticity*, Academic Press.

Claerbout, J. F., 1970, Coarse grid calculations of waves in inhomogeneous media with application to delineation of complicated seismic structure, *Geophysics*, **35**, 407-418.

Claerbout, J. F., 1971, Toward a unified theory of reflector mapping, *Geophysics*, **36**, 467-481.

Claerbout, J. F., 1976, *Fundamentals of Geophysical Data Processing*, McGraw Hill Inc.

Claerbout, J. F., 1985, *Imaging the Earth's Interior*, Blackwell Scientific Publications.

Claerbout, J. F., and Doherty, S.M., 1972, Downward continuation of moveout corrected seismograms, *Geophysics*, **37**, 741-768.

Clayton, R., and Engquist, B., 1977, Absorbing boundary conditions for acoustic and elastic wave equations, *Bull. Seism. Soc. Am.*, **67**, 1529-1540.

Dai, N., and Kanasewich, E.R., 1992, One-way equation, absorbing boundary and seismic migration, *Expanded Abstracts of the technical program with authors biographies*, the 62nd Annual International SEG Meeting, New Orleans.

Dai, N., Kanasewich, E.R., and Vafidis, A., 1992a, Seismic migration and absorbing boundaries with an one-way wave system in heterogeneous media. Submitted for publication.

Dai, N., Kanasewich E.R, and Vafidis, A., 1992b, Simulation of seismic waves in porous media. *Expanded Abstracts of the technical program with authors biographies*, the 62nd Annual International SEG Meeting, New Orleans.

Dai, N., Kanasewich E.R., and Vafidis, A., 1992c, Absorbing boundary conditions for seismic waves in elastic and porous media, Submitted for publication.

Dai, N., Vafidis, A., and Kanasewich, E.R., 1990, Surface seismic simulation in steam injection EOR problem with finite differences, *AOSTRA Journal of Research*, **6**, 199-210.

Dai, N., Vafidis, A., and Kanasewich, E.R., 1992d, Wave propagation in viscoacoustic heterogeneous media: the velocity-pressure finite difference media, Submitted for publication.

Dai, N., Vafidis, A., and Kanasewich, E.R., 1992e, Seismic waves in porous media: high order finite difference solution of Biot's equations. Submitted for publication.

Dry, S. M., and Minster, J. B., 1984, Numerical simulation of attenuated wavefields using Pade approx mant method, *Geoph. J. Roy. Astr. Soc.*, **78**, 105-118.

de la Cruz, V., and Spanos, T. J. T., 1983, Mobilization of ganglia, *J. Am. Inst. Chem. Eng.*, **29**, 854-858.

de la Cruz, V., and Spanos, T. J. T., 1985, Seismic wave propagation in a porous medium, *Geophysics*, **50**, 1556-1565.

de la Cruz, V., and Spanos, T. J. T., 1989, Thermomechanical coupling during seismic wave propagation in a porous mediu,. *J. Geophys. Res.*, **94**, B1, 637-642.

de la Cruz, V., Markushevich, V.M., and Spanos, T.J.T., 1991a, Seismic wave propagation in inhomogeneous porous media, preprint.

de la Cruz, V., Eastwood, S.E., Hickey, C.J., and Spanos, T.J.T., 1991b, Seismic parameters in permeable media, preprint.

de Vries, S. M., 1989, *Propagation of transient acoustic waves in porous media*, Report number Et/Em 1989-06, Delft Technical University of Technology.

Emerman, S.H., Schmidt, W., and Stephen R.A., 1982, An implicit finite-difference formulation of the elastic wave equation, *Geophysics*, **47**, 1521-1526.

Emerman, S. H. and Stephen R. A. 1983, , Comment on absorbing boundary conditions for acoustic and elastic wave equations, *Bull. Seis. Soc. Am.*, **72**, 661-665.

Emmerich, H., and Korn, M., 1987, Incorporation of attenuation into time domain computations of seismic wave fields, *Geophysics*, **52**, 1252- 1264.

Engquist, B., and Majda A.,1977. Absorbing boundary conditions for the numerical simulation of waves, *Math. Comp.* **31**, 629-651.

Engquist, B., and Majda, A., 1979. Radiation boundary conditions for acoustic and elastic wave calculations, *Math. Comp.***32**, 313-357.

Feng, S., and Johnson, D.L., 1983, High-frequency acoustic properties of a fluid/porous solid interface: I. New surface modes, *J. Acoust. Soc. Am.*, **74**, 906-914.

French, W.S., 1975, Computer migration of oblique seismic reflection profiles. *Geophysics*, **40**, 961-980.

Fuchs, K., and Muller, G., 1971, Computation of synthetic seismograms with the reflectivity method and comparison with observations, *Geophys. J. R. Astr. Soc.*, **23**, 417-433.

Gazdag, J., 1978, Wave equation migration with the phase shift method, *Geophysics*, **43**, 1342-1351.

Gazdag, J., 1981, Modeling of the acoustic wave equation with transform methods, *Geophysics*, **46**, 854-859.

Geertsma, J., and Smit, D.C., 1961, Some aspects of elastic wave propagation in fluid-saturated porous solids, *Geophysics*, **26**, 169-181.

Gottlieb, D., and Turkel, E., 1976, Dissipative two-four methods for time dependent problems, *Math. Comp.*, **30**, 703-723.

Harrison, D.B., Glaister, R.P., and Nelson, H.W., 1979, Reservoir description of Clearwater oil sand Cold Lake, Alberta, Canada, in: R.F. Meyer, C. T. Steele (eds). *The future of heavy crude oil and tar snads*, 264-279.

Hassanzadeh, S., 1991, Acoustic modeling in fluid saturated porous media, *Geophysics*, **56**, 424-435.

Hedstrom, G.W., 1979. Nonreflection boundary conditions for nonlinear hyperbolic systems, *J. Comput. Phys.*, **30**, 222-237` .

Hickey, C.J. 1990, *Numerical studies of Seismic wave propagation in porous media*. M.Sc. Thesis, University of Alberta.

Higdon, R.L., 1986, Absorbing boundary conditions for difference approximations to the multi-dimensional wave equation, *Math. Comp.*, **47**, 437-459.

Higdon, R.L., 1987, Numerical absorbing boundary conditions for the wave equation, *Math. Comp.*, **49**, 65-90

Higdon, R.L., 1991, Absorbing boundary conditions for elastic waves, *Geophysics*, **56**, 231-241.

Hildebrand,F.B.,, 1956, *Introduction to numerical analysis*, New York, McGraw-Hill.

Hron, F., and Kanasewich, E.R., 1971, Synthetic seismograms for deep sounding studies using asymptotic ray theory, *Bull. Seism. Soc. Am.*, **61**, 1169-1200.

Hubral, P., 1977, Time migration—Some ray theoretical aspects, *Geophs. Prosp.*, **25**, 738-745.

Israeli, M., and Orszag, S.A., 1981, Approximation of radiation boundary conditions, *J. Comput. Phys.*, **41**, 115-135.

Jeffreys, H., 1976, *The Earth*, Cambridge Press, 6th edition.

Johnson, D.L., 1986, Recent developments in the acoustic properties of porous media, *Proceedings of the Enrico Fermi Summer School, Course XCIII: Frontiers in Physical Acoustics*, Elsevier, New York, 255-290.

Judson, D.R., Lin, J., Schultz, P.S. and Sherwood, W.C., 1980, Depth migration after stack, *Geophysics*, **45**, 361-375.

Kanasewich, E.R., 1983, *Cold Lake Seismicity Project : Report No 3, April 1983*, Dept. of Physics, University of Alberta, Edmonton, Canada.

Katsube, N., and Caroll, M., 1987, The mixture theory for fluid-filled porous materials, Theory: *J. Appl. Mech.*, **54**, 1-6.

Kelly, K.R., and Marfurt, K.J., 1990, *Numerical Modelling of Seismic Wave Propagation*. Society of Exploration Geophysicist,. 423-424.

Kelly, K.R., Ward, R.W., Treitel, S., and Alford, R.M., 1976, Synthetic seismograms: A finite-difference approach, *Geophysics*, **41**, 2-27.

Keys, R.G., 1985, Absorbing boundary conditions for acoustic media, *Geophysics*, **50**, 892-902.

Kjartansson, E., 1979, Constant Q - wave propagation and attenuation, *J Geophys. Res.*, **84**, 4737-4748.

Knopoff, L., 1964, Q, *Rev. Geophys. Space Phys.*, **2**, 625- 660.

Kosloff, D., and Baysal, E., 1982, Forward modeling by a Fourier method. *Geophysics*, **47**, 1402-1412.

Kosloff, R. and Kosloff, D., 1986, Absorbing boundary for wave propagation problems, *J. Comp. Phys.* **63**, 363-376.

Larner, K.L., Hatton, L., Gibson, B.S., and Hsu, I., 1981, Depth migration of imaged time sections, *Geophysics*, **46**, 734-750.

Levy, 1979, Propagation of waves in a fluid-saturated porous elastic medium, *Int. J. Eng. Sco.*, **17**, 1005-1014.

Macrides, C.G., and Kanasewich, E. R., 1987, Seismic attenuation and Poisson's rations in oil sands from crosshole measurements, *Can. J. Explor. Geoph.*, **23**, 46-55.

Macrides, C., Kanasewich, E.R., and Baratha, S., 1988, Cross-borehole seismic imaging in steam injection projects, *Geophysics*, **53**, 65-75.

Madsen, N.K., Rodrigue, G.H., and Karush, J.I., 1976, Matrix multiplication by diagonals on a vector/parallel processor, *Inform. Proc. Lett.*, **5**, 41-45.

Mahrer, K.D., 1986, An empirical study of instability and improvement of absorbing boundary conditions for elastic wave equation, *Geophysics*, **51**, 1499-1501.

Mason, W.R., 1969, Internal friction mechanism that produces an attenuation in the Earth's crust proportional to frequency,*J. Geophys. Res.*, **74**, 4963-4966.

McMechan, G.A., 1983, Migration by extrapolation of time dependent boundary values, *Geophy. Prosp.*, **31**, 413-420.

Mikhailenko, B. G. and Korneev, V.I., 1984, Calculation of synthetic seismograms for complex subsurface geometries by a combination of finite integral Fourier transforms and finite difference techniques, *J. Geophys.*, **54**, 195-206.

Mitchell, A.R., and Griffiths, D.F., 1981, *The finite difference method in partial differential equations*, Wiley, N.Y..

Norris, A.N., 1985, Radiation from a point source and scattering theory in a fluid-saturated porous solid, *J. Acoust. Soc. Am.*, **77**, 2012-2023.

Nur, A., Walls, J.D., Winkler, K., and De Vilbiss, J., 1980, Effects of fluid saturation on waves in porous rock and relations to hydraulic permeabilit,: *SPEJ*, **24**, 450-458.

Schultz, P.S. and Sherwood, W.C., 1980, Depth migration before stack, *Geophysics*, **45**, 376-393.

Randall, C.J., 1988. Absorbing boundary condition for the elastic wave equation, *Geophysics*, **53**, 611-624.

Randall, C.J., 1989. Absorbing boundary condition for the elastic wave equation, velocity-stress formulation, *Geophysics*, **54**, 1153-1163.

Reshef, M., and Kosloff, D., 1986, Migration of common shot gathers, *Geophysics*, **51**, 324-331.

Reynolds, A.C., 1978, Boundary conditie s for the numerical solution of wave propagation problems, *Geophysics*, **43**, 1099-1110.

Scandrett, C.L., Kriegsmann, G.A., and Achenbach, J.D., 1986, Scattering of a pulse by a cavity in an elastic half-space, *J. Comput. Phys*, **65**, 410-431.

Schneider, W.A., 1978, Integral formulation for migration in two and three dimensions. *Geophysics*, **43**, 49-76.

Sheriff, R.E. and Geldart L.P., 1983, *Exploration seismology*, Cambridge University Press.

Slattery, J.C., 1969, Single phase flow through porous media, *J. Am. Inst. Chem. Eng.*, **15**, 866-872.

Smith, W. D., 1975, The application of finite-element analysis to body wave propagation problems, *Geophys. J. Roy. Astr. Soc.*, **42**, 747-768.

Sochacki, J., Kubichek, R., George, J., Fletcher, W.R., and Smithson, S., 1987, Absorbing boundary condition and surface waves, *Geophysics*, **52**, 60-71.

Stacey, R., 1988, Improved transparent boundary formulations for the elastic wave equation, *Bull. Seism. Soc. Am.* **78**, 2089-2097

Stoll, R. D., 1974, Acoustic waves in marine sediments, in *Physics of Sound in Marine Sediments*, Hampton, L., ed., Plenum, New York.

Stolt, R.H., 1978, Migration by Fourier transform, *Geophysics*, **43**, 23-48.

Strang, G., 1968, On the construction and comparison of difference schemes *SIAM J. Num. Anal.*, **5**, 506-517.

Sun, R. and McMechan, G., 1986, Pre-stack reverse time migration for elastic waves with application to VSP profiles. *Proc. IEEE,* **74,** 457-465.

Tal-Ezer, H., Carcione, J.M., and Kosloff, D., 1990, An accurate and efficient scheme for wave propagation in linear viscoelastic media, *Geophysics,* **55,** 1366-1379.

Thompson, K.W., 1987. Time dependent boundary conditions for hyperbolic systems, *J. Comput. Phys.,* **68,** 1-24.

Tosaya, C.A., Nur, A.M., and Da Prat, G., 1984, Monitoring of Thermal EOR Fronts by seismic methods: Western Energy Frontiers, *Proc. Soc. Petr. Eng.,* **54,** 179-186.

Tsingas, C., 1990, *Seismic reflection imaging over thermally enhanced oil recovery site,* Ph.D. thesis, University. of Alberta.

Tsingas, C. and Kanasewich, E.R., 1990, Pre-stack shot gather migration and imaging a steam zone using a migrated omega-x stack. *Can. J. Explor. Geoph.,* **26,** 17-32

Turkel, E., 1974, Phase error and stability of second order methods for hyperbolic problems, *J. Comp. Phys.,* **15,** 226-250.

Turkel, E., 1980, On the practical use of high order methods for hyperbolic systems, *J. Comp. Phys.,* **35,** 319-340.

Vafidis, A., 1988, *Supercomputer finite-difference methods for seismic wave propagation*: Ph.D. thesis, Univ. of Alberta, Edmonton, Canada.

Vafidis, A., Abramovici, F., and Kanasewich, E.R., 1992, Elastic wave propagation using fully vectorized high order finite differences, *Geophysics,* **57,** 218-232.

Vafidis, A., and Kanasewich, E.R., 1991, Modelling crosshole seismic data in steam injection problems with finite differences, *Can. J. Explor. Geophysics,* **27,** 23-33.

Virieux, J., 1984, SH-wave propagation in heterogeneous media: Velocity-stress finite difference method, *Geophysics,* **49,** 1933-1957.

Virieux, J., 1986, P-SV wave propagation in heterogeneous media: Velocity-stress finite difference method, *Geophysics,* **51,** 889-901.

Wang, Z., and Nur, A., 1988, Effect of temperature on seismic wave velocities in rocks saturated with hydrocarbons, *SPE Reservoir Engineer,* **3,** 158-164.

Whitaker, S., 1969, Advances in the theory of fluid motion in porous media, *Ind. Eng. Chem.*, **61**, (12), 14-28.

Winkler, K   . Dispersion analysis of velocity and attenuation in Berea sandstone, *J. Geoph.* ,   . **90**, 6793-6800.

Yew, C.H. and Jogi, P.N., 1976, Study of wave motions in fluid saturated rocks, *J. Acous. Soc. Am.*, **60**, 2-8.

Yew, C.H. and Jogi, P.N., 1978, The determination of Biot's parameters for sandstones Part 1: Static tests, *Experimental Mechanics*, 167-172.

Zheng, B., 1989, *Higher order terms in asymptotic ray theory:* Ph.D. Thesis, University of Alberta.

Zhu, X., and McMechan, G.A., 1991, Finite-difference modeling of the seismic response of fluid-saturated, porous, elastic media using Biot theory, *Geophysics*, **56**, 328-339.

APPENDIX A

DERIVATION OF EQUATIONS (2.2.5) AND (2.2.6)

Biot's (1956a) equations for wave motion in the elastic isotropic porous solid containing a viscous fluid were established in the context of uniform porosity. He extended his wave equation (Biot, 1962a) to include inhomogeneous porosity. In the extended form, a total stress tensor Π of the bulk material and the fluid pressure p are used instead of the solid stress tensor Σ^s and the quatity s. The quantities Π and p are related to Σ^s and s by

$$\Pi = \Sigma^s + s\mathbf{I} , \qquad (A. 1)$$

and

$$p = - \frac{s}{\eta_o} . \qquad (A. 2)$$

The quantities Π and p can be given by

$$\Pi = (\lambda + \alpha M)\nabla \cdot \mathbf{u}^s \mathbf{I} + \mu_s \left[\nabla \cdot \mathbf{u}^s + (\nabla \cdot \mathbf{u}^s)^\mathrm{T} \right] + \alpha M \nabla [\eta_o(\mathbf{u}^f - \mathbf{u}^s)] \qquad (A. 3)$$

and

$$p = - M \nabla [\eta_o(\mathbf{u}^f - \mathbf{u}^s)] - \alpha M \nabla \cdot \mathbf{u}^s \qquad (A. 4)$$

where λ and μ_s are the Lame coefficient and shear modulus of the solid material,

$$\alpha = 1 - \frac{K_b}{K_s} \, , \tag{A.5}$$

and

$$M = \frac{1}{\dfrac{\eta_o}{K_f} + \dfrac{\alpha - \eta_o}{K_s}} \, , \tag{A.6}$$

with K_s, K_f and K_b denoting the bulk modulus of the solid material, the pore fluid and the dry porous frame, respectively.

From (A.1), (A.2), (A.3) and (A.4) we have

$$s = Q\nabla \cdot \mathbf{u}^s + R\nabla \cdot \mathbf{u}^f + \frac{R}{\eta_o}\nabla \eta_o \cdot \left(\mathbf{u}^f - \mathbf{u}^s\right) \tag{A.7}$$

and

$$\Sigma^s = (P - 2N)\nabla \cdot \mathbf{u}^s \mathbf{I} + N\left[\nabla \mathbf{u}^s + \left(\nabla \mathbf{u}^s\right)^T\right] + Q\nabla \cdot \mathbf{u}^f \, \mathbf{I} + \frac{Q}{\eta_o}\nabla \eta_o \cdot \left(\mathbf{u}^f - \mathbf{u}^s\right) \mathbf{I} \, , \tag{A.8}$$

where

$$N = \mu_o \, , \tag{A.9}$$

$$P = \lambda + M(\alpha - \eta_o)^2 + 2\mu_s \, , \tag{A.10}$$

$$Q = \eta_o(\alpha - \eta_o)M \, , \tag{A.11}$$

and

$$R = \eta_o^2 M \, . \tag{A.12}$$

APPENDIX B

DERIVATION OF THE DE LA CRUZ AND SPANOS MACROSCOPIC EQUATIONS

Let $G_f(x,t)$ be a physical quantity associated with the fluid in a porous medium. The volume average of G_f over a region V is defined as

$$\langle G_f \rangle = \frac{1}{V} \int_v G_f(x,t)dV . \tag{B.1}$$

A related quantity, called the intrinsic volume average, is defined by

$$\overline{G_f} = \frac{1}{V_f} \int_v G_f(x,t)dV = \frac{1}{\eta}\langle G_f \rangle , \tag{B.2}$$

which is the volume average over the fluid volume V_f in V. In (B.2) η denotes the porosity of the medium and is given by $\eta = V_f/V$.

The volume averaging theorems (Slattery,1969; Whitaker,1969) can be expressed as

$$\langle \partial_i G_f \rangle = \partial_i \langle G_f \rangle + \int_{A_{fs}} G_f n_i dA \tag{B.3}$$

for spatial derivatives and

$$\langle \partial_t G_f \rangle = \partial_t \langle G_f \rangle - \int_{A_{fs}} G_f v \cdot n \, dA \tag{B.4}$$

for time derivatives, where A_{fs} refers to the fluid-solid interfaces in the volume V, n is the unit normal on those interfaces, directed toward the solid, and v is the particle velocity on the interfaces. Replacing f with s in (B.3) and (B.4) one can have similar relations for a physical quantity associated with the solid.

Upon applying (B.3) and (B.4) to microscopic equations (2.3.1) to (2.3.4) in Chapter 2, one has

$$\rho_0^s \partial_t \langle u_i^s \rangle = \partial_k \langle \sigma_{ik}^s \rangle + \frac{1}{V} \int_{A_{sf}} \sigma_{ik}^s n_k dA \ , \tag{B.5}$$

$$\rho_0^f \partial_t \langle v_i^f \rangle = \partial_k (\langle \sigma_{ik}^f \rangle - \delta_{ik} \langle p^f \rangle) + \frac{1}{V} \int_{A_{fs}} (\sigma_{ik}^f - \delta_{ik} p^f) n_k dA \ , \tag{B.6}$$

$$\langle \sigma_{ik}^s \rangle = K_s \delta_{ik} [\partial_l \langle u_l^s \rangle - (\eta - \eta_0)] + \mu_s (\partial_k \langle u_i^s \rangle + \partial_i \langle u_k^s \rangle - \frac{2}{3} \delta_{ik} \partial_l \langle u_l^s \rangle) + \mu_s I_{ik}^s \tag{B.7}$$

$$\langle \sigma_{ik}^f \rangle = \mu_f (\partial_k \langle v_i^f \rangle + \partial_i \langle v_k^f \rangle - \frac{2}{3} \delta_{ik} \partial_l \langle v_l^f \rangle) + \mu_f I_{ik}^f \ , \tag{B.8}$$

where ρ_0^s, ρ_0^f are the static density of the solid and fluid respectively, η, η_0 denote the porosity and the static porosity of the medium, and

$$I_{ik}^s = \frac{1}{V} \int_{A_{sf}} (u_i^s n_k + u_k^s n_i - \frac{2}{3} \delta_{ik} u_l^s n_l) dA \ , \tag{B.9}$$

$$I_{ik}^f = \frac{1}{V} \int_{A_{fs}} (v_i^f n_k + v_k^f n_i - \frac{2}{3} \delta_{ik} v_l^f n_l) dA \ , \tag{B.10}$$

where we have used

$$\frac{1}{V}\int_{A_{sf}} \mathbf{u}^s \cdot d\mathbf{A} = -(\eta - \eta_o) ,$$

(B.11)

$$\frac{1}{V}\int_{A_{fs}} v_i^f n_i dA = \frac{\partial \eta}{\partial t} .$$

(B.12)

Following the condition (2.3.6) in Chapter 2, the integrals in (B.5) and (B.6) are related by the equation

$$I_i = \frac{1}{V}\int_{A_{sf}} \sigma_{ik}^s n_k dA = -\frac{1}{V}\int_{A_{fs}} \left(\sigma_{ik}^f - \delta_{ik} p^f\right) n_k dA$$

(B.13)

which can be explained as a body force density (per unit volume) exerted on the fluid by the solid matrix across the interface. For steady flow of fluid in porous media, I_i is related to the Darcian resistance which is proportional to the relative velocity between the fluid and solid. For nonsteady flow, an extra term proportional to the relative acceleration is added (de la Cruz and Spanos, 1985, 1989). For statistically isotropic porous media, I_i is given by

$$I_i = \frac{\mu_f \eta_o^2}{K}\left(v_i^f - v_i^s\right) - \rho_{12}\partial_i\left(v_i^f - v_i^s\right) ,$$

(B.14)

where K is the permeability and ρ_{12} is called the induced mass coefficient.

De la Cruz et al. (1991a) noticed that I_{ik}^s does not vanish if the porosity is non-uniform. They suggest

$$I_{ik}^s = \left[\frac{\delta}{\eta_o}\left\langle u_i^f\right\rangle + \frac{(1-\delta)}{1-\eta_o}\left\langle u_i^s\right\rangle\right]\partial_k\eta_o + \left[\frac{\delta}{\eta_o}\left\langle u_k^f\right\rangle + \frac{(1-\delta)}{1-\eta_o}\left\langle u_k^s\right\rangle\right]\partial_i\eta_o$$

$$-\frac{2}{3}\,\delta_{ik}\left[\frac{\delta}{\eta_o}\langle u_l^f\rangle + \frac{(1-\delta)}{1-\eta_o}\langle u_l^s\rangle\right]\partial_l\eta_o \ ,$$

(B.15)

which is a first order quantity in displacement and vanishes when the porosity is uniform. Since $I_{ik}^f = \partial_t I_{ik}^s$ following condition (2.3.5) in Chapter 2, by taking the time derivative of (B.15), one obtains

$$I_{ik}^f = -\left[\frac{\delta}{\eta_o}\langle v_i^f\rangle + \frac{(1-\delta)}{1-\eta_o}\langle v_i^s\rangle\right]\partial_k\eta_o - \left[\frac{\delta}{\eta_o}\langle v_k^f\rangle + \frac{(1-\delta)}{1-\eta_o}\langle v_k^s\rangle\right]\partial_i\eta_o$$

$$+\frac{2}{3}\,\delta_{ik}\left[\frac{\delta}{\eta_o}\langle v_l^f\rangle + \frac{(1-\delta)}{1-\eta_o}\langle v_l^s\rangle\right]\partial_l\eta_o$$

(B.16)

Based upon the volume average of the microscopic equation of continuity for the fluid and the analysis of the pressure-density relationship for fluids, de la Cruz et al. (1991a) introduced the following macroscopic equation

$$\frac{1}{\eta_o K_f}\,\partial_t\langle p^f\rangle = -\frac{1}{\eta_o}\,\partial_t\eta - \frac{\partial_l\langle\langle\rho_b^f\rangle v_l^f\rangle}{\langle\rho_b^f\rangle} \ .$$

(B.17)

They suggest (de la Cruz et al., 1991a,b) that

$$\partial_t\eta = \frac{\delta_s}{1-\eta_o}\,\partial_l\langle v_l^s\rangle - \frac{\delta_f}{\eta_o}\,\partial_l\langle v_l^f\rangle - \left[\frac{\delta_l}{1-\eta_o}\langle v_l^s\rangle + \frac{(1-\delta_l)}{\eta_o}\langle v_l^f\rangle\right]\partial_l\eta_o \ ,$$

(B.18)

where δ_s, δ_f, δ and δ_l are macroscopic parameters of the porous medium. In particular, δ_s and δ_f are given by

$$\delta_s = \frac{\eta_o K_s[(1-\eta_o)K_s - K_b]}{K_f\,[(1-\eta_o)K_s - K_b] + \eta_o K_s K_f} \ ,$$

(B.19)

$$\delta_f = \frac{\eta_o K_f[(1-\eta_o)K_s - K_b]}{K_f\,[(1-\eta_o)\,K_s - K_b]\,+\,\eta_o K_s K_f} \ ,$$
<div align="right">(B.20)</div>

While δ and δ_f must be determined experimentally. They are the subject of continuing theoretical studies.

Substituting eq.(B.9), (B.10) and (B.13) to (B.18) into (B.5)to (B.8), and writing them in tensor form, we obtain the macroscopic equations (2.3.7) to (2.3.11) in Chapter 2, where the brackets < > are dropped for convenience. The coefficients in equations (2.3.7) to (2.3.11) are given by

$$D_{11} = \left(\rho_o^s - \frac{\rho_{12}}{1-\eta_o}\right) ,$$
<div align="right">(B.21)</div>

$$D_{12} = \frac{\rho_{12}}{\eta_o} ,$$
<div align="right">(B.22)</div>

$$D_{21} = \frac{\rho_{12}}{1-\eta_o} ,$$
<div align="right">(B.23)</div>

$$D_{22} = \left(\rho_o^f - \frac{\rho_{12}}{\eta_o}\right) ,$$
<div align="right">(B.24)</div>

$$b = \frac{\mu_f \eta_o^2}{K} ,$$
<div align="right">(B.25)</div>

$$A = K_s + \frac{4}{3}\mu_s - \frac{\delta_s K_s}{1-\eta_o} ,$$
<div align="right">(B.26)</div>

$$B = \frac{\delta_f K_s}{\eta_o} ,$$
<div align="right">(B.27)</div>

$$C = \frac{\delta_s K_f}{1-\eta_o} ,$$
<div align="right">(B.28)</div>

$$E = K_f \left(1 - \frac{\delta_f}{\eta_o} \right) , \tag{B.29}$$

$$H_A = K_s \delta_A - \frac{2}{3} \mu_s \frac{1-\delta}{1-\eta_o} , \tag{B.30}$$

$$H_B = K_s \delta_B + \frac{2}{3} \mu_s \frac{\delta}{\eta_o} , \tag{B.31}$$

$$N_f = \mu_s \frac{\delta}{\eta_o} , \tag{B.32}$$

$$N_s = \mu_s \frac{1-\delta}{1-\eta_o} , \tag{B.33}$$

$$F_A = K_f \delta_A , \tag{B.34}$$

$$F_B = K_f \delta_B , \tag{B.35}$$

$$\delta_A = \frac{1}{1-\eta_o} \left(\delta_I - \frac{\delta_s}{1-\eta_o} \right) , \tag{B.36}$$

and

$$\delta_B = \frac{1}{\eta_o} \left(\delta_I - 1 + \frac{\delta_f}{\eta_o} \right) . \tag{B.37}$$

APPENDIX C

THE TRUNCATION ERROR
OF THE MACCORMACK TYPE FINITE DIFFERENCE SCHEME

Definition A finite difference scheme is called of order (p,q) if its truncation error E has the form (Gottlieb and Turkel 1976)

$$E = \Delta t\, h(\Delta t, \Delta x),$$

$$h = O\!\left((\Delta x)^q\right) \quad \text{whenever} \quad \Delta t = O\!\left((\Delta x)^{q/p}\right) \tag{C. 1}.$$

Gottlieb and Turkel (1976) proposed several two-step schemes similar to the original MacCormack scheme for a first order hyperbolic system in one dimension

$$\frac{\partial \mathbf{u}}{\partial t} = \mathbf{A}\,\frac{\partial \mathbf{u}}{\partial x} + \mathbf{Cu} \tag{C. 2}$$

One of those schemes consists of a 'predictor'

$$\mathbf{u}_j^{(1)} = \mathbf{u}_j^n + p\mathbf{A}\!\left[\alpha\Delta_x\mathbf{u}_j^n + \beta\Delta_x\!\left(\Delta_x\mathbf{u}_j^n\right)\right] + \Delta t\,\mathbf{Cu}_j^n \tag{C. 3}$$

and a 'corrector'

$$u_j^{n+1} = \frac{1}{2}\left(u_j^n + u_j^n\right) + \frac{p}{2}A\left[\kappa\nabla_x u_j^{(1)} + \gamma\nabla_x\left(\nabla_x u_j^{(1)}\right)\right] + \Delta t C u_j^{(1)}$$
(C. 4)

where p denotes the mesh ratio $\Delta t/\Delta x$, the subscripts represent the grid points on the x-axis and the superscript represents the grid point on the t-axis, and the forward difference operator Δ_x and the backward difference operator ∇_x are defined by $\Delta_x u_j = u_{j+1} - u_j$ and $\nabla_x u_j = u_j - u_{j-1}$, respectively. For $\alpha = \kappa = 1$ and $b = -\gamma = 1/6$ the predictor and the corrector become equations (2.5.4) and (2.5.5) in Chapter 2, respectively. In order to calculate the truncation error of this scheme, the difference operators are expanded in Taylor serieses

$$\Delta_x u_j = u_{j+1} - u_j = \Delta x u_x + \frac{\Delta x^2}{2}u_{xx} + \frac{\Delta x^3}{6}u_{xxx} + \frac{\Delta x^4}{24}u_{xxxx} + O\left(\Delta x^5\right),$$
(C. 5)

$$\Delta_x\left(\Delta_x u_j\right) = \Delta x^2 u_{xx} + \Delta x^3 u_{xxx} + \frac{7\Delta x^4}{12}u_{xxxx} + O\left(\Delta x^5\right),$$
(C. 6)

$$\nabla_x u_j = u_j - u_{j-1} = \Delta x u_x - \frac{\Delta x^2}{2}u_{xx} + \frac{\Delta x^3}{6}u_{xxx} - \frac{\Delta x^4}{24}u_{xxxx} + O\left(\Delta x^5\right),$$
(C. 7)

and

$$\nabla_x\left(\nabla_x u_j\right) = \Delta x^2 u_{xx} - \Delta x^3 u_{xxx} + \frac{7\Delta x^4}{12}u_{xxxx} + O\left(\Delta x^5\right),$$
(C. 8)

where the subscripts on the right hand side of equations (C.5) - (C.8) denote partial derivatives with respect to the indicated coordinate. To simplify the notation where the time index n or space index j is miss, u is defined at time $n\Delta t$ or space location $j\Delta x$. Substitution of (C. 5) , (C. 6) into (C. 3) and (C. 7), (C. 8) into (C. 4) gives

$$u^{(1)} = u^n + A\left[\Delta t u_x + \frac{\Delta t\Delta x}{3}u_{xx} - \frac{\Delta t\Delta x^3}{18}u_{xxxx} + O\left(\Delta t\Delta x^4\right)\right] + \Delta t C u,$$
(C.9)

and

$$\mathbf{u}^{n+1} = \frac{1}{2}\left(\mathbf{u}^n + \mathbf{u}^{(1)}\right) + A\left[\frac{\Delta t}{2}\mathbf{u}_x^{(1)} - \frac{\Delta t \Delta x}{6}\mathbf{u}_{xx}^{(1)} + \frac{\Delta t \Delta x^3}{36}\mathbf{u}_{xxxx}^{(1)} + O\left(\Delta t \Delta x^4\right)\right] + \frac{\Delta t}{2}C\mathbf{u}^{(1)}$$

$$(C.\ 10)$$

or

$$\mathbf{u}^{n+1} = \mathbf{u}^n + \Delta t A\mathbf{u}_x^n + \Delta t C\mathbf{u} + \frac{\Delta t^2}{2}\left[A(A\mathbf{u}_x^n)_x + A(C\mathbf{u}^n)_x + C(A\mathbf{u}_x + C\mathbf{u})\right]$$

$$- \frac{\Delta x \Delta t^2}{6}\left[A(A_x\mathbf{u}_x^n)_x + A(C\mathbf{u}^n)_{xx} - CA\mathbf{u}_{xx}^n\right] + O\left(\Delta x^2 \Delta t^2\right) + O\left(\Delta t \Delta x^4\right). \qquad (C.\ 11)$$

On the other hand, by substituting $\mathbf{u}_t = A\mathbf{u}_x + C\mathbf{u}$, and

$$\mathbf{u}_{tt} = (A\mathbf{u}_x + C\mathbf{u})_t = A\mathbf{u}_{xt} + C\mathbf{u}_t = A\mathbf{u}_{tx} + CA\mathbf{u}_x + CC\mathbf{u}$$

$$= (A\mathbf{u}_t)_x - A_x\mathbf{u}_t + CA\mathbf{u}_x + CC\mathbf{u}$$

$$= (AA\mathbf{u}_x + AC\mathbf{u})_x - A_x(A\mathbf{u}_x + C\mathbf{u}) + CA\mathbf{u}_x + CC\mathbf{u}$$

$$= AA_x\mathbf{u}_x + AA\mathbf{u}_{xx} + AC_x\mathbf{u} + AC\mathbf{u}_x + CA\mathbf{u}_x + CC\mathbf{u}$$

$$= A(A\mathbf{u}_x + C\mathbf{u})_x + C(A\mathbf{u}_x + C\mathbf{u}) \qquad (C.\ 12\ )$$

into the Taylor expansion of $\mathbf{u}$, namely

$$\mathbf{u}^{n+1} = \mathbf{u}^n + \Delta t \mathbf{u}_t + \frac{\Delta t^2}{2}\mathbf{u}_{tt} + O\left(\Delta t^3\right), \qquad (C.\ 13)$$

one has

$$u^{n+1} = u^n + \Delta t A u_x^n + \Delta t Cu + \frac{\Delta t}{2}^2 [A(Au_x + Cu)_x + C(Au_x + Cu)] + O(\Delta t^3).$$

(C. 14)

The truncation error is given by the difference between equation (C. 11) and (C. 14):

$$E_1 = -\frac{\Delta x \Delta t}{6}^2 [A(A_x u_x^n)_x + A(Cu^n)_{xx} - CAu_{xx}^n] + O(\Delta x^2 \Delta t^2) + O(\Delta t^3) + O(\Delta t \Delta x^4).$$

(C. 15)

The scheme given in equations (2.5.4) and (2.5.5) has a variant defined by using backward differences in the predictor and forward differences in the corrector. Similarly the truncation error of this variant can be found as

$$E_2 = \frac{\Delta x \Delta t}{6}^2 [A(A_x u_x^n)_x + A(Cu^n)_{xx} - CAu_{xx}^n] + O(\Delta x^2 \Delta t^2) + O(\Delta t^3) + O(\Delta t \Delta x^4).$$

(C. 16)

Alternating these two variants at successive time levels will cancel the $\Delta x \Delta t^2$ error term and yield a (2,4) scheme even for variable coefficients according to the definition (C. 1).

APPENDIX D

THE EIGENVALUES AND EIGENVECTORS OF THE C-S SYSTEM
AND THE BIOT SYSTEM

In the following discussion eigenvalues and eigenvectors of the matrices **A** and **B** in the C-S system (2.3.40) are derived. The eigenvalues and eigenvectors of the matrices **A** and **B** in the Biot system (2.2.26) can be obtained by comparing the elements in these matrices of the C-S system and the Biot system (Appendix E).

In order to find the eigenvalues of matrix **A** given in equation (2.2.27) one solves the characteristic equation

$$\det (\mathbf{A} - \lambda \mathbf{I}) = 0 , \tag{D. 1}$$

or

$$\det \begin{bmatrix} -\lambda & 0 & R_{22} & 0 & 0 & 0 & 0 & R_{12} \\ 0 & -\lambda & 0 & 0 & R_{22} & 0 & 0 & 0 \\ A & 0 & -\lambda & 0 & 0 & B & 0 & 0 \\ A-2\mu_s & 0 & 0 & -\lambda & 0 & B & 0 & 0 \\ 0 & \mu_s & 0 & 0 & -\lambda & 0 & 0 & 0 \\ 0 & 0 & -R_{21} & 0 & 0 & -\lambda & 0 & -R_{11} \\ 0 & 0 & 0 & 0 & -R_{21} & 0 & -\lambda & 0 \\ -C & 0 & 0 & 0 & 0 & -E & 0 & -\lambda \end{bmatrix} = 0 . \tag{D. 2}$$

Expanding equation (D. 2) one has

$$\lambda^2\left(\lambda^2 - \mu_s R_{22}\right)\left[\lambda^4 + \lambda^2(R_{11}E + R_{22}A - R_{12}C - R_{12}B) + (AE - BC)(R_{11}R_{22} - R_{12}R_{21})\right] = 0 .$$

(D. 3)

The solutions of (D. 3), which are the eigenvalues of **A**, can be written as

$$\left(\lambda_1, \lambda_2, \lambda_3, \lambda_4, \lambda_5, \lambda_6, \lambda_7, \lambda_8\right) = (-V_f, -V_r, -V_s, 0, 0, V_f, V_r, V_s) ,$$

(D. 4)

where V_f, V_r, and V_s, are the high frequency limit of the propagation velocity of the fast P wave, S wave and slow P wave. V_f and V_s are given in section 2.4 (see equations (2.4.29) and (2.4.30)). V_r is given by

$$V_r = \sqrt{\mu_s R_{22}} .$$

(D. 5)

It is readily shown that matrix **B** has the same eigenvalues as matrix **A** by replacing matrix **A** in equation (D. 1) with matrix **B** as given in equation (2.3.42).

A left eigenvector l_A^i of matrix **A** corresponding to eigenvalue λ_i is a row vector defined by

$$l_A^i \mathbf{A} = \lambda_i l_A^i .$$

(D. 6)

A right eigenvector r_A^i of matrix **A** corresponding to eigenvalue λ_i is a column vector defined by

$$\mathbf{A} r_A^i = \lambda_i r_A^i .$$

(D. 7)

If we use $\mathbf{L}_A$ to denote a matrix whose rows are composed of the left eigenvectors of matrix $\mathbf{A}$ and $\mathbf{R}_A$ to denote a matrix whose columns are composed of the right eigenvectors of matrix $\mathbf{A}$ corresponding to the eigenvalues in the order given by (D. 4), then we have

$$
\mathbf{L}_A = \begin{bmatrix}
1 & 0 & -l_{13} & 0 & 0 & l_{16} & 0 & -l_{18} \\
0 & 1 & 0 & 0 & -l_{25} & 0 & 0 & 0 \\
1 & 0 & -l_{33} & 0 & 0 & l_{36} & 0 & -l_{38} \\
0 & 0 & l_{43} & 1 & 0 & 0 & 0 & l_{48} \\
0 & l_{52} & 0 & 0 & 0 & 0 & 1 & 0 \\
1 & 0 & l_{33} & 0 & 0 & l_{36} & 0 & l_{38} \\
0 & 1 & 0 & 0 & l_{25} & 0 & 0 & 0 \\
1 & 0 & l_{13} & 0 & 0 & l_{16} & 0 & l_{18}
\end{bmatrix} ,
\tag{D. 8}
$$

where

$$
l_{13} = \frac{V_f(CR_{22} - ER_{21})}{R_{21}(BC - EA) + V_f^2 C} ,
\tag{D. 9}
$$

$$
l_{16} = \frac{R_{22}}{R_{21}} - \frac{V_f^2(CR_{22} - ER_{21})}{R_{21}^2(BC - EA) + R_{21}V_f^2 C} ,
\tag{D. 10}
$$

$$
l_{18} = \frac{AV_f(CR_{22} - ER_{21})}{C R_{21}(BC - EA) + V_f^2 C^2} - \frac{V_f}{C} ,
\tag{D. 11}
$$

$$
l_{25} = \sqrt{\frac{R_{22}}{\mu_s}} ,
\tag{D. 12}
$$

$$
l_{33} = \frac{V_s(CR_{22} - ER_{21})}{R_{21}(BC - EA) + V_f^2 C} ,
\tag{D. 13}
$$

$$
l_{36} = \frac{R_{22}}{R_{21}} - \frac{V_s^2(CR_{22} - ER_{21})}{R_{21}^2(BC - EA) + R_{21}V_s^2 C} ,
\tag{D. 14}
$$

$$
l_{38} = \frac{AV_s(CR_{22} - ER_{21})}{C R_{21}(BC - EA) + V_s^2 C^2} - \frac{V_s}{C} ,
\tag{D. 15}
$$

$$l_{45} = - \frac{E(2\mu_s - A) + BC}{BC - AE} ,$$

(D. 16)

$$l_{48} = - \frac{AB + B(2\mu_s - A)}{BC - AE} ,$$

(D. 17)

$$l_{52} = \frac{R_{21}}{R_{22}} ;$$

(D. 18)

and

$$\mathbf{R}_A = \begin{bmatrix} 1 & 0 & 1 & 0 & 0 & 1 & 0 & 1 \\ 0 & 1 & 0 & 0 & 0 & 0 & 1 & 0 \\ -r_{31} & 0 & -r_{33} & 0 & 0 & r_{33} & 0 & r_{31} \\ -r_{41} & 0 & -r_{43} & 1 & 0 & r_{43} & 0 & r_{41} \\ 0 & -r_{52} & 0 & 0 & 0 & 0 & r_{52} & 0 \\ r_{61} & 0 & r_{63} & 0 & 0 & r_{63} & 0 & r_{61} \\ 0 & r_{72} & 0 & 0 & 1 & 0 & r_{72} & 0 \\ -r_{81} & 0 & -r_{83} & 0 & 0 & r_{83} & 0 & r_{81} \end{bmatrix} ,$$

(D. 19)

where

$$r_{31} = \frac{BV_f^2 - R_{12}(EA-CB)}{(R_{22}B - R_{12}E)V_f} ,$$

(D. 20)

$$r_{41} = \frac{BV_f^2 - R_{12}(EA-CB)}{(R_{22}B - R_{12}E)V_f} - \frac{2\mu_s}{V_f} ,$$

(D. 21)

$$r_{61} = \frac{BV_f^2 - R_{12}(EA-CB)}{(R_{22}B - R_{12}E)B} - \frac{A}{B} ,$$

(D. 22)

$$r_{81} = \frac{R_{22}(EA-CB) - EV_f^2}{(R_{22}B - R_{12}E)V_f} ,$$

(D. 23)

$$r_{52} = \sqrt{\frac{\mu_s}{R_{22}}} \ , \tag{D. 24}$$

$$r_{72} = -\frac{R_{21}}{R_{22}} \ , \tag{D. 25}$$

$$r_{33} = \frac{BV_s^2 - R_{12}(EA-CB)}{(R_{22}B - R_{12}E)V_s} \ , \tag{D. 26}$$

$$r_{43} = \frac{BV_s^2 - R_{12}(EA-CB)}{(R_{22}B - R_{12}E)V_s} - \frac{2\mu_s}{V_s} \ , \tag{D. 27}$$

$$r_{63} = \frac{BV_s^2 - R_{12}(EA-CB)}{(R_{22}B - R_{12}E)B} - \frac{A}{B} \ , \tag{D. 28}$$

$$r_{83} = \frac{R_{22}(EA-CB) - EV_s^2}{(R_{22}B - R_{12}E)V_s} \ . \tag{D. 29}$$

Similarly, a left eigenvector l_B^i of matrix B corresponding to eigenvalue λ_i is a row vector which satisfies

$$l_B^i B = \lambda_i l_B^i \ . \tag{D. 30}$$

A right eigenvector r_B^i of matrix B corresponding to eigenvalue λ_i is a column vector which satisfies

$$B r_B^i = \lambda_i r_B^i \ . \tag{D. 31}$$

If we use L_B to denote a matrix whose rows are composed of the left eigenvectors of matrix B and R_B to denote a matrix whose columns are composed of the right eigenvectors of matrix B corresponding to the eigenvalues in the order given by (D. 4), then we have

$$
L_B = \begin{bmatrix}
0 & 1 & 0 & -s_{14} & 0 & 0 & s_{17} & -s_{18} \\
1 & 0 & 0 & 0 & -s_{25} & 0 & 0 & 0 \\
0 & 1 & 0 & -s_{34} & 0 & 0 & s_{37} & -s_{38} \\
0 & 0 & 1 & s_{44} & 0 & 0 & 0 & s_{48} \\
s_{51} & 0 & 0 & 0 & 0 & 1 & 0 & 0 \\
0 & 1 & 0 & s_{34} & 0 & 0 & s_{37} & s_{38} \\
1 & 0 & 0 & 0 & s_{25} & 0 & 0 & 0 \\
0 & 1 & 0 & s_{14} & 0 & 0 & s_{17} & s_{18}
\end{bmatrix} ,
\tag{D. 32}
$$

where

$$
s_{14} = \frac{V_f(CR_{22} - ER_{21})}{(CB - EA)R_{21} + CV_f^2} ,
\tag{D. 33}
$$

$$
s_{17} = \frac{1}{R_{21}}\left[R_{22} - \frac{V_f^2(CR_{22} - ER_{21})}{(CB - EA)R_{21} + CV_f^2} \right] ,
\tag{D. 34}
$$

$$
s_{18} = \frac{1}{C}\left[\frac{AV_f(CR_{22} - ER_{21})}{(CB - EA)R_{21} + CV_f^2} - V_f \right] ,
$$

$$
s_{25} = \sqrt{\frac{R_{22}}{\mu_s}} ,
\tag{D. 35}
$$

$$
s_{34} = \frac{V_s(CR_{22} - ER_{21})}{(CB - EA)R_{22} + CV_s^2} ,
\tag{D. 36}
$$

$$
s_{37} = \frac{1}{R_{21}}\left[R_{22} - \frac{V_s^2(CR_{22} - ER_{21})}{(CB - EA)R_{21} + CV_s^2} \right] ,
\tag{D. 37}
$$

$$
s_{38} = \frac{1}{C}\left[\frac{AV_s(CR_{22} - ER_{21})}{(CB - EA)R_{22} + CV_s^2} - V_s \right] ,
\tag{D. 38}
$$

$$
s_{51} = \frac{R_{21}}{R_{22}} ,
\tag{D. 39}
$$

$$s_{44} = \frac{2E\mu_s}{AE - CB} - 1 \ ,$$

(D. 40)

$$s_{48} = \frac{2B\mu_s}{AE - CB} \ ,$$

(D. 41)

and

$$\mathbf{R}_B = \begin{bmatrix} 0 & 1 & 0 & 0 & 0 & 0 & 1 & 0 \\ 1 & 0 & 1 & 0 & 0 & 1 & 0 & 1 \\ -t_{31} & 0 & -t_{33} & 1 & 0 & t_{33} & 0 & t_{31} \\ -t_{41} & 0 & -t_{43} & 0 & 0 & t_{43} & 0 & t_{41} \\ 0 & -t_{52} & 0 & 0 & 0 & 0 & t_{52} & 0 \\ 0 & t_{62} & 0 & 0 & 1 & 0 & t_{62} & 0 \\ t_{71} & 0 & t_{73} & 0 & 0 & t_{73} & 0 & t_{71} \\ -t_{81} & 0 & -t_{83} & 0 & 0 & t_{83} & 0 & t_{81} \end{bmatrix} \ ,$$

(D. 42)

where

$$t_{31} = \frac{A - 2\mu_s}{V_f} + \frac{B}{V_f}\left(\frac{V_f^2 - AR_{22} + CR_{12}}{BR_{22} - ER_{12}}\right) \ ,$$

(D. 43)

$$t_{41} = \frac{A}{V_f} + \frac{B}{V_f}\left(\frac{V_f^2 - AR_{22} + CR_{12}}{BR_{22} - ER_{12}}\right) \ ,$$

(D. 44)

$$t_{71} = \frac{V_f^2 - AR_{22} + CR_{12}}{BR_{22} - ER_{12}} \ ,$$

(D. 45)

$$t_{81} = \frac{V_f}{R_{12}} - \frac{R_{22}}{R_{12}}\left[\frac{A}{V_f} + \frac{B}{V_f}\left(\frac{V_f^2 - AR_{22} + CR_{12}}{BR_{22} - ER_{12}}\right)\right] \ ,$$

(D. 46)

$$t_{52} = \sqrt{\frac{\mu_s}{R_{22}}} \ ,$$

(D. 47)

$$t_{62} = -\frac{R_{21}}{R_{22}} \ ,$$

(D. 48)

$$t_{33} = \frac{A - 2\mu_s}{V_s} + \frac{B}{V_s}\left(\frac{V_s^2 - AR_{22} + CR_{12}}{BR_{22} - ER_{12}}\right),$$

(D. 49)

$$t_{43} = \frac{A}{V_s} + \frac{B}{V_s}\left(\frac{V_s^2 - AR_{22} + CR_{12}}{BR_{22} - ER_{12}}\right),$$

(D. 50)

$$t_{73} = \frac{V_s^2 - AR_{22} + CR_{12}}{BR_{22} - ER_{12}},$$

(D. 51)

$$t_{83} = \frac{V_s}{R_{12}} - \frac{R_{22}}{R_{12}}\left[\frac{A}{V_s} + \frac{B}{V_s}\left(\frac{V_s^2 - AR_{22} + CR_{12}}{BR_{22} - ER_{12}}\right)\right].$$

(D. 52)

It can be shown that

$$\mathbf{L}_A \mathbf{R}_A = \mathbf{N}_A$$

(D. 53)

and

$$\mathbf{L}_B \mathbf{R}_B = \mathbf{N}_B$$

(D. 54)

where $\mathbf{N}_A$ and $\mathbf{N}_B$ are diagonal matrices whose diagonal elements are non-zero real numbers. These numbers can be used as factors to normalize the eigenvectors.

APPENDIX E

A COMPARISON OF THE COEFFICIENTS OF THE BIOT SYSTEM
AND THE C-S SYSTEM

Comparisons of the elements of the matrices E_0, A_0, B_0 and C_0 in the Biot system (2.3.28) and the C-S system (2.2.18) are given in tables E.1, E.2, E.3 and E.4 respectively.

Table E. 1: A comparison of the non-zero elements in matrix E_0
of the Biot system and the C-S system

Inconstant element in E_0	Biot system		C-S system	
$E_{11} = E_{22}$	ρ_{11}:	$(1-\eta_o)\rho_o^s - \rho_{12}$	D_{11}:	$\rho_o^s - \dfrac{\rho_{12}}{1-\eta_o}$
$E_{16} = E_{27}$	ρ_{12}:		D_{12}:	$\dfrac{\rho_{12}}{\eta_o}$
$E_{61} = E_{72}$	ρ_{12}:		D_{21}:	$\dfrac{\rho_{12}}{1-\eta_o}$
$E_{66} = E_{77}$	ρ_{22}:	$\eta_o\rho_o^f - \rho_{12}$	D_{22}:	$\rho_o^f - \dfrac{\rho_{12}}{\eta_o}$

Table E. 2: A comparison of the non-zero elements in matrix A_0 of Biot system and C-S system

Inconstant element in A_0	Biot system	C-S system
A_{31}	P: $\dfrac{(1-\eta_o)K_s\left(1-\eta_o - \frac{K_b}{K_s}\right) + \eta_o\frac{K_bK_s}{K_f}}{1-\eta_o - \frac{K_b}{K_s} + \eta_o\frac{K_s}{K_f}} + \frac{4}{3}\mu_s$	A: $\quad K_s + \frac{4}{3}\mu_s - \dfrac{\delta_s K_s}{1-\eta_o}$ *
A_{41}	P-$2N$:	A-$2\mu_s$:
A_{81}	Q: $\dfrac{\eta_o[(1-\eta_o)K_s - \eta_o K_b]}{1-\eta_o - \frac{K_b}{K_s} + \eta_o\frac{K_s}{K_f}}$	$-C$: $\quad C = \dfrac{\delta_s K_f}{1-\eta_o}$ *
A_{52}	N: $\quad (1-\eta_o)\mu_s$	μ_s:
$A_{36}=A_{46}$	Q:	B: $\quad \dfrac{\delta_f K_s}{\eta_o}$ *
A_{86}	R: $\dfrac{\eta_o^2 K_s}{1-\eta_o - \frac{K_b}{K_s} + \eta_o\frac{K_s}{K_f}}$	E: $\quad E = K_f\left(1 - \dfrac{\delta_f}{\eta_o}\right)$ *

* $\delta_s = \dfrac{\eta_o(1-\eta_o)(K_s - K_b)}{\eta_o K_s + (1-\eta_o)K_f}$, $\delta_f = \dfrac{\eta_f(1-\eta_o)K_f}{\eta_o K_s + (1-\eta_o)K_f}$

Table E.3: A comparison of the non-zero elements in matrix B_0

of the Biot system and the C-S system

Inconstant element in B_0	Biot system	C-S system
B_{41}	N	μ_s
B_{32}	$P\text{-}2N$	$A\text{-}2\mu_s$
B_{42}	P	A
B_{48}	Q	$\text{-}C$
$B_{37}= B_{47}$	Q	B
B_{87}	R	$\text{-}E$

Table E.3: A comparison of the non-zero elements in matrix C_0
of the Biot system and the C-S system

non-zero element in C_0	Biot system	C-S system [*]
$C_{11}=C_{22}$	$-b$: $\quad b = -\dfrac{\eta_o^2 \mu_f}{K}$	$\dfrac{-b}{1-\eta_o}$: $\quad b = -\dfrac{\eta_o^2 \mu_f}{K}$
$C_{16}=C_{27}$	b	$\dfrac{b}{\eta_o}$
$C_{61}=C_{72}$	b	$\dfrac{b}{1-\eta_o}$
$C_{66}=C_{77}$	$-b$	$-\dfrac{b}{\eta_o}$
C_{31}	$-\dfrac{Q}{\eta_o}\dfrac{\partial \eta_o}{\partial x}$: $\quad Q = \dfrac{\eta_o[(1-\eta_o)K_s - \eta_o K_b]}{1-\eta_o - \dfrac{K_b}{K_s} + \eta_o\dfrac{K_s}{K_f}}$	$N_A\dfrac{\partial \eta_o}{\partial x}$: $\quad N_A = K_s\delta_A + \dfrac{4}{3}\mu_s\dfrac{1-\delta}{1-\eta_c}$
C_{41}	$-\dfrac{Q}{\eta_o}\dfrac{\partial \eta_o}{\partial x}$	$H_A\dfrac{\partial \eta_o}{\partial x}$: $\quad H_A = K_s\delta_A - \dfrac{2}{3}\mu_s\dfrac{1-\delta}{1-\eta_o}$
C_{32}	$-\dfrac{Q}{\eta_o}\dfrac{\partial \eta_o}{\partial z}$	$H_A\dfrac{\partial \eta_o}{\partial z}$
C_{42}	$-\dfrac{Q}{\eta_o}\dfrac{\partial \eta_o}{\partial z}$	$N_A\dfrac{\partial \eta_o}{\partial z}$
C_{36}	$\dfrac{Q}{\eta_o}\dfrac{\partial \eta_o}{\partial x}$	$N_B\dfrac{\partial \eta_o}{\partial x}$: $\quad N_B = \dfrac{4\delta\mu_s}{3\eta_o} - K_s\delta_B$
C_{46}	$\dfrac{Q}{\eta_o}\dfrac{\partial \eta_o}{\partial x}$	$-H_B\dfrac{\partial \eta_o}{\partial x}$: $\quad H_B = K_s\delta_B + \dfrac{2}{3}\mu_s\dfrac{\delta}{\eta_o}$
C_{37}	$\dfrac{Q}{\eta_o}\dfrac{\partial \eta_o}{\partial z}$	$-H_B\dfrac{\partial \eta_o}{\partial z}$

$$C_{47} \qquad \frac{Q}{\eta_o}\frac{\partial \eta_o}{\partial z} \qquad\qquad\qquad N_B \frac{\partial \eta_o}{\partial z}$$

$$C_{51} \qquad\qquad\qquad\qquad N_s \frac{\partial \eta_o}{\partial z}: \quad N_s = \mu_s \frac{1-\delta}{1-\eta_o}$$

$$C_{52} \qquad\qquad\qquad\qquad N_s \frac{\partial \eta_o}{\partial x}$$

$$C_{56} \qquad\qquad\qquad\qquad N_f \frac{\partial \eta_o}{\partial z}: \quad N_f = \mu_s \frac{\delta}{\eta_o}$$

$$C_{57} \qquad\qquad\qquad\qquad N_f \frac{\partial \eta_o}{\partial x}$$

$$C_{81} \qquad -\frac{R}{\eta_o}\frac{\partial \eta_o}{\partial x}: \quad R = \frac{\eta_o^2 K_s}{1-\eta_o - \dfrac{K_b}{K_s} + \eta_o \dfrac{K_s}{K_f}} \qquad F_A \frac{\partial \eta_o}{\partial x}: \quad F_A = K_f \delta_A$$

$$C_{82} \qquad -\frac{R}{\eta_o}\frac{\partial \eta_o}{\partial z} \qquad\qquad\qquad F_A \frac{\partial \eta_o}{\partial z}$$

$$C_{86} \qquad \frac{R}{\eta_o}\frac{\partial \eta_o}{\partial x} \qquad\qquad -G_x: \qquad K_f \delta_B \frac{\partial \eta_o}{\partial x} + \frac{K_f}{\rho_o^f}\frac{\partial \rho_o^f}{\partial x}$$

$$C_{87} \qquad \frac{R}{\eta_o}\frac{\partial \eta_o}{\partial z} \qquad\qquad G_z: \qquad K_f \delta_B \frac{\partial \eta_o}{\partial z} + \frac{K_f}{\rho_o^f}\frac{\partial \rho_o^f}{\partial z}$$

$$* \quad \delta_A = \frac{1}{1-\eta_o}\left(\delta_I - \frac{\delta_s}{1-\eta_o}\right) \ , \qquad \delta_B = \frac{1}{\eta_o}\left(\delta_I - 1 + \frac{\delta_f}{\eta_o}\right) .$$

APPENDIX F

PHYSICAL PARAMETERS AND COEFFICIENTS OF THE BIOT SYSTEM AND THE C-S SYSTEM FOR COLD LAKE SHALES AND SANDSTONES

Table F.1: Physical parameters and coefficients of the Biot system and the C-S system for Cold Lake shale

Basic parameters		Biot system		C-S system	
ρ_o^s (kg/m³)	2211	ρ_{11} (kg/m3)	2200	D_{11} (kg/m3)	2221
ρ_o^f (kg/m³)	1040	ρ_{22} (kg/m3)	20.8	D_{22} (kg/m3)	2080
η_o	0.01	ρ_{12} (kg/m3)	-10.4	D_{12} (kg/m3)	-1040
				D_{21} (kg/m3)	-10.4
K_s (N/m²)	6.97E9	P (N/m2)	1.1735E10	A (N/m2)	1.16157E10
μ_s (N/m²)	3.575E9	N (N/m2)	3.539E9	μ_s (N/m2)	3.575E9
K_b (N/m²)	6.6897E9	Q (N/m2)	1.30741E6	B (N/m2)	6.77983E9
K_f (N/m²)	2.51E9			C (N/m2)	7.21183E6
K (1/m²)	1.E-16	R (N/m2)	2.463E7	E (N/m2)	6.84832E6
μ_f (Ns/m²)	1E-3	b (N s m4)	1E9	b (N s m4)	1E9
		V_f (m/s)	2301	V_f (m/s)	2304
		V_r (m/s)	1270	V_f (m/s)	1270
		V_s (m/s)	1087	V_f (m/s)	180

Table F.2: Physical parameters and coefficients of the Biot system and the C-S system for Cold Lake sandstone saturated with gas

Basic parameters		Biot system		C-S system	
ρ^s (kg/m³)	2650	ρ_{11} (kg/m3)	1766	D_{11} (kg/m3)	2655
ρ^f (kg/m³)	10	ρ_{22} (kg/m3)	6.7	D_{22} (kg/m3)	20
η	0.335	ρ_{12} (kg/m3)	-3.35	D_{12} (kg/m3)	-10
				D_{21} (kg/m3)	-5
K_s (N/m²)	3.67E10	P (N/m2)	6.1329E9	A (N/m2)	8.09936E9
μ_s (N/m²)	4.4E9	N (N/m2)	2.926E9	μ_s (N/m2)	4.4E9
K_b (N/m²)	2.23E9	Q (N/m2)	8.72456E5	B (N/m2)	2.8662E6
K_f (N/m2)	1.44E6			C (N/m2)	1.35615E6
K (1/m2)	1.E-12	R (N/m2)	4.837E6	E (N/m2)	1.44389E6
μ_f (Ns/m2)	2.2E-5	b (N s m4)	2.47E6	b (N s m4)	2.47E6
		V_f (m/s)	1865	V_f (m/s)	1748
		V_r (m/s)	1287	V_f (m/s)	1287
		V_s (m/s)	269	V_f (m/s)	269

Table F.3: Physical parameters and coefficients of the Biot system and the C-S system for Cold Lake sandstone saturated with bitumen

Basic parameters		Biot system		C-S system	
ρ^s (kg/m^3)	2650	ρ_{11} (kg/m3)	2092	D_{11} (kg/m3)	3146
ρ^f (kg/m^3)	985	ρ_{22} (kg/m3)	660	D_{22} (kg/m3)	1970
η	0.335	ρ_{12} (kg/m3)	-330	D_{12} (kg/m3)	-985
				D_{21} (kg/m3)	-496
K_s (N/m^2)	3.67E10	P (N/m2)	7.8412E9	A (N/m2)	1.09993E10
μ_s (N/m^2)	4.4E9	N (N/m2)	2.926E9	μ_s (N/m2)	4.4E9
K_b (N/m^2)	2.23E9	Q (N/m2)	9.47998E8	B (N/m2)	3.09045E9
K_f (N/m2)	1.7E9			C (N/m2)	1.46225E9
K (1/m2)	1.E-12	R (N/m2)	5.256E8	E (N/m2)	1.55685E9
μ_f (Ns/m2)	1.5E2	b (N s m4)	1.68E13	b (N s m4)	1.68E13
		V_f (m/s)	2215	V_f (m/s)	2169
		V_r (m/s)	1232	V_f (m/s)	1232
		V_s (m/s)	718	V_f (m/s)	685

Table F.4: **Physical parameters and coefficients of the Biot system and the C-S system for Cold Lake sandstone saturated with water**

Basic parameters		Biot system		C-S system	
ρ^s (kg/m^3)	2650	ρ_{11} (kg/m3)	2111	D_{11} (kg/m3)	3174
ρ^f (kg/m^3)	1040	ρ_{22} (kg/m3)	696.8	D_{22} (kg/m3)	2080
η	0.335	ρ_{12} (kg/m3)	-348	D_{12} (kg/m3)	-1040
				D_{21} (kg/m3)	-524
K_s (N/m^2)	3.67E10	P (N/m2)	8.56648E9	A (N/m2)	1.22171E10
μ_s (N/m^2)	4.4E9	N (N/m2)	2.926E9	μ_s (N/m2)	4.4E9
K_b (N/m^2)	2.23E9	Q (N/m2)	1.35E9	B (N/m2)	4.38695E9
K_f (N/m2)	2.51E9			C (N/m2)	2.07568E9
K (1/m2)	1.E-12	R (N/m2)	7.285E8	E (N/m2)	2.20997E9
μ_f (Ns/m2)	1.5E1	b (N s m4)	1.68E12	b (N s m4)	1.68E12
		V_f (m/s)	2386	V_f (m/s)	2358
		V_r (m/s)	1229	V_f (m/s)	1229
		V_s (m/s)	773	V_f (m/s)	729

Table G1: Physical parameters and coefficients of Biot system for the model shown in Figure 2.6.14 on page 82

Layer	ρ_b^s	ρ_b^f	ρ_{12}	η_b	K_s	K	μ_s	K_b	K_f	μ_f	ρ_{11}	ρ_{22}	P	N	Q	R	b	V_f	V_r	V_s
	kg/m3	( )	( )			N/m2				(Ns/m2)	kg/m			N/m2			(Nsm4)		m/s	
1	2250	1040	-260	0.25	5.2E9	1E-12	2.4E9	2.2E9	2.5E9	1E-3	1947	520	5.3E9	1.8E9	5.2R8	3.8R8	6E7	1856	1005	733
2	2300	1040	-104	0.1	5.3E9	1E-13	2.9E9	3.8E9	2.5E9	1E-3	2174	208	7.6E9	2.6E9	2.4E8	1.4E8	1E9	1950	1100	764
3	2400	1040	-104	0.05	5.8E9	1E-13	3.3E9	3.7E9	2.5E9	1E-3	2384	156	9.2E9	3.1E9	2.1E8	3.4E7	3E8	2030	1162	514
4	2480	1040	-104	0.03	6.1E9	1E-13	3.7E9	5.7E9	2.5E9	1E-3	2510	135	1.1E10	3.6E9	6.9E7	4.7E7	9E8	2097	1212	860
5	2211	1040	-10	0.01	6.9E9	1E-16	3.6E9	6.7E9	2.5E9	1E-3	2200	21	1.2E10	3.5E9	1.3E6	2.5E7	1E9	2301	1270	1087
6	2650	985	-330	0.33	3.7E10	1E-12	4.4E9	2.2E9	1.7E9..1	.5E2	2092	660	7.8E9	9.5E8	5.3E8		1.7E13	2215	1232	718
7	2670	1040	-104	0.02	9.4E9	1E-13	5.6E9	8.9E9	2.5E9	1E-3	2720	125	1.6E10	5.5E9	4.5E7	3.8E7	4E8	2500	1443	953
8	2700	1040	-104	0.05	2.6E10	1E-14	1.7E10	2.5E10	2.5E9	1E-3	2670	156	4.7E10	1.7E10	3E7	9.6E6	3E9	4200	2487	958
S*	2650	10	-3.4	0.33	3.7E10	1E-12	4.4E9	2.2E9	1.4E6	2.2E-5	1770	7	6.1E9	2.9E9	8.7E5	4.8E6	2E6	1748	1287	269
HB*	2650	900	-302	0.33	3.7E10	1E-12	4.4E9	2.2E9	1.2E9	3E-1	2046	603	7.4E9	2.6E9	6.8E8	3.8E8	1E12	1950	1237	675

S: steam;   HB: heated bitumen

END

18-08-93

FIN